Università degli Studi di Palermo

DIPARTIMENTO DI CHIMICA E FISICA DELLA TERRA
ED APPLICAZIONI ALLE GEORISORSE E AI RISCHI NATURALI
C.F.T.A.

RELATIONSHIPS BETWEEN MAFIC AND FELSIC MAGMATISM AT PANTELLERIA: A PETROLOGICAL STUDY ON INTERMEDIATE TRACHYTE MAGMAS

PhD thesis by:
Nunzia Romengo

Tutor:
Prof. S. G. Rotolo (GEO/07)

Coordinator:
Prof. F. Parello

Co-tutor:
Dott.ssa P. Landi(GEO/07)
Istituto Nazionale di Geofisica e Vulcanologia (INGV) - *Pisa, Italy*

Reviewers:

A. Gioncada - Dipartimento di Scienze della Terra- Università degli Studi di Pisa - via S. Maria, 53 - 56126 Pisa (Italy)

J. White - Department of Geography & Geology Eastern Kentucky University 521 Lancaster Ave., Roark 103 (USA)

DOTTORATO DI RICERCA IN GEOCHIMICA XXI CICLO
Jan 2007 – Dec 2010

CONTENTS

Abstract

Pantelleria, besides to represent the type locality for pantellerite, a Fe-rich peralkaline rhyolite, is well known in the petrological literature for the bimodality of the erupted products: a mafic end-member which includes mildly alkali basalts, and a felsic end-member which consists of trachytes (mildly peralkaline or metaluminous) and pantellerites with a complete lack of intermediate compositions between these two compositional groups.

Trachytes are the less evolved felsic compositions thus represent the crucial rock-type to investigate the relationships among mafic (parental) magmas and felsic (derivative) melts.

The central aims of this thesis:

- petrogenesis of trachytes and their relationships with parental basalts:

The petrogenesis of the trachytes is of particular importance, since they have been erupted in a narrow age-interval: final phases of the eruption of the Green Tuff (~45ka) and initial phases of the post-Cinque Denti caldera magmatism (±35-29ka).

In particular the discovery of a products (a benmoreiite lava flow) resulting from mixing processes between mafic and trachytic magmas gives evidence that basaltic magmas intruded into the trachytic magma chamber below the caldera associated with episodes of refilling from depth of the residing trachytic magma body. It can be regarded as a physical evidence of a strict relationships between basaltic and trachytic magmas. This study confirms a Daly gap between alkali-basaltic products (SiO_2 ~ 48 wt%) and trachytic rocks (SiO_2 ~ 64 wt %).

- pre-eruptive conditions (T, P, H_2O_{melt}) of trachytes:

The principal focus of this thesis was the reconstruction of pre-eruptive conditions of eruptions at Mt Gibele, by crystallization experiments, performed at T = 900-950 °C, P= 1.0 - 1.5 kb, for a variable H_2O_{melt} in a total of 12 charges.

Experimental Phase equilibria characterize clinopyroxene as the liquidus-phase, followed by alkali feldspar and olivine. T-P- H_2O_{melt} pre-eruptive conditions of trachyte magma are closely reproduced by 2 Runs that match closely phase abundance and phase composition of the natural sample. Thus we propose as the most likely

storage/crystallization conditions for trachyte magma at: T = 950 °C, P= 1.5 kb, H_2O_{melt} = 2.5- 2.8 wt %;

- petrogenetic relationships between trachytes and pantellerites:

We were able to produce a pantellerite liquid (Na+K/Al = 1.24) at the following conditions: T = 950 °C, P = 1 kb, H_2O_{melt} = 1.6 wt %, at a total crystal content of 73 wt %. These conditions are very different from the inferred pre-eruptive T-P-H_2O of pantellerite magma (Di Carlo et al., 2010), being much higher in temperature and at an H_2O_{melt} unrealistically low.

Nevertheless, we are allowed to assess that pantellerites are derivative of parental trachyte magma after 70 % of crystal fractionation, and this agrees with independent estimates, either geochemical or via thermodinamical modelling.

INTRODUCTION

The Island of Pantelleria represents the emerged portion of a large volcanic edifice rising up from the Sicily Channel Rift.

Pantelleria, besides to represent the type locality for pantellerite, a Fe-rich peralkaline rhyolite, is well known in the petrological literature for the bimodality in the erupted products: a mafic end-member which includes mildly alkali basalts, and a felsic end-member which consists of trachytes (mildly peralkaline or metaluminous) and pantellerites with a complete lack of intermediate compositions between these two compositional groups.

Given their occurrence in a variety of geotectonic settings, the petrogenesis of pantellerites is a highly debated issue and although some recent experimental petrology studies (Scaillet & MacDonald, 2001, 2003, 2006; Di Carlo et al., 2010) and petrological papers (White et al., 2005, 2009) shed light on several aspects regarding phase equilibria, assessment of T-P pre-eruptive conditions, the role of dissolved H_2O and fO_2 , some questions still remain unclear. Among these latter we may include the origin of the Daly gap in basalt-rhyolite volcanic suites, the petrogenetic link between mafic and felsic end-members.

At Pantelleria, **pantellerites** were erupted either as pyroclastic flows, or as pumice fall deposits or else as lavas flows. **Trachytes** on the contrary, were erupted dominantly as lava flows and, to a lesser extent, are found as enclaves in some young pantelleritic lava flows. Trachytes are the less evolved erupted felsic composition and consequently represent the crucial rock-type to investigate the relationships among mafic (parental) magmas and felsic (derivative) melts.

At Pantelleria the existing petrogenetic models for pantellerites (for a more general review see Scaillet and MacDonald, 2001) can be summarized in:

- Protracted fractional crystallization (FC hereafter) from an alkali basalt parental magma (Civetta et al., 1998) to trachyte (~ 75 % of solid removed) and later to pantellerites (~ 90 % of solid removed). This model has been developed purely on

geochemical grounds, while more recently White et al. (2009), added valuable petrological constraints to the fractional crystallization model.

- no direct consanguinity between mafic and felsic magmas. Following this hypothesis, trachytes are the result of a two-step process that encompasses the low-degree partial melting of alkali-rich mafic cumulates followed by fractional crystallization at low-pressure (Lowenstern and Mahood, 1991; Avanzinelli et al., 2004).

Although there is a general consensus that pantellerite is most likely deriving from trachyte via fractional crystallization of an assemblage dominated by alkali feldspar at relatively low pressures and fO_2 ($\leq$ FMQ) (Civetta et al.,1998; Avanzinelli et al., 2004; White et al., 2005; 2009; Di Carlo et al., 2010), the origin of trachytes still remains ambiguous.

In fact, according to White et al. (2009), trachytes can suffer of a significant degree of feldspar accumulation that prevents them to be strictly representative of a liquid, rather a crystal mush.

The central aims of this study can be outlined as follows:

1. to examine primarily the petrogenesis of a suite of metaluminous to slightly peralkaline trachytes and secondarily of some selected pantellerites.
2. individuate inter formational petrologic variability in the commonly considered "homogeneous", trachyte body.
3. to focus on detailed petrological definition including trace elements in key mineral phase (clinopyroxenes).
4. perform thermodynamic modelling (MELTS code) in order to explore the viability of fractional crystallization (FC) process and its adherence to natural products.
5. after that all these points were assessed we performed a small number of focused crystallization experiments in the range 900- 950 °C, 1.0-1.5 kbar, $H_2O_{melt} \leq 3.0$ wt%, fO_2 ca. FMQ in order to more constrain pre-eruptive conditions. All the experiments were carried out at CNRS-Institute des Sciences d' Orleans.

CHAPTER 1

GEOLOGY AND ERUPTIVE HISTORY OF THE PANTELLERIA

1.1 The Sicily Channel Rift Zone (SCRZ)

The island of Pantelleria is set in the Sicily Channel Rift Zone (SCRZ), a continental domain belonging to the Pelagian Block, the northern promontory of the African plate. The Sicily Channel was characterized since Pliocene by transtensional tectonics (Boccaletti et al., 1987; Catalano et al. 2008) coupled to diffuse mafic alkaline volcanism, subaerial (Linosa and Pantelleria islands) and submarine (Graham and Nameless Banks).

The SCRZ consists of three basins: the Pantelleria Trough, the Linosa Trough, and the Malta Trough. Volcanism occurs in all but the Malta Trough, and include two islands (Pantelleria and Linosa) and several seamounts. The thickness of the crust throughout most of the Pelagian Block is 25-35 km, thinning to 16-17 km in the SCRZ (Civile et al., 2008).

The Pantelleria Trough is characterized by high average heat flow values 100±20 mW/m^2 and a strong positive Bouguer anomaly 65-103 mGal (Berrino & Capuano, 1995; Argnani & Torelli, 2001; Civile et al., 2008).

A strong magnetic anomaly suggests the presence of abundant basaltic material at depth (Della Vedova et al., 1995).

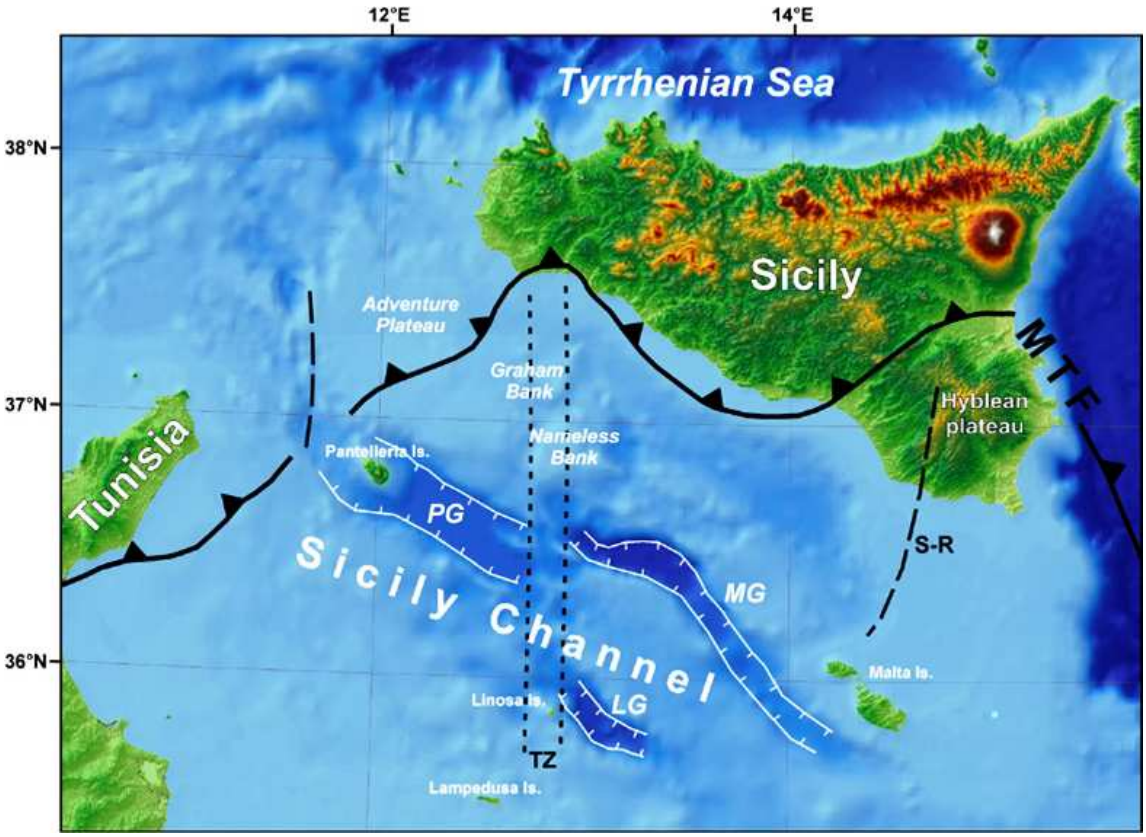

Fig. 1.1 - Morphological map of the Sicily Channel and surrounding regions. The Pantelleria graben (PG), the Malta graben (MG), and the Linosa graben (LG) are the principal tectonic depressions of the Sicily Channel. The external deformation front of the Maghrebides–southern Apennines (MTF), TZ indicates the broadly N-trending transfer zone discussed in the text, and S–R indicates the Scicli–Ragusa fault system. (From Civile et al., 2010).

Submarine magmatism in the Sicily Channel rift began during the early Pliocene, the oldest basaltic sample was dredged up from the Nameless Bank and dated at 10Ma (Beccaluva et al. 1981). The two most recent eruptions in the SCRZ were submarine, and occurred in the Graham Bank in 1831 and in the "Foerstner volcano" 5km NW offshore Pantelleria in 1891 (Washington 1909, Berrino & Capuano et al., 1995; Calanchi et al., 1989; Rotolo et al., 2006)

1.2 Pantelleria island volcanic complex

The island of Pantelleria represents the emerged part of a large volcanic edifice, whose submerged portion rises about 1000 meters above the sea floor. Pantelleria is elliptical in shape, with a NW-SE long axis oriented in strict agreement with the Sicily Channel Rift Zone.

Two concentric (nested) caldera rims represent the main structural feature of the island:

(i) the old caldera (age ca. 114 ka) named “La Vecchia” by caldera (Mahood & Hildreth (1986), and

(ii) the young caldera, named “Cinque Denti” by Mahood & Hildreth (1986) or “Monastero” by Cornette et al. (1983). This latter is related to the eruption of the Green Tuff ignimbrite, 50 ka B.P. (Civetta et al., 1984; Mahood & Hildreth, 1986).

Fig.1.2 - The two concentric caldera rims: “La Vecchia” caldera is the older and the more external; “Cinque Denti” is the younger and more internal and the circles point out of the eruptive centers.

The volcanological evolution of the island can be summarized as follows:

(1) an early period ~300-120 ka, which was dominated by pantellerite lava flows and subordinate ignimbrite or welded tuffs sheets. Ages as old as 500 ka were determined only in alkali granite cognate enclaves within the Green Tuff ignimbrite (Rotolo & Villa, 2001), These old sequences are exposed at Salto La Vecchia –Balata dei Turchi area (Sud-Est side of the island);

(2) an intermediate period (120-50 ka), characterized by large explosive eruptions emplacing several ignimbrite sheets, the oldest of them associated with the collapse of the "La Vecchia" caldera (~114 ka, Mahood & Hildreth). The SW, S, SE, and N rims of this depression are still discernible**.** The common character of all the ignimbrites at Pantelleria is the extreme degree of welding and rheomorphism (i.e. post-depositional flowage); both phenomena contribute to obliterate the primary structures of the deposits;

(3) The Plinian eruption of the Green Tuff (GT), that covered the whole island and whose fine ashes travelled as far as Dodecannnese (Margari et al, 2007). Its age has been estimated at between 50 ka (Mahood and Hildreth, 1986) and 45 ka (Civetta et al., 1988);

(4) the post Green Tuff volcanism (44-30 ka). This period began with the eruption of Mt Gibele-Montagna Grande thick trachytic lava flows (~ 44-37 ka; Mahood and Hildreth, 1986) that cover two thirds of the Cinque Denti Caldera. During this period effusion of pantellerite lava flows alternated with the emplacement of lava domes and with low-energy strombolian to subplinian eruptions of pantellerite magmas;

(5) after the eruption of the Mt Gibele- Montagna Grande trachytes the eruptive style turned to effusions of pantellerite lava flows which alternated with low-energy strombolian/subplinian eruption of pantellerite magmas, resulting in a complex interfingering of pumice fall sequences in the northern side of Montagna Grande (Rotolo et al., 2007), and in lesser amount on the other fault limited sides of Montagna

Grande block. Montagna Grande was uplifted and separated from the source vent of Mt Gibele, in recent times (~ 29-18 ka). Cuddia Randazzo and Cuddia del Gallo explosive and effusive eruptions represent the most recent volcanic events on the island (6 ka, Civetta et al., 1998; Speranza et al., in press; La felice et al., in prep.)

Fig. 1.3 - Cuddia Randazzo and Cuddia del Gallo eruptive centers, as seen from Mueggen.

It is important to stress out that the felsic post-Green Tuff volcanism activity was centred dominantly within the caldera rims, but, almost contemporaneously, basaltic magmas were erupted (scoria cones, lava flows) (**fig.1.4**) in the N side of the island, well beyond the caldera rims (with only exception of the Khartibucale hawaiite scoria cone, exactly over the caldera rim, close to Cala Cinque Denti).

Fig. 1.4 C. Rosse (Mursia), a basalt scoria cone in the north side of the island.

Taken as whole, alkali basalts represent around 5 vol.% of outcropping rocks, trachytes ca. 15 vol.%, the remaining 80 vol.% being pantellerites (Mahood and Hildreth, 1986).

1.3 THE GREEN TUFF ERUPTION

The Plinian eruption of the Green Tuff (GT), associated with the "Cinque Denti" caldera collapse, represents a major divide in the Pantelleria eruptive history, being the last large explosive eruption, and the most powerful of the island as well.

The Green Tuff consists of a complex sequence of air fall deposits, surge deposits, and welded to reomorphic pyroclastic flows. It presents a compositional zoning upwards from pantellerite to comenditic trachyte (Mahood & Hildreth,1986; Civetta et al., 1988), due to the emptying of chemically zoned magma chamber (Ferla & Meli, 2006).

The DRE volume of the products was estimated, by Mahood & Hildreth (1986) at around 2.5 km^3**.** Wolff and Wright (1981) estimated instead the erupted volume of the Green Tuff at 7 km^3 (DRE), assuming that all of the products on the island of Pantelleria are of plinian origin and a dispersal direction that extends to the NE to include the location of the Y-6 ash layer in the eastern Mediterranean.

Making exception for the basal fall layer, preserved only in the easternmost sections of the island, the Green Tuff shows pervasive welding and rheomorphism throughout the sequence.

The Green Tuff was variably interpreted by former Authors as a sequence of welded pyroclastic flows (Borsi et al., 1963; Villari,1969; 1974; Orsi & Sheridam, 1984), as a welded pyroclastic fall (Wright, 1980; Wolff & Wright, 1981) or as a combination of welded pyroclastic fall and compound ignimbrite (Mahood & Hildreth, 1986).

The eruption of the Green Tuff was accompanied by collapse of a caldera 6x7 km in size, which occupies the SW part of the island (**fig.1.2**).

1.4 POST-GREEN TUFF VOLCANISM (50-6 ka)

Based on K-Ar datings, stratigraphycal data and location of the vents, Civetta et al. (1988) and Orsi et al. (1991) splitted the post Green Tuff volcanism into 5 cycles of activity. According to these authors, the Green Tuff is regarded as the first eruptive cycle of the recent history of the island. However, new stratigraphycal data and $^{40}Ar/^{39}Ar$ ages (La Felice et al., in prep.) suggest that this scheme have to be partially modified.

1.4a – The Montagna Grande trachyte

After a period of quiescence of at least 10 ka, the Green Tuff eruption was followed by the emission of Mt Gibele - Montagna Grande trachytic lava flows (2^{nd} silicic cycle according to Civetta et al., 1988, Orsi et al., 1991) from the source vent of the Mt. Gibele vent. K-Ar dating gives ages from 35 +/- 8 ka to 28 +/- 16 ka (Mahood & Hildreth, 1986). Mt. Gibele is an edifice located within the young caldera (fig.1.2). The trachyte lavas gradually built a shield-like edifice which filled two thirds of the caldera, for a volume estimated at 3 km^3.

On the basis of their K–Ar data, although affected by large quoted 1 sigma errors, Mahood & Hildreth (1986) considered the Mt. Gibele trachyte flows as a prolongation of the “Green Tuff” eruptive cycle.

After the emplacement of the trachytes, in at least 6 stocked lava flows pile, a major tectonic uplift (vertical offset > 200 m) separated Mt Gibele from Montagna Grande in recent times (~ 29-18 ka, Mahood & Hildreth, 1986).

The faults that are bordering the E and W sides of Montagna Grande, were used as a preferential ascent pathways for pantellerite magmas that were emplaced as small domes (the two Mt. Gibile cones on the W) or small pumice cones (C. del Moro and Carbonara on the E).

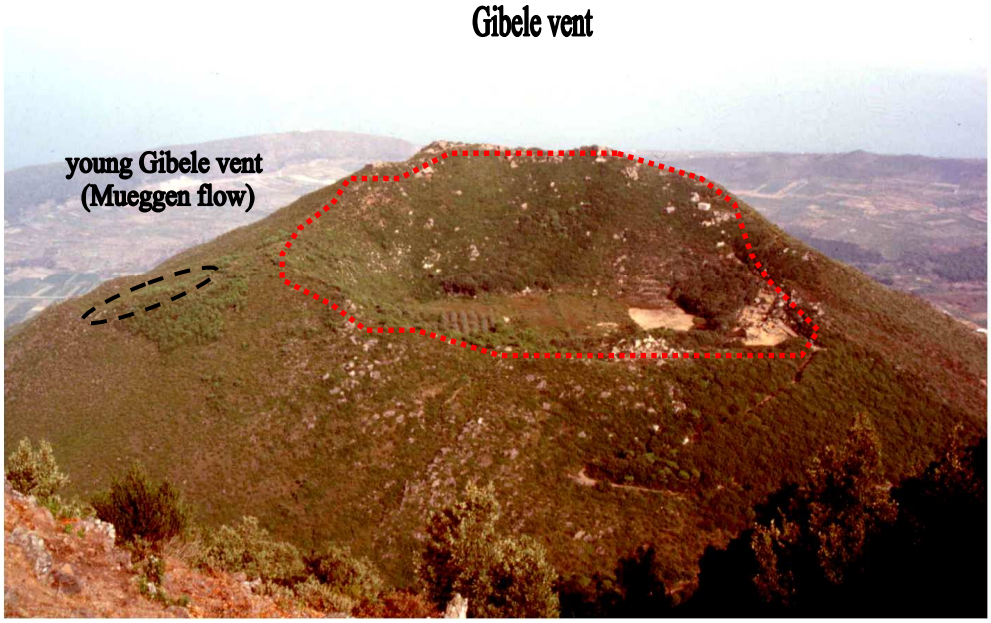

Fig. 1.5 The Mt. Gibele source vent of trachyte lavas, as seen from Montagna Grande.

Mahood & Hildreth (1986) stated that caldera-filling trachyte eruption was due to an isostatic compensation for the caldera collapse, given that the erupted volume of trachyte is comparable with the difference between the Green Tuff and the caldera volumes.

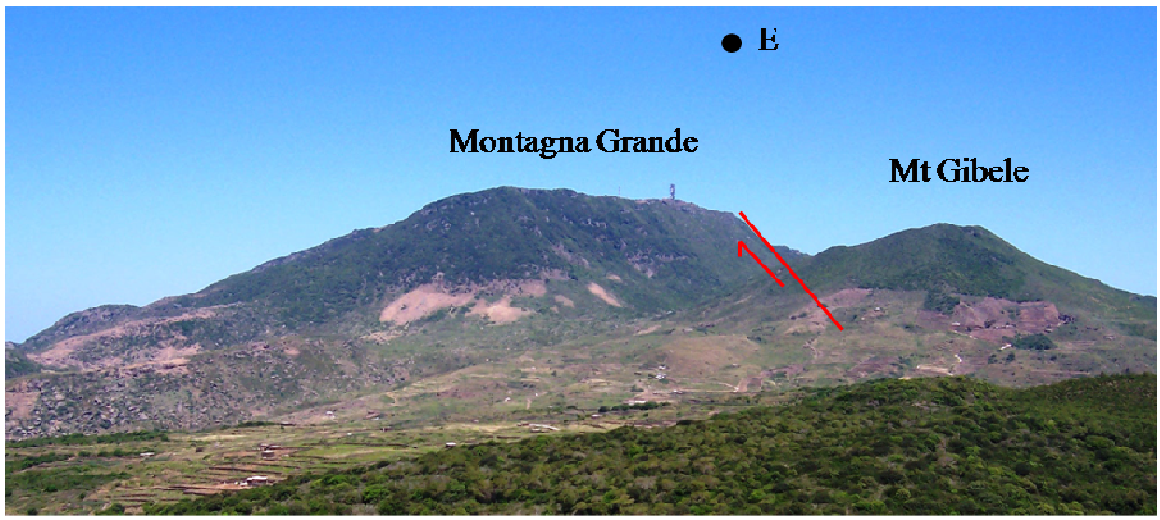

Fig. 1.6 The Mt. Gibele source vent (height 700 m) of trachyte lavas and the uplifted block of Montagna Grande (height 836 m) seen from W (Rekhale).

1.4b – Post trachytic phase felsic volcanism.

The period spanning the age interval 20-6 ka was probably the most fertile in eruption frequency of the post-Green Tuff history. Eruptions occurred from tens of eruptive centers (Rotolo et al, 2007 and references therein fig.1.7) located within the caldera rims, and mostly around the base of the intracaldera trachyte shield from radial fractures and along the fractures bounding the Montagna Grande tilted block.

The volcanic activity is characterized by effusive events and low-energy from strombolian to subplinian eruptions, emplacing lava flows, lava domes and pumice fall deposits. All the erupted magmas have pantelleritic composition. Trachytic magmas are present only as enclaves which reach 20-30 vol.% of the whole erupted products in Cuddia Randazzo and Gelfiser eruptions (Mahood and Hildreth,1986; Perugini et al., 2002).

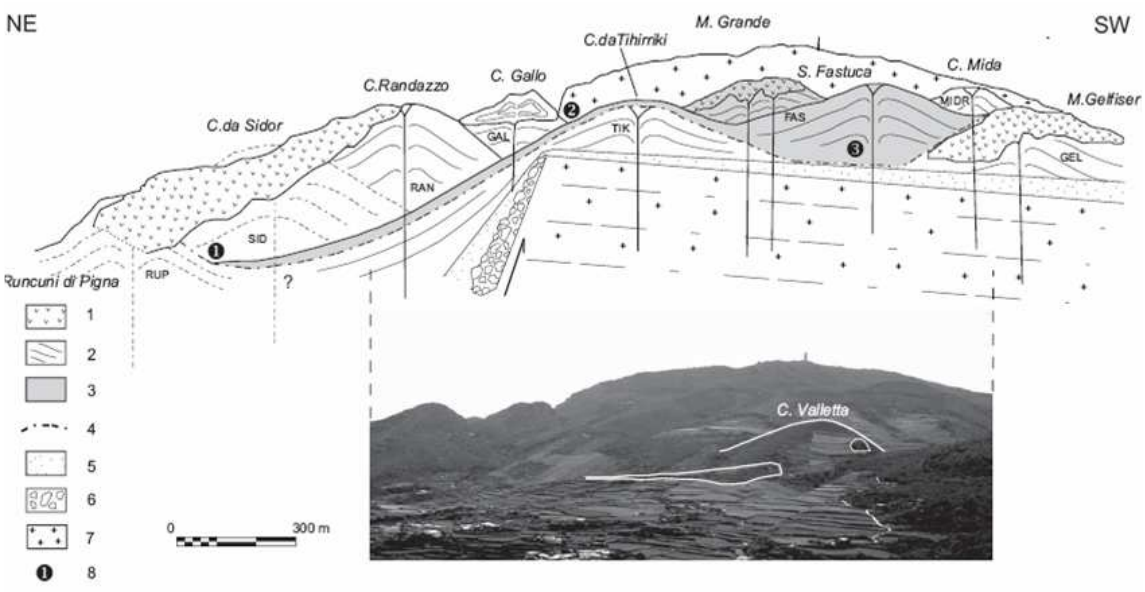

Fig. 1.7 Stratigraphic relationships between different post-caldera eruptive units in the area shown in the photo (photo taken from the caldera rim located 2 km NE of C. Randazzo), (from Rotolo et al., 2007).

CHAPTER 2

REVIEW OF PETROGENETIC HYPOTHESIS AND PHASE EQUILIBRIA CONSTRAINTS ON PANTELLERIA MAGMAS

Pantelleria island is well known in the petrographic literature for the presence of a bimodal suite including transitional basalts and hawaiites as mafic end member (SiO_2 45-52 wt %) and metaluminous to peralkaline trachytes and pantellerites as felsic end member (SiO_2 > 62 wt %).

Rocks of intermediate composition such as mugearites, benmoreite and mafic trachytes been found only as xenoliths (Villari, 1974; Civetta et al., 1984; Ferla et al., 2006). The lack of intermediate composition in bimodal suite (Daly Gap) is a common feature in the alkaline/peralkaline volcanism in continental rift and oceanic island settings.

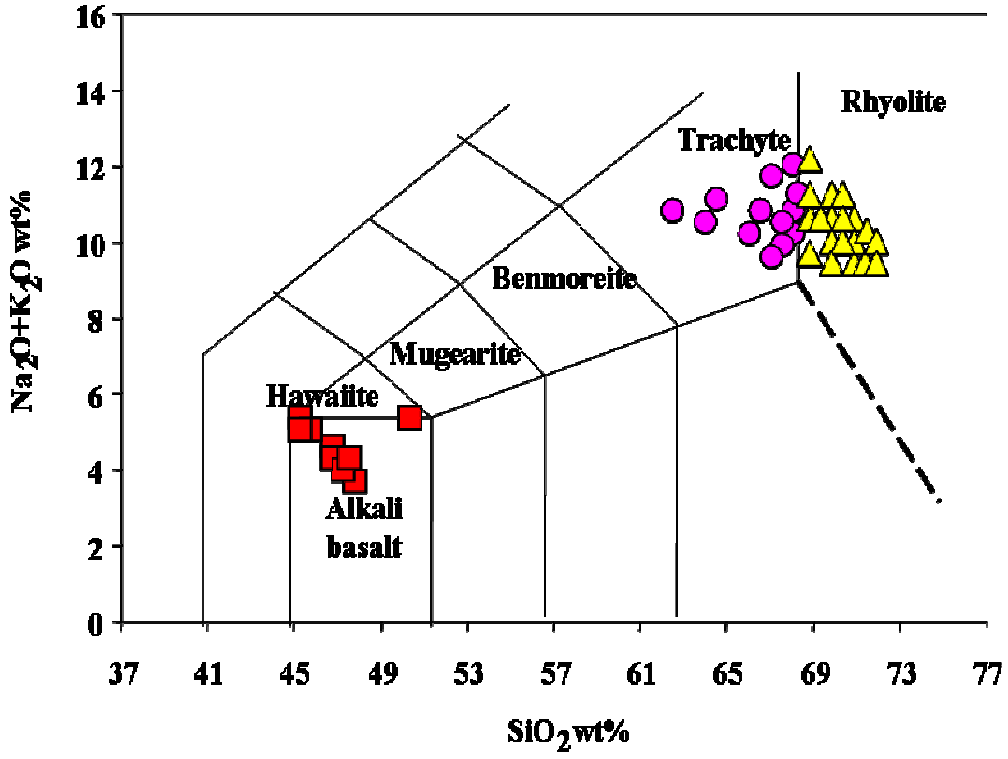

Fig. 2.1 Total alkali-silica (TAS) classification diagrams of Pantelleria volcanic rocks. (From Civetta et al., 1998). Square = basalts and hawaiites, circles = trachytes, triangles = rhyolites.

2.1 - Mafic magmas -

The mafic rocks at Pantelleria range from slightly hy-normative transitional basalts/hawaiites to ne-normative alkali basalts (Civetta et al. 1998).

Two main groups of basalts, respectively erupted before and after Green Tuff, have been recognized on the basis of major and trace chemical composition (Avanzinelli et al., 2004; Civetta et al., 1991; Civetta et al., 1998; White et al., 2009). K-Ar data give ages of 118±9 ka, 83±5 ka, and ~20-30 ka (Mahood and Hildreth, 1986; Civetta, 1984).

Basalts younger than 50 ka have lower TiO_2 and P_2O_5 contents and lower incompatible element and LREE abundances than the older ones. The different chemistry is though to be due to a different degrees of partial melting of a deep mantle source. In particular, $^{87}Sr/^{86}Sr$ ratios, that cluster around 0.7029 to 0.7032 (Civetta et al., 1998) in the mafic rocks, show that the primary mafic magnas were derived from mantle material which had been depleted in incompatible elements by a much earlier episode of magma generation. None of the mafic rocks from Pantelleria have petrological characteristics of really primary magmas.

Nd isotopic ratios show a restricted range of values in mafic rocks $^{143}Nd/^{144}Nd$ (0.5129 to 0.5130).

Sr and Nd isotope ratios are similar to those in OIBs or enriched MORBs; in contrast, the Pb isotope ratios, $^{206}Pb/^{204}Pb$ (19.13 to 19.94), $^{207}Pb/^{204}Pb$ (15.60 to 15.67), $^{208}Pb/^{204}Pb$ (39.08 to 39.62) are more variable. The proportion of several trace elements (e.g. Ce/Pb, Nb/U, Th/U) suggests a MORB type mantle sources contaminated with HIMU-like material (Esperanca & Crisci, 1995) or EMI+HIMU (Civetta et al., 1998).

Helium $^{3}He/^{4}He$ ratios of 7.3 Ra and $\delta^{13}C$ of - 4.5 ‰ measured in the free gases and dissolved helium and carbon in waters (respectively 1.0- 6.3 Ra and -7.1 to - 0.9‰) suggest a MORB-like source (Parello et al., 2000).

2.2 - Felsic end member: trachytes to pantellerites-

The felsic end member includes a variety of magmas from metaluminous trachytes to pantellerites, the Fe-rich peralkaline rhyolites typical of the island.

From the isotopic point of view, trachytes have $^{87}Sr/^{86}Sr$ (0.7031-0.7033) and Pantellerites considerable higher than $^{87}Sr/^{86}Sr > 0.7034$ (Civetta et al., 1994, 1998). Only few samples fall outside this range.

Based on geochemistry and mineralogy the following groups of silicic magmas can been distinguished (Civetta et al., 1998; Avanzinelli et al., 2004; White et al., 2005; White et al., 2009):

a) metaluminous trachytes (AI < 1; where Agpaitic Index = molar $(Na_2O + K_2O)/Al_2O_3$) with low incompatible trace element (ITE) such as Rb, Zr, Nb and Th, (low ITE trachytes) but high content of Ba, and positive Eu anomalies;

b) metaluminous trachytes with high contents (AI < 1) of Rb, Zr, Nb but lower Ba and negative Eu anomalies (high ITE trachytes);

c) comenditic trachytes (SiO_2= 66.0-67.0 wt%, 1 < AI < 1.3), with modest LREE enrichment, similar to those of the pantellerites;

d) strongly peralkaline (SiO_2 > 69.0 wt%, AI > 1.3 to 2.1) magmas from pantelleritic trachytes to pantellerites.

Geochemical and petrological evidence led White et al. (2005) to separate felsic rocks into five categories, each typified by different phenocryst assemblages, melt agpaitic index**,** oxygen fugacity (fO_2) and temperature (see Table 2.1).

Sample:	SiO_2 wt%	AI	ΔFMQ	Temperature	Mineral assemblages
1.	< 65.0	<1.3	-0.7 -1.1	880-990	augite + fayalite + ilmenite + magnetite
2.	67.0	1.4	-0.5	~800	augite + fayalite + ilmenite
3.	< 68.0	1.5-1.6	-0.2	760-750	hedembergite + fayalite + aenigmatite + quartz
4.	< 72.0	1.6-1.7	0.0	740-700	Na-hedembergite or aegirine-augite + ilmenite + aenigmatite + quartz + ferrorichterite
5.	70.0	2.0	/	~700	aegirine-augite + aenigmatite + quartz

Table 2.1 Variation in mineralogy, temperature and oxygen fugacity in a suite of peralkaline to strongly peralkaline rocks at Pantelleria (from White et al., 2005). AI = Agpaitic index: molar $(Na_2O + K_2O)/Al_2O_3$.

The comendites and pantellerites are characterized by enrichment in LREE and HFSE as Cs, Rb, Zr, Nb, Y, Th, Hf and a strong depletion of Ba, Sr, Co, Ni, Sc with peralkalinity increasing.

2.3 Petrogenesis of felsic rocks

The origin of the trachytes at Pantelleria, and more in general in the continental rift zones where the Daly Gap is present, remains a puzzling issue in the volcanological literature. Two main models have been proposed at Pantelleria:

1. extremely protracted fractional crystallization from an alkali basalt parental magma (Civetta et al., 1998; Avanzinelli et al., 2008; White et al., 2009);
2. low-degree partial melting of alkali gabbros cumulates to generate trachytoid melts, successively evolving into pantelleritic magmas by low-pressure crystal fractional (Lowenstern and Mahood, 1991).

The subsequent low-pressure differentiation of the trachypantellerite magma resulted in the formation of anorthoclase-cumulate trachytes and residual pantellerite (Mahood & Stimac, 1990; Mahood et al., 1990; Lowenstern & Mahood, 1991).

In general to achieve increase in peralkalinity, a Ca-rich plagioclase is removed from a basaltic magma. The processes is able to achieve the enrichment in alkalies, depleting in the mean time derivative liquids in alumina, ***"the plagioclase effect"*** of Bowen (1945).

Once peralkalinity is approached, the removal of K-feldspar ensures a rapid increase in peralkalinity dictated by the fractionation of K-feldspar. ***"orthoclase effect"*** is counterbalanced by the crystallisation of Na-bearing minerals: aenigmatite, Na-clinopyroxene (at high fO_2) or amphibole (at low fO_2), ***"the pyroxene effect"*** of Scaillet and MacDonald, 2003. Crystallisation of these minerals is able to efficiently buffer the increase in melt peralkalinity to Agpaitic Index ± 2.

Pantelleria provides proof of the existence of a stratified magma chamber with the pantellerite magma localized in the higher part, the anorthoclase-rich trachytic magma in the middle part and the basaltic magma localized below the trachyte in the lower part (Civetta *et al*., 1984, 1988, 1998; Mahood & Hildreth, 1986).

2.4 Hypothesis about the origin of “Daly Gap”

One of the main problems in studies of peralkaline complexes, is the lack of rocks of intermediate composition between basalt and trachyte, constituting the so-called ‘Daly Gap’.

Ferla et al. (2006) suggested that the ‘benmoreitic’ enclaves in Pantelleria volcanic rocks are probably formed by the mixing between an FM-1 basalt, rising along dykes, and overlying trachytic magma and are not representative of magma of intermediate composition. Although the chemical composition of the enclaves fills the ‘Daly Gap’, they do not represent a continuous liquid line of descent from mafic to felsic magma compositions.

Several models have been proposed for the origin of the Daly Gap and we briefly report a few of them.

The abrupt chemical separation between mafic and felsic rocks was considered by Mahood and Hildreth (1986) to be due to the presence of a shallow, low-density, mass of felsic magma beneath the central part of the island, beneath the younger caldera, that behaved as a density FILTER (Civetta et al., 1998).

White et al., (2009) have suggested that the compositional gap is the result of inhomogeneous crystallization rate for a given silica increase; to confirm the process of fractional crystallization, Mushkin et al. (2003) suggest that the Daly Gap reflects the relatively low sampling of intermediate compositions during the cooling and crystallization of magma chambers. The mafic compositions evolve slowly because of the small difference in silica content between the melt and the fractionating assemblage.

Also the more felsic compositions evolve slowly because of their low cooling rate combined with the onset of K-feldspar crystallization. The fast evolution and low sampling probability through the intermediate stage reflects the combination of efficient cooling and large difference in silica content between fractionating crystals and the magma.

2.5 Phase equilibrium constraints on pre-eruptive conditions of felsic explosive volcanism, at Pantelleria.

Phase equilibria amassment in experimental investigation is particularly important:

1. to predict the liquid line descent (i.e. direction of derivative liquids) and
2. to make comparison with natural phase assemblage in order to derive pre-eruptive conditions.

2.5.1 Experimental phase equilibria

Recent experimental investigations (Scaillet & Macdonald, 2001, 2003, 2006) and melt inclusions studies (Gioncada & Landi, 2010) have shown that peralkaline melts are rather H_2O-rich. These studies have demonstrated the important role of pressure, water, oxygen fugacity and silica disilicate activity ($aSiO_2$) on the phase equilibria of felsic peralkaline magmas.

The determination of storage conditions of pantelleritic magmas can also provide constraints on the more general problem of the origin of silica-oversaturated peralkaline magmas, which has been extensively debated (see Civetta et al., 1998; Scaillet & Macdonald, 2001; Macdonald et al., 2008).

Di Carlo et al. (2010) present the hydrous phase equilibria of a pantellerite with agpaitic index (= molar Na_2O+K_2O/Al_2O_3) = 1.4, within the pressure range 25-150 MPa and temperatures between 680-800 °C, with oxygen fugacities below the Ni-NiO solid buffer (NNO), and melt water contents (H_2O_{melt}) up to 6 wt % (Fig. 2.2).

The phase relationships at 150 MPa at H_2O-saturation (ca. 6 wt% H_2O_{melt}) clinopyroxene is the liquidus phase, appearing at 760 °C, followed by alkali feldspar and then by quartz whose crystallization is inferred to occur at around 650°C. Aenigmatite is stable at temperatures below 740 °C under H_2O_{melt} poor conditions, and below 680 °C at $H_2O \leq$ 5 wt %. Amphibole begins to crystallize at temperatures lower than 700 °C, and its stability field is drawn as nearly independent of melt water content. Ilmenite was detected in only one charge, at 750 °C and 1.7 wt % H_2O_{melt}.

Phase relationships at 100 MPa show broadly the same pattern as at 150 MPa, with clinopyroxene being the liquidus phase, followed by alkali feldspar and then

quartz. Amphibole begins to crystallize at T < 700 °C, but is not stable at H_2O-saturation at 680 °C, therefore having a negatively sloping stability curve under H_2O-rich conditions. Aenigmatite displays the opposite behaviour, its stability field being limited to water contents > 2.5 wt % at around 680 °C.

Results at 50 MPa (2.7 wt % H_2O_{melt} at saturation) are similar to those at 100 MPa, except that aenigmatite was only identified in one charge near the solidus, hence this phase appears to have a very restricted stability field at this pressure.

The work shows that inference of crystallization pressure on the base of pre-eruptive volatile contents obtained only from melt inclusions analyses may lead to significant errors, if not interpreted in the context of crystal-liquid equilibrium.

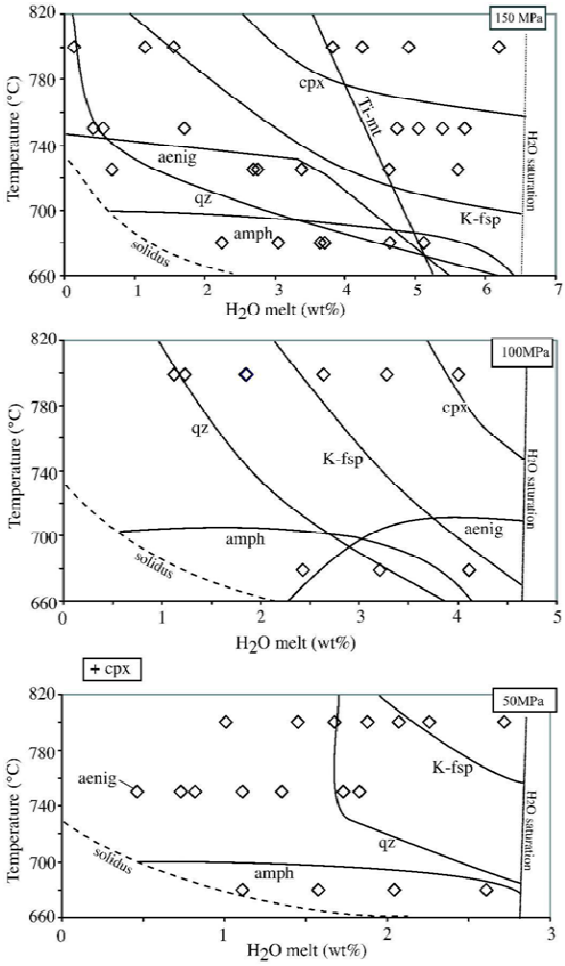

Fig. 2.2 Isothermal-polybaric phase relationships of PAN 01113 pantellerite at: a) 800 °C, b) 750 °C and c) 680 °C. In (c) alkali feldspar and clinopyroxene are always present. The dashed lines represent the water saturation curve experimentally derived for the Pan01113 composition (Di Carlo *et al*, 2010).

CHAPTER 3

TRACHYTES, GREEN TUFF AND PANTELLERITES : FIELD RELATIONSHIPS

3.1Field relationships and sampling

The study area is entirely located within the younger caldera.

We focused primarily on the possibility to better describe/differentiate the Montagna Grande trachyte body, which in the literature is referred to as a homogeneous eruptive body, although detailed data are lacking.

Secondarily we focused also on the Green Tuff sequence, because this was the latest eruption before the trachyte and, given the magnitude and the related caldera collapse, is likely to have thoroughly modified the plumbing system.

Trachytes represent the link between the mafic and felsic poles at Pantelleria **(fig.2.1)**, consequently it is of great importance to understand if some petrological variability within the trachyte body occurs and, if so, to ascertain possible connections with the eruption timing (i.e. early/late episodes).

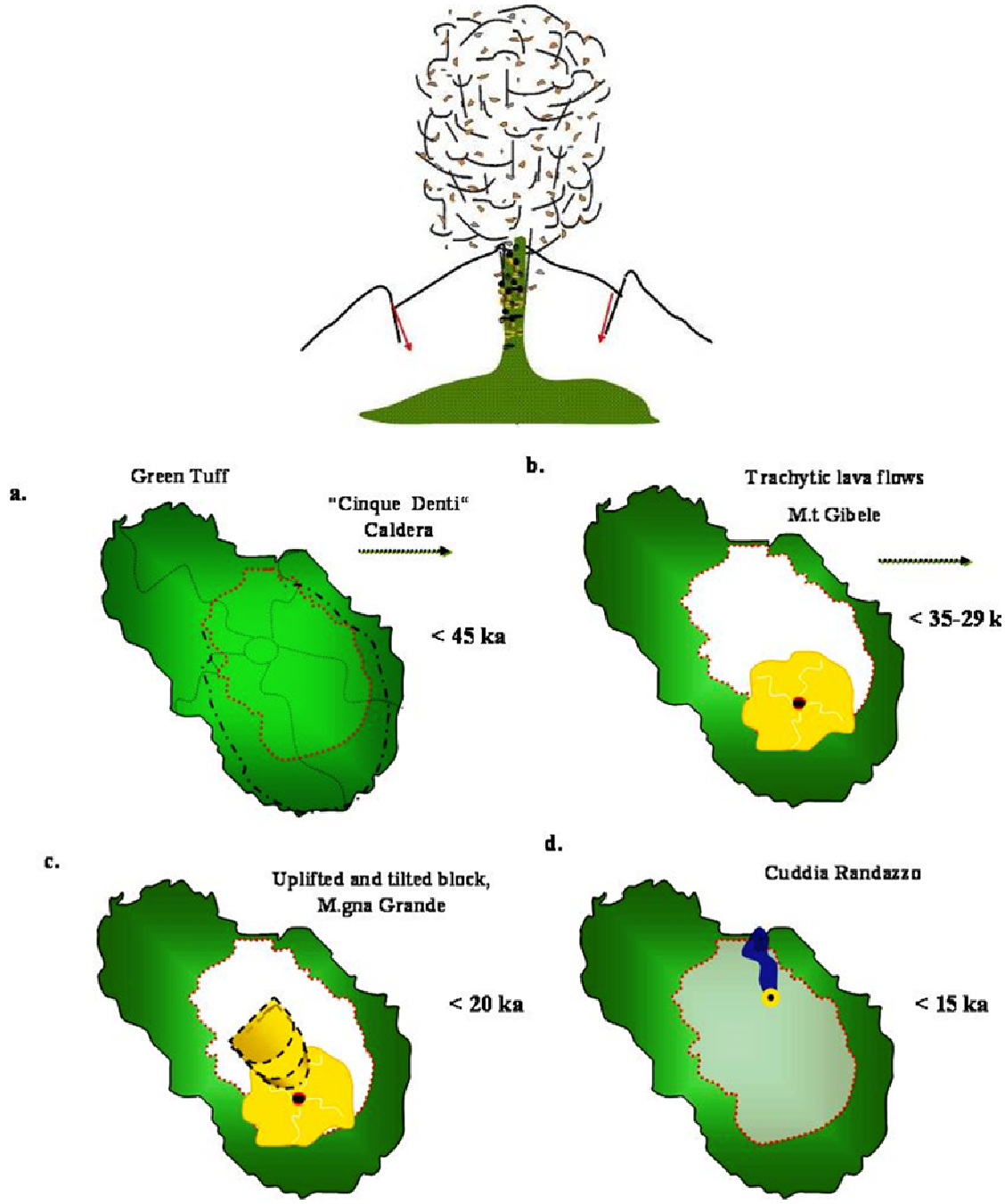

Fig. 3.1 (a) the Green Tuff plinian eruption and related caldera collapse, (b) the trachyte lava flows were poured out from M.t Gibele and filled 2/3 of the caldera; (c) the trapdoor uplift separated the Montagna Grande block from the Mt Gibele source vent and (d) at ca. 6 ka begun the eruptive cycle of Cuddia Randazzo.
Green colour = the Green Tuff plinian eruption
Yellow colour = trachyte lava flow
Blue colour = eruptive strombolian C. Randazzo.

3.2 The Green Tuff sequence

The results of our analysis relate to stratigraphy, distribution, texture, structure show that the major part of the Green Tuff on the island of Pantelleria was emplaced by a pyroclastic density current mechanism (consisting of various flow units) and only a minor part of this unit consists of fall and surge products.

The Green Tuff is the sole ignimbrite (with a high aspect ratio), among the at least 5 erupted at Pantelleria, that entirely drapes the island. The Green Tuff drapes the former topography, showing great reomorphic thickening (up to 30 m) in paleovalleys, while thins out to few cm in the lee-side of the relief.

The most complete eruptive section is visible in few exposures in the NE sector of the island, between the Lake Specchio di Venere and Cala Cinque Denti.

Here, a 3.5 meter thick stratigraphic section allows the recognition of 5 members within the Green Tuff sequence (Orsi and Sheridan, 1984, recognize 8 members in a nearby, not specified, locality).

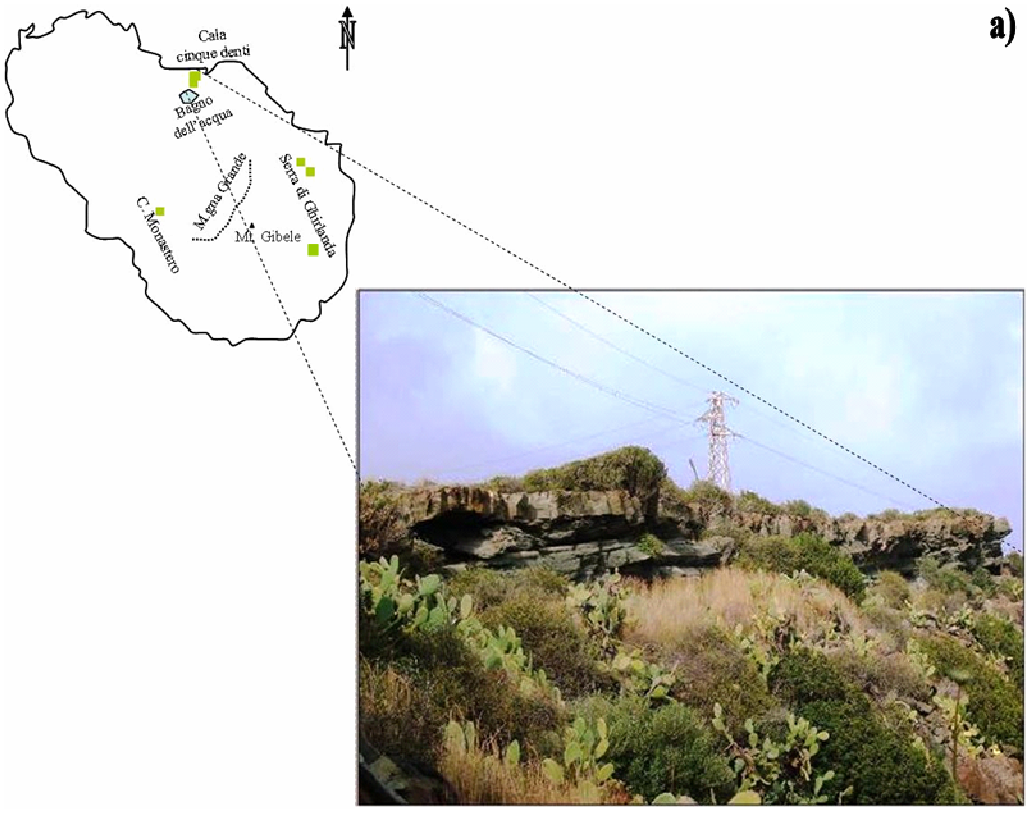

Fig. 3.2 a) Location of the Green Tuff sequence outcrops close to the Lake Bagno dell'acqua.

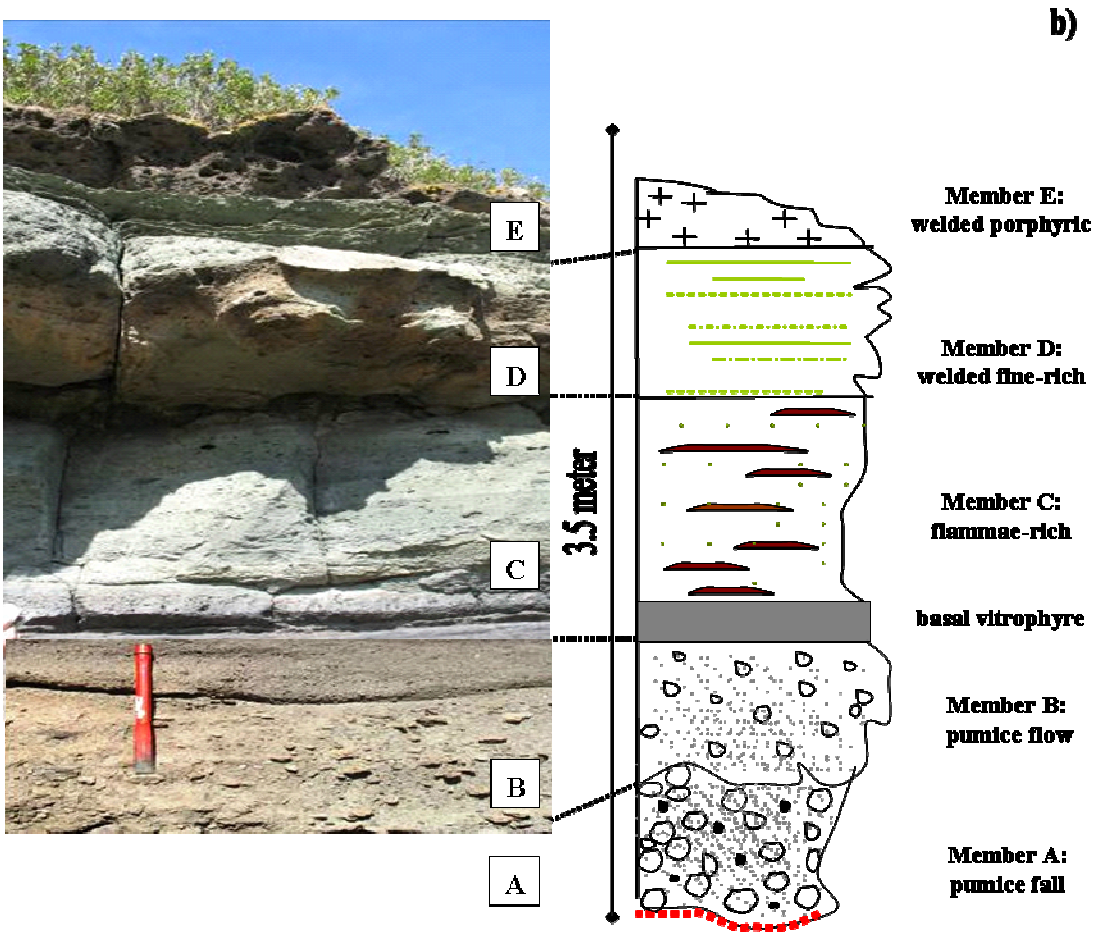

Fig. 3.3 b) a close-up vie of the sequence Cala Cinque Denti for a total thickness of around 3.5 mt. The Green Tuff mantling the inner wall of the caldera Cala Cinque Denti.

Each member is characterized by different eruptive, depositional and textural features. Nonetheless, the upper two thirds of the sequence are strongly affected by welding and rheomorphism that thoroughly obscures the primary features of the deposit.

From bottom to top the sequence consists of:

Member A: The Green Tuff sequence is opened by a plinian **pumice fall** deposit which lies just above a reddish paleosol. This member is to 50-60 cm thick poorly sorted pumice fall, the maximum and mean dimensions of pumice clasts are 5 and 7 cm, respectively. Feldspar is the most abundant mineral.

Non-welded basal pumice have also been found. Lithic clasts are rare in this member.

Member B consists of an ashy deposit with dispersed pumice clast. It is a chaotic, unwelded, **pumice flow** (40-50 cm thick, with maximum and mean pumice dimension

around 3-5 cm), very rich in fine ash, which could be representative of the initial stages of the column collapse. These latter are highly vesicular and contain small amounts of feldspar, clinopyroxene, aenigmatite. The abundance of ashy matrix suggests for this member a flow origin. The pumice-fall beds of this member are very poor in lithics.

Member C consists of a blackish **vitrophyre** (7-10 cm thick) that grades in to a progressively fiammae-poorer median portion of this thickly welded member, whose total thickness is around 70 cm. We consider this member as the result of the emplacement of the first pyroclastic density current.

Member D: Above the vitrophyre the sequence continues with **fines-rich and deeply welded**, to thoroughly pistachio-green portion, which alternates scattered and elongated fiammae and also less welded areas. It contains a large amount of crystals, mostly alkali feldspar up to 1 cm. Lithic clasts are larger and more abundant than in any other member. Higher up the sequence continues with a distinctly more, foliated fabric, prominent respect to the eroded lower members. Fiammae, though rare, are highly stretched, and flow folding is common. We interpreted the lamination of this member as a primary structure probably to be referred to a laminar diluted pyroclastic density current. Rich of ashy matrix.

Member E: This member (50 cm thick) is brownish in colour and rich in alkali feldspar phenocrysts (up to 5 mm in length and with an abundance around 35 vol %). This member is **welded**, has a strongly altered scoriaceous portion, and has been interpreted as the result of the tapping the lower portion of the magma chamber during the last eruptive phases (Civetta et al., 1988).

Members A and B are found only in the east side of the island, but with variable thickness due to the erosive power of the upcoming pyroclastic flow. Member C occurs, from north to south, in great part of the Green Tuff sequences. Member E is found in few localities of the island, among them, Costa Zighidì and Contrada Lago, in opposite sides of the young caldera rim.

3.3 Trachyte lavas

Montagna Grande, the most prominent topographic feature of Pantelleria, occupies the center of the island, fig.1.7.

The volcanic mass has been extensively affected by erosion processes and the traces of the original vents are partially concealed. The mountain shows a rapid flank on the east and south part and gentle slopes in the west and north flanks.

The Montagna Grande uplifted block, as already said in the previous chapter, consist entirely of trachyte stacked lava flows covered by more recent pyroclastic deposits and short pantellerite lava flows; the lava flows of Montagna Grande were separated from their vent at Mt. Gibele by a normal fault **(fig. 1.7)**. Mt. Gibele immediately east of the highest point of the summit ridge, is the largest and most important crater.

Our sampling strategy of the Montagna Grande and Mt. Gibele trachytes body was driven by the field identification of morphological limits of different trachyte flows which were accompanied by subtle macroscopic variations in the petrography of the lavas.

Sample	**0718**	**0748**	**0750**	**0747**	**0732**
Locality	**"Case Ricco"**	**"Montagna Grande Sud"**	**"Montagna Grande Nord"**	**"Favare-Mt. Gibele"**	**"Mueggen"**
K-feldspar	32	28	30-32	30	20
Clinopyroxene	4	6	4	6	3
Olivine	3	<<1	1	2	2
Fe-Ti oxide	1	<<1	2	2	<<1
Tot ph+mph	45%	35%	35%	40%	25%
Groundmass	50%	55%	45%	50%	60%
Vesicles	<5%	10%	20%	10%	15%

Tab. 3.1- Modal abundances (vol.%, void free) derived from BSE images, for trachytes mineral assemblages – ph = pheno > 500µm and mph = micropheno 50-500 µm and groundmass < 50µm.

Mueggen trachytes present lower crystal content than the trachytes from Montagna Grande and "Case Ricco". The last, have, indeed, nearly constant modal crystals, with difference close to the detection limit of the counter pointing methodology.

3.3a – Trachyte “Case Ricco” ***(sample pan0718)***

Here the trachyte thick flow unit is the one that banks against the caldera wall close to Sibà-Sciuvechi alignment a Contrada Monastero.

Fig. 3.4 - Trachyte “Case Ricco” -

The lava is fresh, the colour is light grey, the texture highly porphiritic. The phenocrysts are alkali feldspar as large as 15 mm which form up to 30-35 vol.% of the rock, and subordinate olivines, clinopyroxenes, magnetite.

Phenocrysts are settled in a crystalline groundmass showing well developed flow banding.

3.3b- Trachyte " Montagna Grande Sud" ***(samples pan0747-0748)***

Fig. 3.5 -Trachyte "Montagna Grande Sud"-

Immediately east of the highest point of the summit ridge, there is the largest and most important crater post green tuff. It show an almost circular shape, about 100 meters deep.

Here the trachytes are characterised by high abundance and large size of the alkali-feldspar phenocrysts, > 1cm. They constitute about 25-30 vol.% of the rock. Clinopyroxene (6 wt%) is the most abundant mafic mineral and Olivine is scarce (< 2 wt %).

The typical groundmass is holocrystalline but a little glass may be present occasionally, and some of the Mt. Gibele lavas are quite vitrophyric.

3.3c – Trachyte " MUEGGEN "*(sample pan0732)*

Fig. 3.6 view of the last side of Mt. Gibele and of the young trachyte flow, on the side of Mt. Gibele.

The trachytes are gray lavas usually compact. Alkali-feldspar phenocrysts are relatively small, 1-2 mm, and represent < 20 vol.% of the rock. Minor quantity of grains of augite and olivine are also found.

The typical groundmass is holocrystalline but few glass pockets may be present occasionally. The occurrence of small prisms of amphiboles is peculiar.

3.3d – Trachyte "Montagna Grande Nord" ***(sample pan0750)***

This sample was collected from a ridge at 700 meter a.s.l (**fig.3.7**).

It consists of a usually very compact lavas with light grey colour and highly porphyritic texture. Alkali feldspars form 30-35 vol. % of the rock. Crystals are tabular, highly cleavable, with glistening surfaces, colourless and transparent, and are 2 cm in length. Clinopyroxene, 1-2 mm in length, is the most abundant mafic mineral; the groundmass is light grey and almost aphanitic, though the lens reveals the presence of micro phenocrystals.

3.4 - The mafic lava inter bedded in trachyte

During the field survey, surprisingly, we encountered a short (100 meters) mafic lava flow at the top of the trachytes pile of Montagna Grande, at elevation of 730 meters.

The major importance of this mafic lava flow, is (i) in being the sole mafic magma within the caldera (intracaldera mafic) and (ii) the sole product with intermediate composition (benmoreite, see cap. 4) recovered in the island.

This sample (pan0749) is, dark grey in colour, highly porphyritic (PI = 55-60 vol.%) and shows seriate texture with abundant glomeroporphyric crystal clots.

Macroscopic phenocrysts, in order of decreasing abundance, are: alkali-feldspar, with tabular shape, colourless and transparent, 1-2 mm in length, and large clinopyroxene and olivine crystals (up to 4 mm).

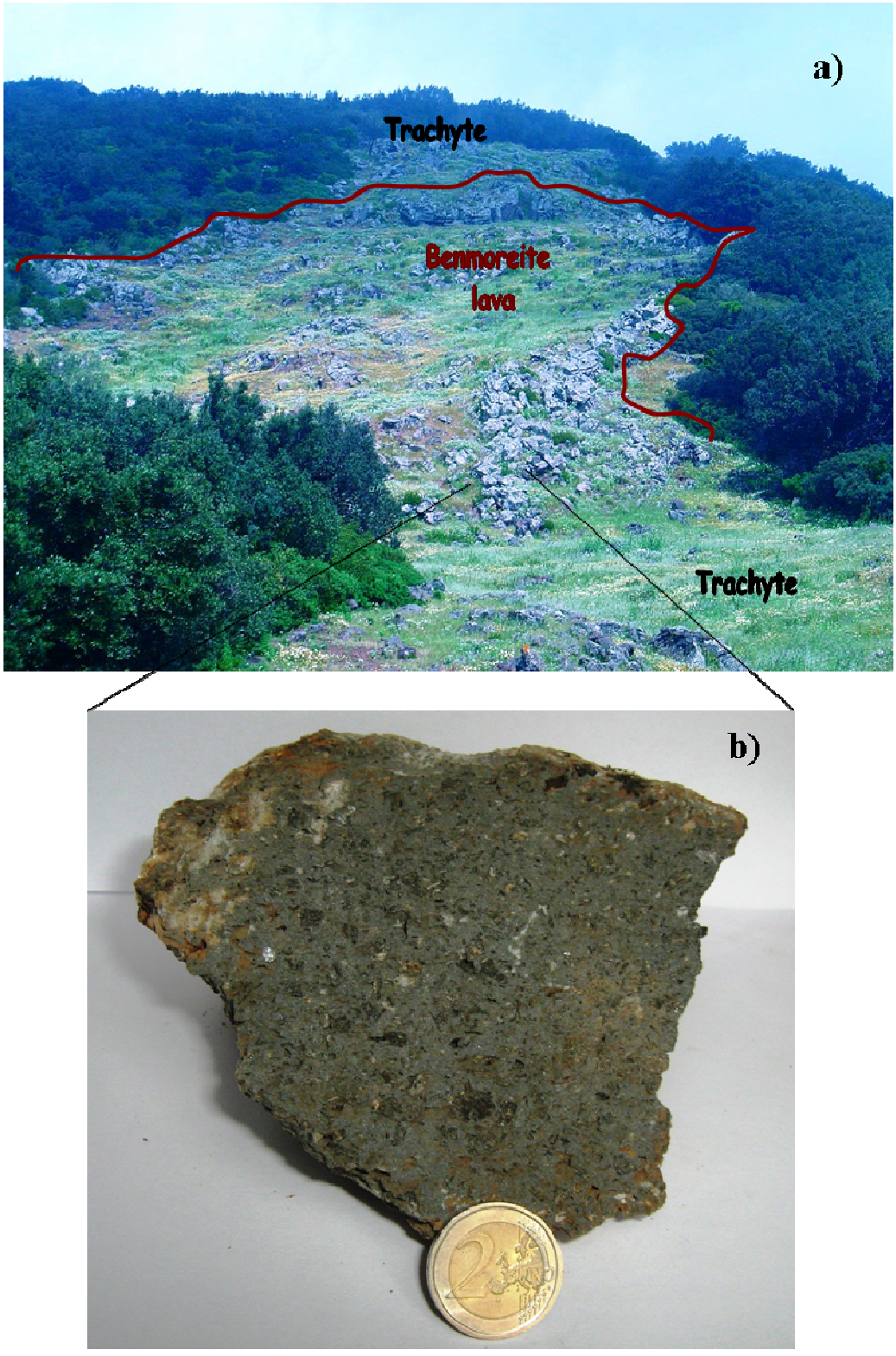

Fig.3.7 a) field view of the benmoreitic lava flow, close to the summit of Montagna Grande and b) hand specimen.

3.5 The trachytic enclaves in C. Randazzo pantellerites

Cuddia Randazzo is a composite structure, 8.2 to 5.5 ka old (Civetta et al., 1988; Speranza et al., 2010), that includes: (i) a pantellerite lava dome, (ii) the dome is broken at the NE termination to originates the 3,5 km long Khaggiar lava field and (iii) an outer pumice ring, partially dissected by the dome collapse, envelopes the dome itself **(fig.3.9)** .

The Randazzo fall deposit thins away from the source-vent and ends out in less than 200 meters, suggesting a strombolian distribution. The juvenile fraction consists of well-inflated coarse pumices (crystals ≤ 20 vol %) and denser, less vesiculated, darker scoriae (crystals ≤ 30 vol. %) associated with abundant bread-crust pumiceous bombs.

A main feature of these deposits is the occurrence of abundant, rounded to ameboidal trachytic enclaves (15-20 vol %), with feldspar megacrysts up to 2 cm, which have been interpreted as comagmatic clasts (Prosperini et al., 2000; Perugini et al. 2002). Lithics of pantelleritic lavas are scarce.

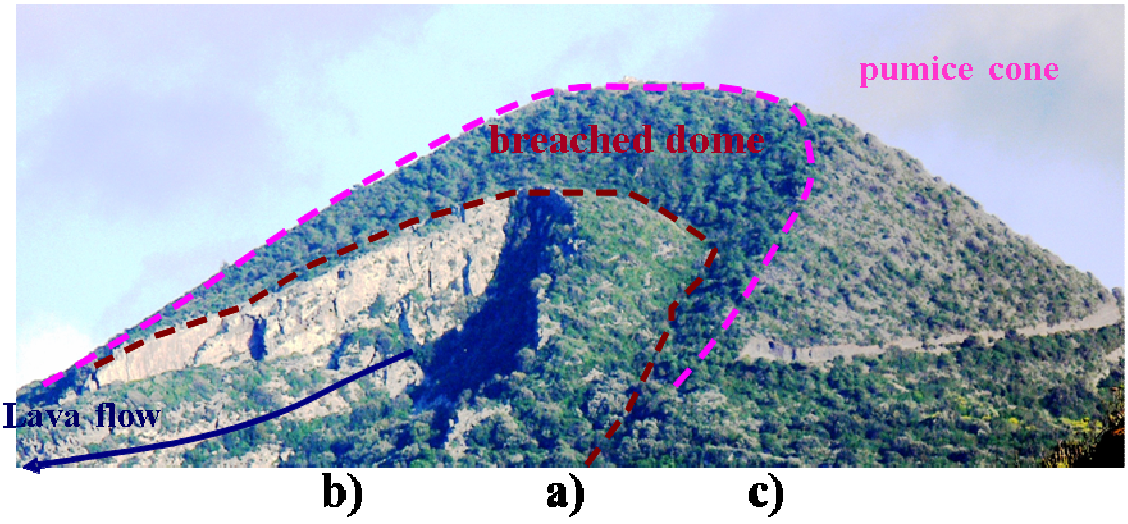

Fig. 3.8 - Cuddia Randazzo is composite structure that includes a core dome (a), a lava flow (c) and a pumice fall (b).

3.5a -Enclaves in lava flow-

The Khaggiar lava flow, originates from the Cuddia Randazzo pumice cone.

The Khaggiar pantellerite lava is a dark-grey glassy rock with small crystals of alkali-feldspar. It also includes abundant fragment with irregular shape, of a light-grey trachyte with large crystals of feldspar. Here after, these fragments will be called ENCLAVES.

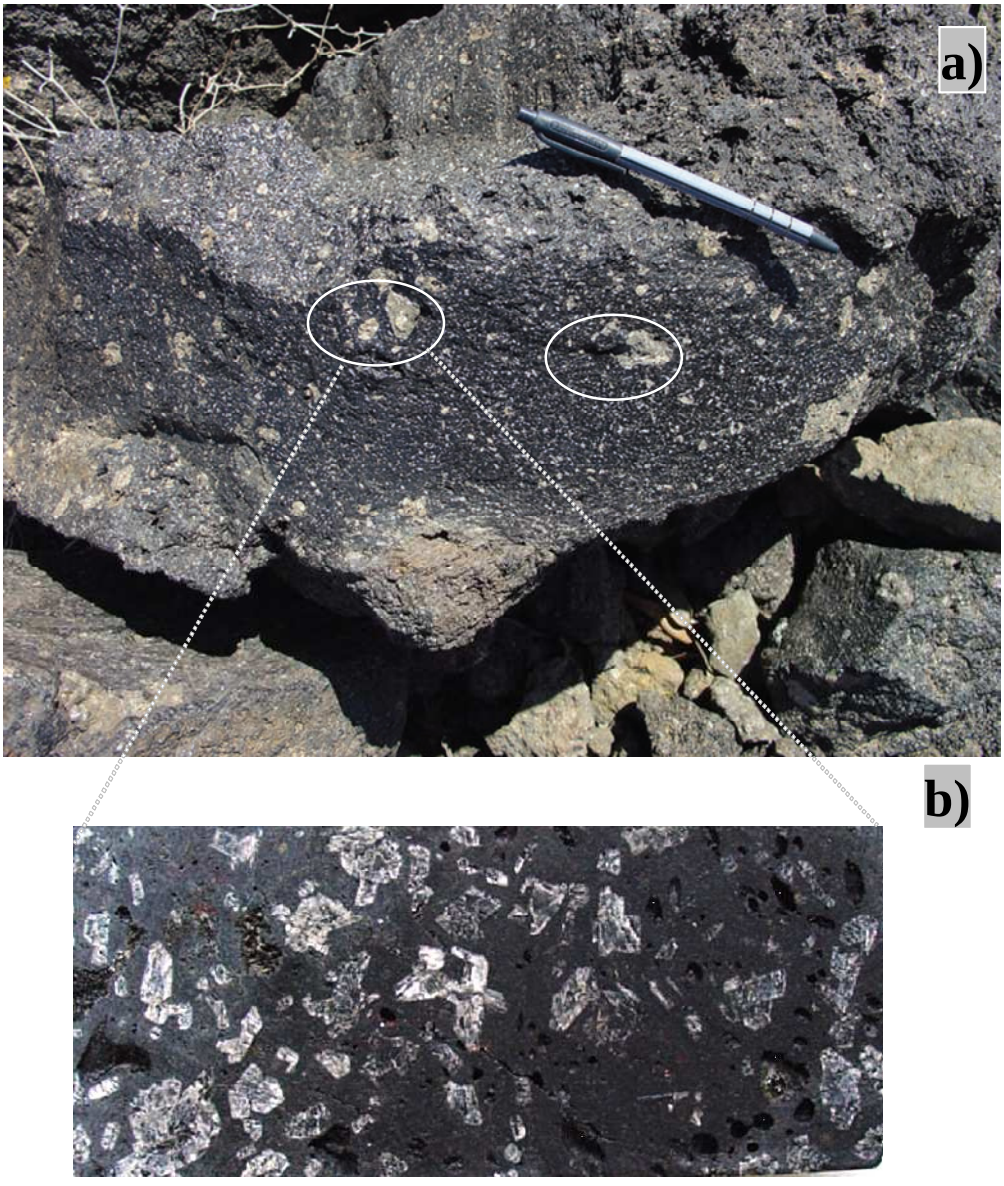

Fig. 3.9 a) Khaggiar flow a population of inclusions which show diffuse, crenulated contacts with the host lava; b) close-up view. It also includes abundant fragment with irregular shape, of a light-grey rock with large crystals of feldspar.

3.5b -Enclaves in the pumice fall-

Similar characteristics can be observed in the pumice cone of Cuddia Randazzo, along the road which cuts the cone on its SW flank. In fact, abundant ENCLAVES with rounded shape and dimensions from few cm to 50-60 cm, are common in the pumice deposit. They are light-grey with large anorthoclase crystals, too.

Perugini et al., 2002 estimated at about 30 vol% of trachytic enclaves in the lava dome of Cuddia Randazzo. Enclaves belonging to the outer portions of the dome show irregular morphologies and high vesicles content if compared to enclaves occurring in the more internal portions of the dome (Perugini et al., 2002).

The textural relationships described above clearly suggest that the porphyritic enclaves represent portions of trachyte magma entrained while still semi-molten into the pantellerite host magma as also suggested by Mahood and Hildreth (1986).

CHAPTER 4

WHOLE-ROCK PETROCHEMISTRY

4.1 General features

Whole-rock analyses and CIPW norm are presented in Table 4.1.

The mafic volcanics have a SiO_2 content ~ 46.4- 47.4 wt %, while the silicic rocks range from 60.9 wt % to 70.6 wt % SiO_2, with a compositional gap between mafic and silicic end members of 11.8 wt %, a part for one single intermediate sample.

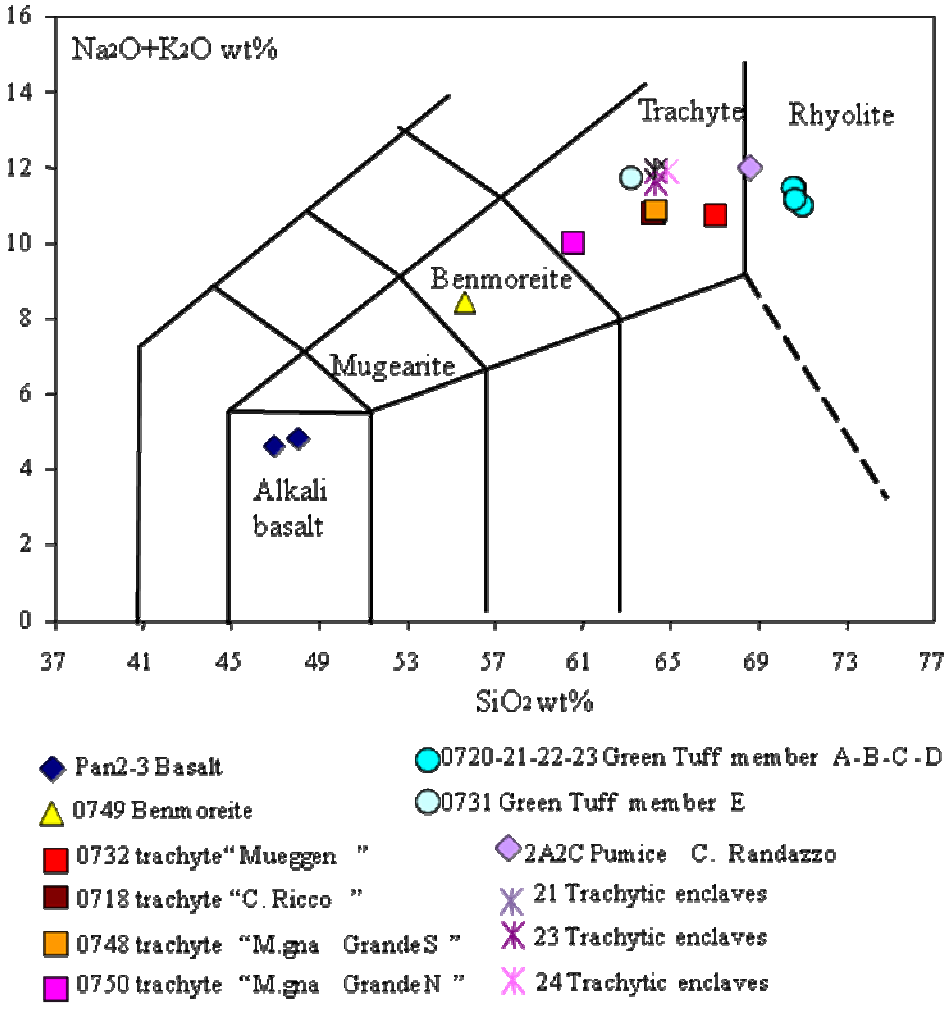

Fig. 4.1 Total-alkali versus silica (TAS) diagram for the classification of volcanic rocks (Le Maitre, 2002).

According to the TAS classification grid (**Fig. 4.1**) the C. Mursia e C. Bruciata products fall in the field of the alkali basalts (SiO_2 = 46.4- 47.4 wt %, Alkali = 4.6-4.8 wt % and nefelina = 3.8- 4.0). The silicic magmas range from trachytes (acmite = 0.0-1.8) to rhyolites (acmite = 2.1- 2.4) with a nearly continuous compositional variation.

In particular, most of trachytes from Montagna Grande (Montagna Grande N, Montagna Grande S. and Case Ricco) are metaluminous trachytes (AI = 0.97 -1.00), a part for one sample (Mueggen) with AI = 1.18.

The trachytic enclaves found in the Cuddia Randazzo pumice cone are peralkaline with AI = 1.1-1.2 (**Table 4.1**). The single intermediate rock found among the lavas of Montagna Grande, has benmoreitic composition with SiO_2 = 55.6 wt % and Alkali = 8.2 wt %. The Green Tuff samples have a peralkaline chemistry ranging from peralkaline trachytes in the upper member (**member E**) to peralkaline rhyolites in the lower members (basal fallout and **members A, B, C, D**).

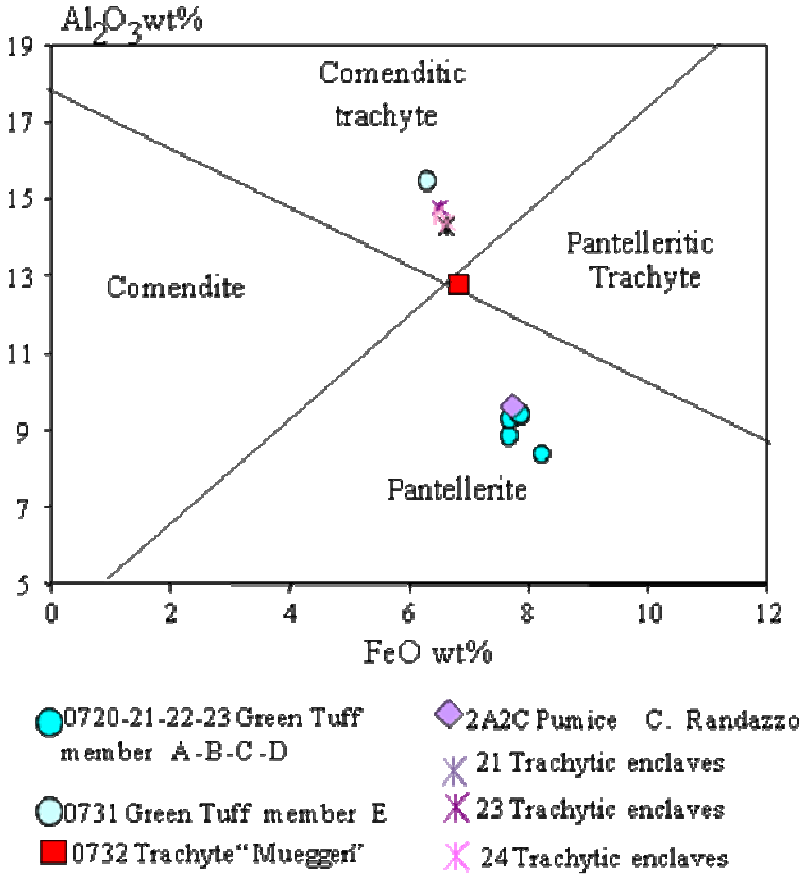

Fig. 4.2 The Macdonald (1974) classification diagram for the classification of peralkaline trachyte and rhyolite.

According to the classification diagram of Macdonald (1974) (**Fig. 4.2**) the composition of the peralkaline rocks range from Comenditic trachyte (Al_2O_3 = 15.7-14.1 wt %; FeO_{tot} = 6.4- 7.1 wt %) to Pantellerite (Al_2O_3 = 8.5- 9.5 wt %; FeO_{tot} = 7.6-8.2 wt %).

4.2 Major and trace element variations

There is a general decrease in MgO, CaO, TiO_2, and P_2O_5, and increase in K_2O with increasing SiO_2 from 46.4 to 70.6 wt %. Na_2O increases from basalt (Na_2O ~ 3.7-3.8 wt %) to trachyte (Na_2O ~ 5.7-6.9 wt %;) , and then slightly decrease in the rhyolites down to Na_2O = 6.1 wt %. FeO_{tot} decreases from 13.1 to 5.6 wt % from basalts to trachytes and increase up to 8.1 wt % in pantelleritic magmas. Al_2O_3 remains nearly constant (around 15.0 wt %) from basalt to trachyte, and decreases down to 8.3 wt % in pantellerite (**Fig. 4.3; Table 4.1**).

Most incompatible trace elements (Rb, Th, Nb, Zr) shows an extreme enrichment from basalt to trachytes, while the compatible (Sr, Cr e V) trace elements show a rapid decrease (down to 20 ppm). (**Fig. 4.4**)

The basaltic products, show REE enrichments by a factor of about 10 to 100 comparated to chondrite values, and are characterized by modest LREE enrichment $(Ce/Yb)_N$ = 6.8-7.6, and a slightly positive Eu anomaly (Eu/Eu* = 1.16-1.18) (**Fig. 4.5a**). Except for TiO_2 > 3.0 wt % in the sample from C. Rosse, the chemical composition of these products, for example 0.7 wt % P_2O_5 and the values of incompatible element and LREE abundances (Sr < 500 ppm, Zr < 160 ppm, Nb < 50 ppm, Ba < 400 ppm, La < 30 ppm), corresponds to the typical composition of the basalts younger than 50 ka discussed in Civetta et al. (1998).

Sample	Pan2	Pan3	749	732	718	748	750	747	720	721	722	723	731	2A2C	Pant21	Pant24	Pant23
Locality	C. Mursia	C. Bruciata	M. Grande	Mueggen	C. Ricco	M. Grande	M. Grande	M. Grande	Cinque Denti	Cinque Denti	Cinque Denti	Cinque Denti	C. Zighidì	C. Randazzo	C. Randazzo	C. Randazzo	C. Randazzo
Rock-type	Basat	Basalt	Benm.	Trach. lava	Trach. lava	Trach. lava	Trach. lava	Trach. lava	P. fall	P. flow	welded eutax.	welded fine-rich	welded fine-depleted	pumice	Trach.	Trach.	Trach.
Formation		Basalt				Trachyte					Green Tuff						
Member									A	B	C	D	E				
SiO_2 wt %	46.39	47.43	55.62	66.82	63.78	63.68	60.94	64.87	70.26	69.82	69.80	70.59	63.07	68.68	64.41	64.48	63.89
TiO_2	3.42	2.96	1.91	0.59	0.75	0.76	1.30	0.74	0.59	0.55	0.60	0.60	0.82	0.65	0.62	0.63	0.76
Al_2O_3	13.99	14.87	14.54	12.68	15.83	15.90	14.59	13.93	9.00	8.51	9.31	9.28	15.66	9.48	14.05	14.27	15.09
Fe_2O_3	14.38	12.61	9.75	7.77	6.16	6.21	8.52	7.19	8.48	9.08	8.53	8.35	7.06	8.75	7.46	7.26	7.06
MnO	0.57	0.58	0.20	0.24	0.19	0.19	0.23	0.23	0.19	0.19	0.11	0.27	0.25	0.11	0.27	0.26	0.25
MgO	5.68	5.73	3.73	0.28	0.52	0.51	1.28	0.33	0.27	0.28	0.26	0.10	0.27	0.38	0.20	0.21	0.38
CaO	10.16	10.20	5.23	0.82	1.87	1.83	2.76	1.03	0.38	0.43	0.40	0.39	0.93	0.58	1.14	1.17	1.48
Na_2O	3.68	3.81	5.25	5.79	6.63	6.56	6.20	6.81	6.21	6.21	6.05	6.42	7.05	6.97	6.87	6.88	6.85
K_2O	0.94	1.02	2.96	5.01	4.22	4.26	3.89	4.54	4.62	4.71	4.83	4.20	4.72	4.63	4.98	4.83	4.96
P_2O_5	0.77	0.78	0.82	0.10	0.15	0.19	0.43	0.14	0.01	0.01	0.02	0.04	0.23	0.43	0.10	0.11	0.08
Tot	100	100	100	100	100	100	100	100	100	100	100	100	100	100	100	100	100
FeO	3.08	11.49	8.95	7.06	5.61	5.67	7.75	6.54	7.53	8.17	7.68	7.52	6.42	7.88	6.93	6.79	6.60
LOI	0.06	0.06	0.67	1.30	0.59	0.07	0.69	0.89	4.45	2.08	1.32	2.00	0.40	3.12	0.36	0.32	0.23
A.I.	0.47	0.53	0.82	0.99	0.97	0.97	0.99	1.16	1.69	1.80	1.63	1.68	1.07	1.58	1.19	1.16	1.10
Mgv	46.78	50.22	45.76	7.43	15.69	15.34	25.05	9.26	6.75	6.48	6.41	2.62	7.84	8.96	5.52	5.89	10.44
CIPW																	
Q	0.00	0.00	0.00	13.59	2.62	2.72	0.73	7.60	27.71	28.00	27.32	27.52	0.83	23.49	6.00	5.62	2.20
Or	5.60	6.00	18.20	29.60	24.91	25.19	22.99	26.83	27.32	27.83	28.54	24.82	27.89	27.38	29.43	28.54	29.31
Ab	20.40	21.80	45.10	37.33	56.07	55.53	52.46	46.37	20.53	17.55	22.43	24.35	54.27	22.98	44.54	46.51	50.00
An	18.88	20.48	7.36	0.00	1.00	1.35	0.49	0.00	0.00	0.00	0.00	0.00	0.00	0.00	0.00	0.00	0.00
Ne	3.95	3.77	0.00	0.00	0.00	0.00	0.00	0.00	0.00	0.00	0.00	0.00	0.00	0.00	0.00	0.00	0.00
Ac	0.00	0.00	0.00	1.87	0.00	0.00	0.00	1.74	2.24	2.41	2.20	2.20	1.70	2.09	1.84	1.80	1.75
Ns	0.00	0.00	0.00	2.22	0.00	0.00	0.00	2.16	4.45	2.08	1.30	2.00	0.80	4.67	2.60	2.20	3.50
Di	26.50	25.20	12.60	3.02	6.39	5.68	8.94	3.70	1.59	1.82	1.60	2.30	2.75	2.50	4.40	4.50	0.60
Ol	14.51	13.77	8.90	0.00	0.00	0.00	0.00	0.00	0.00	0.00	0.00	0.00	0.00	0.00	0.00	0.00	0.00
Mt	1.74	1.53	1.19	0.00	0.75	0.75	1.03	0.00	0.00	0.00	0.00	0.00	0.00	0.00	0.00	0.00	0.00

Hy	0.00	0.00	1.50	10.47	6.08	6.53	9.34	9.10	13.41	14.49	13.30	12.30	9.15	13.68	9.31	9.03	8.12
Il	6.50	5.60	3.60	1.12	1.44	1.44	2.47	1.41	1.12	1.04	1.10	1.10	1.56	1.23	1.18	1.20	1.44
ap	1.83	1.85	1.94	0.24	0.35	0.45	1.02	0.33	0.51	4.21	1.12	1.45	1.89	0.51	1.21	1.10	1.45
Tot	99.92	100.00	100.38	99.46	99.62	99.62	99.47	99.24	98.88	99.43	98.91	98.03	100.84	98.52	100.51	100.49	98.38
Sc ppm	32	29	16	5	4	5	11	9					11	2	6	7	10
V	377	308	120	5	6	5	41	5	10	10	10	5	5	5	5	5	5
Cr	80	110	70	20	20	20	20	20	11	17	9	39	20	20	20	20	20
Co	48	44	18	<1	2	<1	6	2					<1	<1	<1	<1	<1
Ni	30	40	50	20	20	20	20	20	12	12	8	0	20	20	20	20	20
Cu	60	60	20	<10	<10	<10	<10	<10					<10	<10	<10	<10	<10
Zn	120	110	160	260	150	150	170	180					140	340	160	160	130
Rb	19	21	41	98	77	70	65	53	145	148	140	146	39	187	69	69	50
Sr	432	481	352	11	187	184	177	137	3	2	5	12	66	19	12	15	42
Y	32	31	46	113	65	64	59	59	185	195	139	187	49	164	56	54	42
Zr	156	154	405	1309	607	615	489	499	1871	1945	1846	1895	302	1648	469	435	324
Nb	50	49	85	242	123	128	104	111	457	480	459	465	73	389	103	100	72
Ba	341	365	910	89	1058	1048	1048	1151	289	314	314	290	2159	84	429	594	1943
La	27	31	62	147	81	78	67	74	89	95	92	82	56.7	207	69	66	53
Ce	58	66	123	275	153	150	133	139	312	270	300	278	102	386	133	131	105
Pr	7.08	8.13	14	29,3	17	16.4	15	16.3					13.1	43.4	15.4	15	12
Nd	30.1	33.9	53.9	103	62.7	61	55.3	61.2					51.7	153	57.8	55.3	45.8
Sm	6.99	7.72	10.7	19.7	12.1	11.6	11	12					10.3	30.6	11.4	11	9.09
Eu	2.77	3.05	3.96	2.86	3.77	3.66	3.21	4.06					5.04	4.36	2.97	3.21	4.25
Gd	7.56	8.10	10.1	17.7	11	10.4	9.77	11					9.67	30	10.2	9.77	8.23
Tb	1.12	1.17	1.60	3.3	1.94	1.85	1.71	1.88					1.65	5.19	1.8	1.71	1.42
Dy	5.88	6.07	8.87	19.8	11.5	11	9.98	11					9.24	29.9	10.5	9.98	7.99
Ho	1.05	1.06	1.59	3.77	2.25	2.1	1.86	2.06					1.68	5.85	1.96	1.86	1.46
Er	2.78	2.84	4.54	11.5	6.51	6.15	5.42	5.91					4.74	17.4	5.75	5.42	4.2
Tm	0.38	0.40	0.64	1.73	0.96	0.91	0.81	0.87					0.65	2.52	0.85	0.80	0.60
Yb	2.31	2.37	3.96	11.3	6.13	5.84	5.11	5.44					4.06	15.7	5.37	5.11	3.81
Lu	0.33	0.32	0.57	1.68	0.91	0.88	0.77	0.81					0.60	2.27	0.81	0.77	0.57
Hf	4	4.10	9.40	30.3	13.6	13.8	10.3	11.7					7.00	39.1	10.6	10.3	7.5
Th	2.54	2.79	8.59	28.9	12.6	13.5	9.38	10.7					5.04	33.1	9.66	9.38	6.54
U	0.76	0.85	1.88	3.46	3.33	3.23	2.4	2.57					6.2	9.74	2.54	2.40	1.7
$(Ce/Yb)_N$	6.8	7.63	8.47	6.64	6.81	7.00	7.03	6.97					7.43	6.70	6.75	6.99	7.52
Eu/Eu*	1.16	1.18	1.16	0.47	1.00	1.02	1.11	1.08					1.54	0.44	0.84	0.95	1.50

Table 4.1 whole rock analyses. AI = Agpaitic index molar $(Na_2O + K_2O)/Al_2O_3$) LOI = loss on ignition.

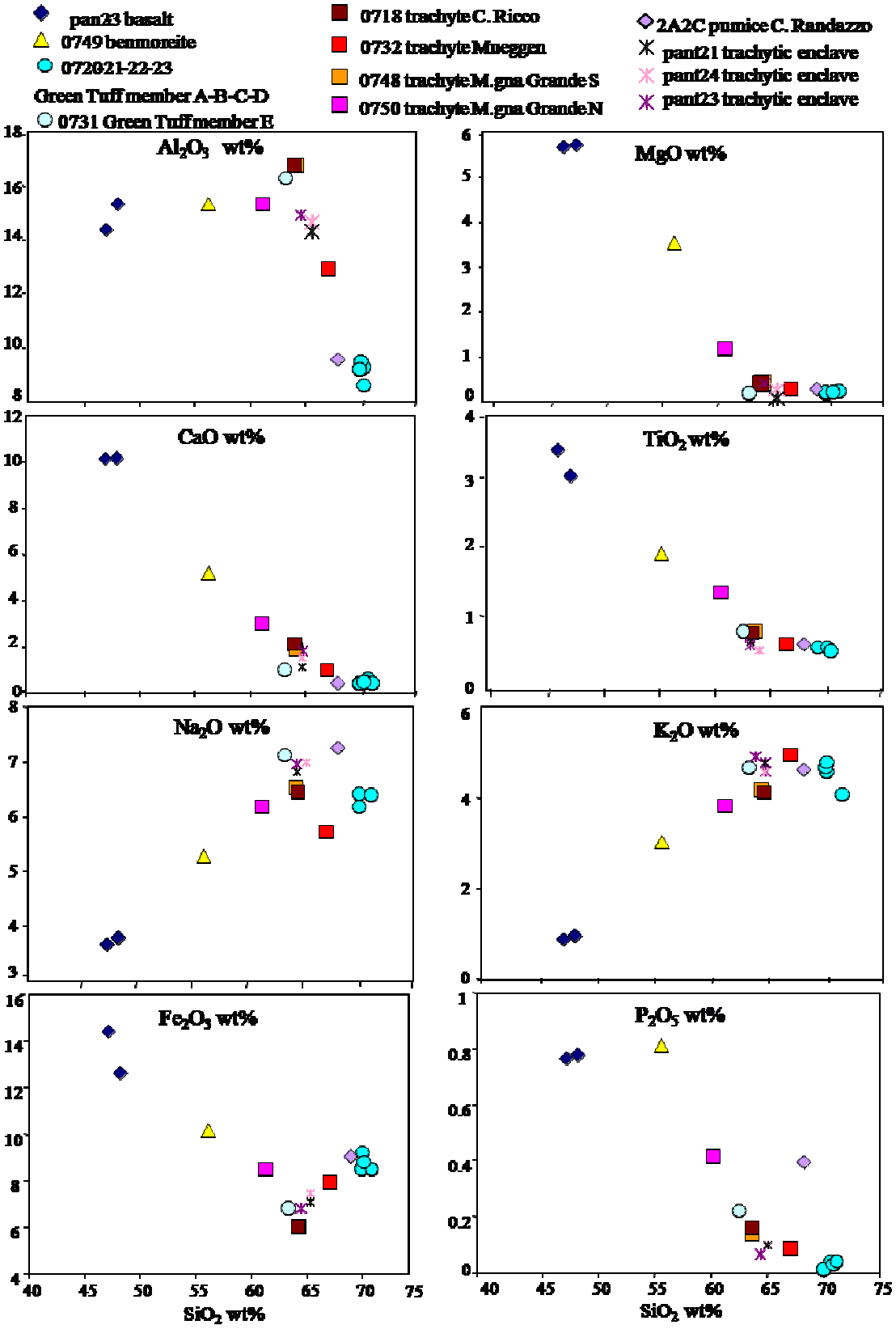

Fig. 4.3 Major-element variation (Harker) diagrams with SiO_2 wt% used as differentiation index.

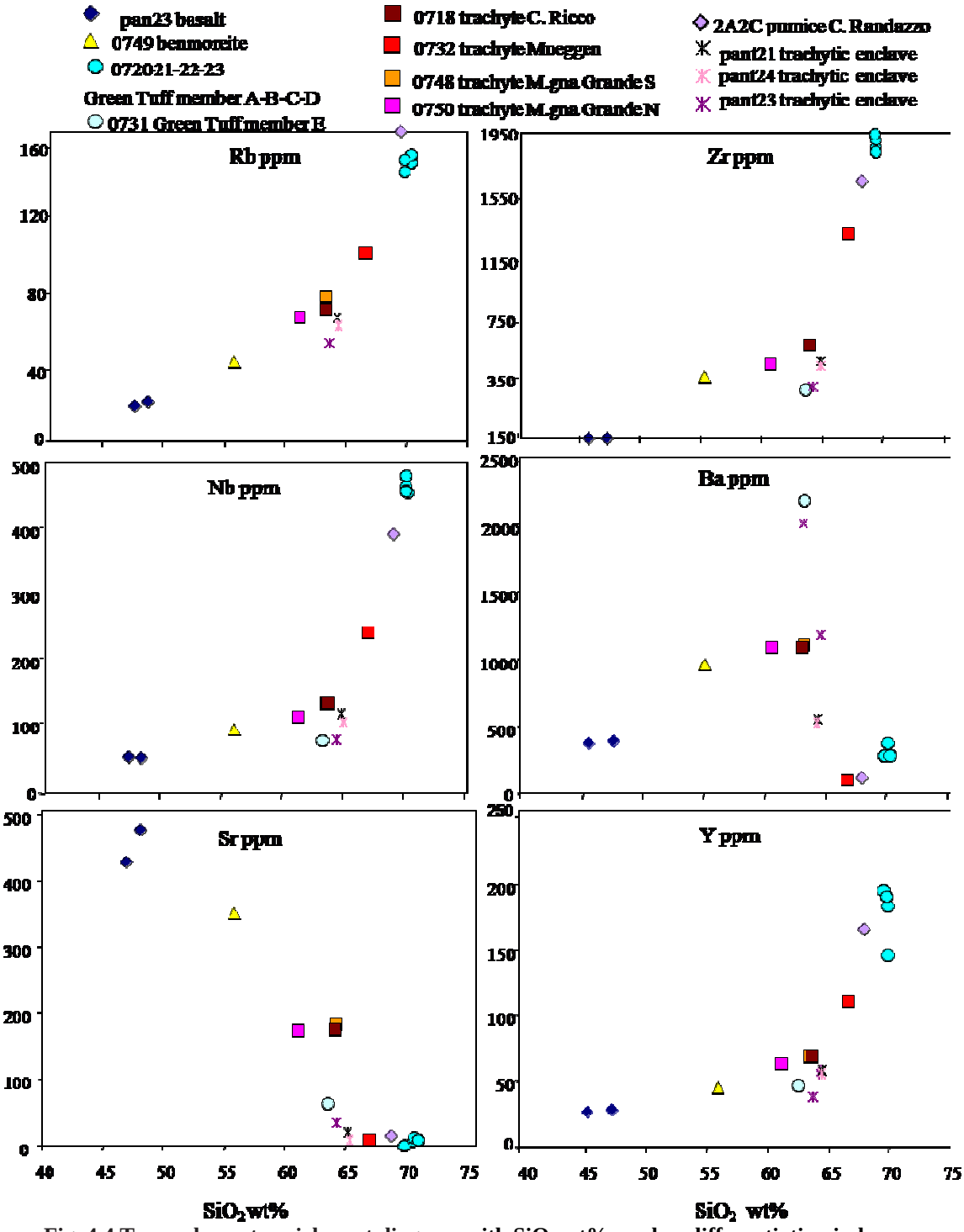

Fig. 4.4 Trace-element enrichment diagram with SiO_2 wt% used as differentiation index.

Trace elements in the **benmoreitic lava** have values intermediate between basalts and trachytes, it is characterized by high LREE enrichment Ce_N/Yb_N = 8.5, and a weak Eu positive spike (Eu/Eu* = 1.16).

What is interesting, trace elements contents of the trachytic samples show a general dispersal in the Harker diagrams. More in detail, three groups can be distinguished.

The metaluminous trachytes from Montagna Grande (Montagna Grande N, Montagna Grande S, Case Ricco), with SiO_2 from 60.9 wt % to 64.8 wt %, show poorly variable contents of incompatible trace elements in the ranges Rb = 53-77 ppm, Zr = 300-615 ppm, Nb = 58-128 ppm, and nearly constant content of Ba = 1048-1128 ppm and Sr = 177-187 ppm.

This values correspond to the chemistry of the High-ITE metaluminous rocks of White et al. (2009).

The peralkaline enclaves in C. Randazzo and the sample from the upper part of the Green Tuff have incompatible trace elements, such as Rb, Zr, Nb, lower than the previous ones, for the same SiO_2 content. Based on the Ba content, this peralkaline (**P**) group can be further divided in two groups:

- **P-High Ba trachytes** (Pant23 and Member E of the Green Tuff) with Ba as high as 1940-2160 ppm;
- **P-Low Ba trachyte** with Ba < 500 ppm (Pant21).

The **"Mueggen"** sample, has a more evolved composition than the Montagna Grande trachytes with low concentrations of Rb (~ 98 ppm), Zr (~ 1309 ppm), Nb (~ 242 ppm), low Ba content (~ 89 ppm) and K/Rb ~ 424. They are compositionally contiguous with the pantellerite samples.

Metaluminous trachytes lavas are characterized by a relatively low LREE enrichment $(Ce/Yb)_N$ = 6.8-7.0 and Eu/Eu*~1. The more evolved trachyte (0732-Mueggen) has higher contents of REE, maintains Ce_N/Yb_N ~ 6.7, and shows an evident negative Eu anomaly Eu/Eu* = 0.47 like to the pantelleritic samples (**Fig. 4.5**).

The trachytic enclaves in the Cuddia Randazzo pumice cone, are characterized by a low LREE enrichment Ce_N/Yb_N = 6.7. The P-Low Ba trachytes show a weakly negative Eu anomaly (Eu/Eu* = 0.84-0.95), while pant23 (Ba-rich) has an evident positive Eu anomaly (Eu/Eu* = 1.50).

The same characteristics (high LREE enrichment Ce_N/Yb_N = 8,50 and Eu/Eu* = 1.56) are found in the Ba-rich trachytes from the top of the Green Tuff (Member E).

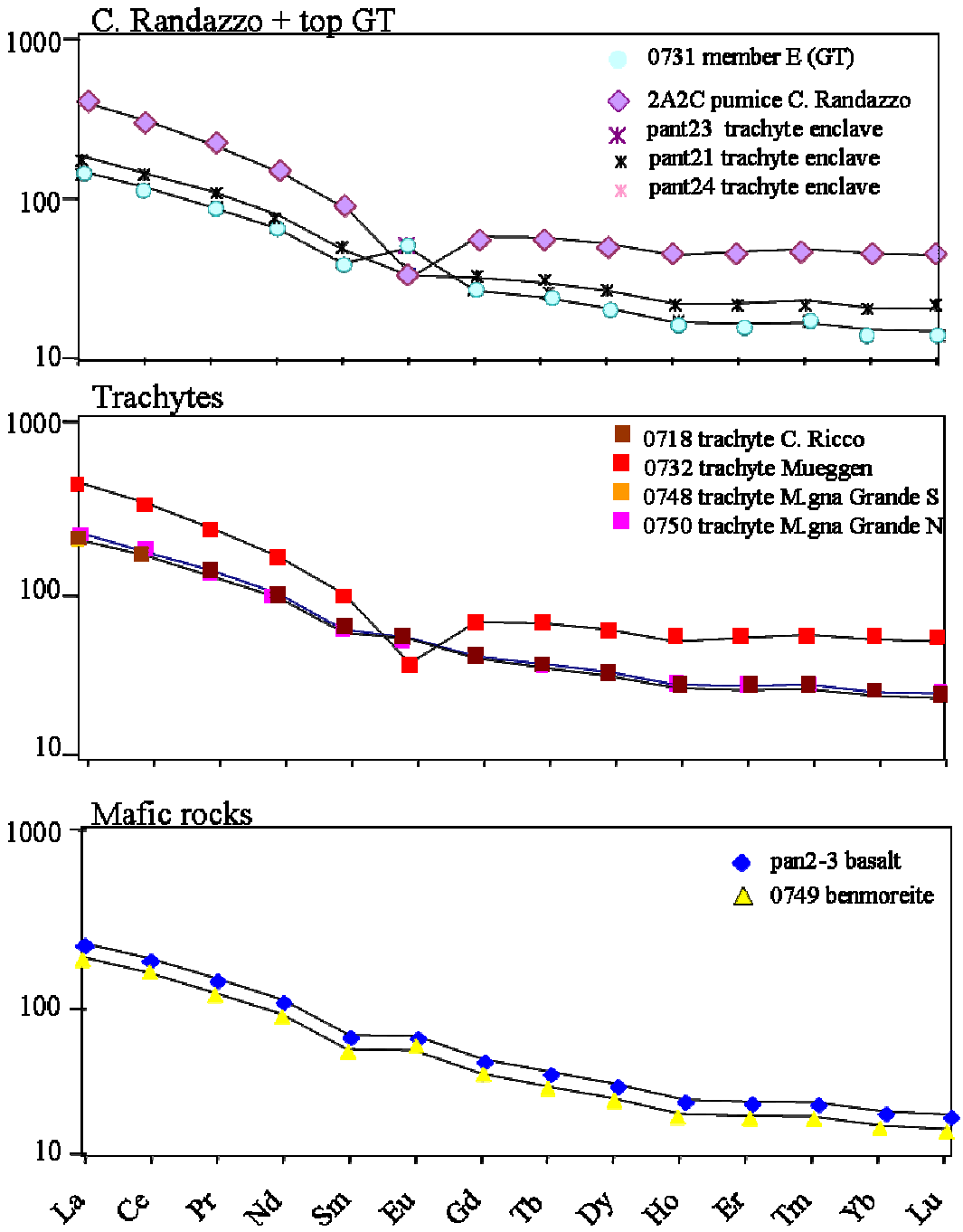

Fig.4.5 Spider diagram Chondrite-normalized (Sun and Mc Donald, 1989) REE abundance diagrams for the rock samples reported can be divided mafic magma, metaluminous and comenditic trachytes and pantelleritic pumice.

CHAPTER 5

PETROGRAPHY AND MINERAL CHEMISTRY
PHENOCRYST ASSEMBLAGES AND COMPOSITIONS

5.1 Extracaldera mafic lavas

The trachybasalts of Cuddia Rosse cone (post-Green Tuff) show porphyritic texture with < 15-20 vol.% of phenocrysts of labradoritic plagioclase (An_{54-68}), clinopyroxene Wo_{40-45}-Fs_{12-16}, olivine Fo_{73-79} and microphenocrysts of Fe-Ti oxide all set in a hypocrystalline to glassy groundmass.

Less frequently subhedral to anhedral olivine crystals are present and are relatively Mg-rich (Fo_{80}) and unzoned.

Phenocrysts are mostly < 1 mm with sporadic larger clinopyroxene (1-1.7 mm).

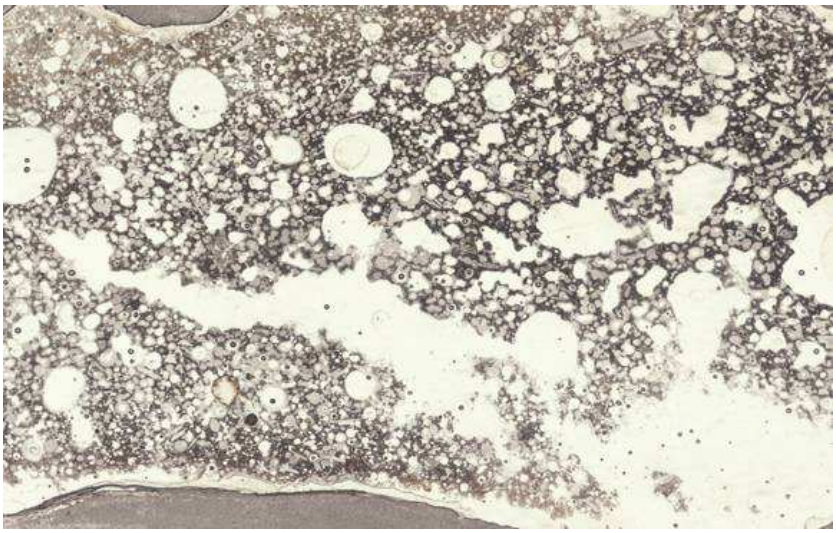

Fig. 5.1 Trachybasaltic scoriae from C. Rosse: thin section under transmitted unpolarized light.

5.2 Trachyte lavas

"Montagna Grande" metaluminous trachyte contains ~ 35-45 wt % of crystals (Table 5.1), mainly anhedral to subhedral alkali feldspars and minor clinopyroxene, olivine and Fe-Ti oxides set in a holocrystalline to ipocrystalline groundmass (Table 3.1).

Sample	**0718**	**0750**	**0748**	**0732**
Locality	**"C. Ricco"**	**"Montagna Grande N"**	**"Montagna Grande S"**	**"Mueggen"**
Olivine	Fo_{19-22} rim Fo_{23-28} core	Fo_{38-40}	Fo_{18-20} rim Fo_{24-26} core	Fo_{8-10}
Feldspar	rim (An_{03-09} Ab_{67-72} Or_{23-27}) core (An_{08-20} Ab_{68-73} Or_{10-18})	Rim ($An_{8-13}Ab_{70-72}Or_{15-22}$) Core ($An_{24-52}Ab_{47-73}Or_{3-12}$)	rim (An_{03-07} Ab_{69-72} Or_{23-25}) core (An_{08-18} Ab_{70-73} Or_{12-16})	(An_{1-5} Ab_{63-72} Or_{21-37})
Na_2O in px	0.08 - 1.01 wt %	0.80 - 1.20 wt %	0.37 - 1.44 wt %	1.16 - 2.02 wt %
Pyroxene	Aug. (Wo_{41-44} $En_{26-34}Fs_{25-32}$)	Aug.($Wo_{40-42}En_{28-33}Fs_{23-28}$) Ti-Augite Fs_{16-18}	Aug. (Wo_{41-44} En_{26-34} Fs_{25-30})	Augite ($Wo_{43-45}En_{13-20}Fs_{25-32}$)
Fe-Ti ox.	Xusp = 0.68- 0.65 Xilm = 0.94- 0.96	Xusp = 0.63- 0.67 Xilm = 0.95- 0.96	Xusp = 0.68- 0.67 Xilm = 0.94- 0.97	Xusp = 0.70- 0.73 Xilm = 0.95- 0.97
Amphibole	-	-	-	Trace (gdm)
Aegirine	-	-	Trace (gdm)	Trace (gdm)
Aenigmatite	-	-	-	Trace (gdm)
Accessory minerals	Apatite Pyrrhotite	Cr-spinel Apatite Pyrrhotite	Apatite Pyrrhotite Sylvite	Apatite Pyrrhotite

Table 5.1 Summary of mineral chemical features determined by SEM-EDS (crystals > 50μm) of the trachytes. Gdm = groundmass < 50μm

In the **less evolved trachyte (sample pan0750, Montagna Grande Nord)** most of feldspars show a large sieve-textured core surrounded by an oscillatory zoned external rim (Fig. 5.2). Based on the chemical composition, three main feldspar populations can be observed:

(1) anorthoclase with nearly homogeneous composition (**An_{5-9} Ab_{70-72} Or_{20-22}**),

(2) plagioclase with labradoritic composition (**An_{54-50} Ab_{44-46} Or_{2-3}**),

(3) directly zoned crystals ranging from labradoritic to oligoclasic core (**An_{24-52} Ab_{47-73} Or_{3-12}**) to anorthoclase (**An_{8-13} Ab_{70-72} Or_{15-22}**) on the rim.

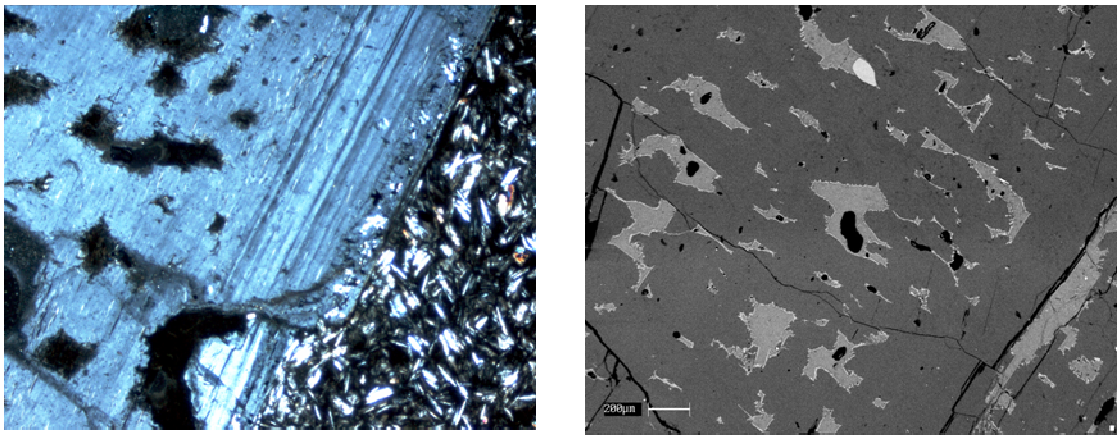

Fig. 5.2 Sample 0750 Montagna Grande N, (a) optical microscope and (b) SEM image (BSE), are evident the patchy areas filled with glass that constitute the sieved cores.

Two populations of clinopyroxene can be recognized:

(1) Augite **$Wo_{40-42}En_{28-33}Fs_{23-28}$**, with TiO_2 < 0.6 wt % and Al_2O_3 < 1 wt %, and

(2) phenocrysts with nearly homogeneous composition **Fs_{16-18}** characterized by TiO_2 1.0 - 1.5 wt % and Al_2O_3 2.7 - 4.0 wt %.

The majority of olivine phenocrysts is euhedral, < 0.5 mm in size, and are characterized by homogeneous composition **Fo_{38-40}**. The groundmass olivine microlites have the same composition **Fo_{38-39}**.

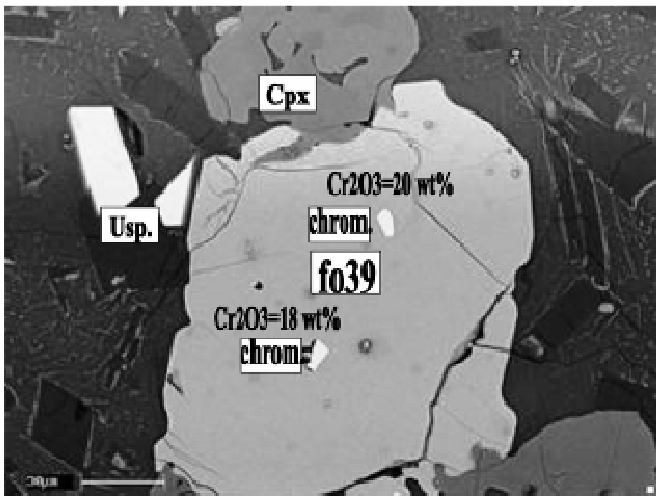

Fig.5.3 Sample 0750 Montagna Grande N, SEM images (BSE) of microcrystalline olivine crystal with rare inclusions of Cr spinels (Cr_2O_3 = 18-20 wt %);

Euhedral crystals of Ti-magnetite (< 500 μm in size) Xusp = 0.63 - 0.67 are abundant, while Ilmenite Xilm = 0.95 - 0.96 occurs mostly in the groundmass. Cr-

spinel with composition **Cr**$^{\#}$ (Cr/(Cr+Al) = 0.60 - 0.71 Cr_2O_3 = 18 - 20 wt % is only enclosed within olivine.

The groundmass is nearly holocrystalline with trace of interstitial glass with agpaitic index AI= 0.94-1.09. The mineral phases the same found as phenocrysts, with accessory chromite, apatite, pyrrhotite mainly included in clinopyroxene.

Trachytes with intermediate composition (pan0718 C. Ricco; pan0748 Montagna Grande Sud) have mm-sized alkali feldspar (up to 5 mm) as dominant mineral phase. It consists of anorthoclase with rim $\mathbf{An_{03–09}Ab_{67–72}Or_{23–27}}$ and core $\mathbf{An_{08-20}Ab_{68-73}Or_{10-18}}$.

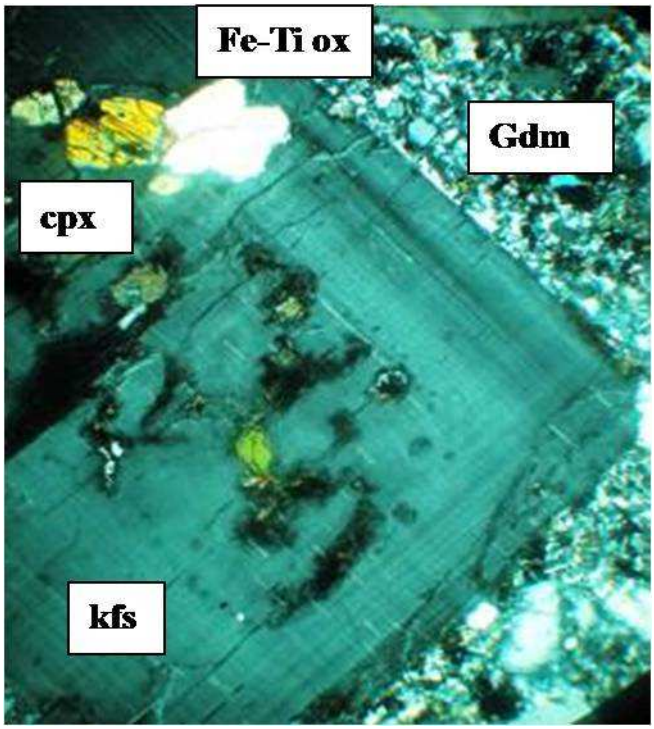

Fig. 5.4 Sample 0748, Montagna Grande Sud. Texture and composition of the crystals anorthoclase, strongly resorbed internally with inclusions di clinopyroxene (crossed polars, 20x). kfs = alkali feldspar, Fe-Ti ox = oxides, cpx = clinopyroxene and gdm = groundmass < 50µm.

Mafic minerals (less than 2 volume % of the total rock) include subhedral augite $\mathbf{Wo_{41–44}En_{26-34}Fs_{25–32}}$ (TiO_2 < 0.5 wt % and Al_2O_3 < 1 wt %), weakly zoned euhedral to subhedral olivine (1 - 0.5 mm) with cores $\mathbf{Fo_{23-28}}$ and rims $\mathbf{Fo_{19-22}}$, euhedral Ti-magnetite Xusp = 0.68 - 0.65 and Imenite Xilm = 0.94 - 0.96. Ilmenite is mostly found in the groundmass and hosted in olivine and clinopyroxene.

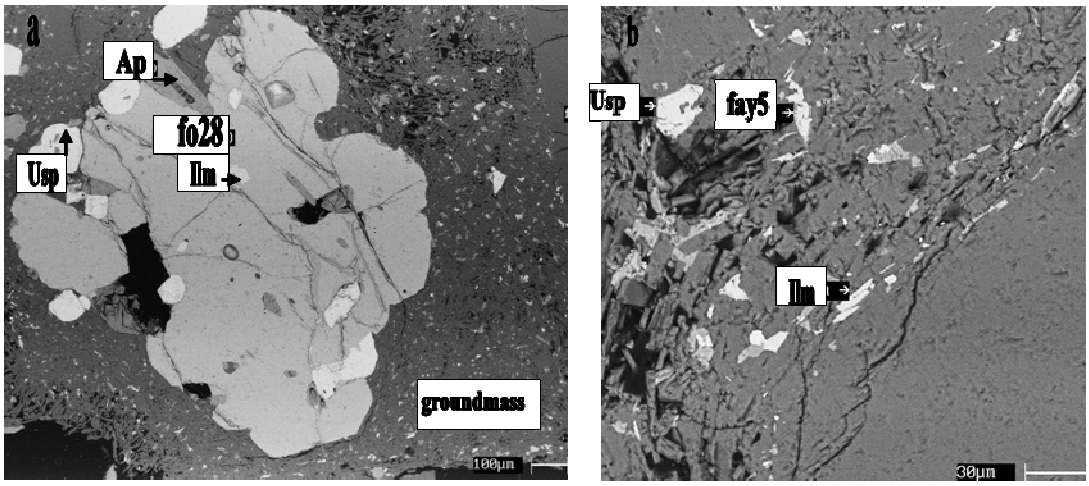

Fig. 5.5 Sample0748 Montagna Grande S, SEM images (BSE) of olivine crystals: a) zoned crystals with abundant inclusions of Fe-Ti oxides; b)The groundmass olivine microlites have composition in the range $Fo_{3\text{-}10}$.

The microcrystalline groundmass is composed of the same mineral phase found as phenocrysts and minor interstitial glass (< 5 vol %). Accessory apatite and pyrrhotite, included in clinopyroxene are common. The olivine microlites have nearly homogeneous composition in the range $\mathbf{Fo_{3\text{-}10}}$.

Trace of sylvite contouring vesicles/holes in feldspar, most likely due to precipitation during low-temperature exsolution of a hypersaline fluid, are also found.

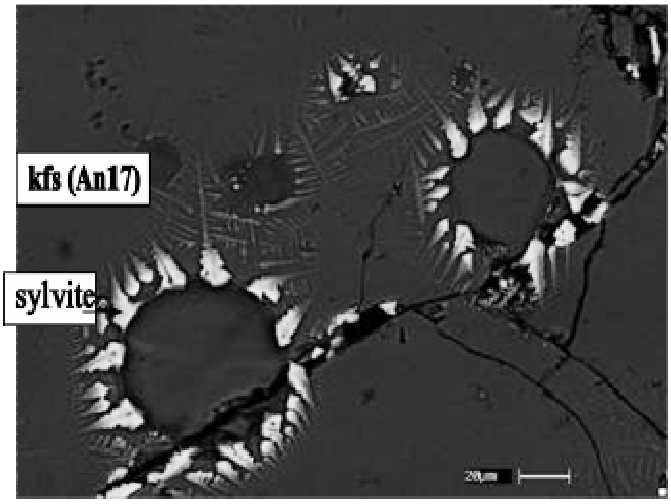

Fig. 5.6 Sample 0748 Montagna Grande Nord, SEM images (BSE) of feldspar crystals $An_{17}Ab_{68}$, with quench sylvite.

In the Mueggen lava (sample pan0732), **the most evolved trachyte**, anorthoclase $\mathbf{An_{1\text{-}5}\,Ab_{63\text{–}72}\,Or_{21\text{–}37}}$ < 1 mm in size, represents the dominant mineral phase, associated with Fe-augite $\mathbf{Wo_{43\text{–}45}\,En_{13\text{-}20}\,Fs_{25\text{–}32}}$ (TiO_2 < 0.5 wt % and Al_2O_3 < 0.5 wt %),

homogeneous olivine **Fo_{8-10}** < 0.5 mm in size, Ti-magnetite Xusp = 0.68 - 0.65, ranging in size from about 0.1 to 1.0 mm and Ilmenite Xilm = 0.94 - 0.96 occurring mostly in the groundmass.

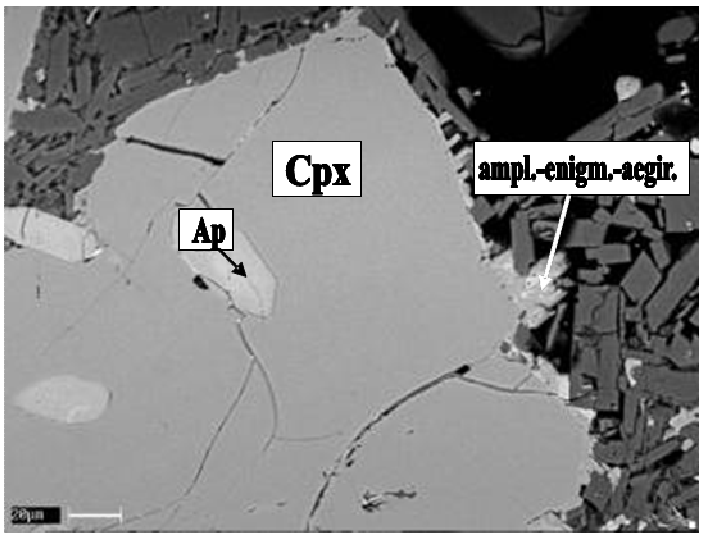

Fig. 5.7 Sample 0732 Mueggen, SEM images (BSE) clinopyroxene phenocrysts with edge of growth with amphibole, aenigmatite, aegirine.

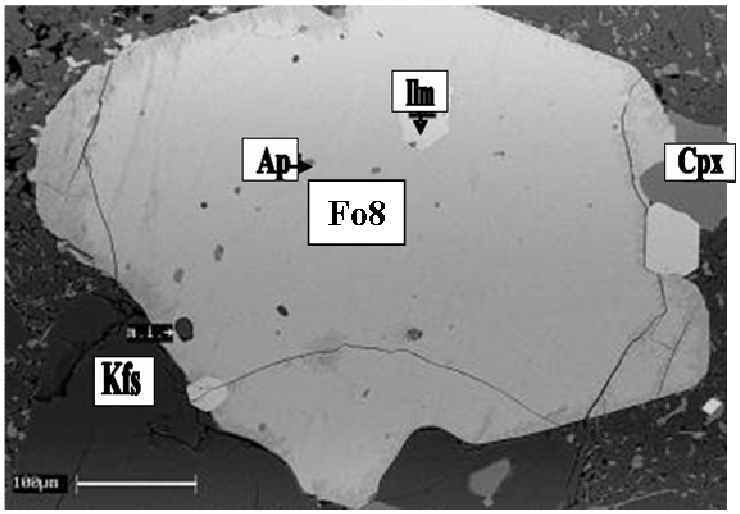

Fig. 5.8 Sample 0732 Mueggen, SEM images (BSE) olivine phenocryst with alteration to the edges.

The microcrystalline groundmass is composed of the some mineral phase found as phenocrysts with accessory apatite, pyrrhotite, mainly included in clinopyroxene.

All phenocrysts are set in a glassy groundmass variably devitrified with aenigmatite and amphibole (Fe-rich) microlites. The olivine microlites have nearly homogeneous composition in the range **Fo_{8-9}**.

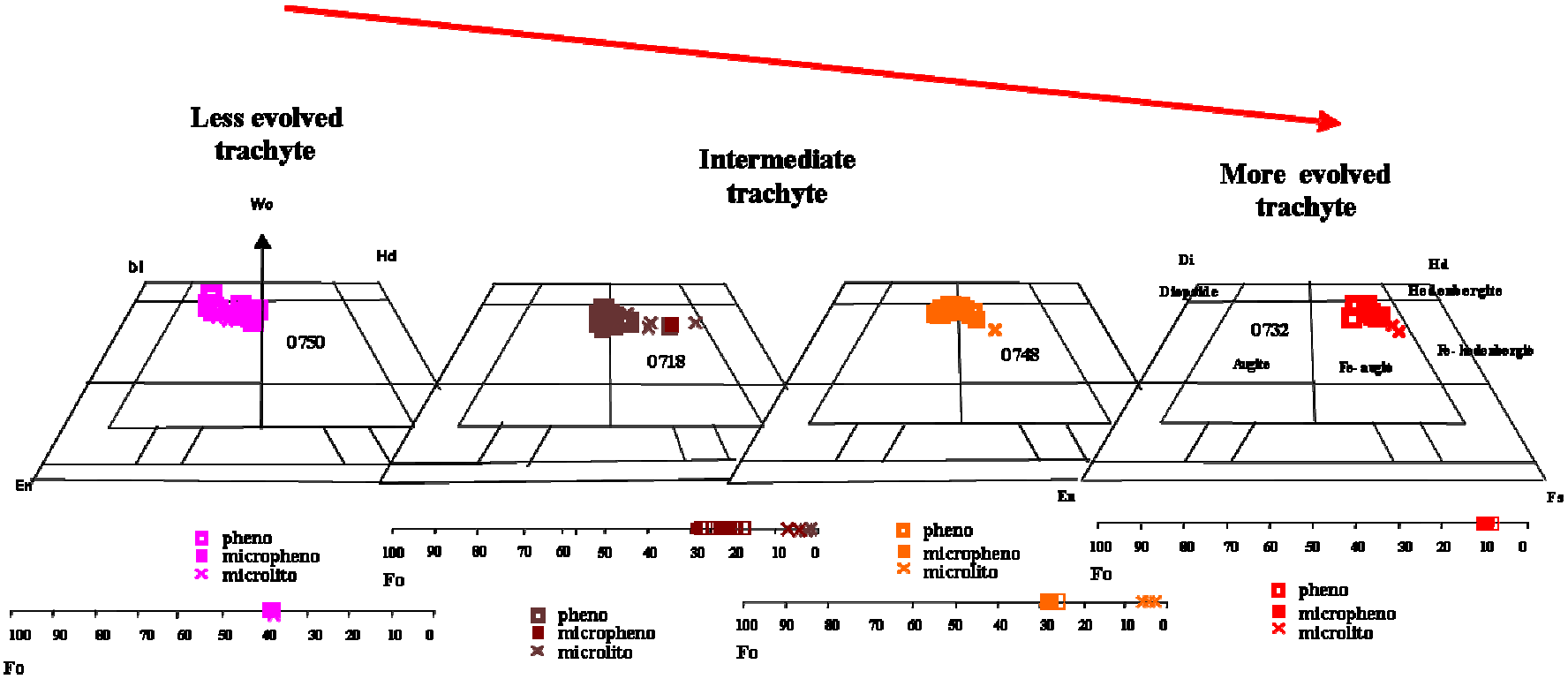

Fig. 5.9 Clinopyroxene classification on the base of quadrilateral components (Morimoto,1989), less evolved trachyte = sample pan0750, intermediate trachytes = samples pan0718-pan0748 and more evolved trachyte = sample pan0732.

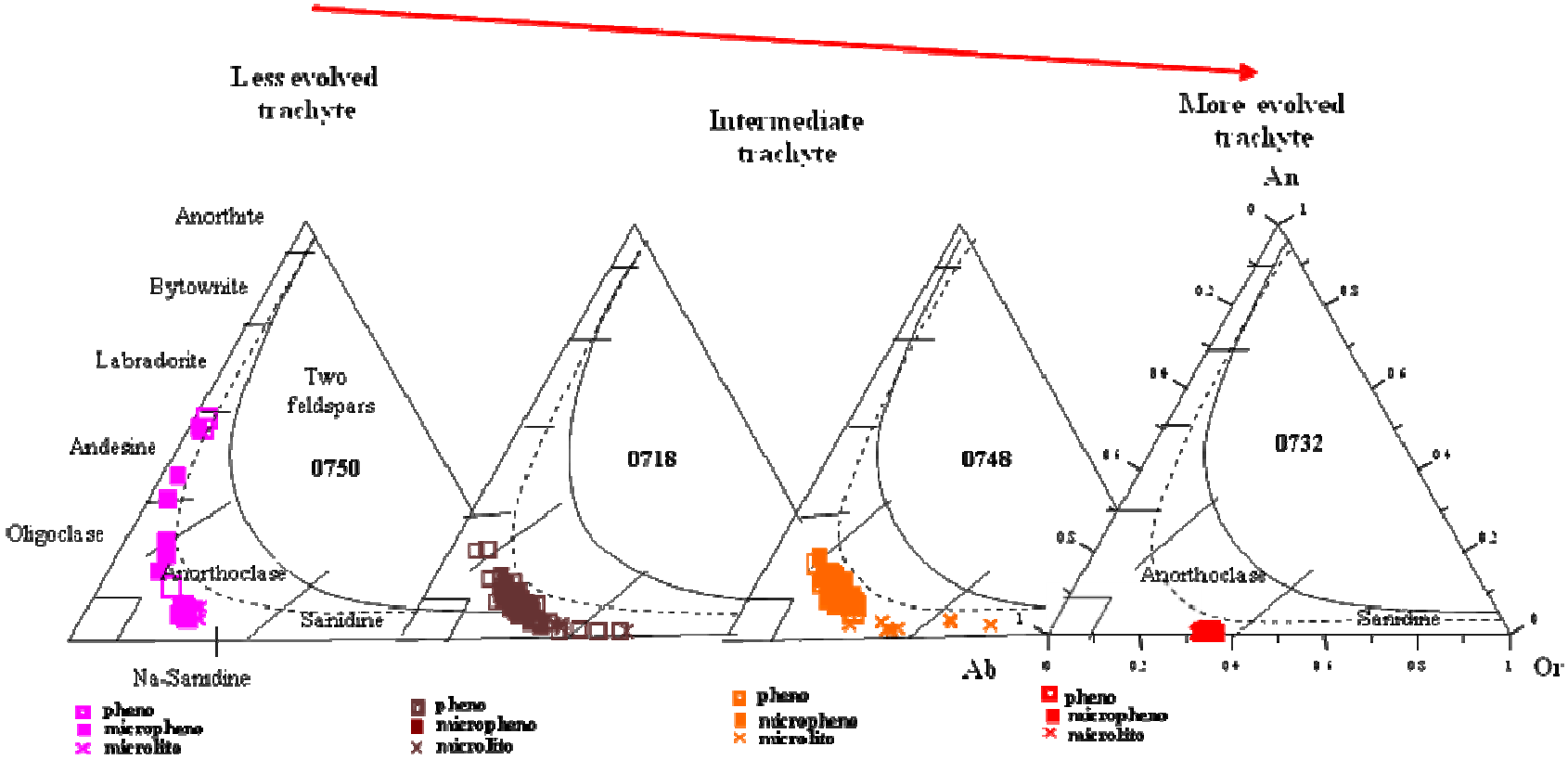

Fig. 5.10 - Compositional variations of plagioclase and alkali feldspar, Less evolved trachyte = sample pan0750- Intermediate trachytes = sample pan0718 -pan0748 and more evolved trachyte = sample pan0732.

5.3 The Green Tuff

All the pantelleritic samples **(member A-B-C-D)** described below have a crystal content ≤ 15 vol %, while the upper trachytic sample (member E) is characterized by higher crystal content ~ 40 volume %.

Crystals in the **Pantellerite** (e.i. member A-B-C-D sample 0720-21-22-23) are euhedral anorthoclase **$An_{0-1}Ab_{60-68}Or_{34-38}$**, commonly < 1 mm, subhedral aegirina-augite **$Wo_{39-43}Fs_{47-53}$** and microphenocrysts of aenigmatite and quartz . Only at the base of the sequence, in the opening **member A** (pumice fall), these mineral are associated with fayalite **Fa_{92-94}.** Crystals are set in a microcrystalline groundmass variably recrystallized with trace of interstitial glass (AI = 1.36 - 1.80). Apatite, pyrrhotite, aegirine, are present as accessory mineral phase, while amphibole occurs only as inclusions in clinopyroxene and feldspar. (**Table 5.2)**

The groundmass is typically holocrystalline and consists of numerous small prisms of aegirine and alkali-feldspar.

The top of the Green Tuff sequence is a **comenditic trachyte** (sample 0731) with phenocrysts of weakly zoned anorthoclase, 1-5 mm in size, (core: **An_{8-10} Ab_{68-73} Or_{22-24};** rim **An_{1-4} Ab_{70-72} Or_{25-28}),** homogeneous clinopyroxene **Wo_{43-44} En_{26-28} Fs_{28-30}** (TiO_2 < 1 wt % and Al_2O_3 < 1 wt %), euhedral olivine < 0.5 mm in size Fo_{22-26}, abundant crystals, up to 1 mm, of Ti-magnetite Xusp = 0.70 - 0.82 (~2 vol.%) and minor Ilmenite Xilm = 0.97 - 0.98 mostly in the groundmass.

Comenditic trachyte has a microcrystalline groundmass (trace of interstitial glass down to 10 vol. %, with AI = 0.92 - 0.98) with accessory apatite and pyrrhotite. The olivine microlites have nearly homogeneous composition in the range $Fo_{7-9.}$

Sample	**0720**	**0721**	**0722**	**0723**	**0731**
Locality	**C. Denti**	**C. Denti**	**C. Denti**	**C. Denti**	**C. Zighidi**
Member	**A**	**B**	**C**	**D**	**E**
Olivine	Fo_{9-12}	-	-	-	Fo_{14-28}
Feldspar	Ab_{62-63} Or_{37-38}	Ab_{66-70} Or_{34-30}	Ab_{64-71} Or_{29-36}	Ab_{60-68} Or_{40-32}	Ab_{69-71} Or_{25-28}
Na_2O in pyroxene	1.44 wt %	1.19-1.50 wt %	2.25-.3.13 wt %	2.2-9.1 wt %	1.0-1.5 wt %
Pyroxene	$Wo_{41-42}En_{10-11}$ Fs_{48-49}	($Wo_{39-40}En_{11-12}Fs_{47-48}$)	(Wo_{39-42} $En_{7-10}Fs_{47-52}$)	(Wo_{39-40} $En_{9-10}Fs_{49-50}$)	(Wo_{43-44} $En_{24-26}Fs_{28-30}$)
Ti-Fe ox.	Xilm = 0.96	-	Xusp = 0.66-0.67 Xilm = 0.98-0.99	Xusp = 0.66-0.73 Xilm = 0.97-0.99	Xusp = 0.74-0.82 Xilm = 0.97-0.99
Amphibole	-	-	Gdm	Gdm	Trace
Aegirine	-	-	Gdm	Trace	Trace
Quartz	Trace	Trace	Trace	Gdm	-
Aenigmatite	Trace	Trace	Trace	Trace	-
Gdm (AI)	1.1-1.7	1.0-1.8	1.6-1.8	1.3-1.5	0.9-1.0

Table 5.2 Summary of mineral chemical features determined by SEM-EDS (phenocrysts only) of the Green Tuff sequence. Agpaitic Index = mol (Na_2O+K_2O) /Al_2O_3. aenig = aenigmatite; amph = amphibole and gdm = groundmass < 50 µm

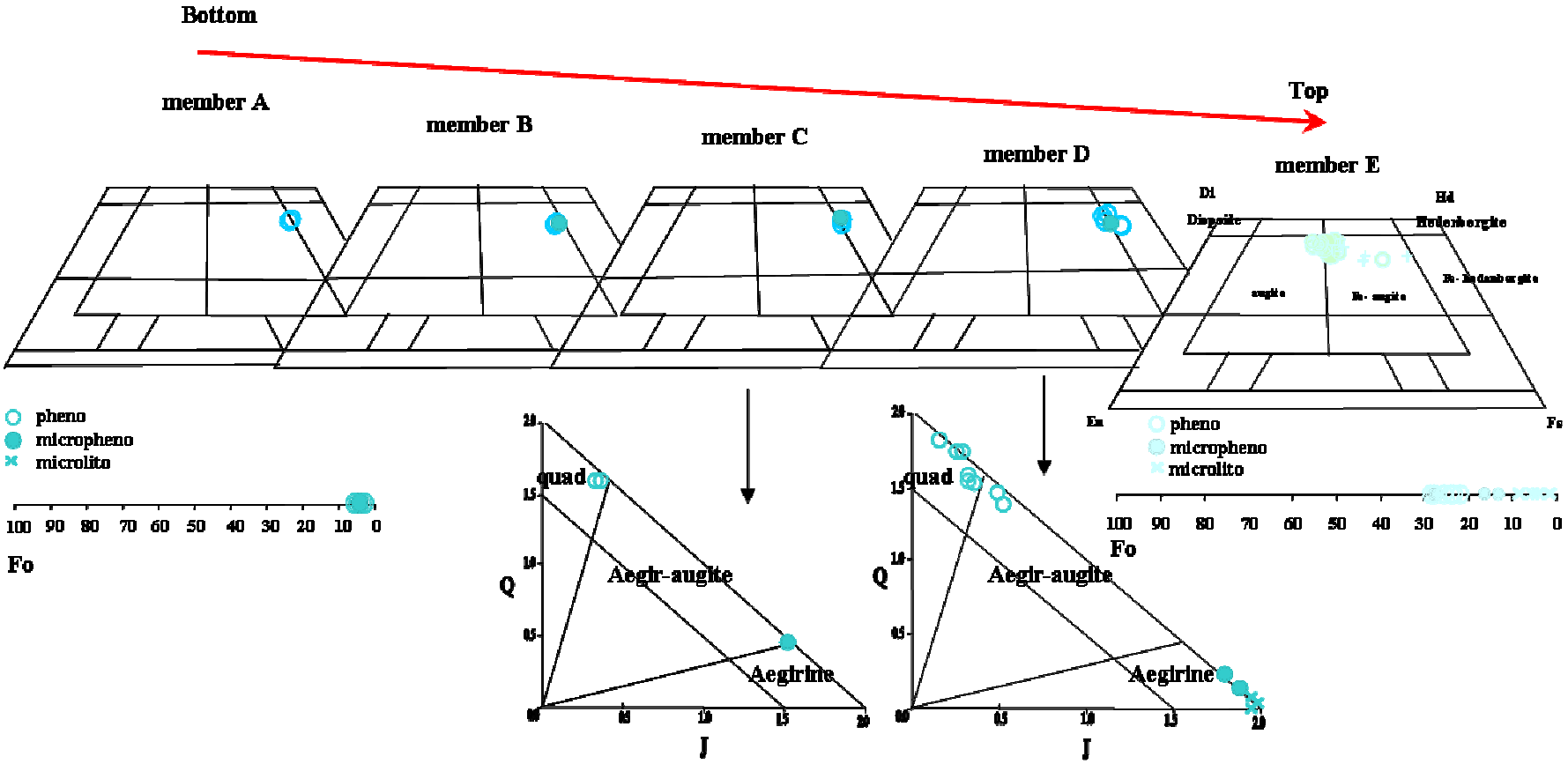

Fig. 5.13 - Clinopyroxene classification on the basis of quadrilateral components (Morimoto, 1989), the members Á-B and E have only pyroxene quadrilateral components while the members C-D have a strong extra-quad composition, thus we also present. The diagram for Na-rich pyroxenes (modified after Morimoto et al., 1988). Q = Ca + Mg + Fe2+; J = 2Na (atoms per formula unit).

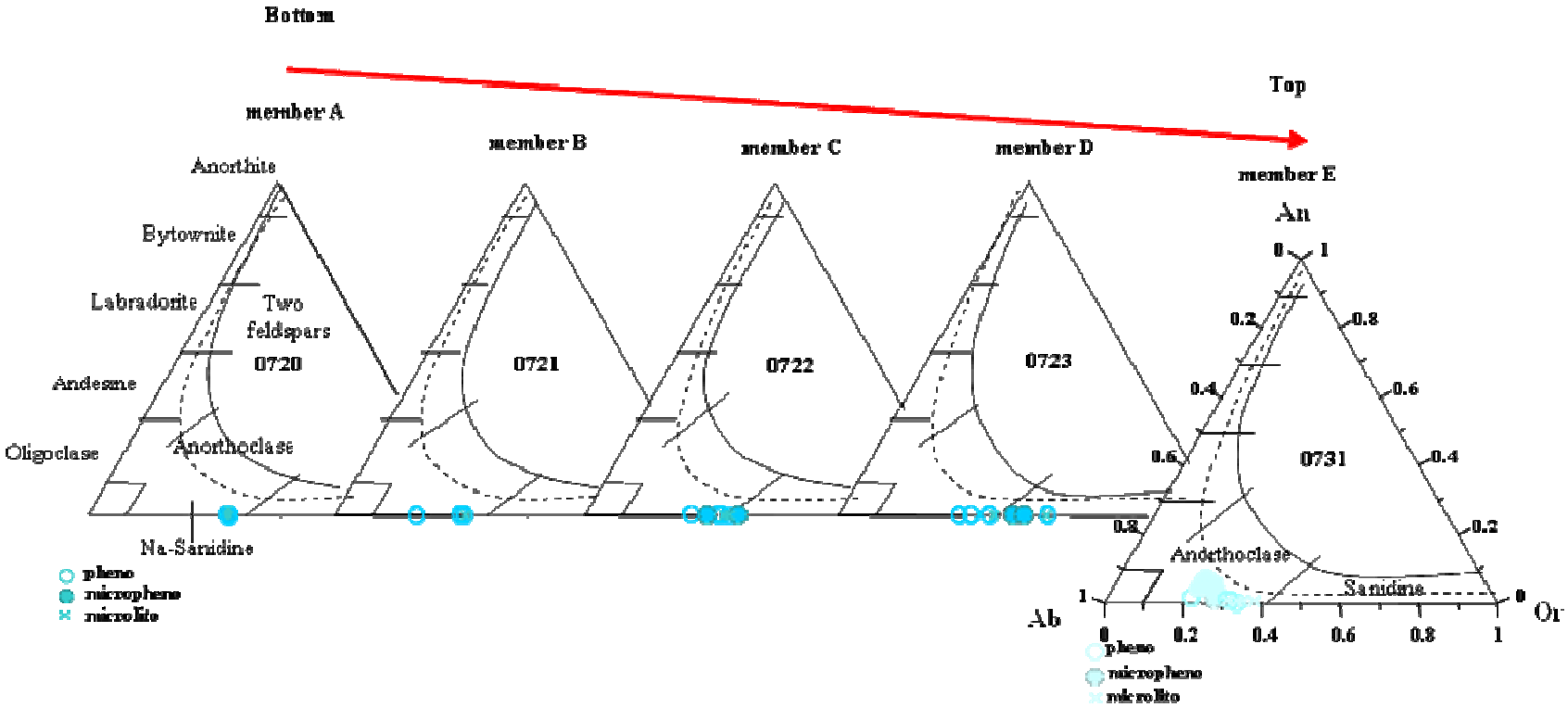

Fig. 5.14 Compositional variations of feldspar the Green Tuff sequence, top green tuff (member E), and (members A-B-C-D).

5.4 The Randazzo pumice cone

Pumice of Cuddia Randazzo are per-alkaline rhyolites (pantellerites) with SiO_2 = 66.1 - 66.5 wt %, $K_2O + Na_2O$ = 9.4 - 10.7 wt % and Agpaitic Index between 1.3 and 1.6 (**Table 4.1**).

They hold ~10 vol % phenocrysts of anorthoclase < 2 mm with nearly homogeneous composition $\mathbf{Or_{32-38}Ab_{60-68}}$**, An < 1.6** mole %, Fe_2O_3 = 0.3-2 wt %, and aenigmatite associated with minor hedembergitic clinopyroxene ($\mathbf{Fs_{28-40}Wo_{36-44}En_{4-14}}$ and $\mathbf{Ae_{16-24}}$), ilmenite, ±magnetite, ±fayalite $\mathbf{Fo_{3-8}}$.

The groundmass is glassy to poorly-crystalline. Microphenocrysts and/or microlites of quartz are sporadic or absent. In the Randazzo products phenocrysts have commonly rounded shape. It is likely due to pre-eruptive heating caused by mixing between pantelleritic and hotter trachytic magmas, found as abundant enclaves and xenocrysts (Mahood et al., 1986; Prosperini et al, 2000).

The characteristics of the trachytic enclaves can be observed in the pumice cone of Cuddia Randazzo, along the road which cuts the cone on its SW flank. Here, abundant enclaves with spheroidal to ameboidal shape with crenulated margins ranging from few cm to 50 - 60 cm, are common in the pumice deposit. Enclaves (sample pant21-22-23) are light-grey in colour and are characterized by large anorthoclase crystals, up to 1.5 cm (**Fig. 5.15**).

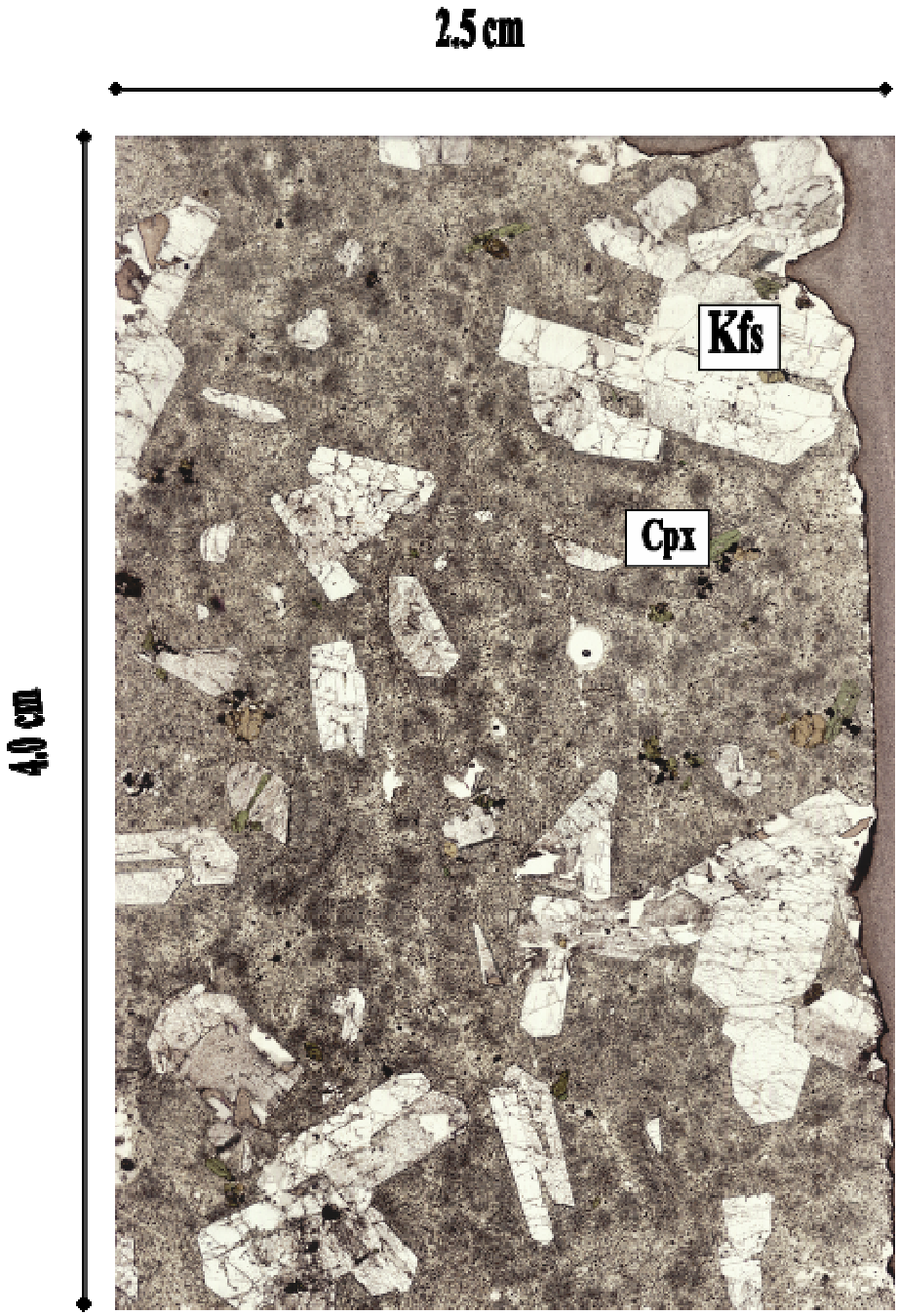

Fig. 5.15 -Trachyte enclave pant23 of C. Randazzo: thin section under transmitted light.

The BaO-rich enclaves pant23 (see par.4.2, BaO = 1940 ppm) contains phenocrysts of anorthoclase in the range $\mathbf{Ab_{64\text{-}70}An_{2\text{-}16}}$ with a BaO content up to 2.5 wt % (i.e. Celsian composition up to 4 mole %), Olivine $\mathbf{(Fo_{20\text{-}30})}$, Clinopyroxene $\mathbf{(Wo_{42\text{-}45}\ En_{20\text{-}28}\ Fs_{30\text{-}39})}$ and minor magnetite.

The sample pant21-24 (BaO < 600 ppm) show more evolved mineral chemistry with anorthoclase **$Ab_{63-67}An < 4$** and BaO < 1 wt %, Olivine (**Fo_{9-16}**), Clinopyroxene (**$Wo_{39-42}En_{18-23}Fs_{39-45}$**) and minor oxides (**Figs 5.16, 5.17**).

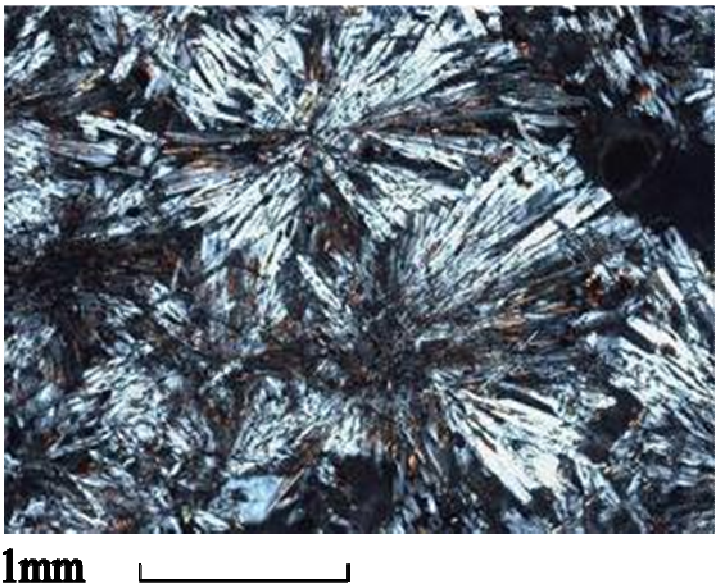

Fig. 5.16 Sample pant21 (trachytic enclave) of C. Randazzo. microphotograph of the spherulitic texture in the groundmass of the trachytic enclaves.

A variability of textures which includes fine spherulites to open, coarse fan-spherulites, hopper to skeletal textures characterize the groundmass of both small-dispersed fragments and blocks (**Figs 5.16, 5.17**).

The mineral composition of the groundmass is close to that of the typical pantellerites and consist of anorthoclase **Ab_{63-65} Or_{32-36} $An_{0.1-0.9}$**, clinopyroxene (**Fs_{40-56}**); rare fayalite; ilmenite (**Ilm_{96-97}**), Ti-magnetite (**Usp_{73-74}**) and strongly peralkaline interstitial glass (AI up to 2.4).

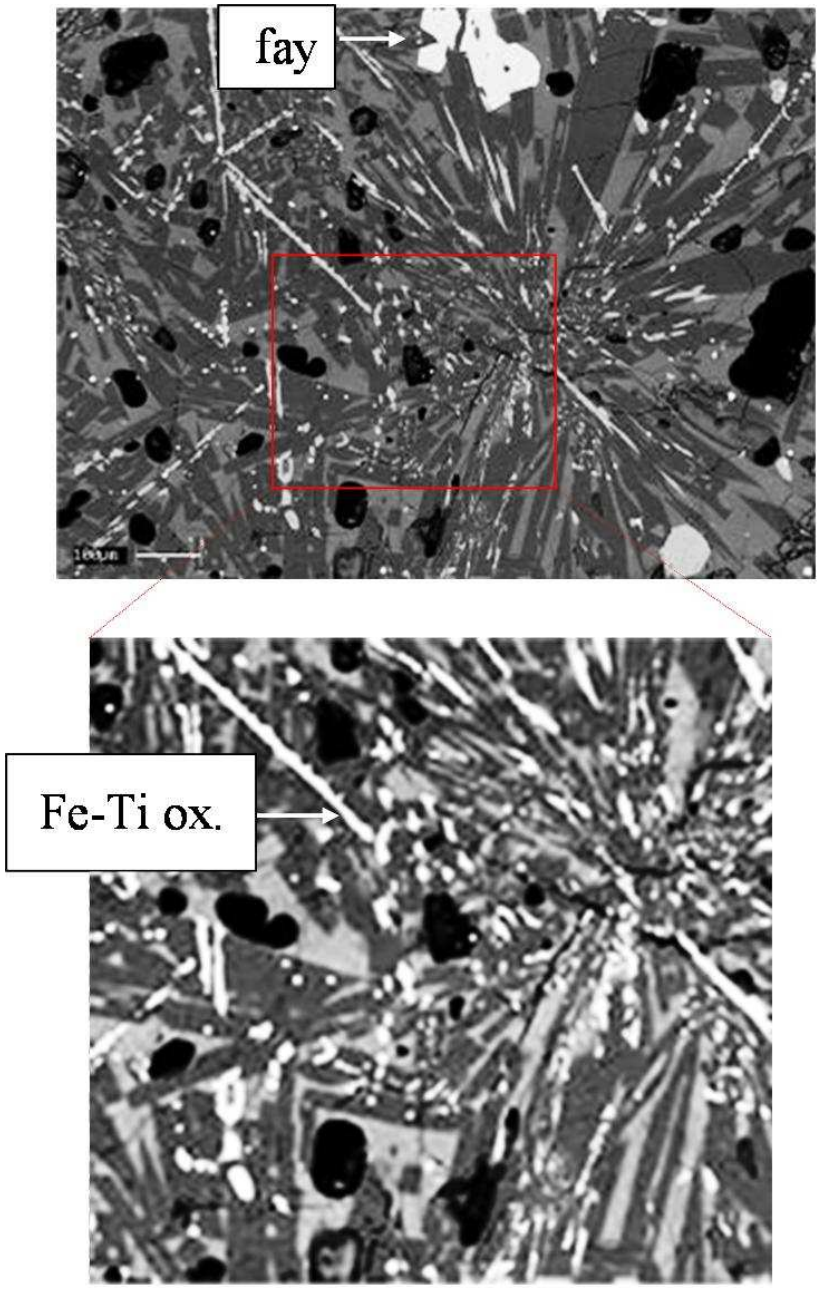

Fig. 5.17 Sample pant21(trachytic enclave) from C. Randazzo, SEM image (BSE), showing spherulitic textures and vesiculated interstitial glass.

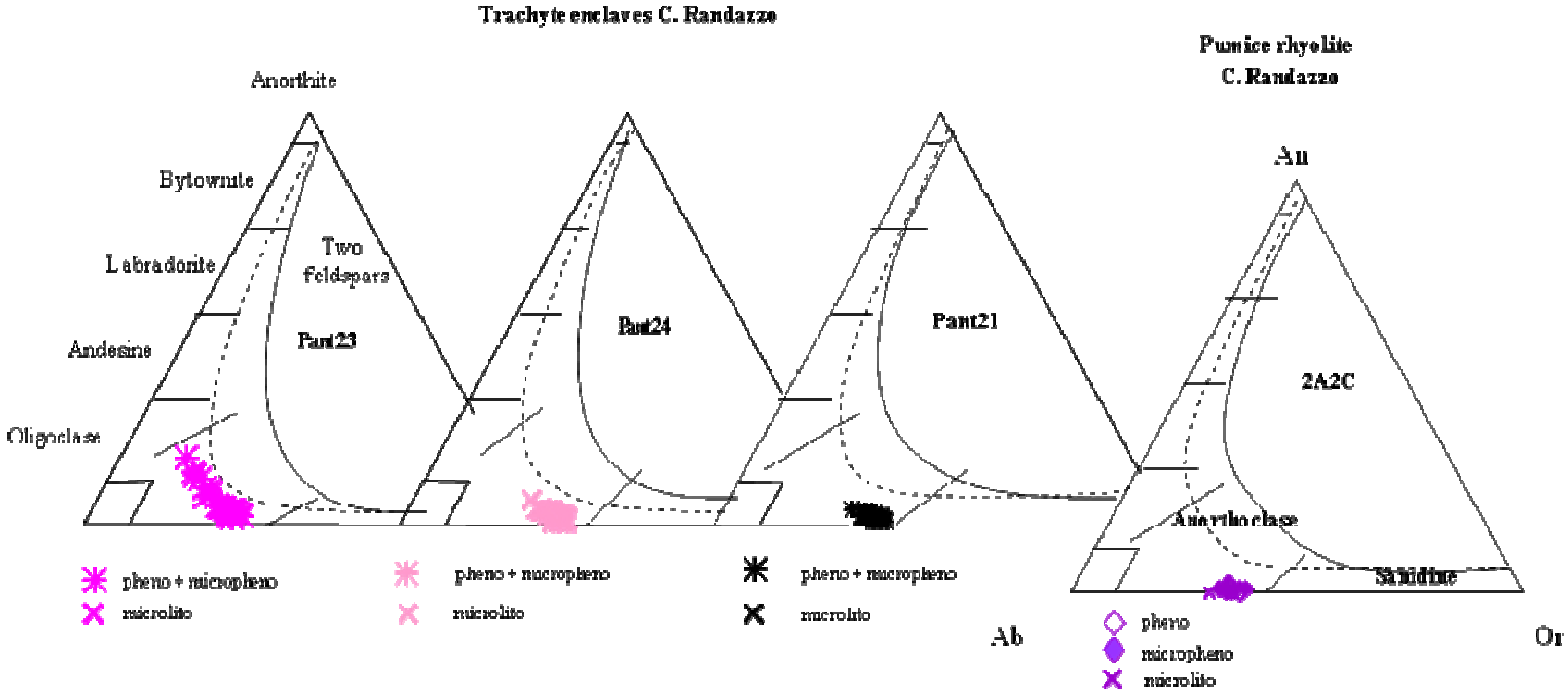

Fig. 5.18 - Trachytic enclaves and pumice in Cuddia Randazzo, compositional variations of alkali feldspar.

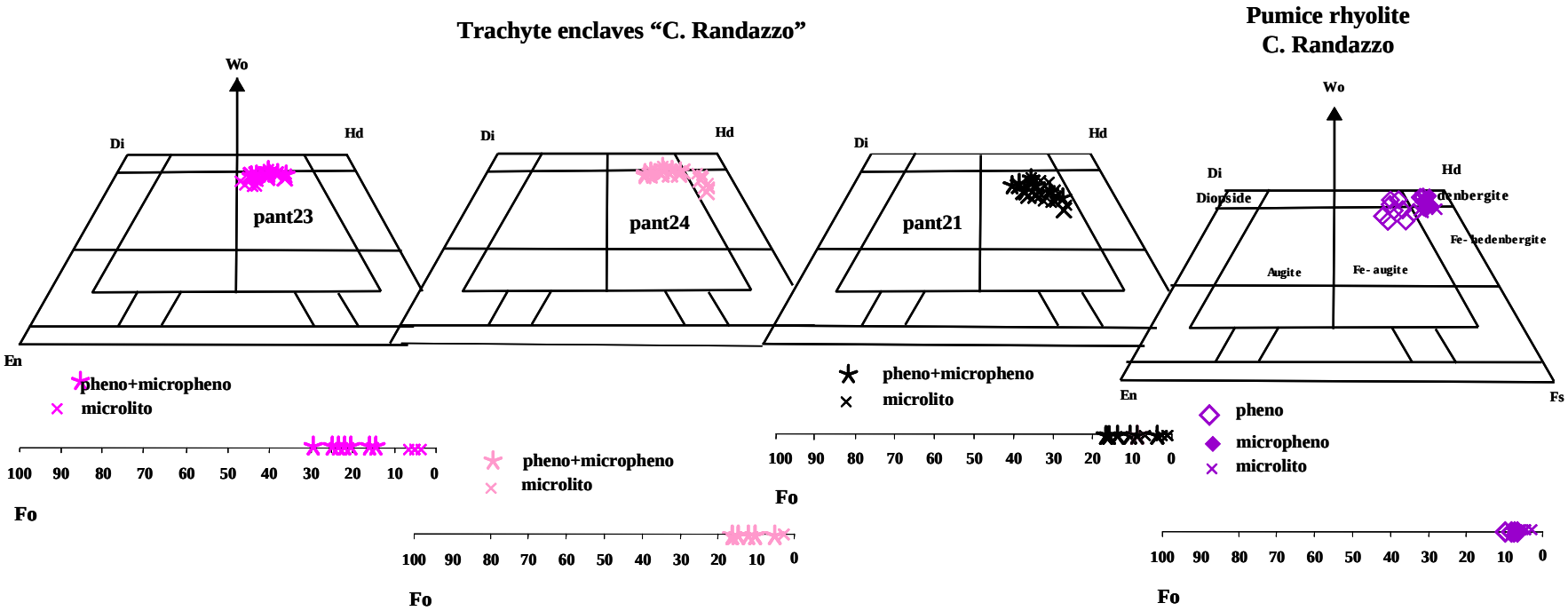

Fig. 5.19 - Trachytic enclaves and pumice in Cuddia Randazzo, clinopyroxene classification on the base of quadrilateral components (Morimoto, 1989).

5.6 Intracaldera mafic lava (Benmoreite 0749)

Lava sample from Montagna Grande with benmoreitic bulk composition has a highly porphyritic (PI = 55-60 vol. %), seriate texture. Phenocrysts, in order of decreasing abundance, are: feldspar, olivine, clinopyroxene, and subordinate magnetite and ilmenite set in a microcrystalline groundmass composed of plagioclase, clinopyroxene, olivine, accessory apatite, pyrrhotite and < 3 vol % of interstitial glass.

Textural characteristics and mineral chemistry, such as the presence of resorbed phenocrysts, reversely and directly zoned crystal with resorbed cores along with microphenocrysts showing textural equilibrium with the groundmass, point to the occurrence of different mineral paragenesis mixed together in the rock.

Three main feldspar populations can be observed: (type A) directly zoned phenocrysts of andesinic plagioclase (**$An_{44\text{-}50}$ $Ab_{47\text{-}50}$**); (type B) microphenocrysts and microlites in the groundmass with andesinic to labradoritic composition (**$An_{24\text{-}70}$ $Ab_{64\text{-}30}$**); (type C) sieve textured phenocrysts, directly zoned from oligoclase (**$An_{25\text{-}10}$ $Ab_{65\text{-}67}$**) to anorthoclase (**$An_{15\text{-}10}$ $Ab_{68\text{-}70}$**).

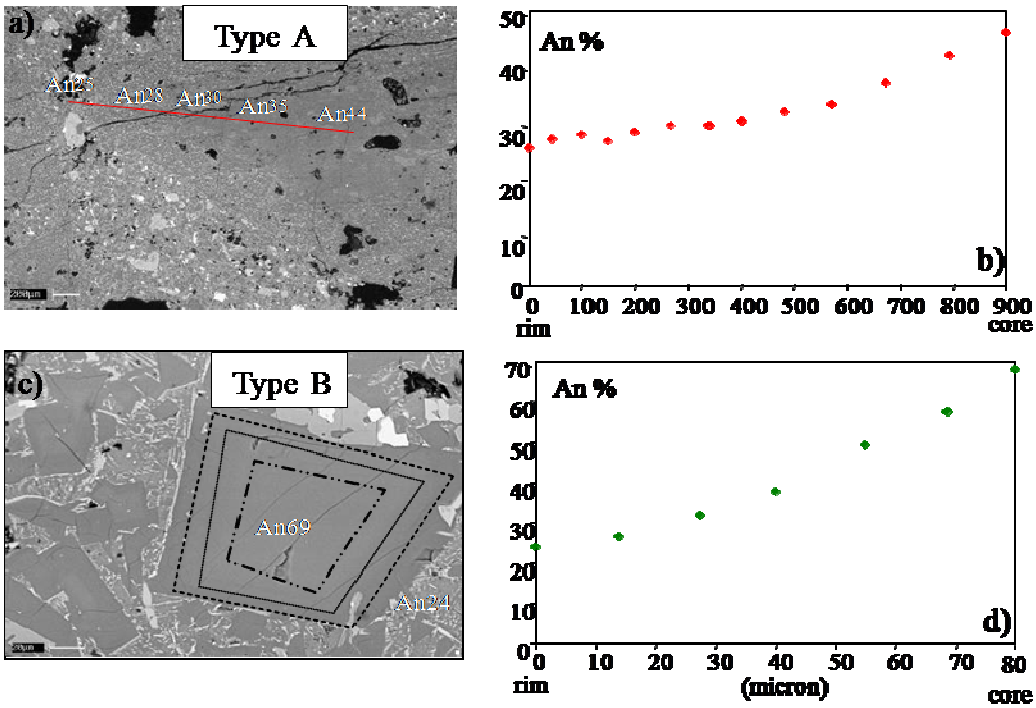

Fig. 5.20 Sample pan0749 of M. Grande N, SEM images (BSE), type A and B feldspar (2a, 2c) and composition traverses (2b, 2d) along a rim-core axis. texture and composition of the feldspar: rounded anorthoclase zoned with sieved textured cores characterized by abundant glass inclusions, and direct zoning (type 1 feldspar). Microlites in the groundmass with direct-zoning (type2).

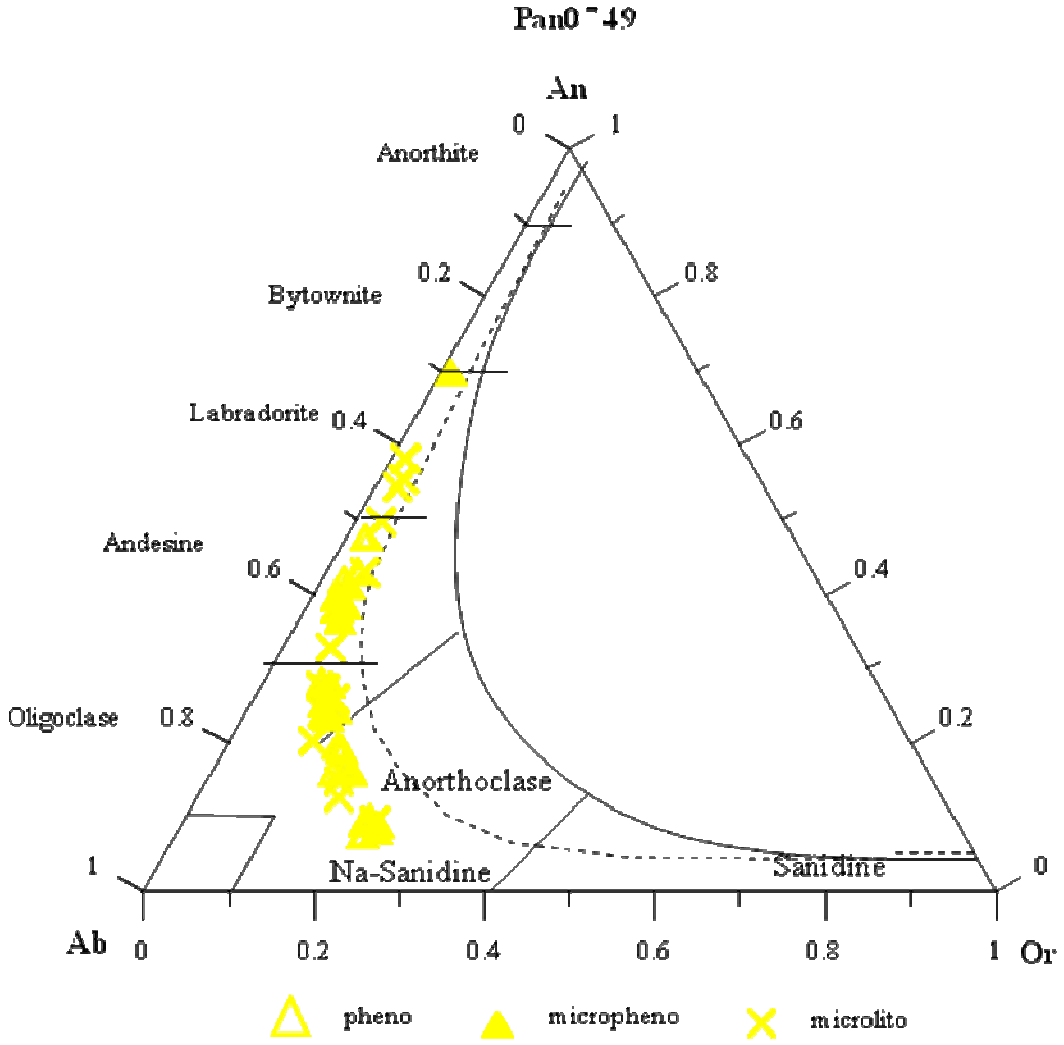

Fig. 5.21 Sample pan0749 of Montagna Grande N, compositional variations of plagioclase and alkali feldspar .

Three populations of clinopyroxene can be recognized: Type A -crystals with Fe-rich cores ($Wo_{40}Fs_{28}$, TiO_2 < 0.7 wt % and Al_2O_3 < 0.9 wt %), close to the composition of the clinopyroxene in the trachytes, and diopidic rims ($Wo_{48}Fs_{12}$, TiO_2 < 3.2 wt % and Al_2O_3 < 7.4 wt %); Type B: rare phenocrysts with nearly homogeneous composition $Wo_{40}Fs_{14}$ characterized by medium-high content of TiO_2 (1.4-2.7 wt%) and Al_2O_3 (3.1-6.0 wt %); Type C: zoned crystals with composition close to that of the Type B in the cores ($Wo_{44}Fs_{18}$, TiO_2 < 3 wt % and Al_2O_3 < 3.8 wt %) and less evolved rims ($Wo_{48}Fs_{11}$, TiO_2 < 3 wt % and Al_2O_3 < 6.6 wt %).

Microphenocrysts in the groundmass have diopsidic composition Fs_8-Fs_{12}.

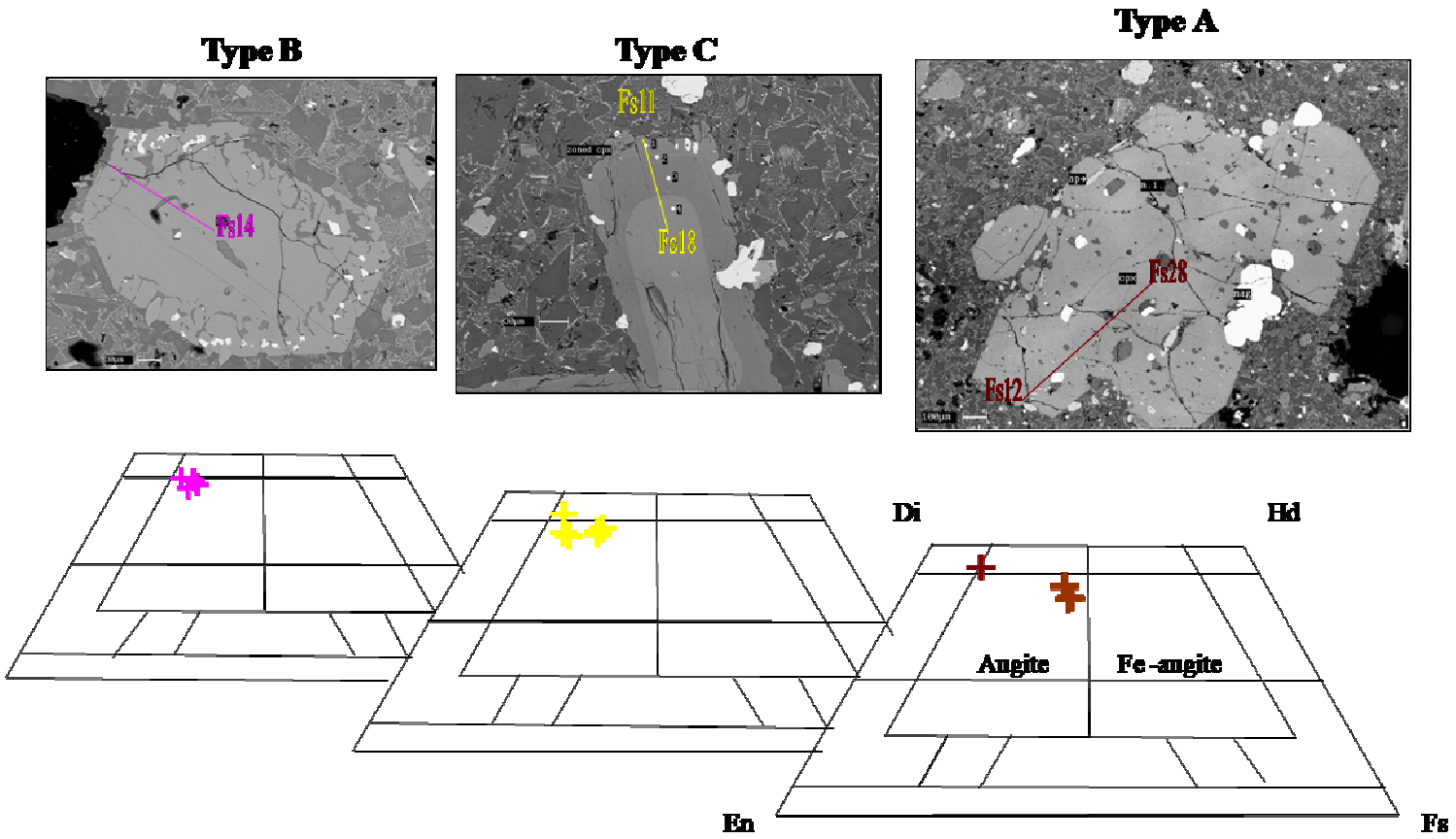

Fig. 5.22 Sample 0749 Montagna Grande, composition traverses along a rim-core axis of pyroxenes : type (b) homogenous, type (a) with inverse zoning and type (c) pyroxene in groundmass.

Olivine crystals show a wide compositional range with a bimodal distribution.

The majority of olivine phenocrysts is euhedral, 1 and 0.5 mm in size, and are characterized by a rather large compositional zoning, ranging from Fo_{80-84} (cores) to Fo_{60-64} (rims) **(Fig. 5.22)**. A second population is represented by skeletal olivines with homogeneous composition $Fo_{54-56.}$ Olivine microlites in the groundmass have nearly homogeneous composition in the range $Fo_{54–64}$ **(Fig. 5.22).**

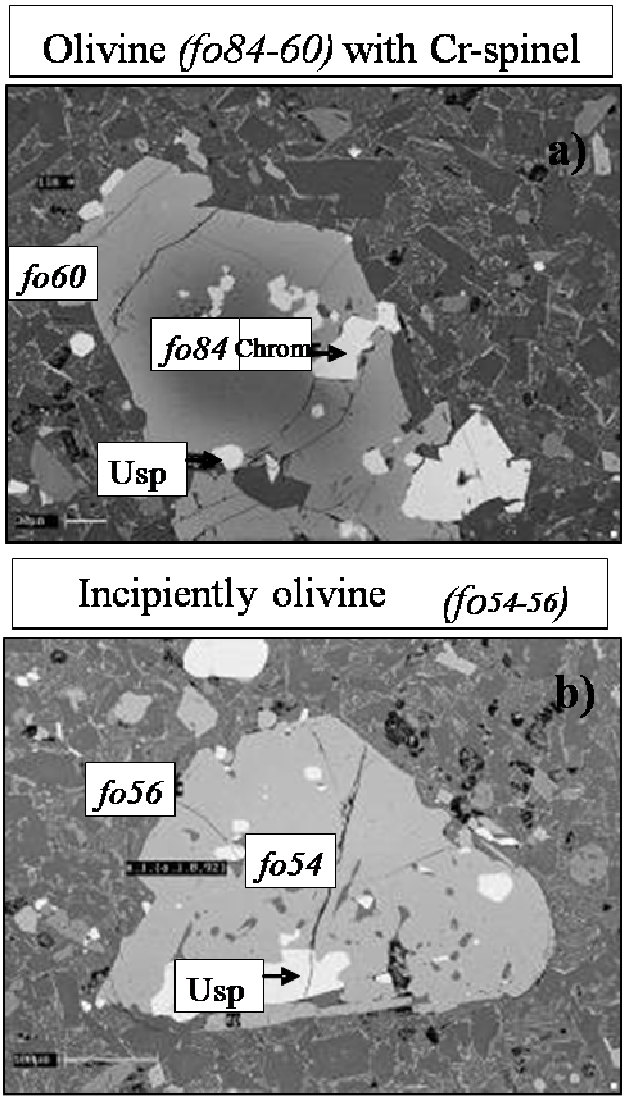

Fig..5.23 Sample pan0749 of Montagna Grande Nord, SEM images (BSE) of olivine crystals. a) zoned crystals core Fo_{84} and rim Fo_{60} with abundant inclusions of Cr-spinels; b) olivine with texture and homogeneous composition. Inclusions of magnetite are peculiar.

Fe-Ti oxides consist of abundant euhedral Ti-magnetite Xusp = 0.65 - 0.72 (< 500 μm in size) and minor Imenite Xilm = 0.94 - 0.96 mostly in the groundmass.

The Cr-spinel is only enclosed as subhedral individuals in olivine with composition Cr# (Cr/(Cr+Al) = 0.60 - 0.67 in olivine Fo_{60-64} and Cr# = 0.43 - 0.47 in olivine Fo_{80-84}.

Glomeroporphyric crystal clots are abundant. They are composed of clinopyroxene Fs_{16-20}, Olivine Fo_{50-60} and magnetite Xusp = 0.70 - 0.71, with apatite and pyrrhotite as accessory minerals.

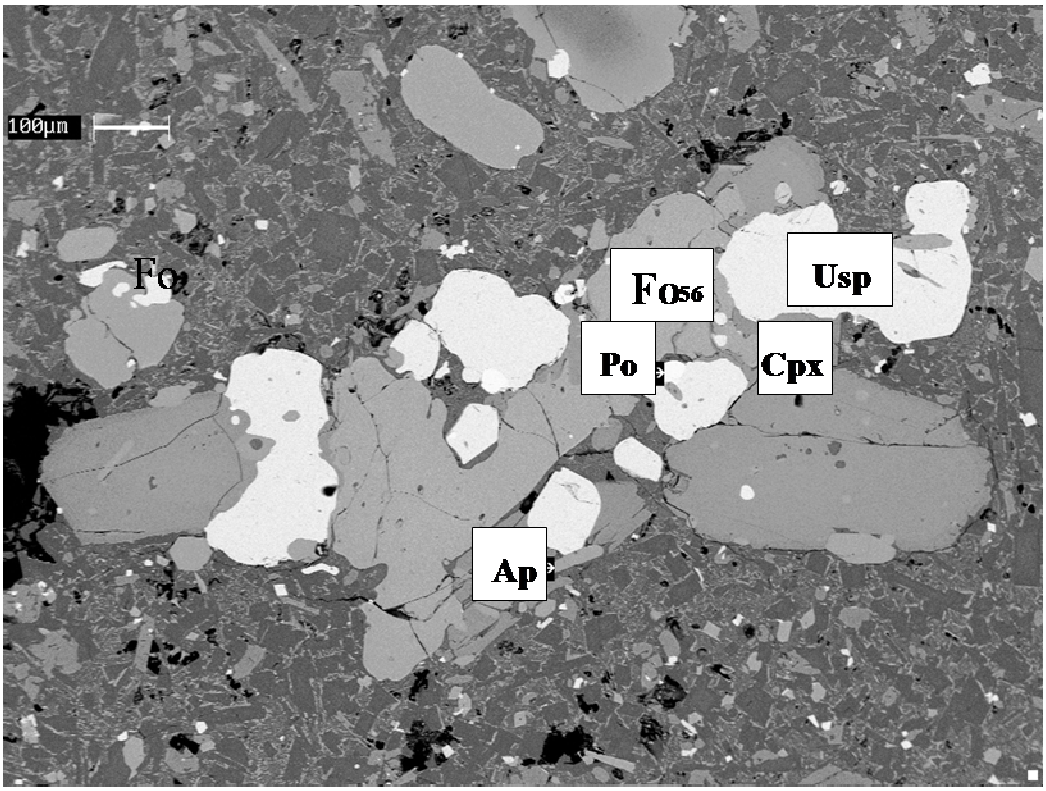

Fig. 5.24 Sample pan0749 of Montagna Grande Nord, SEM images (BSE) of glomeroporphyric crystal composed by clinopyroxene, olivine and magnetite are abundant with apatite and pyrrhotite as accessory minerals.

CHAPTER 6

TRACE ELEMENTS IN MINERAL PHASES,
a key to magma evolution from mafic to felsic liquids

Clinopyroxene is one of the most abundant minerals in igneous rocks and plays a major role in the generation and subsequent differentiation of magma.

Trace element partitioning between clinopyroxene and silicate liquid has therefore been the subject of intense study, especially since the successful application of lattice strain theory to crystal/melt element partitioning in igneous systems.

The determination of partition coefficients for trace elements between minerals and silicate melts $k_{d\ xtal/liq}$ is essential to understanding magmatic processes. These data can be obtained on both natural and experimental samples analyzing mineral phases and melt in equilibrium.

Knowledge of the partitioning of trace elements between mantle minerals and partial melts is fundamental in evaluating partial melting or fraction crystallization processes and determining the dependence of mafic magma genesis on the mineral composition of the mantle sources.

The crystal-liquid partition coefficients are generally assumed to be constant during differentiation, an assumption which is petrologically implausible and which contradicts observed variations in partition coefficients (Jones 1995).

We focus mainly on the partitioning of rare earth elements (REE) between clinopyroxene and melt from alkaline basalt to peralkaline, trachytes and pantellerite.

6.1 Pyroxene chemistry

Trace elements in clinopyroxenes have been analyzed in 7 samples which include rocks with different degree of evolution and trachytes with different geochemistry:

- trachybasalts of C. Rosse (pan 2);
- lava with benmoreitic bulk composition (pan 0749);
- metaluminous trachyte of Case Ricco (pan 0718);

- the more evolved trachyte (Mueggen pan 0732);
- Ba-poor trachytic enclave of C. Randazzo (pant 21);
- Ba-rich trachytic enclave of C. Randazzo (pant 23);
- the rhyolitic pumice of C. Randazzo (pant 2A2C).

The trachybasalts of C. Rosse (pan 2) pyroxenes are salites/augites ($Wo_{44-46}En_{40-42}Fs_{12-14}$), pyroxenes from the lava with benmoreitic bulk rock (pan0749) have salites to augitic composition ($Wo_{46}En_{42}Fs_{12}$ to $Wo_{43}En_{32}Fs_{25}$), the metaluminous trachyte of C: Ricco (pan0718) and the more evolved trachyte of Mueggen (pan0732) show pyroxenes with composition from augite to Fe-augites ($Wo_{41}En_{30}Fs_{29}$ to $Wo_{40}En_{18}Fs_{42}$), the C. Randazzo trachytic enclaves (pant21-23) and pumice (pant2A2C) pyroxenes are Fe-augites to Fe-hedenbergites ($Wo_{42}En_{31}Fs_{27}$ to $Wo_{43}En_{6}Fs_{52}$) (**fig.6.1).**

Compositional differences between hedenbergite and diopside result in contrasting major element cation site assignments. Silicon occupies the T-site and Al makes up any Si shortfall in tetrahedral coordination. Si + Al is approximately equal to 2 a.p.f.u. for all pyroxenes. M1 hosts all Ti^{4+} and also hosts Fe, Mn, and Mg, but significant Ca + Na shortfalls (< 1 a.p.f.u.) in the hedenbergites require that at least some Fe and Mn, and probably Mg, occupy M2. (Olin P. and Wolff J., 2010)

These structural changes should have consequences for trace element partitioning behaviour, which should therefore differ between Fe-rich and the more common Mg-rich pyroxenes.

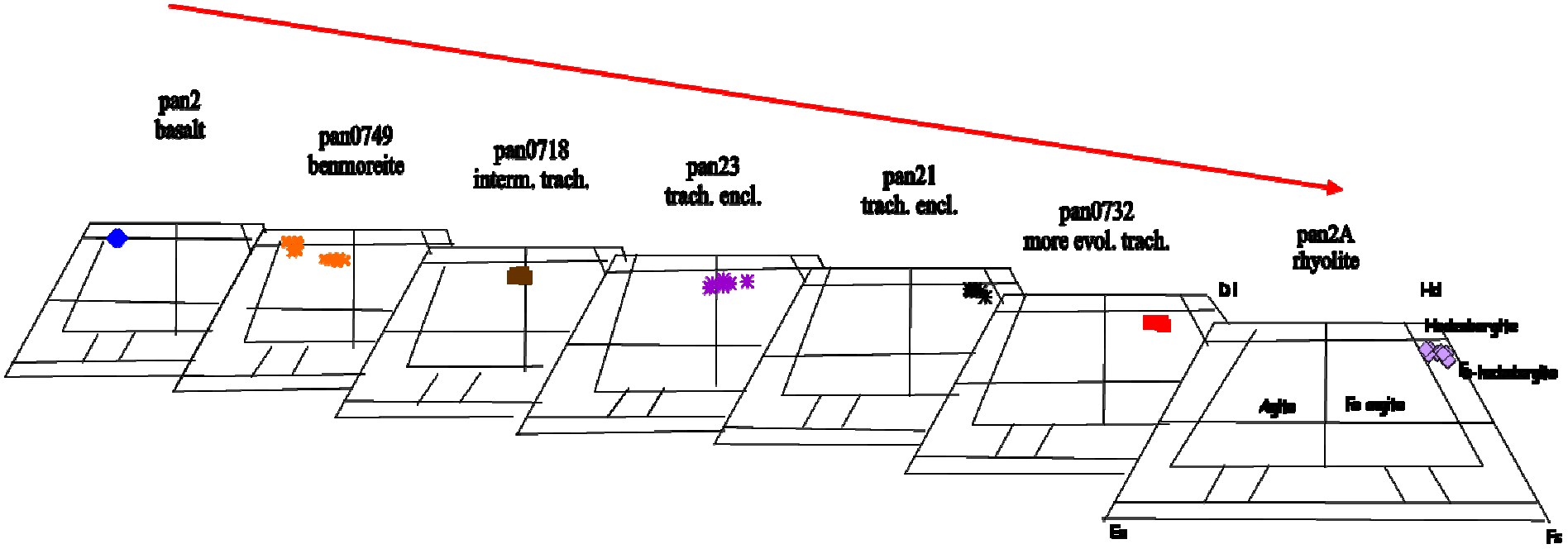

Fig.6.1 Summary of clinopyroxenes composition in samples analyzed for trace elements (LA-ICP-MS).

6.2 Trace element variations in clinopyroxenes from basalt to pantellerite

As a whole from basalt to silicic member only V, Co and Sr show an evident decrease in pyroxene (**Table 6.2**). REE increase steadily from basaltic to silicic rocks following nearly parallel trends i.e. without any relevant charge in slope, for basalt to trachyte, but clinopyroxenes from pantellerite show a marked increase in HREE $(La/Lu)_N$ basalt = 0.80-1.48 and $(La/Lu)_N$ pantellerite = 2.53-2.92 (**Fig. 6.4**).

Among the silicic rocks the Eu anomaly is not observed only in pyroxene of the Ba-rich trachytic enclave from C. Randazzo (pant23) which also show the lower REE contents (**Fig. REE**). While a negative evident Eu anomaly is present in the others trachytes and in the rhyolite. Eu anomally in the more evolved rocks is likely associated with feldspar fractionation.

Nevertheless this general behaviour there is not of a regular increase of REE and incompatible trace elements with decreasing of Mg# (= Mg/Mg + Fe_{tot}) in pyroxene (**Fig. 6.2**). For example Mueggen trachyte shows HREE enrichement higher than the more evolved pantellerites. At least two parallel trends can be seen.

The variations of Zr and Nd vs Mg# in pyroxene highlights two distinct trends which intersect at the basaltic end-member: a ITE-rich trends which includes the metaluminous trachytes of Montagna Grande (high-ITE trachytes), the Fe-rich pyroxene of the "benmoreitic" sample and the more evolved trachyte (Mueggen), and a ITE-poor trend which includes Ba-rich, Ba-poor peralkaline trachytes and peralkaline rhyolites of C. Randazzo. Moreover, pyroxene in the Ba-poor peralkaline trachytes (pant21, SiO_2 = 64.5 wt %) has lower Mg# and higher Ca content than those of the more evolved trachyte of Mueggen (pan0732; SiO_2 = 66.8 wt %) (**Fig. 6.2**).

6.3 Results

The trachyte Mueggen (pan0732) has LREE content close to that of the rhyolite and slightly higher MREE. Only pan0718 (C. Ricco) and the evolved pyroxenes of the benmoreitic sample (pan0749) show the same enrichment of HREE, while in the peralkaline rocks, both trachytes and rhyolites, Lu is more enriched than Yb (**Fig. 6.3**).

The trace elements in pyroxene hosted in the sample Benmoreite pan0749 (with benmoreitic bulk composition) confirm the occurrence of three population of crystals (**Figs. 6.2-6.3**):

(1) a diopsidic pyroxene which has the same chemistry than the pyroxene of the C. Mursia trachybasalts:

(2) Fe-rich pyroxene with the same chemistry than the pyroxene in trachytes, in particular the Casa Ricco trachyte (pan0718);

(3) intermediate composition found as rims of the previous crystals and microphenocrysts.

6.4 Kd of Rare Earth Elements in pyroxene

The lattice structure of clinopyroxene changes in response to changing Fe/Mg and Na/Ca due to the size differences between Na and Ca and Fe and Mg (Cameron and Papike 1980).

K_D values for LREE and HREE are published from a range of magma compositions (Mahood and Hildreth,1983, Mahood and Stimac, 1990).

Kd cpx/liq	**La**	**Ce**	**Kd cpx/liq**	**Yb**	**Lu**
K_d for trachyte melts (Mahood and Stimac, 1990).	0.28	0.48	K_d for trachyte melts (Mahood and Stimac, 1990).	1.4	1.8
K_d For pantellerite melts (Mahood and Stimac, 1990).	0.51	0.81	K_d for pantellerite melts (Mahood and Hildreth,1983).	4.5-6.4	6.1-8.1

Table 6.1 Partition coefficient LREE and HREE in clinopyroxenes

The primary factors controlling the style of trace element partitioning between clinopyroxene and silicate melt are mineral composition and the ionic radius of the substituting cation.

Heavy REE enrichment in Fe-rich clinopyroxenes from felsic magmas is caused by substitution into sixfold coordinated sites (M2 or M1). Increased heavy REE compatibility coincides with the higher Fe and Na contents of these pyroxenes.

One possible explanation, could involve the coupled substitution:

$$Ca^{2+} + Fe^{2+} = Na^{+} + HREE^{3+}$$

One possible problem regards the late crystallization of accessory phases (apatite, pyrrhotite) that concentrate REE and would therefore deplete the melt in REE after pyroxene growth.

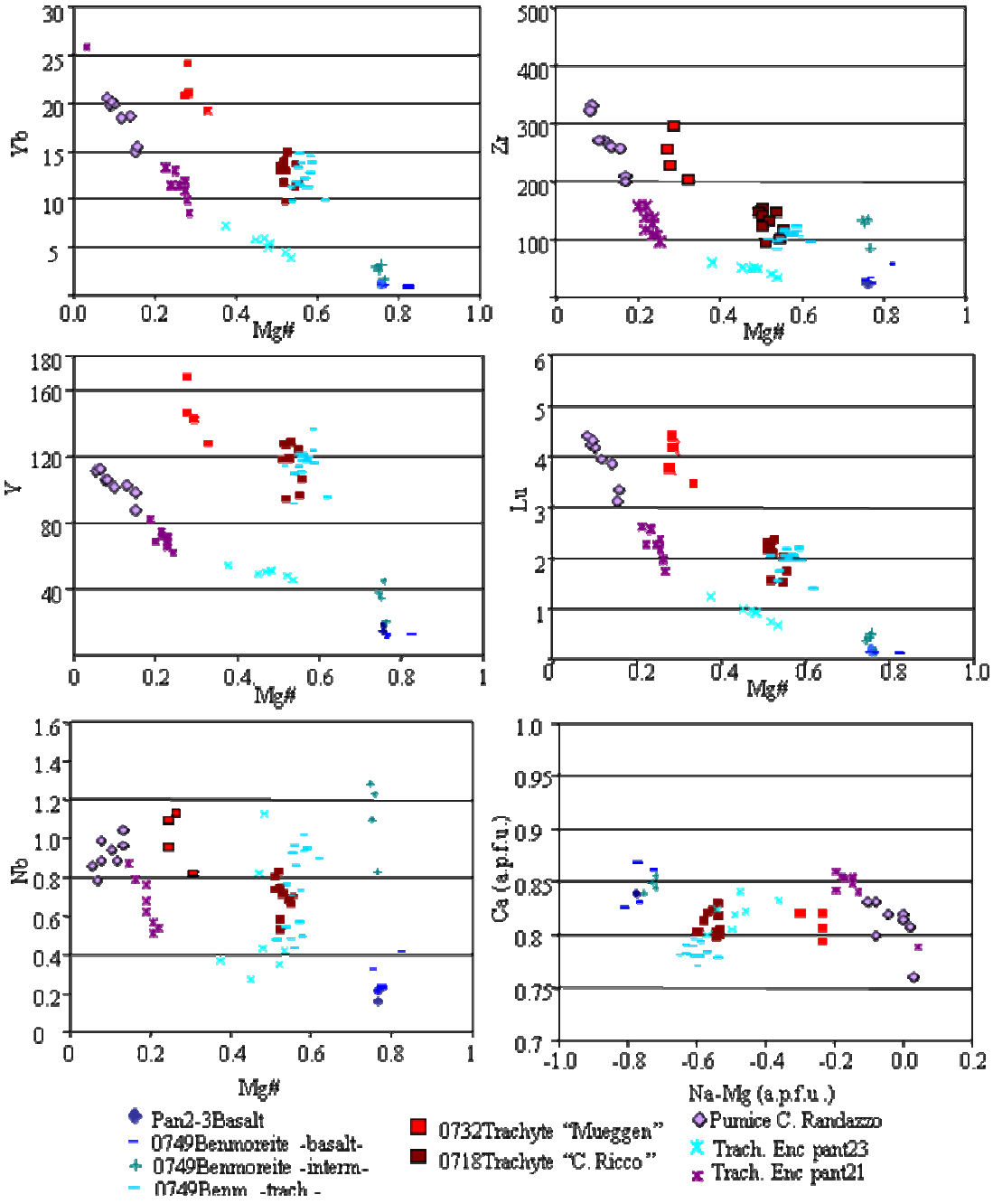

Fig. 6.2 Diagrams Mg# Zr, Mg#-Nd, Mg#-Y and (Na-Mg/Ca) a.p.f.u.

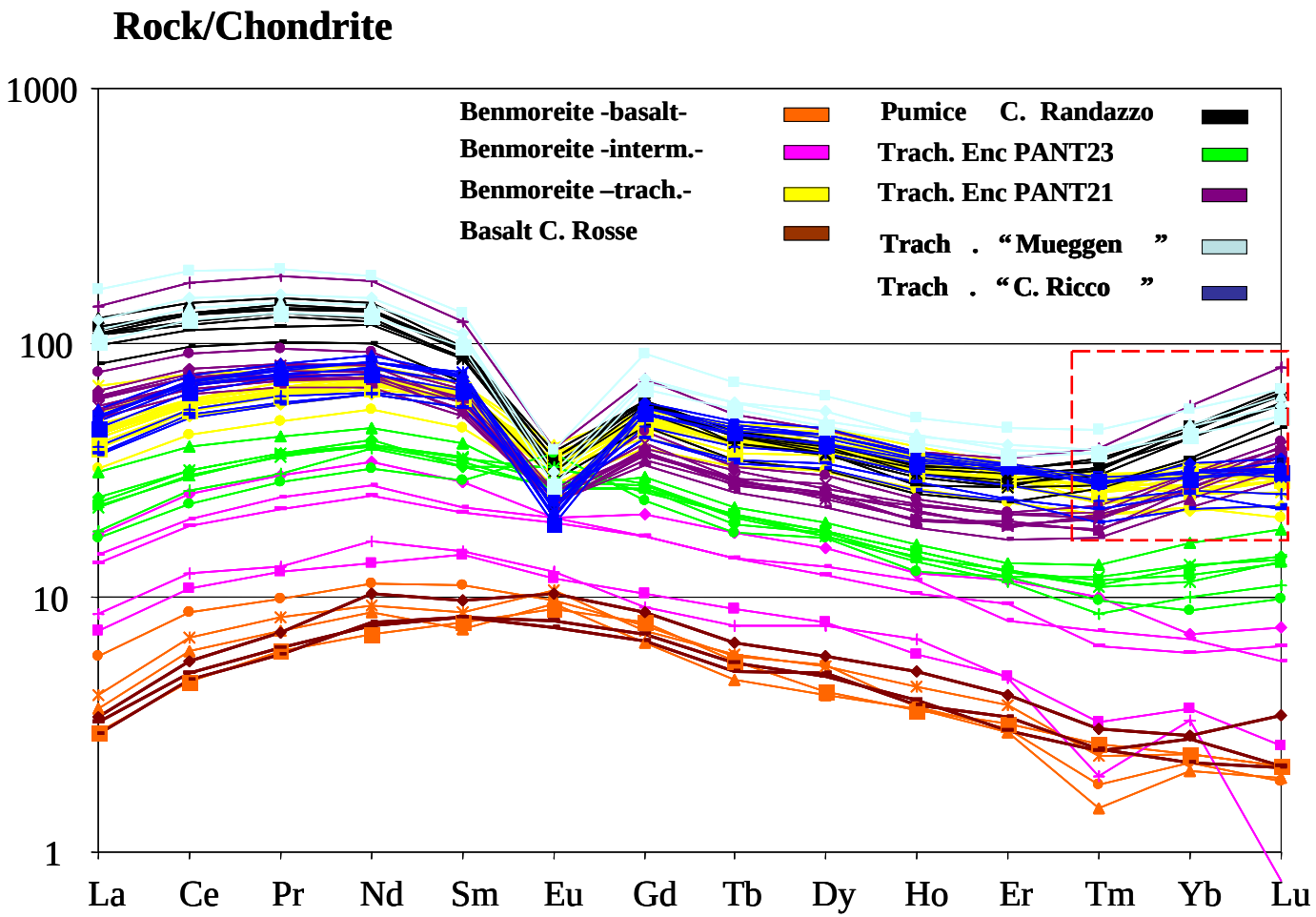

Fig. 6.3 REE in: 1) - 2A2C pumice pantellerite 2) - 0732 trachyte "Mueggen" 3) - 0718 trachyte "C. Ricco" 4) pant21-23 trachytic enclaves 5) 0749 benmoreite -interm-, -basalt- and –trach- and 6) pan2 basalt. Normalizing values are after McDonough and Sun (1995).

Rock type	**Pan2basalt C. Rosse**			**0749 benmoreite Montagna Grande N**									
Sample	**1**	**2**	**3**	**1a**	**1b**	**2a**	**2b**	**2c**	**3a**	**4**	**5a**	**5b**	**5c**
SiO_2 wt%	50.39	49.39	49.89	50.81	51.04	46.79	45.95	51.86	50.91	51.55	51.05	51.20	51.45
Al_2O_3	3.54	4.54	3.24	0.55	0.63	6.29	0.69	0.66	0.65	0.64	0.60	0.65	0.76
TiO_2	1.29	2.19	1.37	0.46	0.54	2.60	0.41	0.54	0.46	0.52	0.52	0.48	0.53
FeO	8.33	8.63	8.41	16.59	17.29	7.73	14.96	14.96	16.36	14.92	15.76	15.92	15.32
MnO	0.21	0.12	0.12	1.05	1.05	0.11	0.96	0.97	1.02	0.93	1.01	1.04	0.96
MgO	14.69	14.72	14.89	10.82	10.36	14.13	13.32	11.77	10.70	11.97	11.32	11.21	11.74
CaO	21.18	20.18	20.82	19.06	18.98	21.02	21.86	19.50	19.45	19.27	18.99	19.07	19.24
NaO	0.39	0.42	0.39	0.62	0.68	0.45	0.45	051	0.59	0.63	0.55	0.61	0.60
Cr_2O_3	0.36	0.26	0.30	0.04	0.00	0.24	0.36	0.02	0.02	0.00	0.00	0.00	0.02
Wo	43.9	43.7	43.9	40.4	40.2	40.6	40.6	41.1	40.6	40.3	40.1	40.2	40.2
En	42.3	42.4	41.3	31.9	30.5	34.4	34.1	31.4	36.0	34.8	33.2	32.8	34.2
Fs	13.8	14.0	14.8	27.8	29.3	25.0	25.4	27.5	23.4	24.9	26.7	27.0	25.6
Li ppm	1.03	0.00	0.54	3.25	2.97	7.38	4.04	3.94	2.67	1.49	3.51	1.60	2.38
Be	0.00	11.87	0.00	1.72	1.23	1.92	2.30	0.00	1.43	4.00	5.48	4.62	0.00
B	7.60	0.00	0.00	1.56	1.55	1.74	3.56	1.87	1.38	3.50	3.29	6.90	3.64
Sc	0.10	0.11	0.10	281	152	107	138	131	130	124	144	38	130
Ti	4002	3820	4302	3176	2915	12729	4025	3448	3449	3303	3280	3238	3154
V	0.30	0.21	0.37	22.16	44.98	257	64.70	59.19	56.48	57.80	50.12	54.17	55.59
Cr	0.38	0.40	0.39	3.53	2.80	2111	5.04	16.80	3.53	6.84	7.12	6.78	7.88
Co	0.04	0.04	0.04	13.39	16.22	38.96	21.46	18.74	16.47	18.81	17.21	15.90	18.45
Ni	0.56	0.72	0.58	1.77	1.96	199	3.98	3.27	2.39	3.89	2.84	1.19	2.75
Zn	0.00	0.00	0.00	271	266	41	287	299	269	238	255	260	264
Rb	2.13	2.05	2.14	0.07	0.05	0.08	0.07	0.12	0.11	0.17	0.15	0.25	0.15
Sr	3.29	4.19	3.37	17.29	20.18	54.61	27.69	16.94	26.37	18.43	17.40	17.26	17.57
Y	2.17	2.48	2.61	91.90	114	20.69	136	123	109	116	121	120	120
Zr	0.22	0.21	0.32	83	100	84.60	121	112	94.79	104	109	116	109
Nb	0.00	0.00	0.00	0.54	0.48	0.83	0.93	1.01	0.76	0.95	0.86	0.43	0.49
Cs	0.00	0.03	0.00	0.01	0.01	0.02	0.02	0.02	0.01	0.03	0.03	0.31	0.02
Ba	2.93	3.41	3.27	0.05	0.05	0.09	0.18	0.82	0.64	0.18	0.18	0.19	0.18
La	4.75	5.66	5.05	25.19	28.45	4.78	34.47	30.94	44.33	25.13	28.97	29.66	28.04
Ce	6.00	7.35	6.35	83.63	96.68	17.56	112	97.48	124	88.19	95.20	97.36	92.64
Pr	7.96	10.31	7.81	14.65	16.99	3.23	20.17	16.96	19.76	15.63	16.50	17.87	16.41
Nd	8.37	9.71	8.42	78.05	88.04	17.15	102	92.89	99.54	82	89.97	89.90	87.82
Sm	7.63	10.38	8.06	22.63	25.84	6.00	28.01	25.11	28.03	24.68	26.30	23.92	24.39
Eu	6.79	8.75	7.16	4.91	5.04	1.84	6.14	4.90	5.62	4.19	4.98	5.02	4.66
Gd	5.14	6.63	5.50	23.15	26.51	5.64	29.38	27.53	27.62	25.32	26.56	29.78	26.30
Td	5.04	5.91	4.94	3.46	4.11	0.89	5.86	5.30	4.72	4.72	5.56	5.61	4.84
Dy	3.77	5.10	3.95	20.95	26.45	5.40	31.22	28.80	26.61	24.38	26.76	30.52	29.33
Ho	3.41	4.17	2.99	3.91	4.89	0.89	5.86	5.30	4.72	4.72	5.56	5.61	4.84
Er	2.55	3.04	2.51	10.39	12.57	2.14	14.74	14.27	12.05	13.10	12.98	14.34	14.37
Tm	2.24	2.86	2.79	1.44	1.75	0.22	2.01	2.02	1.60	1.75	2.09	1.94	1.89
Yb	2.15	3.45	2.20	9.73	12.08	1.61	14.48	12.68	11.19	13.89	13.72	14.77	11.18
Lu	3.39	3.85	6.41	1.54	2.04	0.18	2.22	2.16	1.75	1.94	1.98	2.17	1.95
Hf	0.85	0.74	1.80	2.85	3.59	3.69	4.69	4.64	3.41	3.21	4.48	4.57	4.24
Ta	10.56	0.00	0.61	0.03	0.02	0.15	0.02	0.06	0.04	0.05	0.04	0.02	0.02
Pb	0.00	0.13	0.13	0.13	0.09	0.07	0.12	0.12	0.08	0.16	0.15	0.17	0.12
Th	0.00	0.23	0.00	0.02	0.03	0.06	0.08	0.06	0.15	0.05	0.03	0.02	0.08
U	1.03	0.00	0.54	0.01	0.01	0.01	0.03	0.01	0.05	0.02	0.01	0.00	0.01
Na/Ca	0.03	0.02	0.04	0.03	0.04	0.02	0.02	0.03	0.03	0.03	0.03	0.03	0.03
Zr/Th	0.91	0.85	0.85	0.91	0.85	0.85	0.82	0.79	1.13	0.76	0.79	0.81	0.77
Ce/Y	2.76	2.96	2.43	2.35	2.19	2.97	2.11	2.10	3.02	1.74	1.90	1.80	2.27
$(Ce/Yb)_N$	0.76	0.58	0.79	0.70	0.69	0.50	0.77	0.78	1.00	0.64	0.69	0.78	0.72
$(La/Sm)_N$	0.39	0.34	0.39	1.70	1.45	2.81	1.62	1.49	2.63	1.35	1.52	1.42	1.49
$(La/Lu)_N$	1.40	1.47	0.79	0.70	0.69	0.50	0.77	0.78	1.00	0.64	0.69	0.78	0.72
Eu/Eu*	1.21	1.20	1.17	0.66	0.59	0.96	0.65	0.57	0.62	0.51	0.58	0.57	0.56

Table 6.2 - Major elements by EMP and trace elements by LA-ICP-MS of pyroxene in selected rock samples.

Rock type	**0749 benmoreite**													
	Montagna Grande N													
Sample	**6a**	**6b**	**8a**	**8b**	**8c**	**8d**	**9a**	**9b**	**14a**	**15a**	**15b**	**18a**	**18b**	**18c**
SiO_2 wt%	51.27	51.58	47.36	47.28	46.76	51.89	51.22	51.46	48.28	50.88	51.76	47.28	49.79	50.03
Al_2O_3	0.50	0.65	6.15	6.05	6.80	1.40	0.54	0.58	5.26	0.57	0.61	5.24	3.27	3.13
TiO_2	0.46	0.42	2.36	2.32	2.72	0.72	0.43	0.46	1.88	0.42	0.46	1.67	1.37	1.47
FeO	16.47	15.38	8.31	8.09	7.76	13.49	16.17	15.98	6.34	15.38	15.67	6.00	8.79	8.26
MnO	1.04	1.10	0.10	0.15	0.15	0.84	1.08	1.06	0.12	0.96	1.01	0.10	0.32	0.18
MgO	11.22	11.53	13.69	13.77	13.64	12.38	11.15	11.15	15.16	11.43	11.05	13.78	15.15	14.60
CaO	18.86	19.63	21.23	21.28	21.56	19.41	19.04	19.06	21.94	19.21	19.46	21.61	20.62	20.84
NaO	0.56	0.57	0.54	0.51	0.48	0.65	0.57	0.59	0.45	0.61	0.56	0.43	0.38	0.48
Cr_2O_3	0.00	0.00	0.08	0.09	0.23	0.00	0.03	0.00	0.34	0.00	0.01	0.02	0.06	0.04
Wo	40.6	41.1	40.6	40.3	40.1	40.2	40.2	40.6	40.8	39.6	40.9	40.1	40.1	45.3
En	34.1	31.4	36.0	34.8	33.2	32.8	34.2	33.6	32.2	32.8	33.4	32.6	32.6	40.7
Fs	25.4	27.5	23.4	24.9	26.7	27.0	25.6	25.8	27.0	27.6	25.7	27.3	27.3	14.0
Li ppm	2.61	3.22	2.23	5.39	5.91	2.92	3.80	1.91	3.35	5.07	5.09	9.42	7.46	6.60
Be	3.75	0.00	6.15	7.60	7.22	4.36	4.42	2.86	4.09	3.52	2.17	1.65	2.05	0.00
B	2.94	3.16	3.71	3.24	3.82	3.08	3.04	2.33	1.58	3.64	3.39	2.16	0.97	1.44
Sc	136	135	94	112	118	115	166	189	99	128	149	98	108	111
Ti	3242	3282	13943	15817	15639	3961	3333	3378	15046	3437	3579	15031	9142	9139
V	52.22	53.43	318	346	315	101	51.63	44.77	293	62.97	82.84	337	295	294
Cr	5.00	5.16	644	866	865	5.57	6.33	7.60	2435	9.71	4.51	884	305	270
Co	18.44	17.56	38.87	41	36.99	18.46	18.25	19.38	31.99	17.75	18.88	33.14	37.39	35.73
Ni	3.11	2.72	161	185	151	4.73	1.72	1.61	160	2.24	2.60	63.32	39.45	36.16
Zn	264	277	49	63	95	213	270	277	40	206	230	26	39	50
Rb	0.11	0.12	0.10	0.34	0.15	0.13	0.12	0.12	0.16	0.08	0.28	0.06	0.04	0.05
Sr	21.07	22.90	64.89	71.80	65.28	24.44	17.30	16.04	75.23	21.43	23.03	55.64	37.55	41.20
Y	114	118	37.66	40.11	51.42	95.73	122	117	19.47	116	110	10.79	12.74	15.21
Zr	99	105	132	143	152	94.58	105	112	87.86	108	111	32.70	24.12	28.59
Nb	0.48	0.73	1.28	1.25	1.39	0.90	0.70	0.92	1.25	0.57	0.96	0.20	0.23	0.32
Cs	0.02	0.03	0.04	0.05	0.05	00.02	00.03	0.02	0.10	0.03	0.03	0.01	0.01	0.01
Ba	0.10	0.29	0.18	0.06	0.06	0.85	0.19	0.15	1.22	0.10	0.54	0.03	0.07	0.04
La	26.32	28.19	9.56	10.09	12.92	20.87	27.33	29.11	5.55	28.53	27.55	2.36	1.92	2.67
Ce	89.43	93.59	32.97	35.49	46.95	71.26	91.43	97.45	20.27	92.25	92.45	10.08	7.61	11.32
Pr	15.66	16.67	6.28	6.43	8.69	12.44	15.95	16.98	3.37	16.23	15.99	1.89	1.57	2.14
Nd	85.17	86.71	34.21	35.94	48.27	68.26	89.39	91.94	20.94	86.04	86.46	10.91	8.93	11.64
Sm	24.76	24.72	9.15	10.01	12.99	18.89	25.86	26.56	6.20	24.18	24.28	3.06	3.24	3.57
Eu	5.10	5.45	3.17	3.44	3.60	4.30	5.16	5.22	1.94	4.59	5.73	1.45	1.38	1.65
Gd	26.22	27.47	9.41	10.85	13.11	21.02	27.65	25.41	4.97	26.65	26.10	3.60	4.35	4.00
Td	4.67	5.21	1.42	1.61	2.02	3.22	4.15	4.16	0.77	3.99	3.90	0.47	0.56	0.59
Dy	26.37	25.15	8.91	9.33	11.90	21.17	27.63	25.39	5.23	27.19	25.91	2.78	2.90	3.61
Ho	4.67	5.21	1.75	1.75	2.11	3.96	5.11	4.60	1.03	5.29	4.98	0.55	0.54	0.67
Er	13.06	12.89	3.56	4.73	5.86	10.43	13.10	13.08	2.11	13.45	12.07	1.30	1.40	1.65
Tm	1.85	1.90	0.50	0.50	0.78	1.45	1.87	1.78	0.14	1.58	1.65	0.10	0.18	0.16
Yb	11.80	12.11	3.03	3.03	3.61	9.91	13.35	13.19	1.45	11.22	11.44	0.92	1.07	1.07
Lu	1.94	2.04	5,20	6,69	6,84	3,45	3,86	4,38	3,19	4,67	4,00	1,67	1,20	1,38
Hf	3.58	4.02	0,27	0,26	0,38	0,07	0,02	0,03	0,20	0,06	0,03	0,03	0,02	0,03
Ta	0.03	0.05	0,17	0,19	0,17	0,10	0,15	0,17	0,12	0,09	0,16	0,05	0,05	0,05
Pb	0.18	0.18	0,13	0,15	0,12	0,04	0,04	0,04	0,10	0,10	0,03	0,01	0,02	0,01
Th	0.04	0.04	0,01	0,02	0,04	0,01	0,01	0,02	0,01	0,03	0,04	0,00	0,01	0,01
U	0.00	0.01	0,27	0,26	0,38	0,07	0,02	0,03	0,20	0,06	0,03	0,03	0,02	0,03
Na/Ca	0.03	0.03	0.03	0.02	0.02	0.03	0.03	0.03	0.02	0.03	0.03	0.02	0.02	0.02
Zr/Th	0.79	0.79	0.88	0.88	0.91	0.74	0.75	0.83	1.04	0.79	0.84	0.93	0.60	0.74
Ce/Y	2.07	2.11	2.98	3.21	3.55	1.97	1.87	2.02	3.83	2.25	2.21	2.99	1.94	2.88
$(Ce/Yb)_N$	0.67	0.72	0.66	0.63	0.63	0.70	0.67	0.69	0.56	0.74	0.71	0.49	0.37	0.47
$(La/Sm)_N$	1.41	1.44	2.62	2.11	2.29	1.56	1.40	1.51	11.12	1.43	1.48	1.86	1.36	1.87
$(La/Lu)_N$	0.67	0.72	0.66	0.63	0.63	0.70	0.67	0.69	0.56	0.74	0.71	0.49	0.37	0.47
Eu/Eu*	0.61	0.64	1.04	1.01	0.84	0.66	0.59	0.61	1.07	0.55	0.70	1.33	1.12	1.34

Rock type	Pan0718 trachyte "Case Ricco"										Pan0732 trachyte "Mueggen"			
Sample	**1b**	**1a**	**2a**	**2b**	**3a**	**3b**	**4a**	**4b**	**5a**	**5b**	**1a**	**1b**	**2a**	**3a**
SiO_2 wt%	51.64	50.86	51.14	51.38	51.45	51.30	51.71	50.97	51.89	51.50	50.22	50.13	49.98	50.22
Al_2O_3	0.62	0.99	0.67	0.68	0.71	0.79	0.60	0.79	0.88	0.68	0.30	0.30	0.30	0.33
TiO_2	0.47	0.59	0.45	0.52	0.47	0.78	0.47	0.49	0.53	0.51	0.53	0.42	0.38	0.39
FeO	16.64	17.42	17.21	16.83	16.51	15.90	16.82	15.87	17.04	15.86	23.89	23.56	23.32	22.20
MnO	0.96	1.05	1.12	0.95	0.98	0.88	0.95	0.87	1.07	0.88	1.43	1.40	1.35	1.19
MgO	10.45	10.17	10.07	10.20	10.18	10.80	10.23	11.21	10.36	10.80	5.11	5.21	5.20	6.18
CaO	20.30	19.63	19.70	20.09	20.40	20.19	19.68	19.69	19.77	19.94	18.86	19.18	19.33	19.60
NaO	0.47	0.56	0.54	0.51	0.51	0.54	0.50	0.51	0.52	0.45	0.90	0.89	0.83	0.72
Cr_2O_3	0.00	0.00	0.00	0.00	0.00	0.00	0.00	0.00	0.00	0.00	0.00	0.00	0.00	0.00
Wo	41.2	42.2	41.4	42.0	42.6	42.2	41.2	41.2	41.0	41.7	41.5	42.1	42.5	42.5
En	29.7	30.2	29.4	29.7	29.6	31.4	29.8	32.7	29.9	31.4	15.6	15.9	15.9	18.7
Fs	29.1	27.6	29.2	28.3	27.8	26.4	29.0	26.1	29.1	26.9	42.9	42.0	41.6	38.8
Li ppm	19.43	21.47	13.37	16.22	12.45	17.53	14.33	20.90	19.01	20.27	7.67	8.55	8.97	6.61
Be	3.24	3.20	0.71	2.40	0.79	2.83	1.64	2.60	1.28	2.98	2.81	1.99	0.92	2.25
B	1.72	1.52	4.14	1.70	2.55	1.91	1.58	2.05	1.94	2.19	2.66	1.09	2.13	2.01
Sc	153	153	158	167	151	149	154	145	174	169	197	176	200	205
Ti	3530	3943	3616	3870	3454	3820	3560	3772	4247	4314	2865	3090	2699	2660
V	19.01	18.86	16.78	18.78	19.62	24.74	17.06	29.92	20.67	28.64	0.92	1.63	1.02	3.00
Cr	7.46	2.60	2.56	3.42	2.03	2.63	2.34	2.27	2.44	3.28	2.70	2.41	2.61	2.20
Co	13.46	12.32	11.96	11.97	12.29	12.50	11.73	14.03	12.06	12.62	4.94	4.64	5.39	5.77
Ni	1.28	0.54	1.16	1.05	0.67	1.96	1.65	1.25	0.46	0.45	0.34	0.43	0.38	0.53
Zn	279	316	286	290	270	266	285	248	260	242	355	392	370	348
Rb	0.08	0.25	0.05	0.06	0.06	0.06	0.08	0.05	0.06	0.04	0.08	0.07	0.06	0.07
Sr	11.08	14.32	12.36	13.24	14.60	18.01	12.87	20.74	19.74	23.43	2.13	2.12	2.10	2.48
Y	129	135	128	128	119	124	127	107	95	97	176	204	169	154
Zr	122	146	127	139	116	135	128	108	94	96	256	290	227	197
Nb	0.71	0.91	0.74	0.83	0.59	0.68	0.74	0.70	0.53	0.66	1.10	1.12	0.93	0.78
Cs	0.02	0.03	0.01	0.00	0.02	0.03	0.01	0.01	0.01	0.01	0.10	0.02	0.01	0.01
Ba	0.23	0.47	0.09	0.04	0.09	0.11	0.02	0.08	0.15	0.04	0.10	0.08	0.05	0.05
La	33.35	38.07	33.33	35.60	30.01	32.89	31.88	25.39	23.53	24.05	79.88	105	72.77	65.31
Ce	113	127	114	120	103	114	110	88.98	83.12	84.82	243	311	224	200
Pr	19.96	21.90	20.28	21.13	18.59	19.91	18.83	15.64	14.61	14.78	39.45	49.30	36.53	33.46
Nd	105	112	105	111	95	105	100	80	78	79	187	229	178	159
Sm	29.80	32.31	30.18	30.30	26.44	31.17	28.54	24.51	22.57	22.69	44.14	53.25	42.89	39.25
Eu	3.24	4.17	3.47	3.68	2.98	3.35	3.15	3.58	3.81	3.80	4.79	5.84	4.53	4.23
Gd	31.72	32.54	30.11	30.47	28.86	30.29	30.19	25.72	22.96	23.16	39.03	49.55	38.25	35.69
Td	4.89	4.91	4.57	4.72	4.39	4.47	4.61	3.89	3.34	3.42	5.77	6.95	5.75	5.46
Dy	31.05	30.80	29.22	29.52	26.87	29.27	28.55	24.87	21.79	22.59	36.50	41.47	33.40	31.69
Ho	5.57	5.86	5.46	5.42	5.00	5.37	5.24	4.54	3.91	4.21	6.40	7.57	6.46	6.01
Er	14.40	15.43	14.62	14.32	14.44	13.83	14.14	12.06	10.47	10.73	17.41	20.18	16.54	15.68
Tm	1.88	2.18	2.04	1.90	1.97	1.93	1.93	1.62	1.34	1.52	2.57	3.09	2.52	2.50
Yb	14.87	14.84	13.47	13.82	12.93	13.66	13.94	11.63	9.81	11.24	20.82	29.79	25.79	23.39
Lu	2.37	2.42	2.29	2.14	2.10	2.00	2.18	1.73	1.55	1.51	3.80	4.41	4.19	3.48
Hf	4.55	5.19	4.57	5.03	3.56	5.33	4.60	3.50	3.01	3.62	8.49	11.08	7.41	6.02
Ta	0.04	0.05	0.05	0.05	0.02	0.03	0.01	0.02	0.03	0.03	0.04	0.06	0.01	0.01
Pb	0.37	0.23	0.13	0.13	0.12	0.15	0.08	0.12	0.12	0.06	0.32	0.30	0.30	0.26
Th	0.03	0.06	0.03	0.03	0.03	0.03	0.05	0.06	0.02	0.03	0.04	0.03	0.03	0.02
U	0.01	0.02	0.01	0.00	0.01	0.01	0.02	0.02	0.01	0.01	0.01	0.01	0.01	0.01
Na/Ca	0.02	0.03	0.03	0.03	0.03	0.03	0.03	0.03	0.03	0.02	0.05	0.05	0.04	0.04
Zr/Th	3606	2507	3884	5047	4039	4614	2688	1963	3767	3244	6084	10202	7284	9574
Ce/Y	0.88	0.94	0.90	0.94	0.87	0.92	0.86	0.83	0.87	0.88	1.38	1.52	1.32	1.30
$(Ce/Yb)_N$	2.08	2.34	2.33	2.39	2.20	2.29	2.16	2.09	2.32	2.06	3.21	2.86	2.38	2.34
$(La/Sm)_N$	0.70	0.74	0.70	0.74	0.71	0.66	0.70	0.65	0.66	0.67	1.14	1.25	1.07	1.05
$(La/Lu)_N$	1.46	1.63	1.51	1.73	1.48	1.71	1.52	1.52	1.58	1.66	2.18	2.48	1.80	1.95
Eu/Eu*	0.32	0.39	0.35	0.38	0.33	0.33	0.33	0.44	0.51	0.51	0.35	0.35	0.34	0.35

Table 6.2 - Major elements by EMP and trace elements by LA-ICP-MS of pyroxene in selected rock samples

Rock type	**Pant23b trachyte enclave**							**Pant21b trachyte enclave**				
	“ Cuddia Randazzo”							**“ Cuddia Randazzo”**				
Sample	**2a**	**2b**	**3a**	**4a**	**4b**	**5a**	**5b**	**2a**	**2b**	**2c**	**2d**	**2e**
SiO_2 wt%	51.27	51.27	50.99	50.17	51.13	51.59	51.15	49.41	49.07	48.97	48.88	49.08
Al_2O_3	0.70	0.80	0.56	0.64	0.69	0.81	0.88	0.34	0.36	0.35	0.31	0.35
TiO_2	0.66	0.67	0.59	0.60	0.59	0.66	0.59	0.50	0.61	0.56	0.47	0.56
FeO	19.10	17.94	21.00	17.96	18.04	16.70	16.90	24.68	24.64	24.68	25.26	24.68
MnO	1.11	1.10	1.22	0.96	1.13	1.02	0.96	1.41	1.38	1.34	1.33	1.34
MgO	8.76	9.46	7.10	8.96	9.35	10.78	10.32	3.92	4.16	3.68	3.56	4.48
CaO	20.18	19.73	20.20	20.31	20.07	19.80	20.34	19.97	19.89	19.84	19.83	19.87
NaO	0.54	0.54	0.58	0.59	0.59	0.49	0.55	0.65	0.66	0.73	0.74	0.65
Cr_2O_3	0.00	0.00	0.00	0.00	0.00	0.00	0.00	0.00	0.03	0.00	0.00	0.00
Wo	42.3	41.5	42.9	43.4	42.2	41.1	42.4	44.2	44.2	43.6	44.3	44.0
En	25.6	27.7	21.0	26.7	27.4	31.1	29.9	11.4	11.0	12.4	12.3	12.0
Fs	32.1	30.8	36.1	29.9	30.4	27.8	27.7	44.4	44.8	44.0	43.4	44.0
Li ppm	0.68	2.21	1.15	2.54	1.49	1.18	4.35	2.41	3.12	4.70	1.82	4.41
Be	1.78	1.47	2.19	1.78	1.29	2.57	1.47	2.79	2.69	2.27	0.00	3.81
B	-	-	-	-	-	-	-	2.29	1.75	1.87	1.15	0.11
Sc	291	301	285	297	292	271	289	175	187	161	193	204
Ti	4228	4380	4338	4481	4675	5179	5528	3913	4071	4196	3732	3997
V	5.03	6.27	2.14	8.13	9.36	12.93	11.76	0.43	0.55	0.42	0.27	0.52
Cr	1.91	1.75	2.04	2.17	1.75	1.91	2.17	2.75	1.96	2.81	2.05	2.18
Co	3.21	3.58	2.29	3.54	3.53	5.03	4.81	1.76	1.98	1.60	1.71	2.09
Ni	0.50	0.28	0.33	0.40	0.46	0.48	0.45	0.41	0.33	0.39	0.29	0.42
Zn	182	177	224	185	193	152	171	318	317	316	321	278
Rb	0.05	0.22	0.05	0.05	0.04	0.05	0.05	0.09	0.05	0.07	0.11	0.07
Sr	7.65	7.93	4.84	8.27	8.27	10.47	10.69	3.33	3.83	3.52	3.95	3.69
Y	49.74	51.06	54.62	50.53	51.21	45.77	48.73	68.06	74.61	75.42	67.16	66.78
Zr	53.41	52.84	63.04	51.16	53.15	36.48	43.02	113	134	149	118	110
Nb	0.27	1.13	0.37	0.82	0.43	0.42	0.35	0.01	0.01	0.01	0.01	0.01
Cs	0.01	0.01	0.01	0.01	0.01	0.01	0.01	0.01	0.01	0.01	0.01	0.01
Ba	0.13	1.11	0.10	0.09	0.10	0.26	0.36	0.05	0.05	0.19	0.40	0.08
La	15.97	14.76	20.11	14.63	15.40	11.15	11.90	39.80	34.70	33.12	39.90	34.98
Ce	51.24	48.44	63.32	49.02	51.42	37.85	42.66	121	109	120	119	110
Pr	9.41	9.21	10.96	9.07	9.32	7.27	7.85	21.55	19.25	18.45	20.99	18.78
Nd	52.32	49.17	58.34	49.59	50.00	40.23	48.42	0.00	0.00	0.00	0.00	0.00
Sm	13.17	13.83	16.43	14.49	14.19	11.73	13.26	21.64	23.81	26.60	24.77	22.25
Eu	4.20	4.12	4.15	4.37	4.97	5.64	5.02	3.58	3.99	3.67	4.00	3.67
Gd	14.45	14.51	16.20	14.99	15.25	13.04	14.10	19.90	22.05	20.86	20.37	18.88
Td	1.93	2.09	2.22	2.05	2.07	1.77	2.12	2.22	2.05	2.07	1.77	2.12
Dy	12.19	12.36	13.35	11.77	12.29	11.65	11.68	16.50	18.87	17.88	17.38	17.04
Ho	2.14	2.27	2.40	2.15	2.26	1.89	2.07	3.04	3.20	3.46	2.98	2.99
Er	5.63	5.50	5.94	5.32	5.52	5.29	5.04	8.44	8.42	9.31	8.81	8.45
Tm	0.76	0.80	0.91	0.82	0.75	0.66	0.59	1.38	1.40	1.47	1.25	1.26
Yb	5.84	5.42	7.20	5.91	5.08	3.94	4.42	11.90	12.42	13.16	11.84	10.69
Lu	0.98	0.92	1.25	0.95	0.94	0.67	0.75	2.41	2.64	2.59	2.53	2.17
Hf	1.67	1.91	2.31	1.63	1.53	1.16	1.53	4.23	4.55	5.14	4.07	4.21
Ta	0.01	0.06	0.02	0.03	0.03	0.02	0.01	0.02	0.03	0.05	0.01	0.01
Pb	0.06	0.12	0.07	0.08	0.04	0.08	0.04	0.21	0.25	0.28	0.18	0.11
Th	0.01	0.09	0.03	0.02	0.03	0.05	0.02	0.01	0.01	0.01	0.05	0.02
U	0.01	0.02	0.01	0.01	0.01	0.01	0.01	0.01	0.01	0.01	0.01	0.01
Na/Ca	0.03	0.03	0.03	0.03	0.03	0.02	0.03	0.03	0.03	0.04	0.04	0.03
Zr/Th	3816	599	1984	2557	1716	763	1994	10381	13306	11871	2363	6968
Ce/Y	1.03	0.95	1.16	0.97	1.00	0.83	0.88	1.79	1.46	1.59	1.78	1.66
$(Ce/Yb)_N$	2.40	2.44	2.41	2.27	2.77	2.63	2.64	2.80	2.40	2.50	2.76	2.83
$(La/Sm)_N$	0.76	0.67	0.77	0.64	0.68	0.60	0.56	1.16	0.92	0.78	1.01	0.99
$(La/Lu)_N$	1.69	1.66	1.67	1.59	1.70	1.72	1.64	1.71	1.36	1.33	1.64	1.67
Eu/Eu*	0.93	0.89	0.78	0.90	1.03	1.39	1.04	0.53	0.52	0.48	0.54	0.55

Table 6.2 - Major elements by EMP and trace elements by LA-ICP-MS of pyroxene in selected rock samples

Rock type	Pant21b trachyte enclave " Cuddia Randazzo"					Pnt2A rhyolite pumice " Cuddia Randazzo"							
Sample	**4a**	**4b**	**4c**	**5a**	**5b**	**1a**	**1b**	**1c**	**1d**	**4a**	**4b**	**2a**	**2b**
SiO_2 wt%	48.98	48.88	48.83	48.21	49.09	48.79	49.23	49.14	48.91	49.50	48.96	48.70	49.41
Al_2O_3	0.31	0.14	0.35	0.35	0.42	0.15	0.21	0.29	0.24	0.17	0.20	0.35	0.42
TiO_2	0.61	0.41	0.62	0.59	0.59	0.41	0.54	0.58	0.48	0.46	0.50	0.61	0.77
FeO	25.82	29.60	24.09	25.25	24.55	28.42	28.96	26.82	27.68	28.26	28.61	26.87	27.44
MnO	1.25	1.33	1.29	1.41	1.40	1.43	1.44	1.37	1.36	1.34	1.40	1.48	1.61
MgO	3.37	1.16	4.10	3.60	3.95	1.41	1.56	2.60	2.02	1.76	1.66	2.73	2.78
CaO	19.55	18.31	19.91	19.61	19.89	18.45	17.62	19.18	18.70	18.86	18.62	18.72	19.54
NaO	0.80	0.38	0.64	0.74	0.65	1.43	1.44	1.37	1.36	1.34	1.40	1.48	1.61
Cr_2O_3	0.02	0.00	0.00	0.04	0.01	0.00	0.00	0.00	0.00	0.00	0.00	0.00	0.00
Wo	43.7	42.1	44.3	44.0	44.1	42.4	40.7	43.3	42.5	42.7	42.3	42.1	43.4
En	10.5	3.7	12.7	12.2	11.2	4.5	5.0	7.6	6.4	5.5	5.3	8.6	8.6
Fs	45.9	54.2	43.0	43.8	44.7	53.1	54.3	49.0	51.1	51.8	52.4	49.3	48.0
Li ppm	4.70	4.47	2.12	3.03	3.12	4.02	3.77	3.72	3.94	3.73	4.54	5.54	3.11
Be	2.17	1.99	1.24	1.82	2.82	1.04	0.00	0.47	0.00	1.54	1.33	0.67	1.23
B	1.45	2.17	0.92	1.03	0.88	1.00	0.73	0.84	1.42	1.07	1.33	1.23	1.42
Sc	153	68	202	175	195	92	87	125	121	80	72	134	136
Ti	4134	3158	4007	3987	4006	2924	2992	3533	3367	3109	3139	4328	4192
V	0.32	3.19	0.74	0.30	0.57	1.06	1.17	1.16	1.10	0.81	1.02	0.47	0.50
Cr	2.45	1.80	1.78	2.48	2.70	5.33	1.17	2.56	1.43	4.24	2.38	2.04	2.02
Co	1.47	1.45	2.03	1.77	1.69	1.29	1.17	1.44	1.28	1.05	1.38	1.52	1.65
Ni	0.38	0.44	0.28	0.30	0.39	0.19	0.19	0.22	0.23	0.23	0.36	0.42	0.26
Zn	313	331	275	307	306	320	324	333	311	341	348	308	295
Rb	0.06	0.21	0.05	0.07	0.05	0.03	0.02	0.04	0.03	0.05	0.05	0.05	0.04
Sr	3.26	5.31	3.16	3.11	3.61	3.15	3.63	3.66	3.50	3.58	3.50	2.91	3.19
Y	80.78	114	64.25	71.83	69.85	108	107	103	102	103	104	91	94
Zr	154	634	108	134	128	325	328	252	256	269	262	201	190
Nb	0.01	0.01	0.01	0.01	0.01	0.85	1.05	0.87	0.95	0.89	0.77	1.03	1.04
Cs	0.01	0.01	0.01	0.01	0.01	0.01	0.02	0.01	0.01	0.01	0.01	0.01	0.01
Ba	0.14	0.20	0.03	0.08	1.10	0.04	0.03	0.04	0.09	0.03	0.04	0.06	0.07
La	50.68	98.02	32.17	38.48	41.76	75.64	81.00	69.72	70.82	73.06	71.17	55.96	60.39
Ce	148	301	103	108	110	214	233	191	198	211	210	163	174
Pr	24.85	51.21	17.11	18.59	20.49	35.99	37.94	32.51	33.34	34.84	34.55	26.60	28.31
Nd	0.00	0.00	0.00	92.78	0.00	169	181	152	157	168	165	130	141
Sm	27.36	49.45	20.88	24.22	23.83	38.40	39.22	35.89	34.96	37.95	37.36	29.63	33.53
Eu	4.05	5.97	3.63	3.74	3.60	5.79	5.42	4.99	4.80	5.38	5.11	4.67	4.68
Gd	24.45	38.99	18.02	20.21	19.64	32.35	31.27	31.68	30.71	32.21	31.90	26.85	27.74
Td	1.93	2.09	2.22	1.93	2.09	4.44	4.32	4.02	4.27	4.24	4.28	3.58	3.80
Dy	20.29	30.76	15.26	17.05	17.14	27.02	26.91	24.30	24.65	26.34	25.73	22.40	23.72
Ho	3.61	5.55	2.82	3.41	3.26	4.83	4.94	4.43	4.54	4.56	4.76	3.99	3.94
Er	9.42	15.34	7.38	9.25	8.28	13.98	13.86	11.86	12.31	12.63	13.34	10.83	11.37
Tm	1.55	2.62	1.16	1.40	1.43	2.33	2.39	2.20	2.05	2.15	2.18	1.90	1.80
Yb	13.47	25.01	9.99	11.76	11.43	20.61	19.89	18.72	18.55	20.09	10.21	15.69	14.81
Lu	2.79	5.43	1.95	2.50	2.42	4.42	4.25	3.86	3.96	4.19	4.34	3.26	3.21
Hf	5.31	20.59	3.34	4.77	4.44	9.78	10.15	7.71	7.79	7.49	7.43	6.84	6.42
Ta	0.03	0.06	0.03	0.01	0.05	0.05	0.04	0.02	0.03	0.02	0.02	0.03	0.04
Pb	0.16	0.23	0.13	0.14	0.19	0.20	0.16	0.26	0.24	0.32	0.29	0.45	0.20
Th	0.03	0.07	0.01	0.01	0.01	0.00	0.02	0.01	0.02	0.01	0.02	0.01	0.03
U	0.01	0.02	0.01	0.01	0.01	0.00	0.01	0.01	0.00	0.01	0.01	0.01	0.01
Na/Ca	0.04	0.02	0.03	0.03	0.03	0.05	0.05	0.04	0.03	0.04	0.04	0.04	0.03
Zr/Th	5402	8609	11024	10041	14251	6084	10202	7284	9574	6084	10202	7284	9574
Ce/Y	1.84	2.64	1.62	1.51	1.58	1.38	1.52	1.32	1.30	1.38	1.52	1.32	1.31
$(Ce/Yb)_N$	3.02	3.29	2.84	2.52	2.63	3.21	2.86	2.38	2.34	3.21	2.86	2.38	2.34
$(La/Sm)_N$	1.17	1.25	0.97	1.00	1.10	1.78	1.98	1.87	1.86	1.81	1.70	1.78	1.95
$(La/Lu)_N$	1.89	1.87	1.71	1.60	1.77	1.24	1.30	1.22	1.28	1.21	1.20	1.19	1.13
Eu/Eu*	0.48	0.42	0.57	0.52	0.51	0.50	0.47	0.45	0.45	0.47	0.47	0.51	0.47

Table 6.2 - Major elements by EMP and trace elements by LA-ICP-MS of pyroxene in selected rock samples

CHAPTER 7

SECTION 1 : DISCUSSION

The discussion of this first section is divided in two main parts:

- first we deal with the origin of the rock with benmoreitic composition and discuss about the occurrence of the Daly gap at Pantelleria;

- in the latter part we discuss the characteristics of the trachytes and we make inferences on possible petrogenetic processes leading to the origin of their geochemical differences. We also use QUILF and MELTS algorithms to give chemical-physical parameters driving the evolution of the trachytic magmas and investigate their possible petrogenetic origin and their relationships with peralkaline rhyolites. This part will be further investigated through experimental studies in the next section.

7.1 Sample with benmoreitic composition

Petrography and mineral chemistry of the sample benmoreitic in composition, collected at the top of the trachytic lava pile, clearly show distinct mineral paragenesis, summarized in the following:

(i) A trachytic paragenesis includes augitic clinopyroxene Fs_{25-28}, olivine Fo_{54-56} and oligoclase, mainly found as phenocrysts or as cores in phenocrysts.

(ii) Several phenocrysts with less evolved composition include Mg-rich olivine (up to Fo_{84}), diopside-augite pyroxene ~Fs_{10-14} and andesinic plagioclase. As a whole, these compositions pertain to less evolved magmas.

(iii) A third group of minerals is mainly found in the groundmass and rims of the phenocrysts. They show intermediate composition including diopside-augite Fs_{11-18} and olivine Fo_{54-64}.

These data indicate that the benmoreitic sample does not represent a real intermediate magma originated by fractional crystallization of Pantelleria basalts, but it is the result of a mixing process between mafic magmas and trachytes. Microlites and microphenocrysts in the groundmass with intermediate compositions grew during and

after the mixing events, from an intermediate melt resulting from the mixing itself. The presence of the intermediate compositions only as microlito/microphenocrysts and rims on large phenocrysts inherited from the two different end members suggests a short of time elapsed between the mixing event and the eruption of the mixed magma. Likely, the intrusion from depth of mafic magma into the trachytic magma body acted as a trigger of the effusive eruption.

Phenocrysts of clinopyroxene Fs_{14} in the "benmoreitic" sample has the same trace elements chemistry than the pyroxene from Cuddie Rosse scoriae (Fig. 6.2). In particular REE trace trends are basically superposed (Fig. 6.3), suggesting an origin from low TiO_2-P_2O_5 basalts erupted in the past 50 ka at Pantelleria (Civetta et al., 1998). While, olivine Fo_{84} has never found in the alkali basalts from Cuddie Rosse (Fo_{73-79}) and points to slightly less evolved melts.

One of the most relevant points regards the statement of previous Authors who affirmed that basaltic magmas have been erupted only outside the caldera rim in the past 50 ka period (Mahood and Hildreth, 1986; Civetta et al., 1988, 1998). The study of this lava sample, for the first time, testifies to the eruption of basaltic magmas inside the caldera, even if as mafic end member in mixed products. As a result the analyzed mixed lava gives evidences that basaltic magmas were intruded into the trachytic magma bodies below the caldera. Finally, it can be regarded as a physical evidence of a strict relationships between basaltic and trachytic magmas.

Based on the composition of the pyroxene, the mafic magma which mixed with the trachytic residing magma has basically the same chemistry as the magmas which fed the basaltic eruption in the NW part of the island over the same range of time. Accordingly, the age of Cuddie Rosse has been assessed at around 20.000 years and the analyzed mixed sample is one of the younger products of the Montagna Grande lava pile, dated between 20.000 and 30.000 years (Mahood and Hildreth, 1986; Civetta et al., 1984, 1988). According to Gioncada and Landi (2010), the post caldera mafic magmas are not real primitive products. Episodes of magma ponding and crystallization occurred in the upper crust prior to eruption, at pressure of around 2 kbars (~7 km).

Among the analyzed rocks, another evidence of mixing between mafic and more evolved trachytic magmas is given by the less evolved trachytic sample collected in the

northern sector of Montagna Grande (Pan0750, Montagna Grande Nord). This sample hosts minerals with the typical composition of those of the trachytes (anorthoclase, clinopyroxene Fs_{23-28}, olivine Fo_{38-40}) together with less evolved clinopyroxene Fs_{16-18} and plagioclase, from andesine to labradorite, surrounded by rims with anorthoclasic composition. It suggests that the poorly evolved composition of this trachytic sample is the result of a mixing event between more evolved trachytes and minor quantity of less evolved magmas. Interestingly, the pyroxene Fs_{16-18} was also found as microphenocrysts in the "benmoreitic" sample and is associated with melts with intermediate composition (likely benmoreite).

As a whole, previous data confirms that intermediate magmas were not erupted at Pantelleria and a large compositional gap exists between basaltic products (SiO_2 ~ 48 wt %) and trachytic rocks (SiO_2 ~ 64 wt %). Rocks with intermediate composition always show evince of mixing between trachytes and less evolved magmas. Trace of compositions intermediate between the two end members are only found as sporadic crystals (e.g. clinopyroxene Fs_{16-18}) in mixed products.

The origin of the Daly gap at Pantelleria and other similar volcanic systems remains a controversial as well as an amazing argument. Data presented here can't resolve this magmatological puzzle. However we can participate to the discussion on the Daly gap origin giving some suggestions mainly based on mineralogical data.

The occurrence of rocks originated by mixing between mafic and trachytic magmas proves that basaltic melts, possibly rising from depth of 6-8 km, participate to the evolution of the trachytic magma. We can assume a magma ponding zone at shallow levels in the crust, likely at pressure between 1.0 and 1.5 kbars (see below - MELTS calculations and Experimental Results), where chemical-physical conditions force the magmas towards trachytic compositions. When a large trachytic magma body is formed, periodic or continuous intrusions of small batches of deeper mafic magmas maintain active the system. The intrusion of mafic magmas into the trachytic magma body leads to mixing processes between the two end members resulting in melts with intermediate composition, from which crystallize minerals with intermediate characteristics, possibly producing benmoreitic cumulates. In this context, the production of intermediate melts has to be regarded as a transitional event strictly associated with a mixing event.

Following this idea, intermediate magmas (as discrete magma body) effectively do not exist in the magma system feeding the Pantelleria volcanism.

7.2 The trachytes

Bulk rock compositions of the trachytes highlight the occurrence of two different groups, mainly differing in the contents of incompatible trace elements (Figs. 4.2, 4.3 and 4.4): metaluminous trachytes with relatively high ITE (Samples from Montagna Grande Sud and Case Ricco), corresponding to the HITE trachytes of White et al. (2009), and weakly peralkaline trachyte with lower ITE (member E of the Green Tuff and trachyte enclaves in Cuddia Randazzo deposits). In the last group, two samples (trachytic enclave Pant23 and member E of the Green Tuff pan0731) show very high contents of Ba (1940-2160 ppm).

The sample from Mueggen is a more evolved trachyte, close to rhyolitic composition. In the rocks analysed in this work, Low ITE metaluminous trachytes (White et al., 2009) are not found.

Similarly, trace elements in clinopyroxene depict two different trend differing in the content of several ITE elements, the pyroxene hosted in HITE trachytes showing higher contents of ITE. Moreover, pyroxene from the Mueggen sample, the most evolved trachyte belonging to the high ITE pyroxene group, show REE higher than those of the rhyolitic sample from Cuddia Randazzo (Fig. 6.3).

According to White et al. (2009), the coarsely porphyritic texture of some Ba-rich trachytes suggests a significant role of crystal accumulation, in particular alkali feldspar. However, the two Ba-rich trachytes from Cuddia Randazzo and the top of the Green Tuff show several characteristics which contrast with an origin from trachytic magmas via feldspar accumulation. In detail:

- accumulation of feldspar in metaluminous HITE trachytes is not consistent with major element chemistry (Fig.7.1). Addition of anorthoclasic feldspar implies increasing of Al_2O_3 and SiO_2, while Ba-rich samples show lower content of these elements. Also trends of alkalies are not strictly consistent with an accumulation process. If the less evolved trachyte (0750) is taken as initial magma, accumulation of about 60 wt % of feldspars could produce the Ba-rich trachytes at the top of the Green

Tuff (0731). In this case the chemical difference could be the result of mixing with mafic magmas and feldspar accumulation. But, the quantity of feldspars it not consistent with the crystal content of the Ba-rich samples (25-35 wt %).

- the minerals of the Ba-rich trachytes show composition slightly less evolved than those of the peralkaline trachytes with similar composition (Figs.5.18-5.19). The clinopyroxene show lower ITE (e.g. Yb, Y, Zr, Lu) and REE contents than those of the other trachytes and does not show the negative Eu anomaly which characterize the pyroxenes of the other trachytic samples (Figs. 6.2-6.3). A possible hypothesis is that Ba-rich trachytes represent slightly less evolved terms of the Low-ITE peralkaline group. The negative Eu anomaly in clinopyroxene suggest a minor involvement of plagioclase in the evolution of this group of magmas.

According to previous authors, H-ITE metaluminous trachytes can derive from hydrous transitional basalts via fractional crystallization and produce comenditic trachytes and rhyolites as crystallization proceeds (Civetta et al., 1998; Avanzinelli et al.,2004; White et al., 2005, 2009). However, the mineralogical data and the distribution of trace elements in clinopyroxene presented in this work do not exclude the existence of two distinct groups of trachytes (metaluminous H-ITE and peralkaline L-ITE) with different origin, possibly producing slightly different rhyolitic magmas.

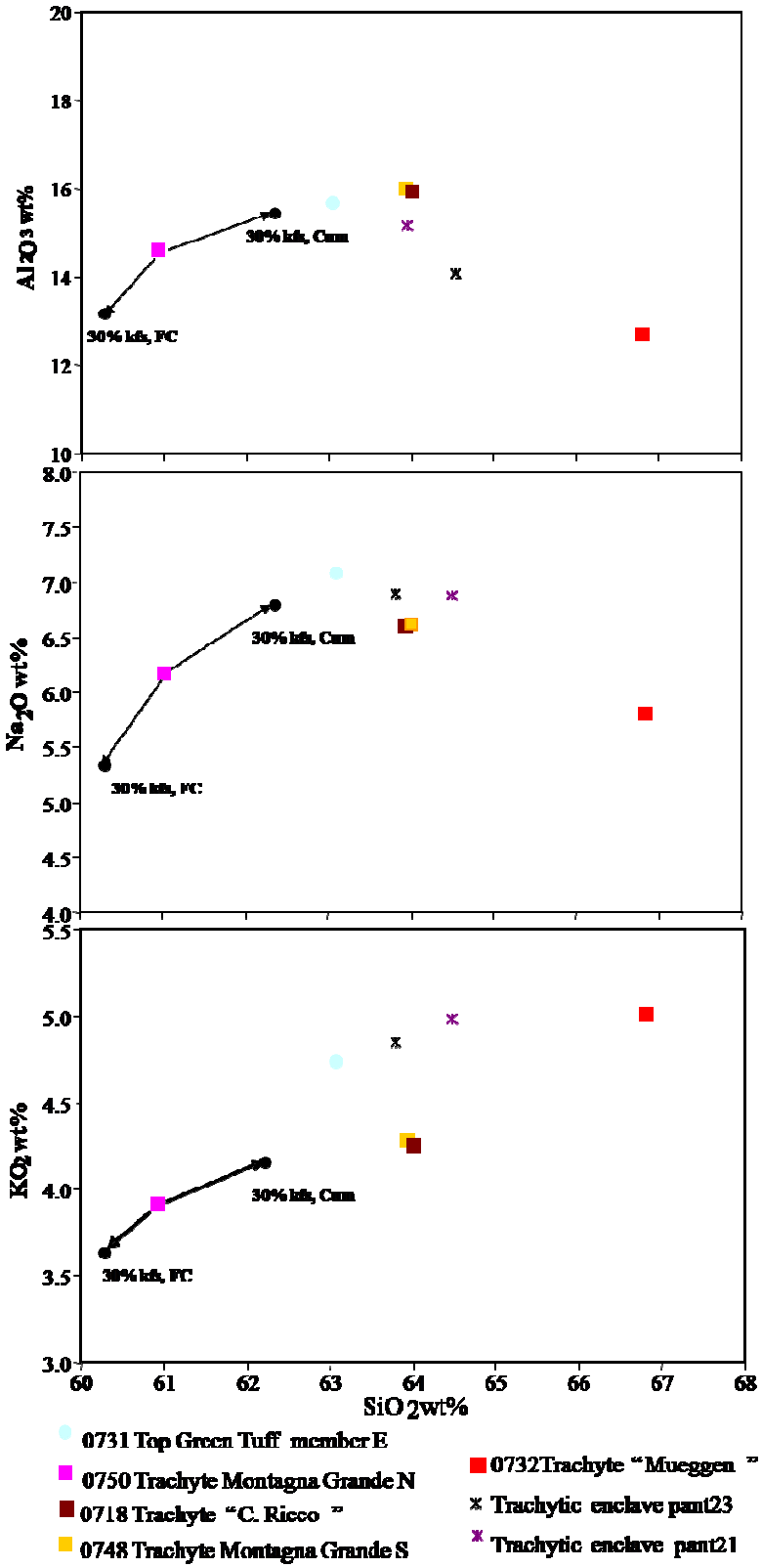

Fig. 7.1 The black arrows show the variation of liquid composition after 30 % of removal (FC) and accumulation (Cum) of anorthoclase feldspar.

7.3 Geothermometry

7.3.1 Pantelleritic magma pre-eruptive conditions

The aim of this section is to define a set of pre-eruptive conditions (*P-T-fO_2 H_2O_{melt}*) for the different rock-types object of this study. This purpose will be achieved basically with two methods: (1) classical geothermobarometric methods such as those involving equilibrium of Fe-Ti oxides and other mineral phases (e.g. the QUILF95 geothermometer) and (2) MELTS code (liquidus Temperature, liquid line of descent).

1) The QUILF thermobarometer has been used in applications involving iron-rich, reduced rocks (Marks and Markl, 2001; White et al., 2005).

Values for intensive thermodynamic parameters were determined with the use of QUILF 95, a program written for Windows 95 that evaluates phase equilibria in the in the QUILF system (i.e. quartz, clinopyroxene, ilmenite, magnetite, fayalite).

Fe-Ti oxides geothermometry: whenever magnetite and ilmenite coexist in the same specimen groundmass we are allowed to apply (Spencer and Lindsey 1981, 1988) in order to derive pre-eruptive T and fO_2.

In the studied samples, ilmenite is scarce compared to Ti-magnetite and rarely both occur within the same thin section, limiting the number of geothermometry calculations. Ideally, oxide pairs should show evidence of textural and chemical equilibrium.

2) MELTS-algorithm (Ghiorso and Sack, 1995; Asimow and Ghiorso, 1998) is widely used to calculate equilibrium phase relations in igneous systems.

MELTS computes phase equilibrium relations by minimization of Gibbs energy given a bulk composition, temperature, pressure, and oxygen fugacity.

To model fractional crystallization, MELTS first determines the liquidus temperature and liquidus phase for the bulk composition and specified parameters. Mineral phases are then subtracted and a new liquid composition is calculated, then the temperature is lowered by 5°C.

MELTS then calculates a new equilibrium phase assemblage, and the process repeats until the solidus temperature, or a temperature specified by the user, has been reached. The whole liquid line of descent is thus calculated.

7.3.2 Mineral assemblages

The trachytic samples are porphyritic, with phenocryst contents ranging from 25 to 35 vol.% (Table 3.1). The principal textural difference between trachytes is that the matrix of trachytes is holo- or hypo-crystalline, while the pantellerites are predominantly glassy.

Intracaldera Trachyte lavas gave the conditions reported below:

- Primitive trachyte, Montagna Grande Nord (sample pan0750), the assemblage fayalite (XFo $_{=}$ 0.437) + ilmenite (XIlm $_{=}$ 0.919) + magnetite (XMt = 0.302) with clinopyroxene Ti-augite (XWo $_{=}$ 0.466 - XEn = 0.439) characterizes trachyte with lower agpaitic index (AI = 0.99), fO_2 around ΔFMQ = - 0.64, and high temperature (973 °C).

- Intermediate trachyte, Montagna Grande Sud (sample pan0748), the assemblage fayalite (XFo $_{=}$ 0.269) + ilmenite + magnetite (XMt = 0.322) with augite (XWo $_{=}$ 0.418 - XEn = 0.285) characterizes trachyte with agpaicity (AI = 0.98), fO_2 around ΔQFM = - 0.74, (ΔFMQ = fO_2 log units below/above the fO_2 defined by the FMQ buffer) and relatively high temperature (870 °C).

- Intermediate trachyte, Case Ricco (sample pan0718), the assemblage fayalite (XFo $_{=}$ 0.224) + ilmenite + magnetite (XMt = 0.322) with augite (XWo $_{=}$ 0399 - XEn = 0.265) characterizes trachyte with agpaicity (AI = 0.98), fO_2 around ΔQFM = - 0.89, (ΔFMQ = fO_2 log units below/above the fO_2 defined by the FMQ buffer) and relatively high temperature (820 °C).

- Evolved trachyte, Mueggen (sample pan0732), the assemblage fayalite (XFo $_{=}$ 0.094) + ilmenite + magnetite (XMt = 0.302) with augite (XEn $_{=}$ 0.145 - XWo = 0.408) characterizes trachytes with agpaicitic index (AI = 1.18), fO_2 around ΔFMQ = - 1.00, and with a temperature (792 °C).

Comenditic trachyte inclusions gave the conditions reported below:

- Primitive trachytic enclave C. Randazzo (sample pant23), with the assemblage fayalite (XFo $_{=}$ 0.207) + ilmenite + magnetite (XMt = 0.227) with Fe-augite (XEn $_{=}$ 0.237 - XWo = 0.420) characterizes trachyte with agpaicity (AI = 1.07), fO_2 around ΔFMQ = - 0.77, and high temperature (895 °C).

- Evolved trachytic enclave C. Randazzo (sample pant21), with the assemblage fayalite (XFo = 0.116) + ilmenite + magnetite (XMt = 0.393) with augite (XEn = 0.158 - XWo = 0.438)characterizes trachytes with agpaicity (AI = 1.19), fO_2 around ΔFMQ = - 0.75, and relatively low temperature (881 °C).

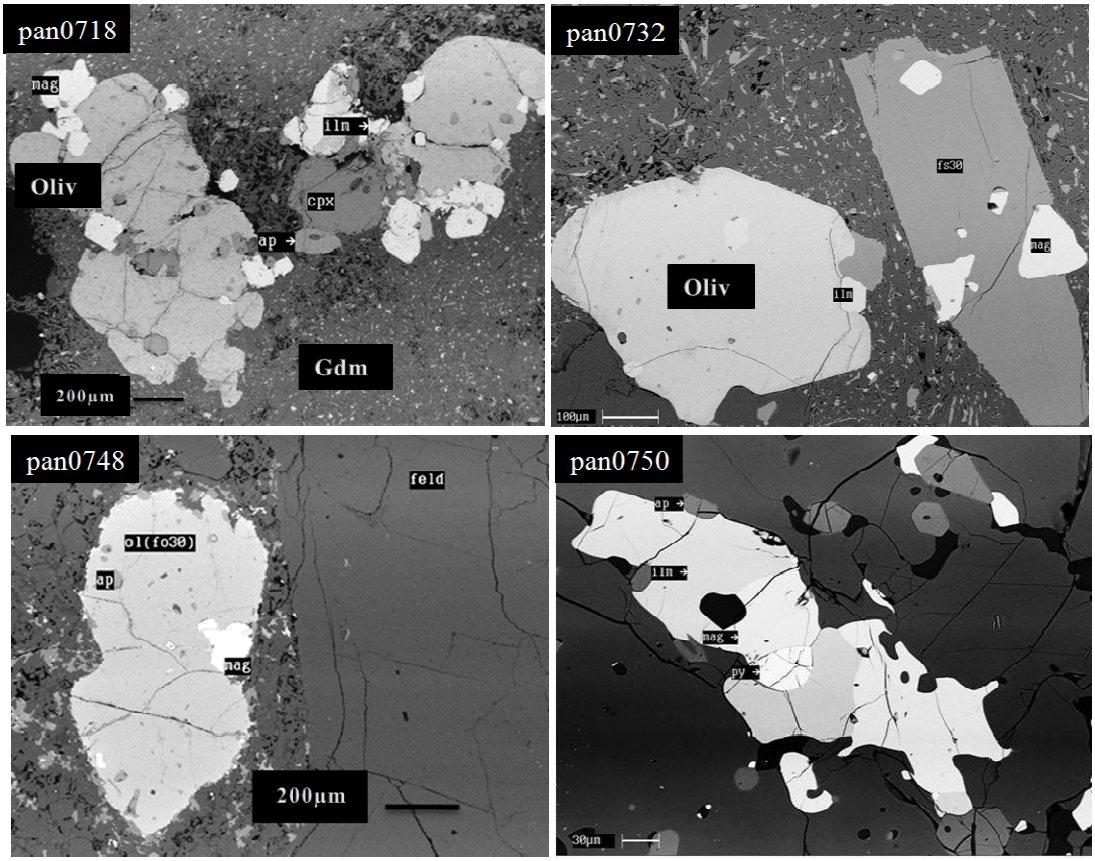

Fig. 7.2. Mineral assemblages of the investigated samples from trachyte flows, phenocrysts are in glassy groundmass in all.

7.3.3 Application of the QUILF thermobarometer

With QUILF95, temperature (T) is calculated based on Fe–Mg–Ca exchange between clinopyroxene and olivine from the following reactions:

$Mg_2SiO_4 + Fe_2Si_2O_6 = Fe_2SiO_4$
$+ Mg_2Si_2O_6$(FeMgOlAug),

$Fe_2SiO_4 + CaFeSi_2O_6 = CaFeSiO_4$
$+ Fe_2Si_2O_6$(FeCaOlAug); and

$Mg_2SiO_4 + CaMgSi_2O_6 = CaMgSiO_4$
$+ Mg_2Si_2O_6$(MgCaOlAug).

Temperature determined from clinopyroxene–olivine equilibria is strongly pressure (P)-dependent, as is silica activity ($aSiO_2$), which varies inversely with P. Thus, if either $aSiO_2$ or P is fixed, the other may be calculated if T is known with QUILF from the following reactions:

$Mg_2Si_2O_6 = Mg_2SiO_4 + SiO_2$(MgOlQAug); and
$Fe_2Si_2O_6 = Fe_2SiO_4 + SiO_2$(FeOlQAug).

Oxygen fugacity (fO_2) can be calculated from equilibrium between fayalite, quartz, and the highly dilute hematite component in ilmenite if T, P, and a_{SiO_2} are known:

$$2Fe_2SiO_4 + O_2 = 2Fe_2O_3 + 2SiO_2(FHQ)$$

The assemblage of Ilmenite + Ti-magnetite + Fe-rich olivine + clinopyroxene and quartz, allowed to apply QUILF equilibria to derive temperature and fO_2 of the magma:

Oxygen fugacity fO_2 can be calculated from equilibrium between fayalite, quartz and the highly dilute hematite component in ilmenite provided that if T, P and a_{SiO2} are known:

$$3Fe_2SiO_4 + O_2 \rightleftharpoons 3SiO_2 + 2Fe_3O_4$$

$$K_{FMQ} = (a^{Fe3O4}{}_{mt})^2 * (a^{SiO2}{}_{qz})^3 / (a^{Fe2SiO4}{}_{ol})^3 * fO_2$$

7.3.4 QUILF results

All the rocks vary within three logarithmic unities below the buffer reaction FMQ in the diagram log fO_2 vs T (°C) (fig.7.2), field rather reduced.

QUILF95 all results were calculated at 1 kbar of pressure, temperature from metaluminous trachyte range from 980 to 780 °C at relative oxygen fugacities fO_2 from -0.60 to -2.65 log units below (ΔFMQ) the fayalite-magnetite-quartz buffer FMQ.

Table 7.1 QUILF. All results are calculated at P = 1500 bar.

		Spinel			Ilmenite			Olivine		Augite		Results			
Sample:		**N-Ti**	**N-Mg**	**N-Mn**	**Hem**	**Gk**	**Py**	**Fo**	**La**	**En**	**Wo**	**T (°C)**	**log fO_2**	**DFMQ**	**SiO_2(Q)**
Intracaldera Trachyte Lavas															
PAN0750	Input	0.685	*0.092*	*0.041*	0.070	0.103	0.030	*0.403*	0.007						
	Calc		0.123	0.032				0.437				973	-11.90	-0.64	0.64
PAN0748	Input	0.668	*0.064*	0.047				0.269	0.007	*0.281*	0.418				
	Calc		0.055							0.285		890	-13.78	-0.74	0.78
PAN0718	Input	0.650	*0.046*	0.044				0.224	0.005	*0.302*	0.399				
	Calc		0.039							0.265		820	-14.61	-0.57	0.89
PAN0732	Input	0.682	*0.015*	*0.053*				0.094	0.007	*0.167*	0.408				
	Calc		0.016							0.145		792	-15.47	-0.84	~1.00
Comenditic Trachyte Inclusions															
Pant23	Input	0.695	*0.035*	0.032				0.207	0.010	*0.230*	0.420				
	Calc		0.046							0.237		895	-13.61	-1.03	0.79
Pant21	Input	0.763	*0.018*	0.056				0.099	0.014	*0.150*	0.438				
	Calc		0.020							0.139		873	-14.62	-1.63	0.77

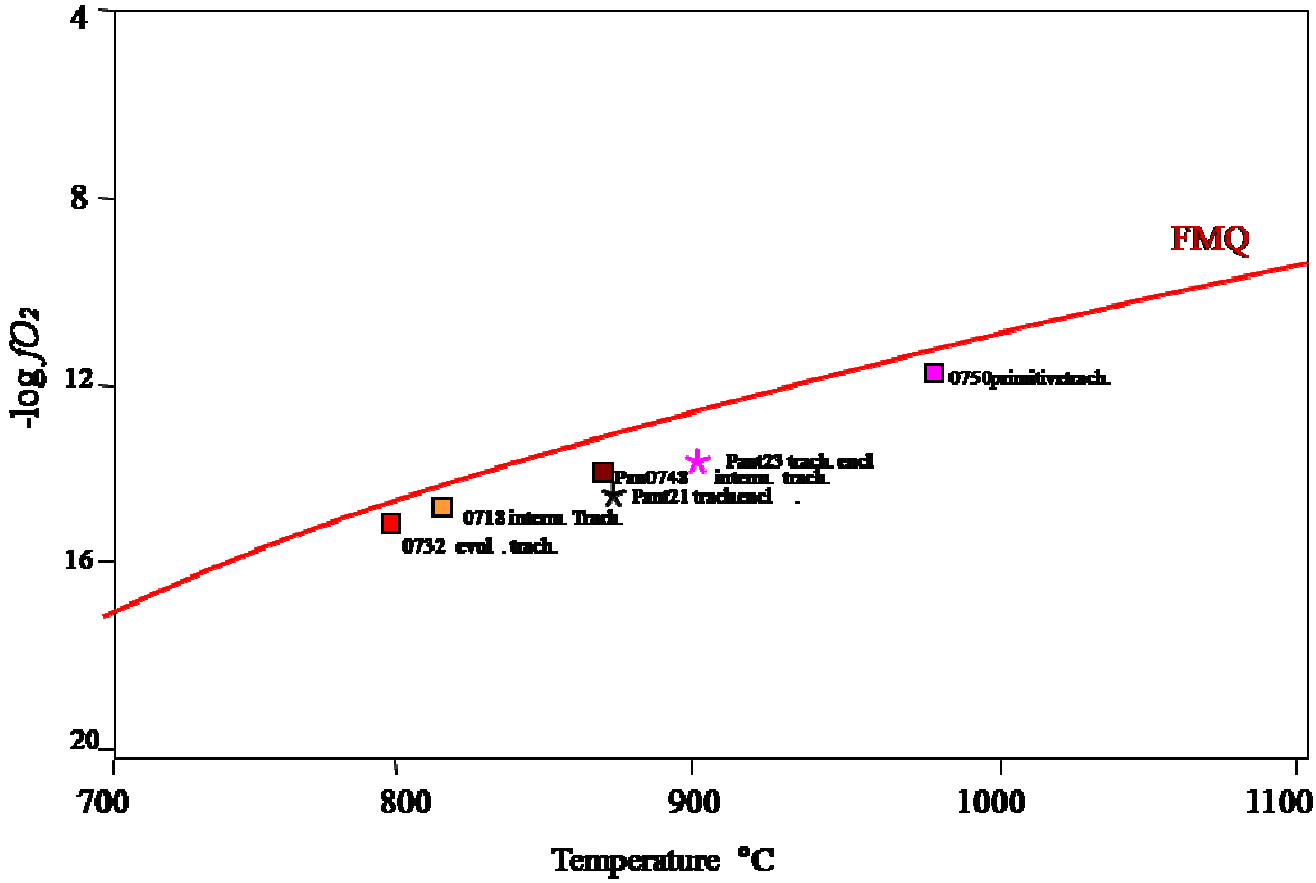

Fig. 7.3 T-fO_2 relationships as determined by QUILF calculations. Note the good fit between magma evolution (phenocrystals assemblage) and declining Temperature.

7.4 Thermodynamic models: modelling the liquid evolutive paths

7.4.1 Basalts to pantellerites

The results of a total of 12 models of fractional crystallization (FC), from basalt to pantellerite, are presented in Figs 7.4 -7.5 -7.6. For each process several trials were made, and only a strict selection is shown here playing with:

- water contents (0.5, **1.0**, **1.5** H_2O wt %), two fO_2 condition (**FMQ-1** and FMQ-2), and two pressures (1 - 2 kbar).

For all the models, temperature was decreased incrementally from a super liquidus trial at 1200 °C. Sample Pan2 "C. Rosse" was selected to represent the parent basaltic magma composition.

The two trials are considered the best fitting:

i. Trial (5) at lower starting water contents is 1.0, olivine is the liquidus phase, with the temperature 1150 °C (QFM-1);

ii. Trial (3) at lower starting water contents is 1.5, olivine is the liquidus phase, with the temperature 1125 °C (QFM-1).

The MELTS models of low pressure (1-2 kbar) fractional crystallization of transitional basalt with 1.0 -1.5 wt % H_2O at oxygen fugacities between FMQ-1 predict that trachyte with agpaitic index between 0.97 and 1.22, water contents between 2.47 and 3.66 wt %, and a temperature between 950 and 990 °C will be produced after 60 - 70 % crystallization (F = 0.40-0.30).

These results are in agreement with temperatures and oxygen fugacities calculated from mineral equilibria in the observed metaluminous trachyte lavas (970 to 870 °C at FMQ-1.0) but produce slightly more alkaline trachyte magmas, where the peralkalinity indices is 0.98-0.99.

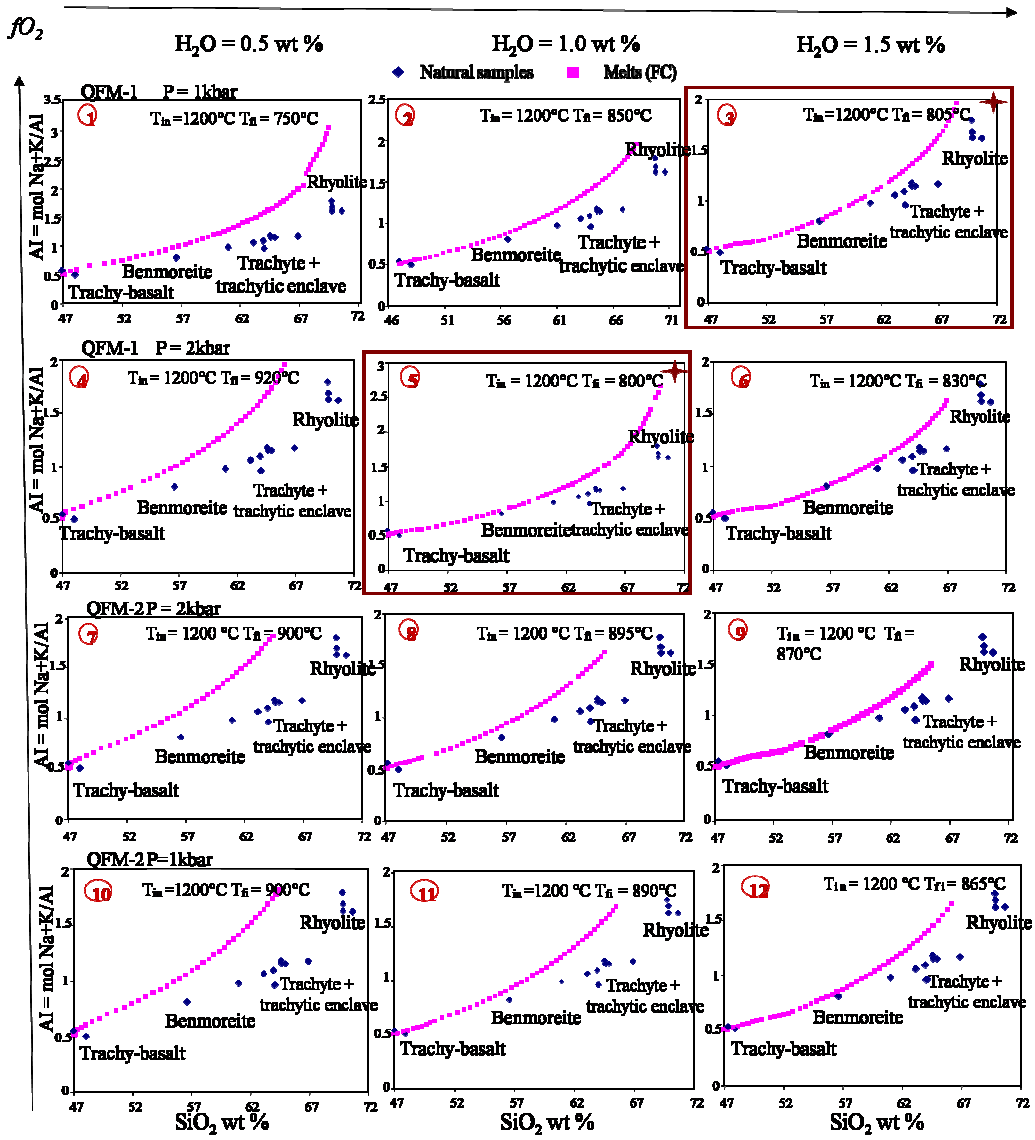

Fig.7.4 results of MELTS modelling from basalt to pantellerite. fO_2 increases from bottom to top, and H_2O_{melt} from left to right. Trials with contour are considered the best fitting.

The two trials obtained at fO_2 QFM-1, $H_2O_{starting\ melt}$ 1.5 wt %, P = 1.0 kbar and fO_2 QFM-1, $H_2O_{starting\ melt}$ 1 wt %, P = 2.0 kbars (3 and 5 in Fig. 7.4) are considered to be the best results .

According to White et al., (2009) Melts calculations predict an origin of the trachytes from basaltic melts at 1-1.5 H_2O wt % via fractional crystallization. The differences in AI and contents of some major elements (in particular Na_2O and FeO) observed between Melts results and natural rhyolitic samples (Figs. 7.5 and 7.6) can be due to the peculiar composition of the mineral phases of the pantelleritic rocks, non completely considered by the Melt code.

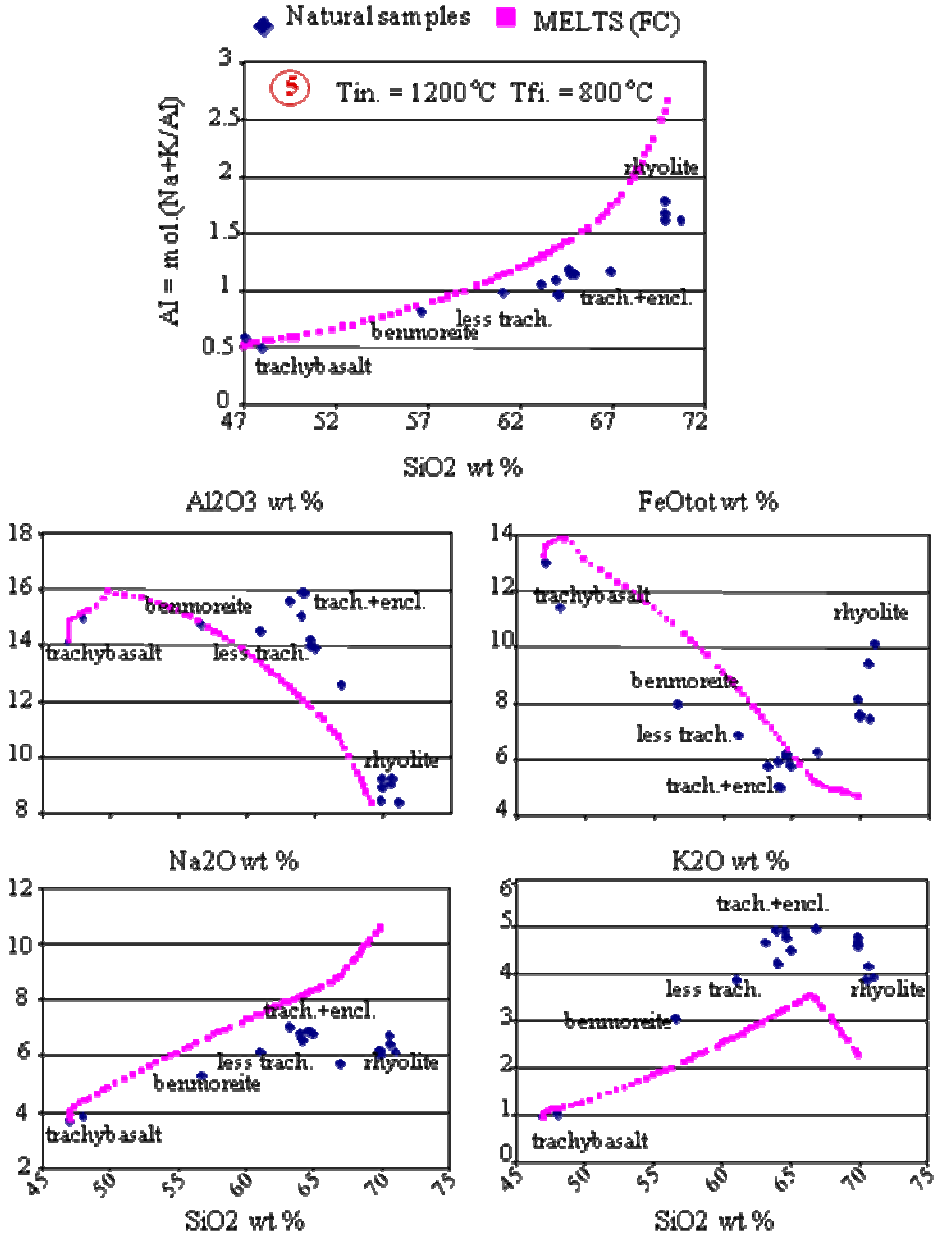

Fig. 7.5 Detailed analyses for major oxides and liquid line of descent (LLD) for trial (3) of fig7.3. Agpaitic Index and oxides anhydrous.

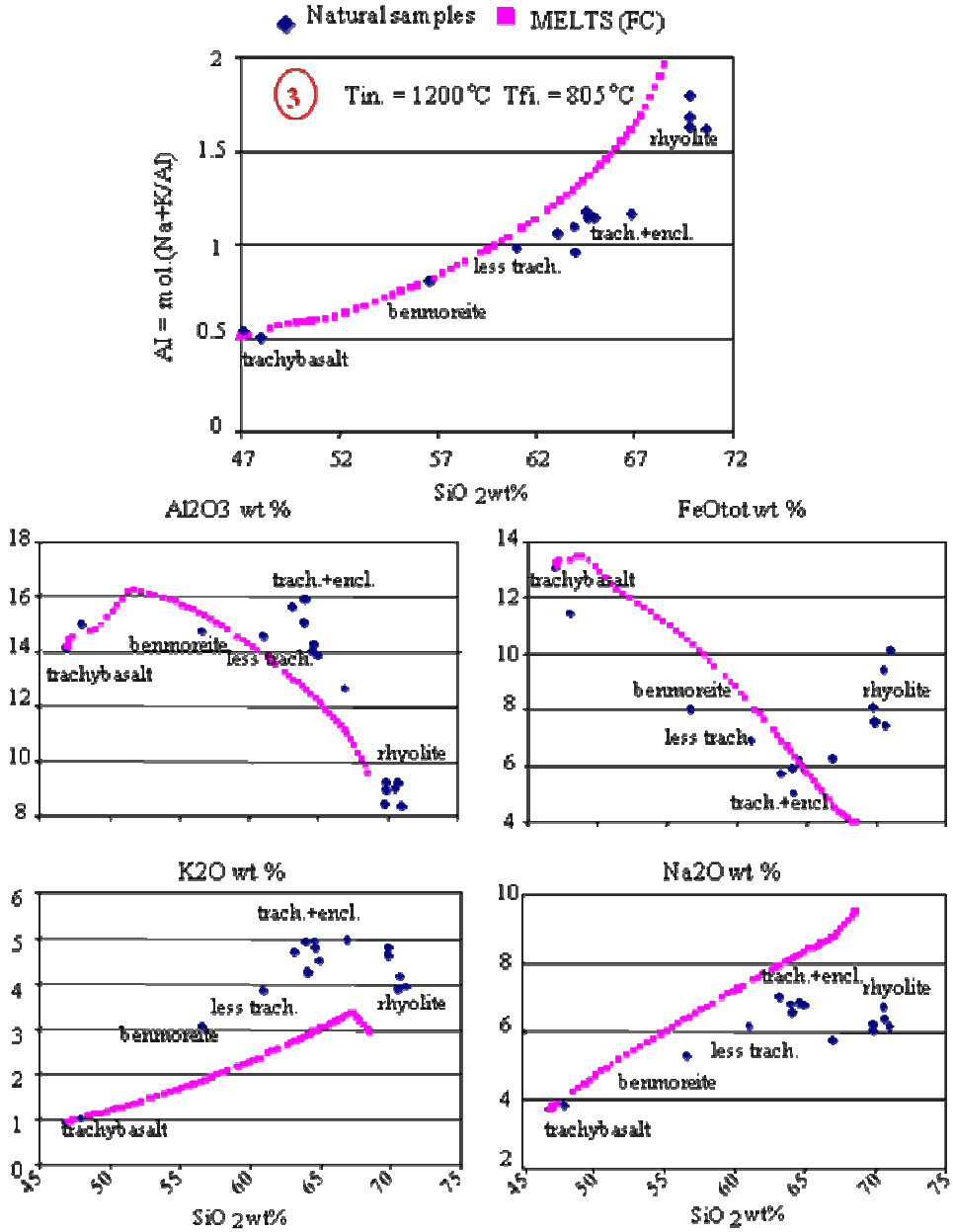

Fig. 7.6 Detailed analyses for major oxides and liquid line of descent(LLD) for trial (5) of fig7.3. Agpaitic Index and oxides anhydrous.

7.4.2 Trachytes to pantellerites

The results of 8 models of fractional crystallization are presented in Figs. 7.7.

There are models that vary between starting water contents (1.0, 3.0, 4.0 wt %), two oxygen buffers (FMQ-1 and FMQ-2), and two pressures (1-2 kbar).

For all models, temperature decreased incrementally from a super liquidus at 950°C. Sample Pan0718 trachyte "Case Ricco" was selected to represent the parent metaluminous magma composition.

Trials performed at QFM-2 give temperatures of the final melts very high, > 800°C, which are not consistent with the temperature suggested for pantelleritic melts by experimental studies (Di Carlo et al., 2010) (Fig. 7.6). Trials obtained at fO_2 QFM-1, $H_2O_{starting\ melt}$ 3 wt % and P from 1.0 to 2.0 kbars, H_2O_{melt} (3 and 5 in Fig. 7.4) are considered to be the best results, suggesting that the more evolved pantelleritic melts can be originated from hydrate trachytic magmas by crystal fractionation in shallow magma chambers

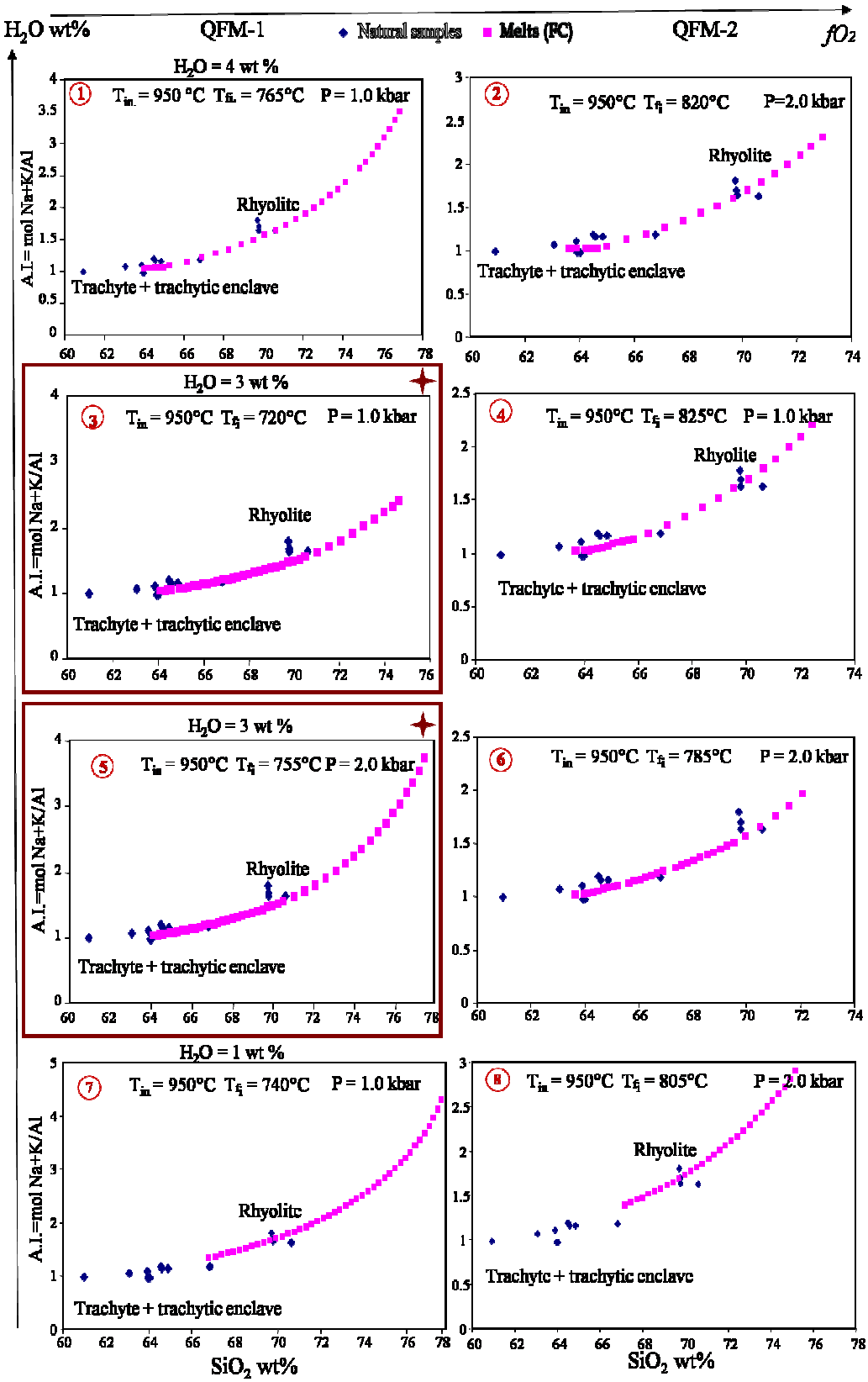

Fig.7.7 results of MELTS modelling from trachyte to pantellerite. H_2O_{melt} increases from bottom to top, fO_2 from left to right. Trials with contour are considered the best fitting.

CHAPTER 8

Experimental Petrology

The reasons that suggested to begin a high pressure, high temperature experimental petrology study are multiple and are briefly outlined below:

- although a knowledge of pre-eruptive conditions (T, P, H_2O_{melt}, fO_2) of trachyte magma, is reasonably assessed by mineral melt equilibria (e.g. White et al. 2005, 2009), tighter constraints are likely to be given by experiments;
- in the past years, and still in progress, a considerable effort has been made to experimentally define pre-eruptive conditions on Pantelleria end member magmas, basalts (Buccheri et al., in preparation) and pantellerites (Di Carlo et al. 2010), and we wish to fill the gap by investigating trachytes.
- the intermediate magmas (i.e. trachytes) are the sole lacking to fully portray the magmatological scenario. This is particularly important also to possibly shed, some light on the origin and significance of the Daly Gap, interpreted in the light of phase equilibria.
- simulation of the liquid line of descent (i.e. the evolution direction of residual progressively trachyte magmas) of hydrous magnas is always more precisely constrained by experiments rather than with computer codes (e.g. Melts).

8.1 The starting material for crystallization experiments

The sample chosen for crystallization experiments is an intermediate trachytic lava (pan0718, see pag.47). It is a strongly porphiritic rock (crystals = 35-40 vol.%) with a microcrystalline groundmass. Silica and potassium content are 64.0 wt % and 4.2 wt% respectively. It has low TiO_2 (0.7 wt %) and relatively high CaO (1.9 wt %) and Al_2O_3 (15.9 wt %) contents.(**Tab. 8.1**).

	Whole rock:	Clinopyroxene pheno	Olivine pheno	Alkali-feldspar pheno	Fe-Ti oxide	Amphibole gdm	Aenigmatite gdm
SiO_2	64.03	51.25	31.21	65.41	0.35	51.54	42.61
TiO_2	0.76	0.55	-	-	22.39	2.33	7.70
Al_2O_3	15.92	0.57	-	21.26	1.21	1.01	0.52
$FeO_{(tot)}$	5.05	15.63	54.24	0.16	69.49	26.37	40.31
MnO	0.19	1.01	2.78	-	1.35	0.78	1.15
MgO	0.52	10.18	10.80	-	0.80	6.37	0.40
CaO	1.89	20.51	0.47	1.75	0.00	5.60	0.16
Na_2O	6.60	0.30	-	8.16	-	4.51	7.38
K_2O	4.25	-	-	2.92	-	1.40	0.00
P_2O_5	0.15	-	-	-	-	-	-
AI	0.97						
Wo		**42.0**					
En		**31.1**					
Fs		**22.0**					
Extra-quad		**5.0**					
Fo			**25.2**				
Fa			**71.1**				
Tef.			**3.7**				
An				**8.8**			
Ab				**73.0**			
Or				**18.2**			
Usp					**73.2**		

Table 8.1 whole-rock chemical analyses of the chosen starting material pan0718 intermediate trachyte (XRF) and minerals (mean of at least 4 analyses) of the natural rock (SEM-EDS). Pheno > 500µm Gdm = groundmass < 50µm.

8.1.1 - Glass preparation and containers

Experiments were all performed in the laboratory of CNRS/INSU, Universite D'Orleans, FRANCE.

We preferred to use as starting material the glass of the natural rock powder, instead of the powder itself, to avoid any problem linked to the persistence of original crystals in the starting mixture.

Glass is simply a convenient starting material to work with the perspective of the attainment of equilibrium. In particular, the use of initially anhydrous starting glasses (e.g. Scaillet et al., 1995; Martel et al., 1999; Scaillet et al., 2007) greatly minimizes nucleation difficulties, especially for feldspars. This is because H_2O under saturation and high degrees of undercooling initially prevail in the experiment, both conditions favouring crystal nucleation.

Crystallization experiments of this type generally yield homogeneous crystalline phases, as crystal growth occurs under fixed conditions. Therefore, this method ensures a close approach to equilibrium.

Single batches of trachyte “C. Ricco” (sample pan0718) were firstly ground (≈ 30-100 μm size) in agate mortar under acetone and then molten in a Piézocéram oven at 1400 °C at 1 atm in a Pt crucible. Two melting cycle (3 hours the each) were done with crushing in between. The resulting glass was embedded in epoxy resin and checked for its absolute homogeneity and possible sodium loss.

A little part of the glass was hand crushed (≈ 20 - 50 μm size) and 30 mg of resulting powder were filled in Au capsules (15 mm length, 2.5 mm Ø internal, 0.2 mm wall thickness) for experiment.

8.1.2 - Experimental charge preparation-

Prior to the sample powder, distilled water and silver oxalate as a CO_2 supplier ($Ag_2C_2O_4$) were loaded at the bottom of each capsule, varying the XH_2O_{loaded} [= moles of H_2O/(H_2O + CO_2)] in the range 0 - 1.0. The initial amount of total fluid 10 %.

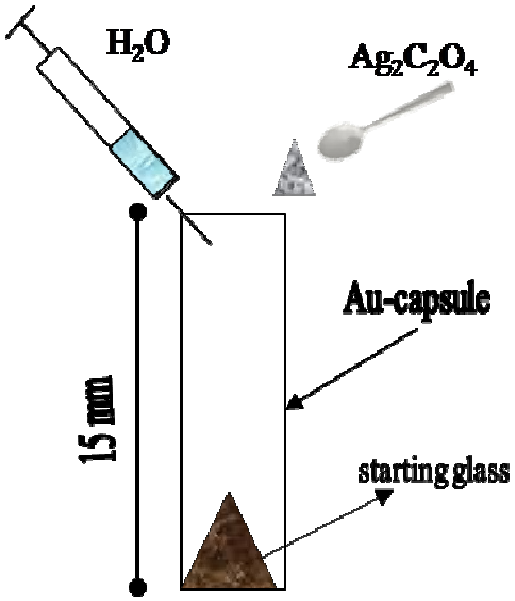

Fig. 8.1 The experimental charge.

Capsules were arc welded, keeping them in a liquid nitrogen bath, in order to prevent water loss. After welding the capsules were weighed, left in an oven overnight and then weighed again to check for leaks (**fig.8.1**). The capsules were then arc welded in a liquid nitrogen bath in order to prevent water loss.

After welding the capsules were weighted, left in an oven at 110° C for 2 hours to improve homogenization of the water distribution within the capsule. The weight of the loaded capsule agreed to within 0.0003 g (the precision of analytic balance) ensuring the closure of the capsules and the impossibility of fluid escapes.

8.1.3 Experimental methods

All experiments were of crystallisation type and were carried out in an Internally Heated Pressure Vessel (IHPV), working vertically and pressurized with Ar-H_2 mixture (**fig.8.2**).

Holloway (1971) provides a thorough description of the experimental machine. The vessel is equipped with an inner furnace, consisting of a double parallel winding of a molybdenum or kanthal wire.The vessel is equipped with an inner furnace, consisting of a double parallel winding of a Mo wire.

Pressure is recorded by a transducer calibrated against a Heise-Bourdon tube gauge (precision 15±20 bar). Three chromel-alumel thermocouples (higher limit: 1300 °C) allowed a continuous control of the temperature in the top, middle and bottom part of the hot spot (i.e. for a length of 4 cm).

The use of Ar - H_2 mixtures with known partial pressure of hydrogen allows to control fO_2 by the reaction $H_2O \leftrightarrow H_2+½O_2$. The equilibrium constant dissociation (K_w) at given T, P permits to fix fO_2, depending on the H_2 loaded and an the H_2O loaded in the capsule.

For each experiment, a separate sensor capsule (see below) was included for the determination of the experimental fO_2. The solid sensors were not analysed, but hydrogen loaded in the autoclave and water content in the capsules define redox condition close to FMQ buffer.

The ***experimental protocol*** consists of:

- loading of the capsules (several capsules can be loaded at the same time);

- tight closure of the vessel, pressurization with H_2 (according to the required fO_2; e.g. for a 1-1.5 kbar total pressure, 6 bar of H_2 ensures fO_2 ~ FMQ), pressurization with Ar, heating up to experimental temperature of the experiments and lastly quenching.

Fig. 8.2 Front vision of Internally Heated Pressure Vessel working vertically (Gros Bleu), equipped with a fast quench device. The two black rubber pipes ensure the water cooling of the furnace. Thermocouples exit wires, fast quench connections and electrical contacts are visible in the lower part of the vessel.

A fast quench device, modified after Roux and Lefevre (1992) was systematically used in order to prevent quench crystallization. The drop quench consists in an alumina tube (Ø 10 mm), in which the samples are placed, hung in the hot spot by two thin (Ø 0.2 mm) Pt wires. At the end of the experiments, Pt wires are melted by a current impulse and the sample drops instantaneously into the coldest part of the vessel (about 50 °C) with a quench rate of about 100 °C/s. This device insures a nearly isobaric quench.

The capsules were weighed to check for leaks and then opened. For each capsule, fragments of the run products were mounted in epoxy and polished for scanning electron microscope (SEM) observations and analyses.

For experiments with $XH_2O = 1.0$, water dissolved in the melt was calculated from Papale et al, 2006, assuming water saturation conditions during the experiment. This was corroborated by the occurrence of bubbles in the run product.

For undersaturated charges ($XH_2O < 1.0$) an empirical relationships of the form:
H_2O (wt %) = $-0.01\ fH_2O^2 + 0.0064\ fH_2O + 0.032$ to calculate the prevailing was used fH_2O.

8.1.4 Control and monitoring of oxygen fugacity

The use Ar-H_2 gas mixture, with known partial pressure of hydrogen, allows to impose variable reducing atmosphere and hence the required final fO_2 for each experiment.

Given that the noble metal of the capsules behaves as an ideal semi-permeable membrane to H_2 **(Chou, 1986)**, the H_2 diffuses vastly into the capsule were it reacts with H_2O establishing the equilibrium The redox state in hydrous systems is controlled by the reaction:

$$H_2O \leftrightarrow H_2 + ½O_2, \quad \textbf{(eq. 7.1)}$$

In other words fO_2 within the vessel can be controlled by adjusting the external H_2 pressure in the system, but is still dependent on the H_2O melt:

$$Kw = H_2O \leftrightarrow H_2 + ½O_2$$

$$\text{thus , } Kw = fH_2O/(fH_2 \cdot fO_2^{0.5})$$

$$fO_2 = (fH_2O/fH_2 \cdot 1/K_w)^2$$

This formulation allows to derive fO_2 provided that fH_2O and fH_2 and are known. Kw and fH_2O of pure water at the T and P of the experiments are obtained by Robie et al. (1979), while for the determination of fH_2 we need to use the solid sensor technique.

For each experiment one sensor capsule was loaded. The sensor consists of two hand-pressed Ni-Pd-NiO pellets of two mixtures ($Ni_{0.15}Pd_{0.85}$-NiO and $Ni_{0.5}Pd_{0.5}$-NiO) loaded with ZrO_2 (to prevent the contact between the two pellets and their contamination with the noble metal of the capsule) and 10 mg of distilled water.

The fO_2 is obtained from which the fH_2 (fH_2 sensor = fH_2 sample) can be calculated and then finally he fO_2 of each sample capsule (we remind is function of the dissolved H_2O within each charge) according to (**eq. 7.1**).

8.1.5 Calculations of fO_2

At fixed hydrogen fugacity in IHPV, the fH_2 inside the capsules is controlled by diffusion of H_2 through the capsule wall and is identical to the fH_2 in the vessel. Hence,
the redox state of the system in each experiment depends on the external redox conditions in the IHPV and on the redox reactions in the capsule. Assuming a negligible
effect of reactions between carbon-bearing species on redox conditions at the studied T and P, the dissociation of water is the main reaction controlling redox equilibria inside the capsules.

Using the estimated aH_2O values, the prevailing fO_2 was calculated for each experiment as $\log fO_2^{capsule} = \log fO_2^{apparent} + 2\log (aH_2O)$ where $\log fO_2$ apparent is the oxygen fugacity that is expected in the system at $aH_2O = 1$.

8.1.6 Attainment of equilibrium

Although we did not perform any reversal or time dependent experiments (mainly because of the Fe-loss problem), to check the attainment of equilibrium in our systems we have several lines of evidence that phases in most experiments have been equilibrated during the run.

At lower temperatures in systems close to the solidus, having a silica-rich residual melt composition, the equilibration kinetics slows down and requires an extremely long duration of the experiments.

Hence, such systems may not reach equilibrium at the laboratory time-scale.
Most samples show evidence of attained equilibrium based on textural and compositional characteristics:

(1) the distribution of mineral phases is homogeneous throughout the samples;

(2) the morphology of the crystals does not indicate any quench crystallization (tails or skeletal forms);

(3) the minerals and glasses have mostly homogeneous compositions;

(4) the crystallization sequence, compositions and proportions of phases follow systematic trends;

Scanning Electron Microscope (SEM-EDS) was used for phase identification and composition. Natural sample and fragments of experimental charges were mounted in epoxy resin and polished for scanning electron microscopy (SEM) observations and chemical analyses (EDS, WDS, see appendix).

CHAPTER 9

9.1 Experimental Results

We performed a series of experiments at 1.0 and 1.5 kbar, in the temperature range of 900-950 °C all with around a 10 % of free fluid phase ($H_2O + CO_2$) coexisting in the melt. For experiments was chosen a range of XH_2O [i.e. moles H_2O/(H_2O+CO_2)] = 1.0, 0.8, 0.6, 0.4 to be loaded with the starting mixture to cover an ample spectrum of conditions. Experimental results are shown in Table 9.1, in which experimental conditions, mass balance results of the phase assemblages and equilibrium coefficients (for clinopyroxenes, olivines and feldspar) are reported.

Table 9.1: Experimental results

Charge	H_2O_{melt}(wt%)	XH_2O_{in}	log fO_2	a $_{H2O}$	ΔNNO	Phase assemblage	$\sum R^2$	ΔFeO	$K_d^{FeMg}{}_{cpx\text{-}liq}$	$K_d^{Fe\text{-}Mg}{}_{ol\text{-}liq}$	$K_d^{Ca\text{-}Na}{}_{pl\text{-}liq}$
"Trachyte C. Ricco"											
Run1, 950°C, P=1.5kbar, 96h, fH_2 = 5.95, X_{Ni} = 0.60, $Au_{90}Pd_{10}$.											
(1-2)	4.39	0.8	-10.65	1.00	0.42	gl(98)+ox(tracce)	0.77	4.2			
(1-3)	4.29	0.6	-10.86	0.78	0.22	gl(81)+cpx(2) +kfs(14)+ox(3)	0.39	2.3	0.19±0.02		0.80±0.1
(1-4)	3.94	0.4	-10.90	0.74	0.17	gl(82)+cpx(1)+kfs(15)+ox(nd)	0.55	4.1 2.5	0.20±0.02 0.18±0.02		0.80±0.2
(1-5)	2.56	0.0	-11.46	0.39	-0.40	gl(65)+cpx(3)+kfs(27)+ol(4)+ox(nd)	0.59			0.30±0.05	0.90±0.1
Run 4, 950°C, P=1.0kbar, 96h, fH_2 = 1.53, X_{Ni}=0.32, $Au_{90}Pd_{10}$.											
(4-1)	6.10	1.0	-9.42	1.00	1.59	gl(99) +ox(tr)	0.67	11			
(4-2)	4.51	0.8	-9.42	1.00	1.59	gl(99)+ox(nd)	0.44	11			
(4-3)	3.08	0.6	-9.79	0.93	1.29	gl(74)+cpx(3)+ kfs(20)+ox(nd)	0.31	0.5	0.27±0.10		0.80±0.1
(4-4)	2.77	0.4	-9.85	0.85	1.26	gl(57)+cpx(5)+kfs(37)+ox(nd) +ol(tr)	1.06	0.5	0.24±0.02		1.10±0.2
(4-5)	1.60	0.0	-10.19	0.66	0.89	gl(27)+cpx(4)+ol(7)+ kfs(62)+ox(nd)	0.38	0.9	0.19±0.02	0.25±0.01	1.20±0.1
Run 2, 900°C, , 100MPa, 48h, $Au_{90}Pd_{10}$ SOME CASPULE FAILED DUE TO CASPULE LEAKAGE, 1 run to be retrieved											
(2-4)	-	0.4	-		-	gl(nd)+cpx(nd)+ kfs(nd)+ox(nd)	-	-	-	-	-
(2-5)	-	0.0	-		-	gl(nd)+cpx(nd)+ kfs(nd)+ox(nd)	-	-	-	-	-
Run 3, 900°C. 150MPa, 48h, SOME CASPULE FAILED DUE TO LEAKAGE 1 run to be retrieved											
(3-3)	-	0.6	-		-	gl(nd)+cpx(nd)+ kfs(nd)+ox(nd)	-	-	-	-	-
(3-5)	-	0.0	-		-	gl(nd)+cpx(nd)+ kfs(nd)+ox(nd)	-	-	-	-	-

Table 9.1 H_2O_{melt} (wt%) Bulk H_2O content of the charge, determinated using the "by difference" method, see text. XH_2Oin initial mole fraction of H_2O of the C–O–H fluid loaded to the capsule. aH_2O calculated after Burnham (1979). ΔNNO= logfO_2 relative to the value of the Ni–NiO buffer (see text); ΔFeO = iron loss (See text). ΣR^2 = sum of square residuals for mass balance results (see text) . Kd calculated with total iron as FeO. Phase abbreviations= phases present and abundances (wt%) gl, glass; k-fsp, K-feldspar; cpx, clinopyroxene; ol, olivine; ox, Fe-Ti oxides.

9.2 Attainment of equilibrium

Attainment of equilibrium has not been tested from reversal experiments. Nevertheless, several textural and chemical criteria, listed below, suggest that near-equilibrium conditions were achieved.

- ***Run duration*.**

In the high temperature range we have considered 96 hours of run duration (on average) as sufficient to closely approach the equilibrium conditions, decreasing experiment duration (to at least 48 h) for lower temperature conditions.

- *Quench* Isobaric quench was achieved with a fast quench-device that ensures a quench rate close to 100 °C/sec.

- *Crystal textures*. Euhedral and platy crystals of olivine are present in low H_2O charges suggesting growth at small degrees of undercooling. Pyroxenes show euhedral , equant, habits. The crystal distributions in the experimental products is uniform (no crystal settling) and seriate crystal sizes were observed due to difference growth rates of the various mineral species (fig. 9.1).

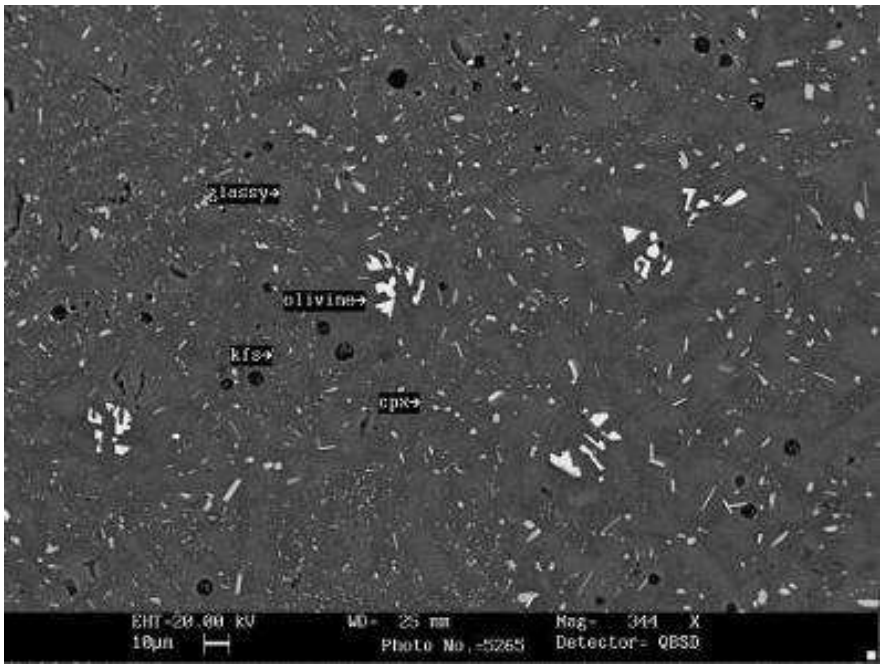

Fig. 9.1 BSE image of run1-5; experiment at P = 1.5 kb and T = 950 °C. Phase assemblage consist of glass (liq), euhedral crystals of olivine (ol) and clinopyroxene (cpx). Feldspar (kfs) is hardly distinguishable from glass in several runs.

- ***Crystal and glass homogeneity.*** The compositional homogeneity of glass and mineral, is highlighted by the low standard deviations of analysis (table 9.2).

- ***Crystal-liquid exchange coefficient.*** The exchange coefficient of exchangeable cations between given mineral phases and the melt (i.e. Fe-Mg exchange for olivine and clinopyroxene $\mathbf{Kd^{Fe\text{-}Mg} = (Fe/Mg)_{xtal} / (Fe/Mg)_{liq}}$ and Ca-Na for feldspar), are also reported in Table 9.1.

$\mathbf{Kd^{Fe\text{-}Mg}}$ was calculated with total iron as FeO. and is considered to represent equilibrium values if in the range 0.22-0.28 for olivine, 0.18-0.25 for clinopyroxene (with FeO = FeO, if instead is calculated with FeO= FeOtot , then the equilibrium K_d lowers of 3-5 units on the 2nd decimal, depending on the Fe^{3+}/Fe^{2+} ratio). The plagioclase Ca-Na exchange coefficient (Ca/Na in plg)/ (Ca/Na in melt) in the range 0.80-1.28.

Iron-loss. The amount of Fe-loss was calculated by mass balance as difference between starting glass FeO and the sum of FeO in all the phases occurring in the given runs. The ΔFeO is always less than 10 wt% in near-liquidus runs with a slight decrease with decreasing liquid proportion.

Based on these petrographic and chemical criteria, we consider that our experiment result closely representing near-equilibrium conditions.

9.3 Trachyte 0718 (Case Ricco) isothermal phase equilibria

Experiments explored a restricted T-P interval (1.5 - 1.0 kbar, 950 °C) for a total of 9 charges, covering a range of water contents from 6.10 to 1.60 wt.% and an fO_2 in the range ΔNNO = - 0.1, + 1.6. The isothermal phase equilibria are reported in Fig. 9.2 , where the) solubility model. Mineral saturation curves are constructed using the experimental data reported in table 9.1.

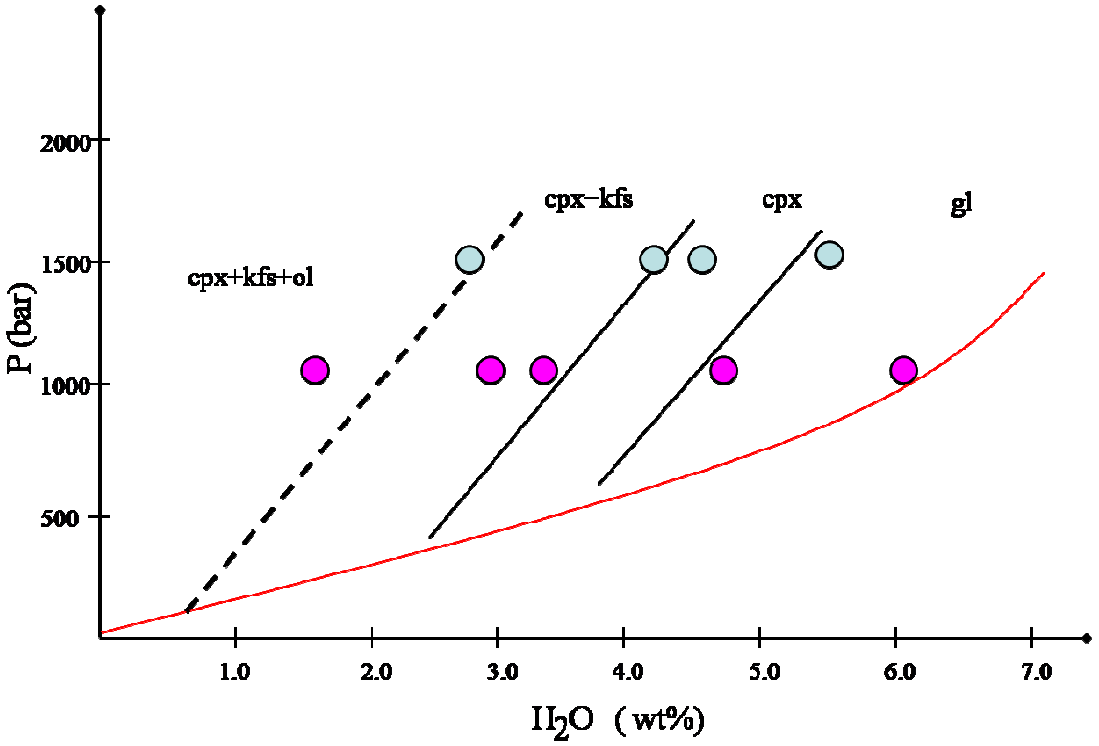

Fig. 9.2 Experimentally determined P-H_2O phase diagram at 950 °C. Data are given in table 9.1 gl, glass; cpx, clinopyroxene; ol, olivine; kfs, feldspar. (H_2O determined "by difference", see text). The red curve is the water saturation, after Papale et al. (2006).

Nine charges were run with mixed H_2O-CO_2 fluids. Water was added as deionized water. The source of CO_2 was $Ag_2C_2O_4$. We chosen XH_2O_{loaded}, defined as $H_2O/(H_2O+CO_2)$ = 1.0, 0.8, 0.6, 0.4 and anhydrous. The loaded amounts of volatiles translate in variable H_2O_{melt} amounts (evaluated with the "by the difference" method (See appendix "Analytical conditions"). CO_2 was always below the FT-IR detection limits.

9.3.1 Phase equilibria

The phase relationships at 1.0-1.5 kbar are shown in Fig.9.2. At H_2O saturation (c. 6.0 wt % H_2O_{melt} at 1.0 kbar, and 7.2 wt % at 1.5 kbar), Fe-Ti oxides are the first phase to crystallize (fig. 9.3b) , followed by clinopyroxene (fig. 9.3c), and by feldspar (fig. 9.3c). Olivine (fig. 9.3d) is the latest phase to crystallize at near-solidus condition (Runs 4-5 and 1-5, table 9.1).

Fe-Ti oxides are always smaller than 3 μm, which makes impossible to obtain reliable SEM-EDS analyses.

Clinopyroxene is euhedral and occurs in small individuals (ca. 10-20 μm), owing to their small size and elongated shape, most clinopyroxene analyses showed glass contamination.

Feldspar occurs in low-H_2O_{melt} experiments. The relative proportion of feldspar tends to increase with decreasing H_2O_{melt} (fig.9.3).

Olivine is distinctly larger in size with respect to clinopyroxene, and occur in those runs with lower H_20 2.50-1.60 wt %. Thus, clinopyroxene + olivine + feldspar (fig. 9.1) is the dominant phase assemblage at low water contents (below 2 wt.%).The presence of bubbles in almost all charges is taken as an evidence of fluid saturation.

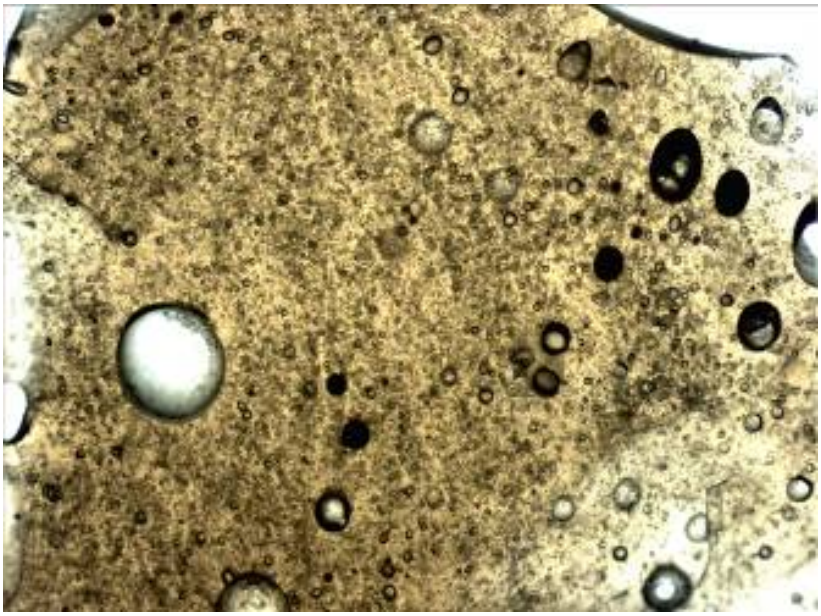

Fig.9.3 Optical microscope (parallel polars, 10x) image of Run 1-3. The presence of bubbles witnesses volatile saturation.

9.4 Cristallinity and phase proportions

Phase proportions were evaluated by mass balance and were considered acceptable for a sum of square residuals ($\sum R^2$ in Table 9.1) < 1.5.

The amount of residual melt varies from 99 wt % to less than 27 wt % in near-solidus runs. Calculated phase proportion show that the crystal content of the charges increases with decreasing pressure and water content (cf. Run 4-4 and 1-5, table 9.1).

Alkali feldspar is the most abundant phase, with a mass proportions varying from trace amounts to over 62 wt % (Run 4-5), followed by clinopyroxene (< 5 wt %) and olivine (< 7 wt %).

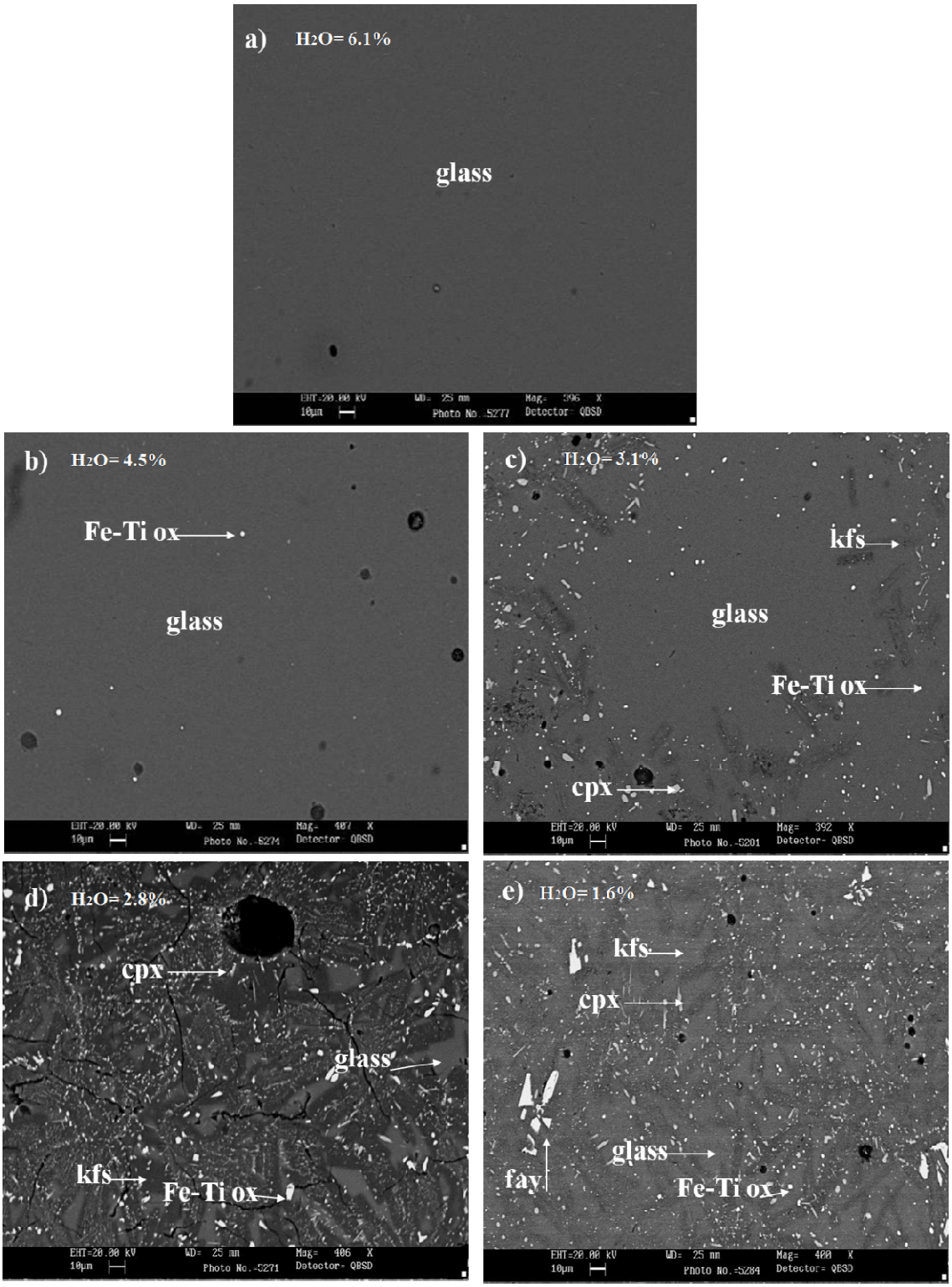

Fig. 9.4 Back-scattered electron images (BSE) of experimental at T = 950 °C, P = 1.0 kbar: a) Run 4-1, b) Run 4-2, c) Run 4-3 d) Run 4-4 and e) Run 4-5.

9.5 Liquid and mineral phase compositions

Glass and mineral compositions are listed in table 9.2. The compositions of mineral phases were determined by SEM-EDS. Glass analyses were mostly obtained by EMP using a defocused beam (see Appendix).

9.5.1 Phase composition

Clinopyroxene composition (table 9.2) varies significantly with the experimental parameters: (fig.9.5) ranges from augite ($Wo_{45}En_{26}Fs_{28}$) to aegirine-augite at P = 1.0 kbar.

- At P = 1.5 kbar clinopyroxene ranges from $Wo_{44}En_{34}Fs_{22}$ to $Wo_{45}En_{26}Fs_{28}$ (fig. 9.7).

- Na_2O in cpx generally increases with decreasing H_2O in the melt to a maximum of 2.9 wt % (aegirine-augite of fig. 9.8).

- CaO in clinopyroxene apparently decreases with decreasing water in the melt (fig. 9.5), from 18-20 wt % to 16 wt % ; however the decrease in CaO_{cpx} is not solely an effect of H_2O but must also be considered as an effect of increasing $(Fe - Na)_{cpx}$ with evolving liquid composition.

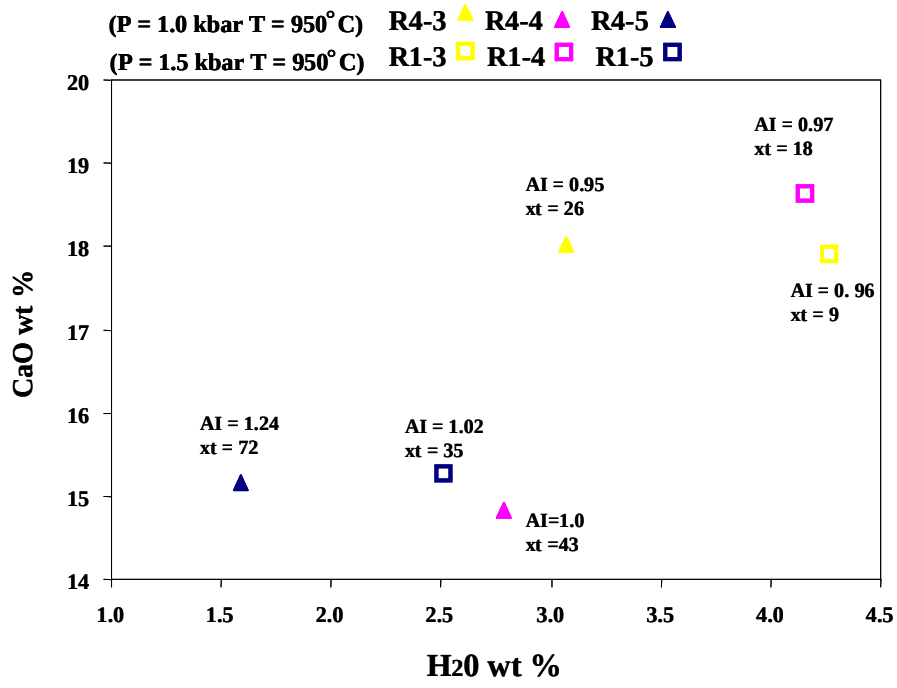

Fig. 9.5 CaO content in clinopyroxene (wt %) vs. water content in the melt. AI = melt agpaitic index; xt = total amount of crystals (wt %) in the charge.

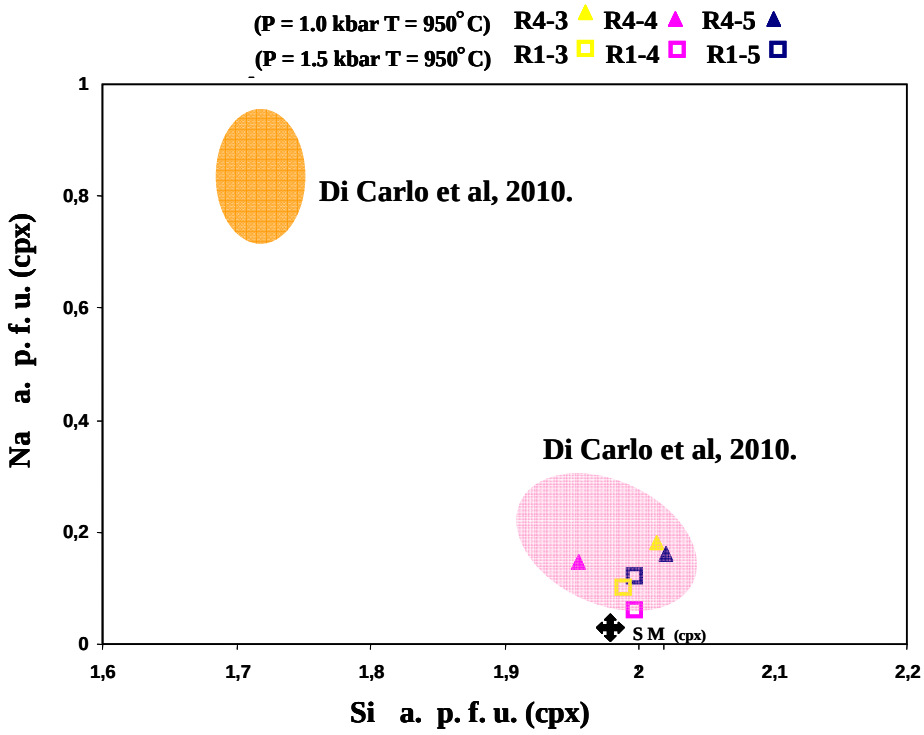

Fig. 9.6 Composition of experimental pyroxenes compared with pyroxene phenocrysts in the starting rock (cross) and with experimental pyroxenes of Di Carlo et al, 2010 on a pantelleritic composition (violet and orange areas represent cpx synthesized at 800-725 and 680°C, respectively).

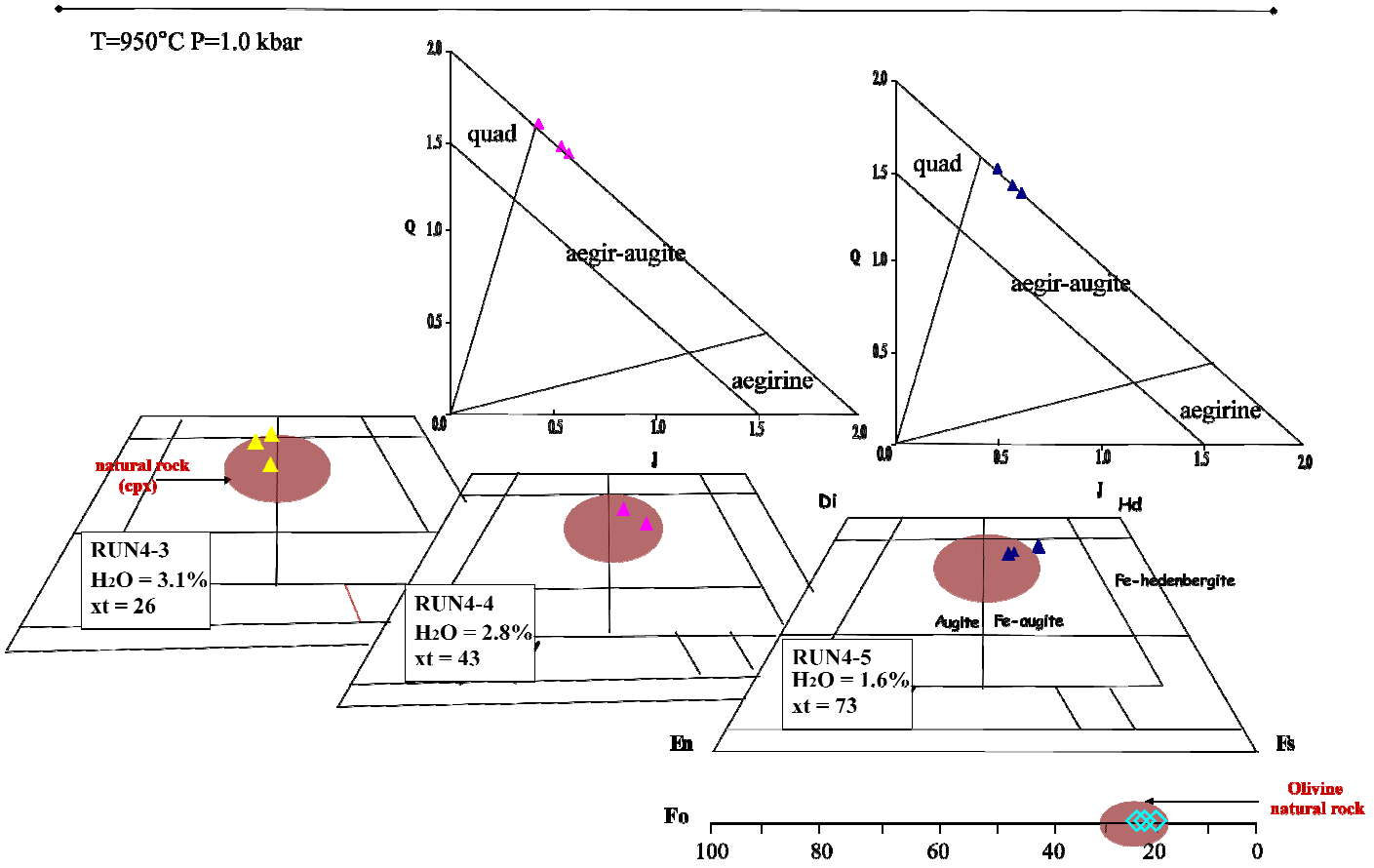

Fig.9.7 Experimental pyroxenes in the Ca-Mg-Fe quadrilateral, and in Q-J diagram (Morimoto, 1989) for those pyroxene whose extra-quad component is > 20%. Natural clinopyroxenes of trachyte 0718 are represented by colored areas, xt = total amount of crystals in the charge (wt %).

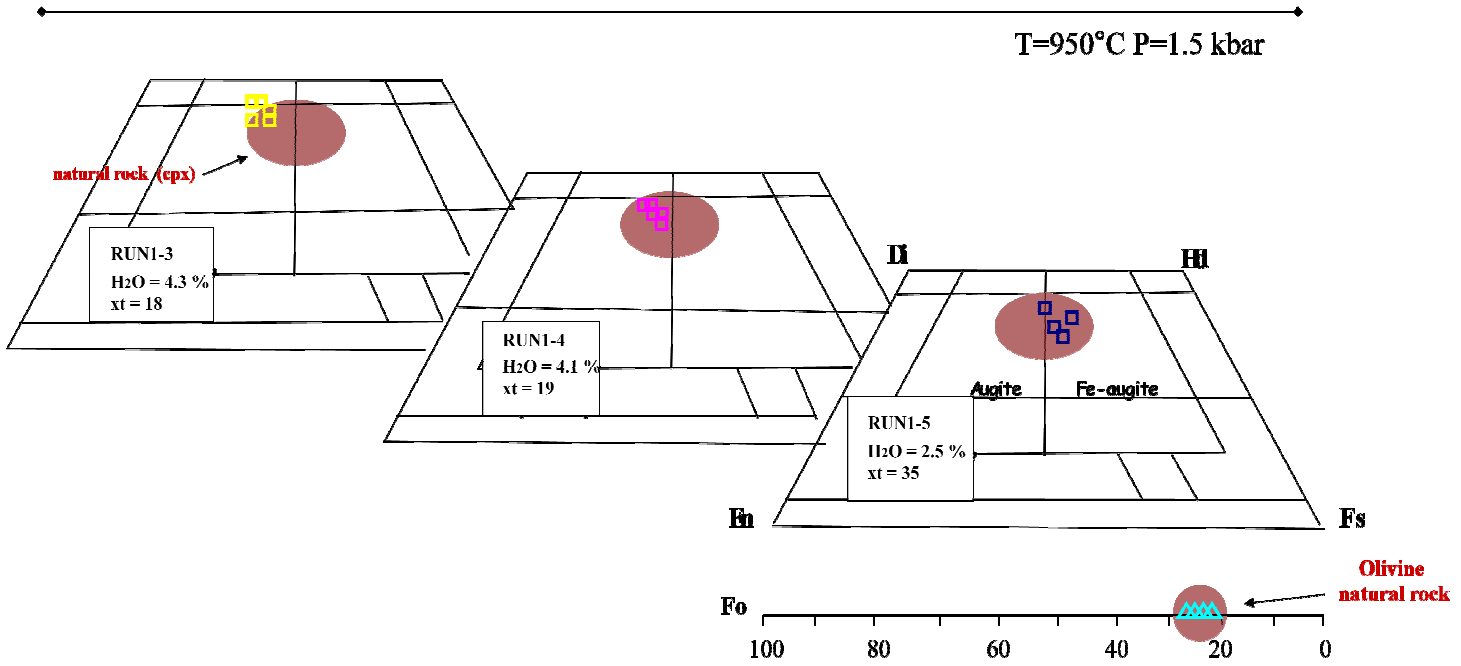

Fig.9.8 Experimental pyroxenes compared to the natural ones (see Fig. 9.5), xt = total amount of crystals in the charge (wt %).

Feldspar always has low **CaO contents (< 3 wt % = An < 11 mol %)** and range from $Ab_{72}Or_{23}$ to $Ab_{65}Or_{28}$. Curiously, the An % shows a decrease with decreasing liquid evolution (Fig. 9.11).

Feldspar composition is not remarkably influenced by variations in T and P, but it shows some variations at different values of H_2O (fig. 9.11) and agpaitic index (fig . 9.14) in the melt . Feldspar are always Na_2O-richer than the coexisting melt, and this difference reaches the maximum value in run 4-5 (Na_2O_{kfs} = 7.5 wt % , Na_2O_{melt} = 4.5 wt % , Table 9.2), characterized by the most evolved melt composition (see below). The K_2O_{kfs} is slightly lower than that of the melt.

The Na/K of feldspars increases with melt peralkalinity (not shown), with the exception of the most peralkaline composition (R 4-5, AI = 1.24, see below).

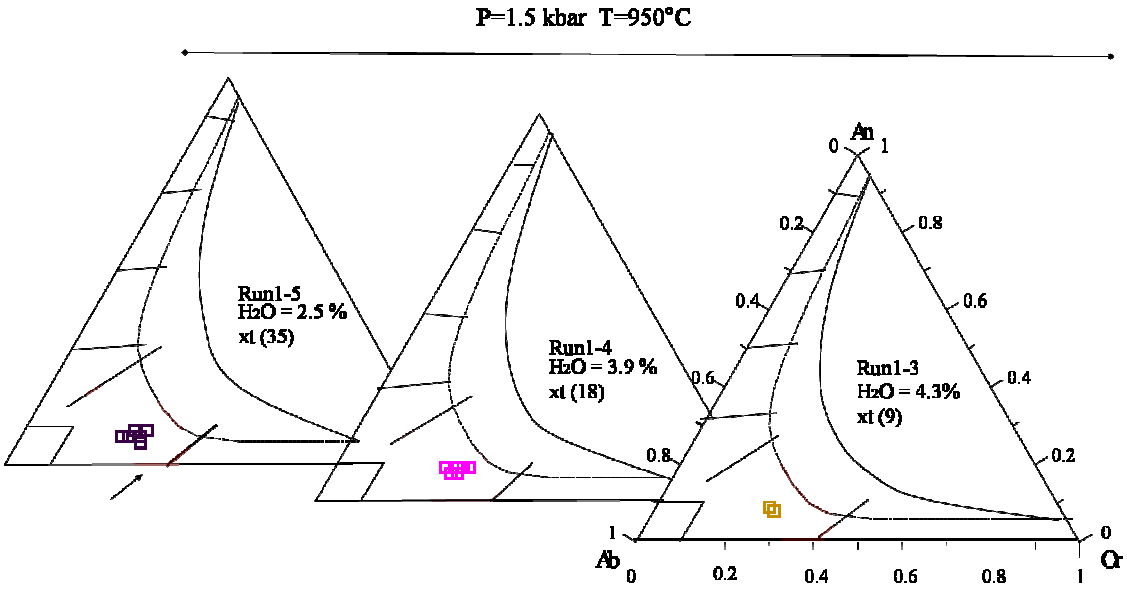

Fig. 9.9 Compositional variations of experimental alkali feldspars, compared with the natural ones (colored areas), xt = total amount crystals in the charge (wt %) .

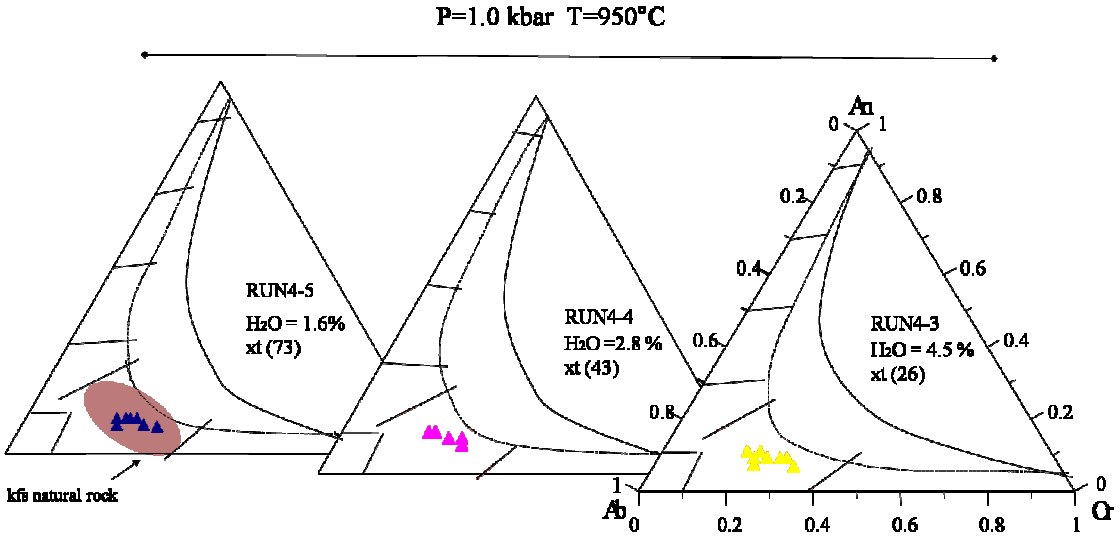

Fig. 9.10 Compositional variations of experimental alkali feldspars, compared with the natural ones (colored areas), xt = total amount crystal in the charge.

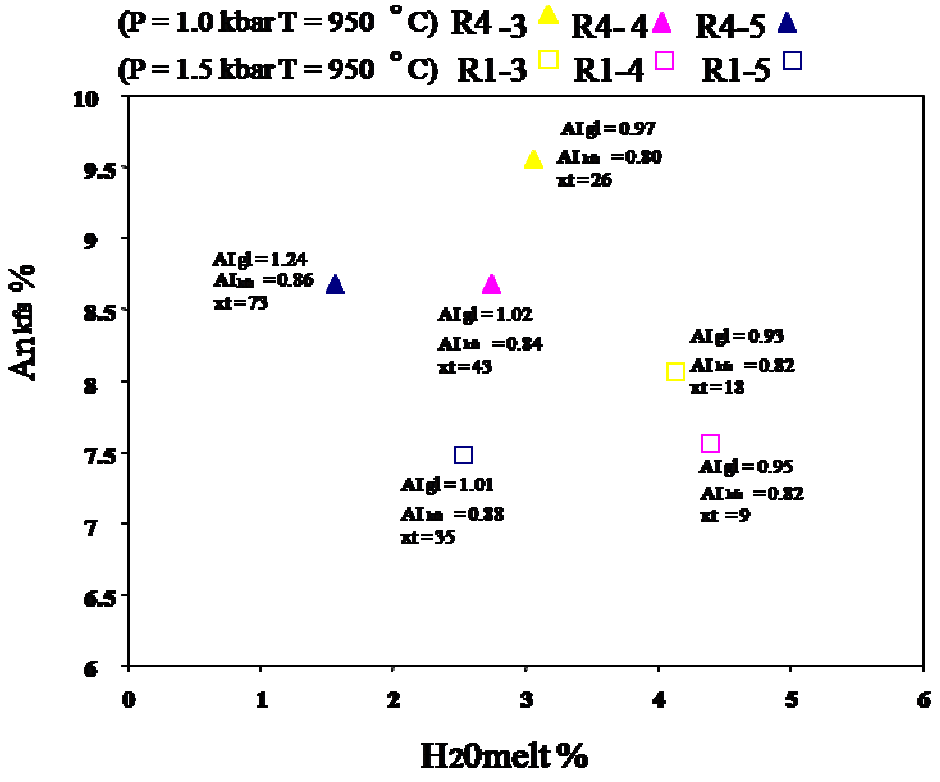

Fig. 9.11 An mol % vs. water content in the melt. Numbers refer to: Agpaitic index of the melt (AI_{gl}), Agp. index of alkali feldspar (AI_{kfs}), and crystal (xt , wt %).

Olivine composition ranges from **Fo_{28}** to **Fo_{21}** in the charges characterized by liquid + clinopyroxene + feldspar + olivine assemblage (Run 1-5 and Run 4-5) and occurs for a restricted range of liquid compositions from AI = 1.0 (Run 1-5) to AI = 1.2 (Run 4-5).

Olivine crystallization occurs between 1.60 and 2.5 % of H_2O. The late crystallization of olivine is in agreement with petrographical observations on the natural samples, and also is coherent with the assumptions of White at al. (2005), who suggested that Fe-rich olivine crystallizes to a maximum melt agpaicity of 1.60.

9.6 composition of experimental melts

Experimental glasses vary their composition coherently with temperature and water content and range from trachyte to rhyolite, covering a silica range between 65.0 to 72.2 wt % (sum of oxides reported at 100 %) (figure 9.12). The melt agpaitic index varies from 0.86 to 1.30 of the most evolved liquid which was obtained at P = 1.5 kb and H_2O = 1.6 wt % (Run 4-5), the agpaitic index of this liquid is AI = 1.24 (table 9.2) for a K_2O = 5.0 wt %. The K_2O concentration increases with decreasing in CaO (fig. 9.16).

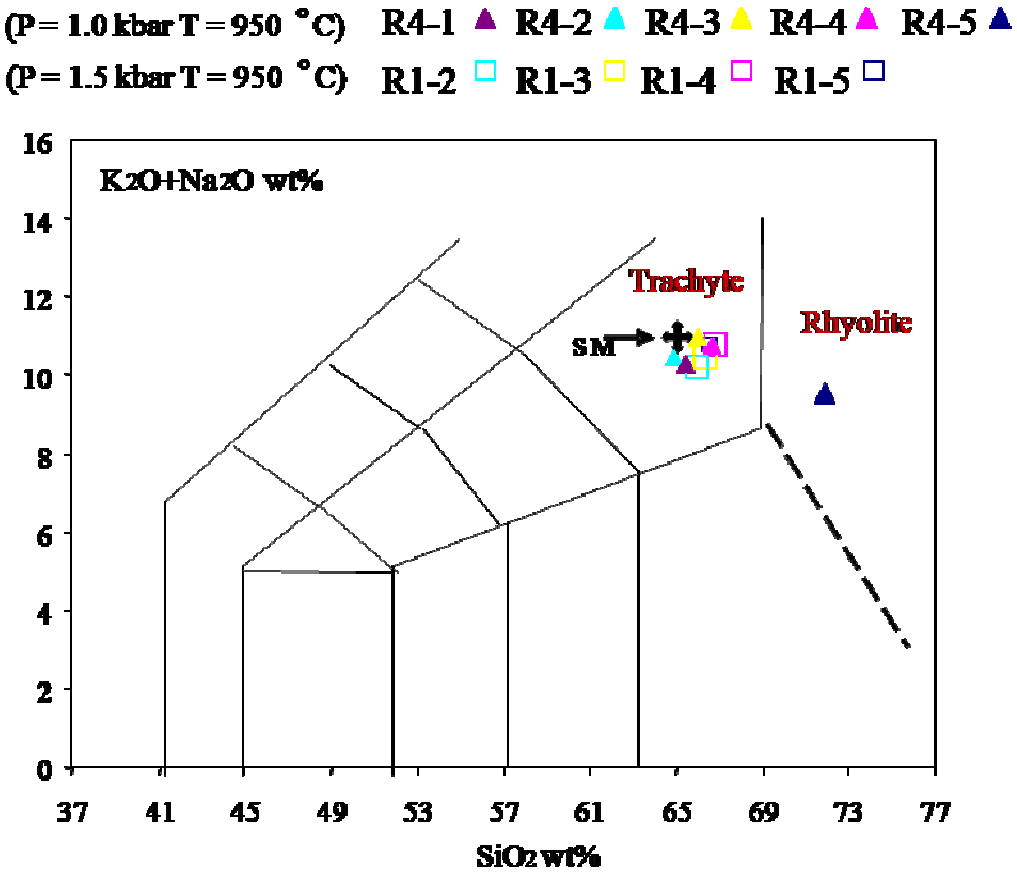

Fig. 9.12 Total-alkali versus silica (TAS) diagram for the classification of experimental glasses (reported to 100 %) as a function of temperature, pressure and phase assemblage. The star represents the starting material composition (SM).

Most of experimental glasses are metaluminous (AI= 0.86 - 1.00). As visible in Fig. 9.13 some liquids move towards less peralkaline compositions (i.e. point to the left of the starting material in Fig, 9.13), and their AI decreases (to 0.92- 0.95) respect to the starting glass composition (AI= 0.97). To explain this anomalous decrease in peralkalinity for this group of experiments we cannot simply invoke the "clinopyroxene-effect" of Scaillet and Mac Donald (2003), since clinopyroxene is only a minor crystallizing phase (Table 9.1), but we have to take in account the crystallizazion of Fe-Ti oxides (R 1-4) that decreases the melt FeO (Fig. 9.13). On the contrary, in those runs where feldspar crystallization becomes more and more abundant, the liquid composition moves towards the normal decrease in Al_2O_3 and increase in FeO (the "orthoclase effect" of Bailey and Schairer, 1964) (bottom directed arrow in Fig.

9.13) increasing at the same time the agpaitic index with respect to the starting composition (to 1.30). Feldspars in these runs are characterized by the lowest agpaitic index (AI_{feld} down to 0.82, Fig. 9.14), i.e. their removal maximizes the increase in melt peralkalinity.

The increasing peralkalinity is accompanied by a dramatic decrease in Al_2O_3 (down to 10.4 wt %) at an SiO_2 = 70.9 wt % (both values are reported as from the microprobe, i.e. totals < 100 %, while on the graphs are reported to 100 %)

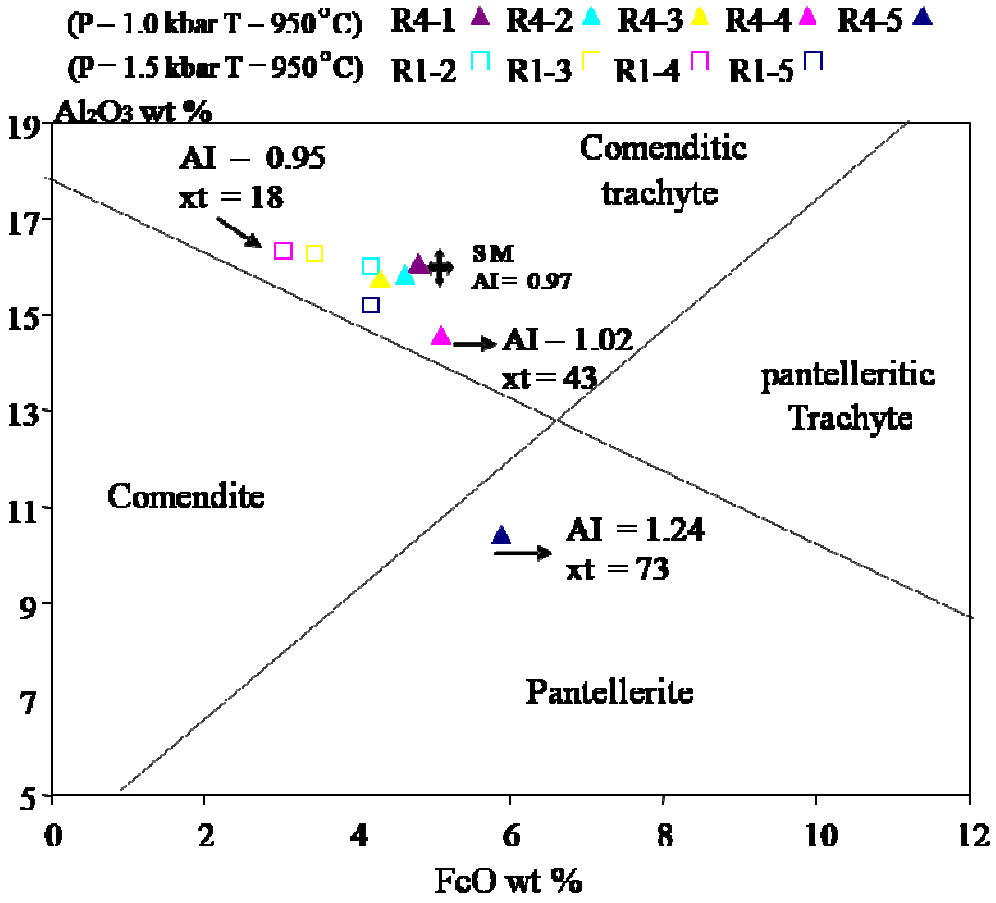

Fig. 9.13 The MacDonald (1974) classification diagram for the classification of experimental glasses, where we projected also liquids with AI < 1 contrarily to the Author's constraints. Numbers refer to the melt agpaitic index (AI) and crystal proportions (xt) (wt %). The star represents the starting material composition (SM). (FeO and Al_2O_3 are reported to 100 %)

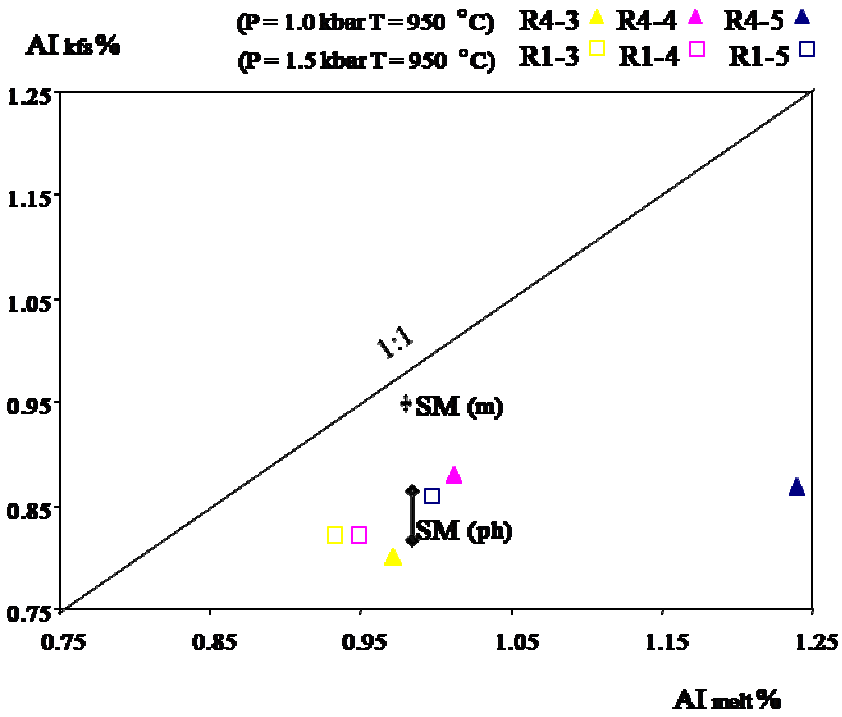

Fig. 9.14 Agpaitic index of the melt (AI_{melt}) vs. Agp. index of alkali feldspar (AI_{kfs}). The compositions of natural phenocrysts (ph) and microlites (m) of the starting trachyte 0718 are also reported.

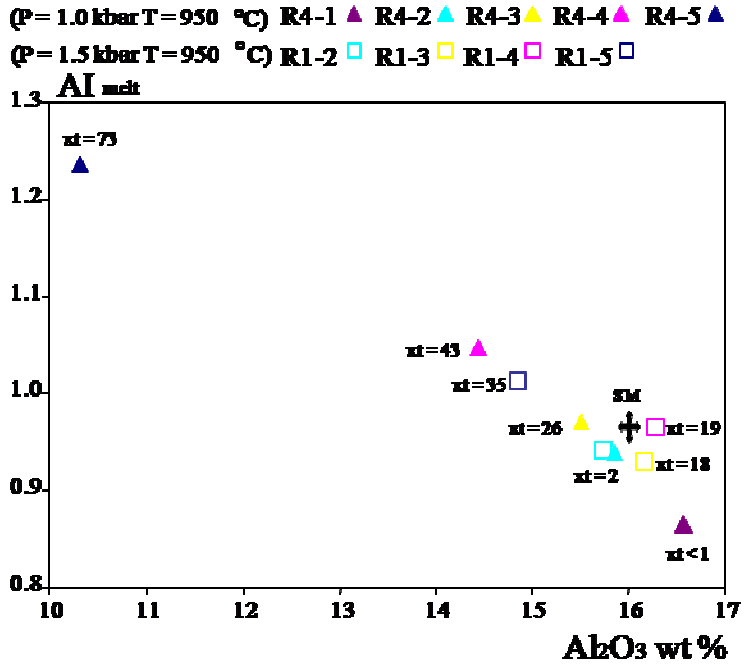

Fig. 9.15 Al_2O_3 (wt %, reported to 100 %) vs agpaitic index (AI) and crystal proportions of the given charge (xt), wt %. The star represents the starting material composition (SM).

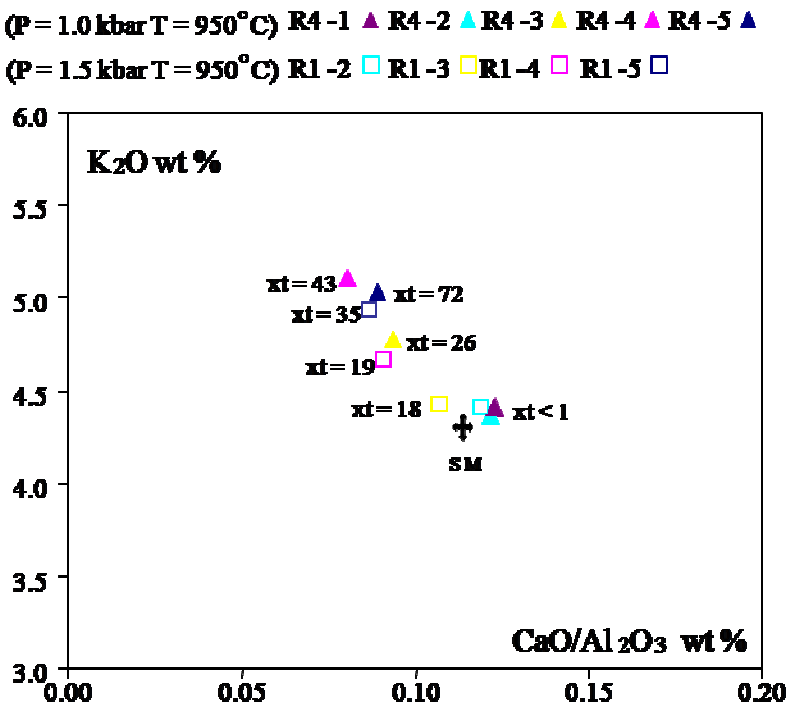

Fig. 9.16 K_2O vs. CaO/Al_2O_3. Potassium content increases steadily, making exception for R 4-5 (xt = 73 %) . The star represents the starting composition (SM); xt = crystal proportions wt %.

Table 9.2 Composition of experimental phases at 1.0 kbar – 950 °C

Charge	TRACH.	R 4-1		R 4-2		R 4-3						R 4-4						R 4-5							
Phase	WR	gl	σ (n=13)	gl	σ (n=12)	gl	σ (n=10)	cpx	σ (n=5)	fsp	σ (n=5)	gl	σ (n=10)	cpx	σ (n=5)	fsp	σ (n=5)	gl	σ (n=10)	cpx	σ (n=5)	ol	σ (n=5)	fsp	σ (n=5)
SiO_2	64.06	61.37	0.48	62.37	0.50	64.13	0.88	50.47	1.57	64.26	0.87	65.12	0.43	52.44	0.50	64.80	1.97	70.89	0.78	53.00	2.11	34.32	0.28	64.72	0.68
TiO_2	0.76	0.75	0.11	0.74	0.07	0.66	0.07	0.78	0.16	0.00	0.00	0.51	0.07	0.81	0.29	0.00	0.00	0.99	0.14	0.65	0.17	0.00	0.00	0.00	0.00
Al_2O_3	15.93	15.04	0.24	15.26	0.17	15.33	0.22	3.87	0.81	20.33	0.90	14.23	0.12	5.53	1.73	19.56	0,34	10.25	0.23	4.57	1.15	0.00	0.00	20.33	0.59
FeO	5.05	4.51	0.07	4.47	0.20	3.98	0.68	14.90	3.58	0.26	0.26	5.00	0.27	16.58	2.54	0.36	0,14	5.46	0.63	14.44	1.16	50.15	1.27	0.63	0.32
MnO	0.19	0.18	0.04	0.21	0.03	0.16	0.03	0.67	0.11	0.00	0.63	0.20	0.03	1.32	0.27	0.00	0,00	0.14	0.05	0.90	0.19	2.62	0.34	0.00	0.00
MgO	0.52	0.56	0.06	0.54	0.02	0.38	0.05	7.77	1.88	0.00	0.00	0.33	0.04	4.92	1.12	0.00	0,00	0.14	0.03	7.63	2.01	8.83	0.84	0.00	0.00
CaO	1.89	1.86	0.08	1.86	0.11	1.43	0.16	17.98	2.26	1.90	0.00	1.14	0.05	14.78	2.02	2.08	0.41	0.85	0.25	15.17	1.60	0.75	0.28	1.81	0.18
Na_2O	6.60	5.57	0.19	5.88	0.11	6.03	0.16	1.94	0.68	6.98	0.91	5.57	0.16	2.38	0.32	7.43	0.61	4.50	0.20	2.42	1.02	0.00	0.00	7.53	0.75
K_2O	4.25	4.11	0.07	4.17	0.05	4.64	0.10	0.00	0.00	4.42	1.08	4.98	0.05	0.00	0.00	4.66	0.50	4.94	0.07	0.00	0.00	0.00	0.00	4.65	0.74
P_2O_5	0.20	0.17	0.03	0.15	0.04	0.18	0.05	0.00	0.00	0.00	0.00	0.16	0.05	0.00	0.00	0.00	0.00	0,24	0.22	0.00	0.00	0.00	0.00	0.00	0.00
Cr2O3	0.00	0.00	0.00	0.00	0.00	0.00	0.00	0.00	0.00	0.00	0.00	0.00	0.00	0.00	0.00	0.00	0.00	0.00	0.00	0.00	0.00	0.00	0.00	0.00	0.00
Tot	100	93.90	-	95.63	-	96.92	-	98.39	-	99.27		97.23	-	98.78	-	98.98	-	98.40	-	98.51	-	96.67	-	99.67	-
Fo	-	-	-	-	-	-	-	-	-			-	-	-	-	-	-	-	-	-	-	24	-	-	-
Wo	-	-	-	-	-	-	-	37	-			-	-	29	-	-	-	-	-	30	-	-	-	-	-
En	-	-	-	-	-	-	-	22	-			-	-	13	-	-	-	-	-	21	-	-	-	-	-
Fs	-	-	-	-	-	-	-	23	-			-	-	25	-	-	-	-	-	22	-	-	-	-	-
extraquad	-	-	-	-	-	-	-	18	-			-	-	33	-	-				27		-	-	-	
An	-	-	-	-	-	-	-	-	-	9		-	-	-	-	10	-	-	-	-	-	-	-	9	-
Ab	-	-	-	-	-	-	-	-	-	64		-	-	-	-	65	-	-	-	-	-	-	-	65	-
Or										27						25								26	
AI	0.97	0.90	-	0.96	-	0.97	-		-	0.82		1.00	-	-	-	0.88	-	1.24	-	-	-	-	-	0.86	-
H2Owt%		5.86	-	4.51	-	3.08	-	-	-			2.77	-	-	-	-	-	1.60	-	-	-	-	-	-	-

Table 9.2 . Composition of experimental phases at P= 1.5 kbar, T= 950 °C

Charge	TRACH.	R 1-2		R 1-3						R 1-4						R 1-5							
Phase	WR	gl	σ (n=12)	gl	σ (n=10)	cpx	σ (n=3)	fsp	σ (n=3)	gl	σ (n=11)	cpx	σ (n=6)	fsp	σ (n=7)	gl	σ (n=8)	cpx	σ (n=5)	ol	σ (n=8)	fsp	σ (n=6)
SiO_2	64.06	61.73	0.41	63.58	0.31	52.98	0.31	65.11	0.31	64.17	0.55	52.44	0.94	64.25	0.78	65.32	0.52	51.96	1.65	33.16	0.92	65.19	1.02
TiO_2	0.76	0.66	0.05	0.76	0.08	0.66	0.23	0.00	0.23	0.69	0.08	0.56	0.36	0.00	0.00	0.59	0.05	0.70	0.22	0.00	0.00	0.00	0.00
$Al2O_3$	15.93	14.67	0.26	15.54	0.22	3.39	0.88	19.74	0.88	15.69	0.14	1.73	0.43	20.08	0.77	14.77	0.47	3.29	1.48	0.00	0.00	20.20	0.67
FeO	5.05	3.66	0.16	3.26	0.12	12.37	1.19	0.40	1.19	2.84	0.20	14.54	1.09	1.64	0.26	4.14	0.35	18.25	2.48	52.46	1.74	0.38	0.12
MnO	0.19	0.09	0.05	0.16	0.02	0.85	0.19	0.00	0.19	0.17	0.04	1.01	0.17	0.00	0.16	0.19	0.04	1.37	0.19	2.72	0.23	0.00	0.18
MgO	0.52	0.49	0.04	0.42	0.04	10.03	0.71	0.00	0.71	0.37	0.03	9.91	0.07	0.00	0.66	0.25	0.05	7.33	0.79	9.11	1.14	0.00	0.44
CaO	1.89	1.69	0.08	1.65	0.12	17.88	1.59	1.54	1.59	1.43	0.09	18.67	0.46	1.60	0.44	1.29	0.15	15.37	0.44	0.50	0.14	1.48	0.29
Na_2O	6.60	5.60	0.06	5.97	0.09	1.49	0.39	7.39	0.39	6.11	0.12	1.47	0.10	7.07	0.00	5.86	0.15	1.67	0.42	0.00	0.00	7.28	0.00
K_2O	4.25	4.09	0.03	4.28	0.06	0.00	0.00	4.79	0.00	4.47	0.06	0.00	0.00	4.48	0.00	4.86	0.18	0.00	0.00	0.00	0.00	4.26	0.00
P_2O_5	0.20	0.10	0,02	0.11	0.04	0.00	0.00	0.00	0.00	0.13	0.05	0.00	0.00	0.00	0.00	0.10	0.04	0.00	0.00	0.00	0.00	0.00	0.00
Cr_2O_3	0.00	0.00	0.00	0.00	0.00	0.05	0.00	0.00	0.00	0.00	0.00	0.00	0.00	0.00	0.00	0.00	0.00	0.00	0.00	0.00	0.00	0.00	0.00
Tot	100	94.59	-	95.72	-	99.66	-		-	96.07	-	99.85	-	99.12	-	97.39	-	99.91	-	97.95	-	98.79	-
Fo	-	-	-	-	-	-	-		-	-	-	-	-	-	-	-	-	-	-	24	-	-	-
Wo	-	-	-	-	-	36	-		-	-	-	38	-	-	-	-	-	31	-	-	-	-	-
En	-	-	-	-	-	28	-		-	-	-	28	-	-	-	-	-	21	-	-	-	-	-
Fs	-	-	-	-	-	19	-		-	-	-	23	-	-	-	-	-	29	-	-	-	-	-
extraquad	-	-	-	-	-	18	-		-	-	-	12	-	-	-	-	-	19		-	-	-	
An	-	-	-	-	-	-	-	*7*	-	-	-	-	-	8	-	-	-	-	-	-	-	7	-
Ab	-	-	-	-	-	-	-	*65*	-	-	-	-	-	65	-	-	-	-	-	-	-	67	-
Or								*28*						27								26	
AI	0.97	0.92	-	0.95	-	-	-	0.80	-	0.95	-	-	-	0.82	-	1.00	-	-	-	-	-	0.82	-
H2Owt%		4.39	-	4.29	-	-	-		-	3.94	-	-	-	-	-	2.56	-	-	-	-	-	-	-

SECTION 2: DISCUSSION

PREVIOUS EXPERIMENTAL STUDIES

Unfortunately the existing experimental database on metaluminous/slightly peraluminous is very restricted, the comendite ND 002 of Scaillet and Mac Donald (2001) from the Olkaria complex has a comparable AI (1.05) to our starting sample, but at much higher silica and lower alumina. This means that we cannot rely on pre-existing experimental data base to compare with.

PRE-ERUPTIVE CONDITIONS OF THE TRACHYTIC MAGMA

The limited number of experiments done do not allow an in-depth discussion about Pre-eruptive conditions of trachyte magma at Pantelleria, nevertheless, the represent an important link with experimental studies carried out on a more evolved pantellerite composition from Pantelleria (Di Carlo et al., 2010). A more robust basis for discussion can be reached if we merge with complementary data derived by thermodynamic modelling (White at al.,2009; this thesis).

Consequently is possible to narrow the T-P constraints for crystallization of trachyte magmas to the following conditions: P = 1.0 - 1.5 kbar, T= 900-950 °C (See chapter 7).

Phase proportions obtained from experiment and Run 1-5 and subordinately Run 4-4, Table 9.3 are the closer to those observed in the natural rock . The compositions of clinopyroxene, alkali feldspar and olivine are Fs_{36-37}, $Ab_{65-66}Or_{26-28}$, and Fo_{24}, respectively, and when compared with the natural phenocrysts (Fs_{26}-$_{32,}$ $Ab_{68}Or_{22}$, Fo_{24}) strengthen the above consideration. Thus we propose as most likely pre-eruptive conditions for trachyte magma: P = 1.5 kb, T = 950 °C, H_2O = 2.5 - 2.8 wt%.

	R1.5 (P = 1.5 kb; T = 950 °C; H_2O = 2.5 wt%)	R4.4 (P = 1.0 kb; T= 950°C; H_2O = 2.8 wt%)	Starting material
K-feldspar	27	37	31
Clinopyroxene	3	5	2
Olivine	4	Tr	2
Fe-Ti oxides	Tr	Tr	1
Crystal tot %	35	43	36

TAB 9.3 Comparison of crystal abundances of runs 1.5 and 4.4 (wt %) with the natural rock (for this latter, modal abundances volume %, as reported in Table 3.1, were converted in wt %)

This hypothesis has an indirect confirmation by recent geophysical studies (Mattia et al., 2007) that suggest for Pantelleria, the presence of a magma reservoir at a depth of about 4 km, which corresponds to a lithostatic pressure slightly over 100 MPa (if an average crustal density = 2.6 g /cm^3 is taken.

RELATIONSHIPS WITH DERIVATIVE LIQUIDS

We were able to produce a pantellerite liquid (AI = 1.24, Run 4-5) at the following conditions : P = 1 kb; T = 950°C, H_2O = 1.6, for a total crystal content of 73 wt %.

These conditions are very different from the inferred pre-eruptive T-P-H_2O, being particularly much higher in temperature and at a water content unrealistically low (cf. Di Carlo et al., 2010). Thus, more experiments are needed to better address this argument, and in particular should be focused to explore lower T and higher H_2O conditions. Nevertheless we are allowed to say that the pantellerites are derivative of parental trachyte magma after 70 wt% of crystal fractionation.

This latter datum agrees well with independent calculations developed either geochemically (Civetta et al., 1998) or thermodynamically (White et al., 2009).

CONCLUSIVE REMARKS

Chemical and mineralogical study of samples from Montagna Grande lava pile and trachytic enclaves in more recent explosive products allow to focus on some aspects of the magma history in the past 50 ka at Pantelleria island:

- the occurrence of a products resulting from mixing processes between mafic and trachytic magmas gives evidence that basaltic magmas were intruded into the trachytic magma bodies below the caldera. The mafic end member shows characteristics close to those of the alkali basalts erupted outside the caldera in the past 50 ka. It can be regarded as a physical evidence of a strict relationships between basaltic and trachytic magmas;
- this study confirms a Daly gap between alkali-basaltic products (SiO_2~48 wt%) and trachytic rocks (SiO_2~64 wt%). Trace of intermediate compositions between the two end members are only found as sporadic crystals in mixed products and likely represent transitional events strictly associated with episodes of refilling from depth of the residing trachytic magma body;
- based on chemical composition of the trachytes and trace elements in clinopyroxene, two groups of trachytes ca be recognized (metaluminous High ITE and peraluminous Low ITE trachytes) which possibly depict two distinct petrogenetic trends;
- as a whole, trachytes can derive from alkali basalts via crystal fractionation. Different physical-chemical conditions, such as volatile pressure, oxygen fugacity, crystallization of accessory mineral phases, can determine different evolutionary trends, leading to trachytic magmas with different chemistry.

Crystallization experiments performed at T = 900-950 °C, P= 1.0 - 1.5 kb, H_2O_{melt} = 1.6 – 6.1 wt % , allow us to place some further constraints:

- pre-eruptive conditions: trachyte magma T-P- H_2O_{melt} conditions are closely reproduced by Runs 1-5 and 4-4, that match phase abundance and phase composition of the natural sample. Thus we propose as the most likely storage/crystallization conditions for trachyte magma at: T = 950 °C, P = 1.5 kb, H_2O_{melt} = 2.5- 2.8 wt %;
- Some experimental melts are characterized by a slight decrease in their peralkalinity (AI_{melt} down to 0.92), we invoke the "pyroxene effect" coupled to Fe-Ti oxides crystallization in a few feldspar-poor runs. When Keldspar crystallization becomes overwhelming produces a net increase in melt peralkalinity, emphasized also low peralkalinity of the feldspars themselves (AI_{feld} down to 0.82- 0.84);
- derivative melts: we were able to produce a pantellerite liquid (AI = 1.24, Run 4-5) at the following conditions: T = 950 °C, P = 1 kb, H_2O_{melt} = 1.6 wt %, at a total crystal content of 73 wt %. These conditions are very different from the inferred pre-eruptive T-P-H_2O of pantellerite magma (Di Carlo et al., 2010), being much higher in temperature and at an H_2O_{melt} unrealistically low. Thus, more experiments are needed to better address this argument, focused to explore the low-T and H_2O-rich region. Nevertheless, we are allowed to assess that pantellerites are derivative of parental trachyte magma after 70 % of crystal fractionation, and this agrees with independent estimates, either geochemical or via thermodinamical modelling.

REFERENCES

Argnani A., Torelli L., 2001. *The Pelagian Shelf and its graben system (Italy/Tunisia). In: Ziegler, P.A., Cavazza, W., Robertson, A.H.F. and Crasquin-Soleau, S. (Editors), Peri-Tethys Memoir 6: Peri-Tethyan Rift/Wrench Basins and Passive Margins.* Mémoires du Muséum National D'Histoire Naturelle **186**, 529-544.

Asimow P.D., Ghiorso M.S. (1998) - *Algorithmic modifications extending MELTS to calculate sub-solidus phase relations.* American Mineralogist **83,** 1127-1131.

Avanzinelli R., Bindi L., Menchetti S. & Conticelli S. (2004) - *Crystallization and genesis of peralkaline magmas from Pantelleria volcano: an integrated petrological and crystal-chemical study*. Lithos **73**, 41-69.

Bailey D.K. & Schairer J.F. (1964) - *Feldspar-liquid equilibria in peralkaline liquids-the orthoclase effect.* Am. Jour. Sci. **262**, 1198-1206.

Beccaluva L., Rossi P.L., Serri G., 1981. *Neogene to Recent volcanism of the southern Tyrrhenian–Sicilian area: implication for a geodynamic evolution of the Calabrian* Arc. Earth Evol. Sci. **3**, 222–238.

Ben-Avraham Z., Nur A., Cello G., 1987. *Active transcurrent fault system along the north African passive margin.* Tectonophyics **141**, 249–260.

Berrino G., Capuano P., 1995. *Gravity anomalies and structures at the island of Pantelleria.* Acta Vulcanologica **7,** 19-26.

Boccaletti M., Cello G. Tortorici L., 1987. *Transtensional tectonics in the Sicily Channel.* J. Struct. Geol. **9**, 869–876.

Brophy J.G. (2008) - *A study of rare earth element (REE)–SiO_2 variations in felsic liquids generated by basalt fractionation and amphibolite melting: a potential test for discriminating between the two different processes.* Contributions Mineral Petrol **158**, 99-111.

Burnham C.W. (1979) - *The importance of volatile constituents. In: Yoder, H. S., Jr., (ed) The evolution of igneous rocks.* Princeton University Press, p. 439-482.

Calanchi N., Colantoni P., Rossi P.L., Saitta M., Serri, G., 1989. *The Strait of Sicily continental rift systems: physiography and petrochemistry of the submarine volcanic centres.* Mar. Geol. **57**, 55– 83.

Cameron K.L., Parker D.F., Sampson D.E. (1996) - *Testing crustal models for the origin of flood rhyolites: a Nd–Pb–Sr isotopic study of the Tertiary Davis Mountains volcanic field, west Texas.* J Geophy Res **101**, 20407–20422

Catalano S., De Guidi G., Lanzafame G., Monaco C., Tortorici L., 2009. *Late Quaternary deformation on the island on Pantelleria: new constraints for the recent tectonic evolution of the Sicily Channel Rift (southern Italy).* J. Geodyn. **48**, 75–82.

Civetta L., Cornette Y., Crisci G., Gillot P. Y., Orsi G. (1983) - *The recent volcanic history of Pantelleria: a new interpretation.* In: Sheridan M.F. & Barberi F. (ends) *Explosive volcanism.* Journ. Volcan. Geot. Res. **17**, 361-373.

Civetta L., Cornette Y., Crisci G., Gillot P.Y., Orsi G. & Requejo C. S. (1984) – *Geology, geochronology and chemical evolution of the island of Pantelleria.* Geol. Mag. **121**, 541-562.

Civetta L., Cornette Y., Crisci G., Gillot P.Y., Orsi G. (1988) - *The eruptive history of Pantelleria (Sicily Channel) in the last 50 ka.* Bull. of Volcanol. **50**, 47-57.

Civetta L., D'Antonio M., Orsi G. & Tilton G. R. (1998) - *The geochemistry of volcanic rocks from Pantelleria Island, Sicily Channel: petrogenesis and characteristics of the mantle source region.* Jour. Petrol. **39**, 1453-1491.

Civile D., Lodolo E., Tortorici L., Lanzafame G., Brancolini G., 2008. - *Relationships between magmatism and tectonics in a continental rift: The Pantelleria Island region (Sicily Channel, Italy).* Marine Geology **251**: 32-46.

Della Vedova B., Pellis G. & Pinna E. (1989). *Studio geofisico dell'area 615–621. di transizione tra il Mar Pelagico e la piana abissale dello Ionio.* Atti dell'8° Convegno del Gruppo Nazionale di Geofisica della Terra Solida, Roma **1,** 543–558.

Devine J. D., Gardner J. E., Brack H. P., Layne G. D. & Rutherford M. J. (1995). Comparison of microanalytical methods for estimating H_2O contents of silicic volcanic glasses. *American Mineralogist* **80**, 319-328.

Di Carlo I., Rotolo S., Scaillet B., Pichavant M., 2007. - *Low-P hydrous phase equilibria of a pantellerite melt: Constraints on pre-eruptive condictions of recent felsic explosive volcanism at Pantelleria.* The Sixth Italian Forum of Earth Sciences, Geoitalia 2007, Rimini, 12-14 September.

Di Carlo I., Rotolo S., Scaillet B., Buccheri V., Pichavant M., 2010. - *Phase Equilibrium Constraints on Pre-eruptive Conditions of Recent Felsic Explosive Volcanism at Pantelleria Island, Italy*. Jour. Petrol. 5**1**, 2245- 2276

Esperanca S. and Crisci, G.M. (1995) - *The island of Pantelleria: a case for the development of DMM-HIMU isotopic composition in a long-lived extensional setting.* Earth Planet. Sci. Lett. **136**, 167–182.

Ferla P. & Meli C. (2006) - *Evidence of magma mixing in the "Daly gap" of alkaline suites: a case study from the enclaves of Pantelleria (Italy).* Jour. Petrol. **147**, 1467-1507.

Foerstner H. (1881). *Nota preliminare sulla geologia dell'isola Pantelleria secondo gli studi fatti negli anni 1874 e 1881*. Bollettino del Reale Comitato Geologico Italiano **12,** 532–556.

Frost B.R., Lindsley D., Anderson D.J., 1988. *Fe–Ti oxide–silicate equilibria: assemblages with fayalitic olivine*. American Mineralogist **73**, 727–740.

Ghiorso M.S., Sack R.O., 1995. - *Chemical mass transfer in magmatic processes. IV. A revised and internally consistent thermodynamic model for the interpolation and extrapolation of liquid-solid equilibria in magmatic systems at elevated temperatures and pressures.* Contributions to Mineralogy and Petrology **119**: 197-212.

Gioncada A. & Landi P. 2010 - *The pre-eruptive volatile contents of recent basaltic and pantelleritic magmas at Pantelleria (Italy).* Journal of Volcanology and Geothermal Research, **191**

Keller J., 1980. *The island of Vulcano*. Rend. Soc. Ital. Miner.Petrol. **36**, 369-414.

Korringa N.K. & Noble D.C. (1972). *Genetic significance of chemical, isotope and petrographic features of some peralkaline salic rocks from the island of Pantelleria.* Earth and Planetary Science Letters **17,** 258–262.

Kovalenko V.I., Hervig R.L. & Sheridan M.F. (1988). *Ion microprobe analyses of trace elements in anorthoclase, hedenbergite, aenigmatite, quartz, apatite and glass in pantellerite: evidence for high H_2O contents in pantellerite melt.* American Mineralogist **73,** 1038–1045.

Le Maitre R.W. (ed.) 2002. *Igneous Rocks. A Classification and Glossary of Terms.* Recommendations of the International Union of Geological Sciences Sub commission on the Systematic of Igneous Rocks, 2nd ed.

Lindsley D.H. & Frost B.R. (1992). - *Equilibria among Fe–Ti oxides, pyroxene, olivine and quartz: Part I.* Theory. American Mineralogist **77**, 987–1003.

Lowenstern J.B. & Mahood G. A. (1991) - *New data on magmatic H_2O contents of pantellerites, with implications for petrogenesis and eruptive dynamics at Pantelleria.* Bull. of Volcanol. **54**, 78-83.

Lowenstern J.B. (1994) - *Chlorine, fluid immiscibility, and degassing in peralkaline magmas from Pantelleria, Italy.* Am. Mineral. **79**, 353-369.

Macdonald R., (1974) - *Nomenclature and petrochemistry of the peralkaline oversatured extrusive rocks*. In*:* Bailey D.K., Barberi F. & MacDonald R. Eds. Oversatured peralkaline volcanic rocks. Bull. of Volcanol. **38**, 498-516. Sp. Issue.

Macdonald R., Scaillet B., 2006. -*The central Kenya peralkaline province: Insights into the evolution of peralkaline salic magmas.* Lithos **91**, 59-73.

Mahood G.A., Baker D.R., 1986. - *Experimental constraints on depths of fractionation of mildly alkalic basalts and associated felsic rocks: Pantelleria, Strait of Sicily.* Contributions to Mineralogy and Petrology **93**, 251-264.

Mahood G.A., Halliday A.N., Hildreth W., 1990. - *Isotopic evidence for the origin of pantellerites in a rift-related alkalic suite: Pantelleria, Italy.* International Volcanology Congress of the International Association of Volcanology and Chemistry of the earth's Interior (IAVECI) Mainz, Abstracts Volume.

Mahood G.A., Stimac J.A., 1990. - *Trace-element partitioning in pantellerites and trachytes.* Geochimica et Cosmochimica Acta **54**, 2257-2276.

Mahood G.A. & Hildreth W. (1983) - *Nested calderas and trapdoor uplift at Pantelleria, Strait of Sicily.* Geology. **11**, 722-726.

Mahood G.A. & Hildreth W. (1986) - *Geology of the peralkaline volcano at Pantelleria, Strait of Sicily.* Bull. of Volcanol. **48**, 143-172.

Margari V., Pyle D.M., Bryant C., Gibbard P.L., 2007. *Mediterranean tephra stratigraphy revisited: results from a long terrestrial sequence on Lesvos Island, Greece*. J. Volcanol. Geotherm. Res. **163,** 34–54.

Marks M. & Markl G. (2001). *Fractionation and assimilation processes in the alkaline augite syenite unit of the Ilimaussaq Intrusion, South Greenland, as deduced from phase equilibria.* Journal of Petrology **42**, 1947-1969.

Martel C., Pichavant M., Holtz F., Scaillet B., Bourdier J.-L. & Traineau H. (1999). *Effects of fO_2 and H_2O on andesite phase relations between 2 and 4 kbar.* Journal of Geophysical Research **104**, 29453-29470.

Mattia M., Bonnacorso A. & Guglielmino F. (2007). *Ground deformations in the island of Pantelleria (Italy): insights into the dynamic of the current inter-eruptive period.* Journal of Geophysical Research **112**.

McDonough W.F. & Sun S.S. (1995) -*The composition of the Earth.* Chem Geol **120**, 223–253

Morimoto N., Fabries J., Ferguson A.K., Ginzburg I.V., Ross M., Seirfert F.A. & Zussman J. (1988) - *Nomenclature of pyroxenes.* Mineral. Mag. **52**, 535-550.

Mushkin, A., Stein, M., Halicz, L., Navon, O., 2002. - *The Daly gap: Low-pressure fractionationand heat loss from a cooling magma chamber.* Geochimica et Cosmochimica Acta **66**, Supplement 1: A539.

O'Neill H.St.C. & Pownceby M.I. (1993), *Thermodynamic data from redox reactions at high temperatures. I An experimental and theoretical assessment of the electrochemical method using stabilised zirconia electrolytes, with revised values for the Fe-"FeO" Co-CoO, Ni-NiO and Cu-Cu_2O oxygen buffers, and new data for the W-$W0_2$ buffer.* Contribution to Mineralogy and Petrology **114,** 296-314.

Orsi G. & Sheridan M. F. (1984) - *The Green Tuff of Pantelleria: rheo-ignimbrite or rheomorphic fall?* Bull. of Volcanol. **47**, 611-626.

Orsi G., Ruvo L. & Scarpati C. (1991/a) - *The recent explosive volcanism at Pantelleria.* Geol. Rundschau. **80**, 187-200.

Papale P. (1997). - *Modelling of the solubility of a one-component H_2O or CO_2 fluid in silicate liquids.* Contributions to Mineralogy and Petrology **126**, 237–251.

Parello F., Allard P., D'Alessandro W., Federico C., Jean-Baptiste P., Catani O. (2000) - *Isotope geochemistry of Pantelleria volcanic fluids, Sicily Channel rift: a mantle volatile end-member for volcanism in southern Europe.* Earth and Planetary Science Letters **180**, 325-339.

Perugini D., Poli G. & Prosperini N. (2002) - *Morphometric analysis of magmatic enclaves: a tool for understanding magma vesiculation and ascent.* Lithos **61**, 225-235.

Pownceby M.I. & O'Neill H. St. C. (1994). *Thermodynamic data from redox reactions at high temperatures. III. Activity-composition relations in Ni-Pd alloys from EMF measurements at 850-1250 K and calibration of the NiO + Ni-Pd assemblage as a redox sensor*. Contributions to Mineralogy and Petrology **116**, 327-339.

Prosperini N., Perugini D., Poli G. & Manetti P. (2000) - *Magmatic enclaves distribution within the Khaggiar lava dome (Pantelleria, Italy): implication for magma chamber dynamics and eruption.* Acta Vulcanologica **12**, 34-47.

Ren M., Omenda P.A., Anthony E.Y., White J.C., Macdonald R., Bailey D.K. (2006). - *Application of the QUILF thermobarometer to the peralkaline trachytes and pantellerites of the Eburru volcanic complex, East African Rift, Kenya.* Lithos **91**, 109–124

Rittmann A. (1967). *Studio geovulcanologico e magmatologico dell' isola di Pantelleria.* Rivista Mineraria Siciliana **106–108,** 147–204.

Robie R.A., Hemkingway B.S. & Fisher J.R. (1979). *Thermodynamic properties of minerals a,d related substances at 298.15 °K and 1 bar (105 Pascals) pressure and at higher temperature.* Geological Survey bulletin **1452**.

Rossi P.L., Tranne C.A., Calanchi N., Lanti E., 1996. *Geology, stratigraphy and volcanological evolution of the island of Linosa (Sicily Channel).* Acta Vulcanologica **8**, 73-90.

Rotolo S., Castorina F., Cellura D. & Pompilio M. (2006). - *Petrology and geochemistry of submarine volcanism in the Sicily Channel Rift.* Jour. Geol. **114**, 355-365.

Rotolo S., La Felice S., Mangalaviti A., Landi P. (2007) - *Geology and petrochemistry of the recent (< 25 KA) silicic volcanism at Pantelleria island.* Bollettino della Società Geologica Italiana **126**, 191-208.

Scaillet B., Pichavant M. & Roux, J. (1995). *Experimental crystallization of leucogranite magmas.* Journal of Petrology **36**, 663-705.

Scaillet B. & Macdonald R. (2001) - *Phase relations of peralkaline silicic magmas and petrogenetic implications.* Journal of Petrology **42**, 825-845.

Scaillet B. & Macdonald R. (2003) - *Experimental constraints on the relationships between peralkaline rhyolites of the Kenia Rift Valley.* Journ. of Petrology **44**, 1867-1894.

Scaillet B. & Pichavant M. (2005). *A model of sulphur solubility for hydrous mafic melts: application to the determination of magmatic fluid compositions of Italian volcanoes.* Annals of Geophysics **48**, 671-698.

Scaillet B. & Macdonald R., (2006) - *Experimental constraints on pre-eruptive conditions of pantelleritic magmas: Evidence from the Eburru complex, Kenya Rift.* Lithos **91**, 95-108.

Sisson T.W. & Grove T.L. (1993B). - *Temperature and H_2O contents of low-MgO high alumina basalts.* Contributions to Mineralogy and Petrology **113**, 167–184.

Tiepolo M., Bottazzi P., Palenzona M., Vannucci R., 2003. - *A laser probe coupled with ICP-double-focusing sector-field mass spectrometer for in situ analysis of geological samples and U–Pb dating of zircon.* Can. Mineral. **41**, 259–272.

Van Achterbergh E., Ryan C.G., Jackson S.E., Griffin W., 2001. *Data reduction software for LA-ICP-MS. In: Sylvester, P. (Ed.), Laser ablation-ICPMS in the earth science.* Mineral. Assoc. Can., vol. **29**, p. 239–243.

Villari L. (1974) - *The Island of Pantelleria.* Bull. Volc. **38**, 680-724.

Washington H.S. (1914) - *The volcanoes and rocks of Pantelleria*. Journal Geol. **21,** 653-713.

White J.C., Holt G.S., Parker D.F., Ren M., 2003. *Trace-element partitioning between alkali feldspar and peralkalic quartz trachyte to rhyolite magma. Part I: Systematics of trace1065 element partitioning.* American Mineralogist **88**, 316-329.

White J.C., Ren M. & Parker D.F. (2005) - *Variation in mineralogy, temperature, and oxygen fugacity in a suite of strongly peralkaline lavas and tuffs, Pantelleria, Italy.* Canad. Mineral. **43**, 1331-1347.

White J.C., Parker D.F. and Ren M. (2009) – *The origin of trachytes and pantellerite from Pantelleria, Italy: Insights from major element, trace element and thermodynamic modelling.* Journ. of Volc. Geoth Res. **179**, 33-55.

Wolff J.A., Wright J.V. (1981) *Rheomorphism of welded tuffs.* Journal of Volcanology and Geothermal Research **10**, 13–34

Wolff, J.A., Wright, J.V., (1981). *Formation of the Green Tuff, Pantelleria.* Bulletin of Volcanology **44**, 681–690.

Wright, J. V. (1980). *Stratigraphy and geology of the welded air-fall tuffs of Pantelleria, Italy.* Geologische Rundschau **6,** 263–291.

APPENDIX

ANALYTICAL TECHNIQUES

XRF ANALYSIS

Whole-rock analyses were carried out on rock chips left in to distilled water overnight in order to minimize the possible absorption of marine aerosol. Samples were ground using an agate mortar.

All the samples were analyzed by electron-dispersive X-ray fluorescence spectroscopy (WDS-XRF) RIGAKU spectrometer, hosted at Dept. C.F.T.A., Univ. of Palermo.

Selected of samples were analyzed for trace-elements by ICP-MS (trace elements) technique at Activation Laboratories, Ancaster, Ontario.

MICROANALYSES (MINERALS AND GLASSES)

SEM-EDS

Lavas and scoriae were reduced to polished thin sections or mounted in epoxy for microanalyses. Mineral and textural analyses were performed using a LEO™ 440 scanning electron microscope coupled to an Oxford-Link EDS, hosted at Dept CFTA. Operating conditions were: 20 kV accelerating voltage and 600 pA beam current, live time 100 s. Natural mineral standards were used to calibrate quantitative analyses.

EMP

A JEOL-JXA-8200, electrone microprobe (combined WDS/EDS micro analyzer) hosted at Istituto Nazionale di Geofisica e Vulcanologia, Rome, was used for major elements analysis of glass and selected clinopyroxenes (i.e. those cpx analysed for trace

elements by LA ICP MS, see below). Operating conditions were voltage 15 kV, beam probe diameter 5 μm and beam current 5 nA for glasses and 14 nA for minerals.

LA-ICP-MS

Trace elements in clinopyroxene were obtained by laser ablation–inductively coupled plasma–mass spectrometry (LA-ICP-MS), using an laser source and Spectrometer at the Consiglio Nazionale delle Ricerche–Istituto de Geoscienze e Georisorse, Pavia, Italy.

LA-ICP-MS is a sensitive analytical method for rapid multi-element determination in the trace, the sample material to be investigated is vaporized in a laser plasma by focussed laser radiation and transported with argon into the inductively coupled plasma ion source of an ICP-MS. The positively charged ions are extracted from the inductively coupled plasma through an interface into the high vacuum of the mass spectrometer and separated in the mass-spectrometric separation system according to their mass/charge ratio and energy/charge ratio and detected by a secondary electron multiplier.

The instrument at CNR- Pavia Laboratory, couples a 266 nm Nd: YAG laser source (Brilliant-Quantel) to a quadrupole ICP-MS (DRCe - Perkin Elmer). The laser was operated at 10 Hz adopting a spot size of 20–40 μm and a pulse energy of about 0.01–0.03 mJ. Selected masses were acquired in peak hopping mode with a dwell time of 10 ms. Each analysis consisted in the acquisition of 60 s on background and 60 s on peak. SRM Nist612 and 44Ca were used as external and internal standard, respectively. Data reduction was carried out with the Glitter software (Van Achterbergh et al., 2001).

Accuracy is estimated to be better than 5% relative (for further details, see Tiepolo et al., 2003).

INFRARED SPECTROSCOPY

The FTIR spectroscopy (Bruker Tensor 27 spectrometer coupled to Hyperion TM Microscope, Dip. CFTA).

Was used to evaluate precisely the H_2O dissolved in a few selected near-liquidus experimental glasses . To solve the Beer-Lambert equation , and to obtain an H_2O value,

were chosen the following variables: molar extinction coefficients were taken from Di Matteo et al., (2004) : 62 (l *mol^{-1} *cm^{-1}) for the 3550 cm^{-1} band, 1.58 (l *mol^{-1} *cm^{-1}) for the 4500 cm^{-1} and 1.36 (l *mol^{-1} *cm^{-1}) for the 5200 cm^{-1}. Either the 3550 cm^{-1} MIR band (H_2O tot) or, when saturated (absorptivity > 1.5) due to high water content or exceedingly thick glass chip (i.e. > 80 microns), were used the 4500 (OH^-) + 5200 (H_2O mol) NIR bands. Melt density was calculated, according to Ochs and Lange, 1999, and varied in the range 2395-2400 g/l in response to variation in H_2O content.

The H_2O concentrations derived from these near-liquidus runs (using the Beer-Lambert equation) were then applied to calibrate the measurement of H_2O by electron microprobe with the by-difference method (Devine, et al., 1995) for all those crystal-rich charges not analyzable by FT-IR. The “by difference” method is based on the assumption that the difference to 100 of the sum of oxides (totals) of glass microprobe analyses, is equal to the amount of dissolved H_2O.

Representative SEM-EDS analyses of K-feldspar.

Sample	**0720**			**0721**			**0722**				**0723**			
Formation	**Green Tuff**			**Green Tuff**			**Green Tuff**				**Green Tuff**			
member	**A**			**B**			**C**				**D**			
	Pumice fall			**Pumice flow**			**Weld. Eutax.**				**Weld. Fines-rich**			
position	**Botton**						**Intermediate**							
Type	mpheno	pheno	pheno	pheno	pheno	mpheno	mpheno	pheno, R	pheno, C	mpheno	mpheno	pheno, R	pheno	pheno	pheno
SiO_2	66.31	65.72	66.49	63.38	66.09	65.88	65.86	66.43	65.79	66.63	66.02	66.43	66.30	65.49	65.21
Al_2O_3	18.66	18.79	18.91	18.17	19.05	18.77	18.77	19.12	19.46	18.68	19.68	19.12	18.94	19.19	19.35
FeO	0.00	0.00	0.00	1.02	0.00	0.00	0.00	0.27	0.37	0.13	0.54	0.27	0.38	0.16	0.40
CaO	0.00	0.07	0.04	0.03	0.03	0.05	0.02	0.06	0.15	0.00	0.22	0.06	0.07	0.04	0.04
Na_2O	7.27	7.39	7.25	13.37	7.98	8.02	7.80	7.41	7.56	7.03	8.49	7.41	8.08	7.26	5.24
K_2O	6.43	6.43	6.53	5.58	6.00	6.01	6.11	6.08	6.42	6.55	5.00	6.08	5.67	7.25	9.80
An	0.0	0.3	0.2	0.1	0.2	0.3	0.1	0.3	0.3	0.0	0.3	0.3	0.3	0.2	0.2
Ab	63.2	63.3	62.7	78.3	66.8	66.8	65.9	64.8	63.7	62.0	71.3	64.8	68.2	60.3	44.8
Or	36.8	36.3	37.1	21.6	33.0	32.9	34.0	34.9	35.6	38.0	27.7	34.9	31.5	39.6	55.1

Sample	**0731**															
Formation	**Green Tuff**															
member	**E**															
	Welded fines-depleted															
position	**Top**															
Type	pheno, R	pheno, I	pheno, C	pheno, R	pheno, I	pheno, C	pheno, R	pheno, I	pheno, C	mpheno, R	mpheno, C	mpheno, R	mpheno, C	micro	micro	micro
SiO_2	65.79	64.70	64.39	65.04	65.05	64.93	65.35	64.90	65.27	64.83	64.76	64.55	64.44	65.29	63,36	65.38
Al_2O_3	19.44	20.80	21.19	21.14	20.89	20.41	20.40	20.33	20.61	20.57	20.42	20.51	20.74	19.41	20.15	18.88
FeO	0.64	0.17	0.26	0.25	0.37	0.33	0.36	0.27	0.21	0.23	0.15	0.17	0.17	1.01	0.61	1.05
CaO	0.31	0.97	1.62	1.09	1.42	0.83	0.88	0.95	1.03	1.03	0.93	1.06	1.37	0.22	0.47	0.58
Na_2O	8.44	8.67	8.28	8.42	7.91	8.09	8.25	8.17	7.94	8.02	8.33	8.50	8.36	7.90	10.47	7.48
K_2O	5.15	4.39	3.94	4.34	3.96	4.66	4.58	4.64	4.35	4.48	4.59	4.44	4.31	5.65	4.37	6.20
An	1.4	4.4	7.6	5.1	6.9	3.9	4.2	4.5	5.0	4.9	4.3	4.9	6.3	1.1	1.9	2.7
Ab	70.4	71.7	70.3	70.9	70.0	69.7	70.2	69.5	69.8	69.5	70.2	70.8	69.9	67.3	77.0	63.0
Or	28.2	23.9	22.0	24.0	23.0	26.4	25.6	26.0	25.2	25.5	25.5	24.3	23.7	31.7	21.1	34.3

All mineral analyses were recalculated to 100 %. Pheno = phenocrysts and mpheno = microphenocrysts (> 50 µm). Micro = microlites (< 50 µm); R= rim, C = core, I = intermediate; An = anorthite, Ab = albite, Or =orthoclase (mol%).

Representative SEM-EDS analyses of K-feldspar.

Sample	**0718**																	
Formation	**Trachyte**																	
Litology	**Trachyte "Case Ricco"**																	
Type	pheno, R	pheno, I	pheno, C	pheno, R	pheno, I	pheno, C	pheno, R	mpheno,	mpheno	mpheno, R	mpheno,	mpheno, R	mpheno, C	micro	micro	micro	micro	micro
SiO_2	65.24	65.7	64.76	66.28	65.41	65.49	66.08	63.61	66.13	65.06	66.80	62.17	64.86	63.96	64.17	64.49	66.20	65.47
Al_2O_3	20.65	20.75	21.05	19.81	21.26	21.22	19.91	21.74	19.59	20.96	18.42	23.20	20.24	21.88	21.42	21.53	20.08	20.13
FeO	0.41	0.16	0.21	0.55	0.16	0.17	0.41	0.51	0.33	0.23	0.57	0.46	0.66	0.34	0.35	0.27	0.48	0.86
CaO	1.13	1.39	1.69	0.44	1.75	1.64	0.98	2.48	2.55	1.44	0.00	4.13	0.71	2.63	2.47	2.24	0.61	0.73
Na_2O	7.94	8.11	8.31	8.15	8.16	8.24	8.17	8.19	8.09	8.64	6.03	8.14	8.21	8.38	8.17	8.43	7.69	7.9
K_2O	4.3	3.88	3.26	4.77	2.92	3.01	4.02	2.87	4.87	3.67	8.18	1.50	4.85	2.19	2.89	2.8	4.59	4.51
BaO	0.33	0.00	0.71	0.00	0.34	0.25	0.44	0.60	0.44	0.00	0.00	0.40	0.48	0.61	0.72	0.24	0.34	0.40
An	5.5	6.7	8.2	2.1	8.8	8.1	4.8	12.0	13.6	1.5	11.9	6.7	5.7	7.3	9.2	7.3	5.1	4.4
Ab	69.7	70.9	73.0	70.7	73.9	74.1	71.9	71.5	71.7	69.2	69.7	71.6	73.5	71.1	71.7	72.3	70.7	69.5
Or	24.8	22.3	18.8	27.2	17.4	17.8	23.3	16.5	14.7	29.3	18.4	21.7	20.8	21.6	19.1	20.4	24.2	26.1

Sample	**0748**																	
Formation	**Trachyte**																	
Litology	**Trachyte "Montagna Grande Sud"**																	
Type	pheno, R	pheno, I	pheno, C	pheno, R	pheno, I	pheno, C	pheno, R	pheno, C	pheno, R	pheno, C	pheno, R	pheno, C	mpheno, R	mpheno, I	mpheno, C	micro	micro	micro	micro
SiO_2	64.46	64.13	62.93	63.02	63.36	61.37	64.95	63.77	63.85	63.25	64.07	64.58	63.61	62.70	61.40	67.84	69.27	66.69	65.71
Al_2O_3	20.76	21.64	22.45	22.62	22.74	23.30	21.37	21.34	20.86	22.34	20.98	20.45	21.69	22.46	23.22	15.73	15.55	18.26	19.48
FeO	0.47	0.09	0.32	0.17	0.01	0.00	0.00	-0.04	0.72	0.20	0.40	0.73	0.03	0.06	0.39	0.07	0.00	0.08	0.67
CaO	1.71	2.32	3.03	2.65	3.04	3.76	1.79	1.93	1.64	2.38	1.08	1.49	2.64	3.21	4.08	0.51	0.58	0.25	0.31
Na_2O	8.17	8.17	8.28	7.90	8.03	8.70	8.09	8.66	8.61	8.27	8.10	8.03	8.66	8.15	8.37	4.42	4.29	7.45	7.30
K_2O	4.18	2.99	2.54	2.66	2.62	1.89	3.67	3.44	3.55	3.02	4.34	4.25	2.95	2.60	1.84	6.24	5.99	5.86	6.35
BaO	0.24	0.28	0.21	0.53	0.22	0.20	0.28	0.26	0.27	0.15	0.59	0.93	0.31	0.49	0.61	2.51	2.61	1.20	0.75
An	7.9	11.2	14.4	13.2	14.7	17.3	8.6	8.9	7.6	11.4	5.2	7.1	12.1	15.3	19.1	3.2	3.7	1.2	1.5
Ab	68.9	71.6	71.2	71.1	70.2	72.4	70.4	72.2	72.7	71.5	70.1	68.9	71.8	70.0	70.7	50.2	50.2	65.1	62.6
Or	23.2	17.2	14.4	15.8	15.1	10.4	21.0	18.9	19.7	17.2	24.7	24.0	16.1	14.7	10.2	46.6	46.1	33.7	35.9

All mineral analyses were recalculated to 100 %. Pheno = phenocrysts and mpheno = microphenocrysts (> 50 µm). Micro = microlites (< 50 µm); R= rim, C = core, I = intermediate; An = Anorthite, Ab = Albite, Or = Orthoclase (mol %).

Representative SEM-EDS analyses of K-feldspar.

Sample	**0750**																		
Formation	**Trachyte**																		
Litology	**Trachyte "Montagna Grande Nord"**																		
Type	pheno, R	pheno, C	pheno, R	pheno, I	pheno, C	pheno, R	pheno, I	pheno, C	pheno, R	pheno, C	mpheno, R	mpheno, I	mpheno, C	mpheno, R	mpheno, C	micro	micro	micro	micro
SiO_2	65.00	64.60	63.90	64.06	64.61	63.52	53.42	53.54	64.46	56.08	64.89	60.89	59.99	62.42	53.51	63.91	63.66	64.4	65.20
Al_2O_3	21.08	21.18	21.39	21.32	21.16	22.00	28.78	28.21	20.92	26.88	20.31	23.34	24.21	22.69	29.08	20.88	21.23	21.07	19.50
FeO	0.00	0.00	0.00	0.00	0.00	0.00	0.00	0.00	0.00	0.00	0.00	0.00	0.00	0.00	0.00	0.00	0.00	1.02	0.00
CaO	1.15	1.60	1.81	1.83	1.46	2.77	11.19	10.95	1.36	8.75	1.39	4.48	5.18	3.60	10.84	1.55	1.86	1.66	1.13
Na_2O	8.33	8.41	8.27	8.56	8.16	8.44	5.17	5.55	8.47	7.03	8.66	8.26	8.09	8.58	5.51	8.50	8.23	7.52	8.16
K_2O	3.92	4.05	3.49	3.58	3.66	2.72	0.45	0.55	3.96	0.59	3.58	1.82	1.55	1.87	0.35	4.17	3.57	3.98	4.42
BaO	0.00	0.00	0.00	0.00	0.00	0.00	0.00	0.00	0.00	0.00	0.00	0.00	0.00	0.00	0.00	0.00	0.00	0.00	0.00
An	5.5	7.4	8.7	8.5	7.1	13.0	53.1	50.6	6.3	39.5	6.5	20.7	23.9	16.9	51.1	7.1	8.9	8.3	5.3
Ab	72.2	70.3	71.5	71.8	71.7	71.8	44.4	46.4	71.6	57.4	73.5	69.2	67.6	72.7	47.0	70.2	70.9	68.0	69.8
Or	22.3	22.3	19.8	19.8	21.2	15.2	2.6	3.0	22.1	3.2	20.0	10.1	8.5	10.4	2.0	22.7	20.3	23.7	24.9

Sample	**0732**																		
Formation	**Trachyte**																		
Litology	**Trachyte "Mueggen"**																		
Type	pheno, R	pheno, C	pheno, I	pheno, C	pheno, I	pheno, R	pheno, C	pheno, I	pheno, R	pheno, C	pheno, R	mpheno, C	mpheno, R	mpheno, C	mpheno, R	micro	micro	micro	micro
SiO_2	65.72	65.96	65.75	66.03	65.67	65.97	65.34	66.19	66.10	65.69	65.98	65.61	65.94	66.03	65.80	66.10	66.59	65.99	65.72
Al_2O_3	19.50	19.08	19.72	19.31	19.30	19.16	19.23	19.80	19.31	19.42	19.01	18.14	19.08	18.51	19.16	19.21	18.28	18.62	19.50
FeO	0.57	0.35	0.27	0.40	0.41	0.16	0.21	0.21	0.55	0.68	0.88	1.86	0.78	1.45	0.54	0.33	1.53	1.10	0.57
CaO	0.08	0.16	0.12	0.24	0.11	0.08	0.22	0.20	0.11	0.14	0.06	0.20	0.11	0.02	0.05	0.17	0.12	0.26	0.08
Na_2O	7.56	7.70	7.73	7.61	7.75	7.89	7.92	7.69	7.92	8.10	7.91	7.61	8.00	7.84	7.68	7.72	7.88	7.59	7.56
K_2O	6.51	6.26	6.39	6.32	6.44	6.37	6.39	6.17	6.01	5.98	6.03	5.79	5.81	5.94	6.40	6.20	5.57	6.26	6.51
BaO	0.00	0.00	0.00	0.00	0.00	0.00	0.00	0.00	0.00	0.00	0.00	0.00	0.00	0.00	0.00	0.00	0.00	0.00	0.00
An	0.4	0.7	0.5	1.1	0.5	0.3	1.0	0.9	0.5	0.6	0.3	1.0	0.5	0.1	0.3	0.8	0.6	1.2	0.4
Ab	63.6	64.7	64.4	63.9	64.3	65.1	64.7	64.9	66.4	66.9	66.4	66.0	67.3	66.7	64.4	64.9	67.9	64.1	63.6
Or	36.0	34.6	35.1	35.0	35.2	34.6	34.3	34.2	33.1	32.5	33.3	33.0	32.2	33.2	35.3	34.3	31.6	34.7	36.0

All mineral analyses were recalculated to 100 %. Pheno = phenocrysts and mpheno = microphenocrysts (> 50 µm). Micro = microlites (< 50 µm); R=rim, C = core, I = intermediate; An = Anorthite, Ab = Albite, Or = Orthoclase (mol %).

Representative SEM-EDS analyses of K-feldspar.

Sample	**pant24**																		
Formation																			
Litology	**trachyte enclave**																		
position	**“pumice C. Randazzo”**																		
Type	pheno, R	pheno, C	pheno, R	pheno, C	pheno, R	pheno, C	pheno, R	pheno, C	pheno, R	pheno, I	pheno, C	mpheno, R	mpheno, C	mpheno, R	mpheno, C	micro	micro	micro	micro
SiO_2	65.33	64.90	65.35	65.58	65.83	66.20	65.54	65.26	65.16	64.76	65.81	64.77	64.40	65.49	65.86	65.24	65.50	66.37	65.32
Al_2O_3	19.37	20.06	19.80	19.63	18.69	19.07	19.97	19.84	19.66	20.51	19.90	20.28	20.90	19.67	19.70	19.66	19.83	18.59	19.12
FeO	0.03	0.17	0.37	0.12	0.24	0.00	0.04	0.32	0.36	0.51	0.02	0.65	0.51	0.00	0.17	0.00	0.16	0.29	0.00
CaO	0.47	0.60	0.27	0.26	0.05	0.04	0.28	0.43	0.33	0.67	0.31	0.72	1.18	0.27	0.39	0.40	0.53	0.00	0.00
Na_2O	7.95	7.96	7.42	7.47	7.86	7.64	7.57	7.78	7.79	7.94	7.46	7.81	7.83	7.60	7.37	7.59	7.51	7.48	7.32
K_2O	5.63	5.84	6.20	6.23	5.99	6.33	6.15	5.99	6.22	5.25	6.44	5.26	4.53	6.32	5.98	6.35	6.10	6.30	6.53
BaO	0.00	0.00	0.00	0.00	0.00	0.00	0.00	0.00	0.00	0.00	0.00	0.00	0.00	0.00	0.00	0.00	0.00	0.00	0.00
An	2.2	2.7	1.3	1.2	0.2	0.2	1.3	2.0	1.5	3.2	1.5	3.5	5.7	1.3	1.9	1.8	2.5	0.0	0.0
Ab	66.7	65.6	63.7	63.8	66.5	64.6	64.3	65.0	64.6	67.5	62.9	66.9	68.3	63.8	64.0	63.3	63.6	64.6	63.0
Or	31.1	31.6	35.0	35.0	33.3	35.2	34.4	33.0	33.9	29.4	35.7	29.6	26.0	34.9	34.1	34.9	33.9	35.8	37.0

Sample	**pant21**																		
Litology	**trachyte enclave**																		
position	**“pumice C. Randazzo”**																		
Type	pheno, R	pheno, C	pheno, R	pheno, C	pheno, R	pheno, I	pheno, C	pheno, R	pheno, C	pheno, R	pheno, C	mpheno, R	mpheno, C	mpheno, R	mpheno, C	mpheno, R	micro	micro	micro	micro
SiO_2	65.14	65.63	65.24	65.22	65.60	65.06	65.55	65.65	65.62	65.79	65.05	65.91	65.51	66.05	65.52	65.68	65.31	65.27	65.47	66.21
Al_2O_3	19.81	19.40	19.65	20.04	19.55	20.14	20.22	19.70	19.90	19.80	20.00	19.10	19.37	19.52	19.70	19.78	19.86	19.73	19.61	19.29
FeO	0.27	0.36	0.33	0.20	0.38	0.24	0.39	0.35	0.30	0.31	0.37	0.26	0.15	0.25	0.27	0.21	0.25	0.39	0.42	0.66
CaO	0.29	0.20	0.29	0.53	0.24	0.65	0.73	0.29	0.19	0.28	0.41	0.09	0.13	0.21	0.14	0.30	0.45	0.32	0.27	0.09
Na_2O	7.75	7.29	7.73	7.60	7.56	7.72	8.03	7.54	7.61	7.43	7.48	7.59	7.53	7.59	7.43	7.78	7.54	7.62	7.49	7.68
K_2O	6.03	6.62	6.19	5.79	6.32	5.66	5.08	6.00	6.23	6.27	6.06	6.58	6.38	6.39	6.47	5.80	6.06	6.34	6.28	5.74
BaO	0.27	0.20	0.15	0.36	0.28	0.24	0.14	0.09	0.10	0.12	0.19	0.43	0.28	0.16	0.03	0.10	0.16	0.36	0.07	0.08
							.													
An	1.3	0.9	1.4	2.5	1.1	3.1	3.4	1.4	0.9	1.3	1.9	0.4	0.6	1.0	0.6	1.4	2.1	1.5	1.3	0.4
Ab	65.2	62.0	64.6	64.9	63.8	65.4	68.2	64.7	64.4	63.4	64.0	63.4	63.8	63.7	63.2	66.1	64.0	63.7	63.6	66.7
Or	33.4	37.1	34.0	32.6	35.1	31.6	28.4	33.9	34.7	35.2	34.1	36.2	35.6	35.3	36.2	32.4	33.9	34.8	35.1	32.8

All mineral analyses were recalculated to 100 %. Pheno = phenocrysts and mpheno = microphenocrysts (> 50 µm). Micro = microlites (< 50 µm); R = rim, C = core, I = intermediate; An = Anorthite, Ab = Albite, Or = Orthoclase (mol %).

Representative SEM-EDS analyses of K-feldspar.

Sample	**pant23**																			
Litology	**trachyte enclave**																			
position	**“pumice C. Randazzo”**																			
Type	pheno, R	pheno, I	pheno, C	pheno, R	pheno, I	pheno, C	pheno, R	pheno, C	pheno, R	pheno, C	pheno, R	pheno, C	mpheno, C	mpheno, R	mpheno, C	mpheno, R	micro	micro	micro	micro
SiO_2	66.01	64.40	63.00	65.57	63.79	62.59	65.93	65.42	66.27	65.95	65.65	66.01	64.22	65.02	66.00	65.94	65.85	67.24	66.96	65.28
Al_2O_3	19.70	21.07	21.72	19.98	21.48	22.46	19.42	20.05	19.59	19.89	19.90	20.10	19.93	20.38	19.86	20.03	19.98	18.45	17.08	18.11
FeO	0.72	1.02	1.56	0.65	1.33	1.25	0.83	0.83	0.35	0.45	0.47	0.40	0.67	0.54	0.57	0.38	0.41	0.02	0.61	0.56
CaO	0.65	1.66	2.31	0.78	2.19	3.19	0.41	0.60	0.29	0.61	0.61	0.35	0.77	0.45	0.55	0.54	0.59	0.24	0.36	0.95
Na_2O	7.54	7.52	7.77	7.71	7.57	7.74	7.48	7.35	7.43	7.55	7.45	7.60	7.98	7.85	7.59	7.36	7.43	6.95	7.25	7.43
K_2O	5.14	3.98	3.22	4.93	3.41	2.54	5.44	5.47	5.50	5.31	5.47	5.36	5.89	5.48	5.30	5.48	5.44	6.00	5.53	5.37
BaO	0.20	0.05	0.15	0.10	0.62	0.87	0.00	0.00	0.00	0.00	0.00	0.00	0.00	0.00	0.00	0.00	0.00	0.00	0.20	0.08
An	3.2	8.3	11.4	3.8	11.0	15.8	2.0	2.9	1.4	3.0	3.0	1.7	3.5	2.1	2.7	2.6	2.9	1.0	1.3	4.6
Ab	66.8	68.0	69.6	67.7	68.7	69.3	66.3	65.2	66.3	66.3	65.4	67.1	65.0	67.1	66.7	65.3	65.5	63.8	66.4	64.7
Or	30.0	23.7	19.0	28.5	20.4	15.0	31.7	31.9	32.3	30.7	31.6	31.2	31.5	30.8	30.6	32.1	31.6	35.2	33.3	30.8

Sample	**0749**																						
Litology	**Benmoreite**																						
Type	pheno, C	pheno, I	pheno, R	Pheno	pheno	pheno,	pheno,	pheno, C	pheno, R	pheno, R	pheno, I	pheno, C	pheno, R	pheno, I	pheno, C	pheno, R	pheno, I	pheno, R	pheno, C	pheno, C	pheno, C	pheno, C	pheno, R	pheno, I
SiO_2	62.38	61.92	59.87	57.76	57.44	57.23	55.80	65.06	65.18	59.09	61.62	63.89	59.19	57.05	55.84	60.67	63.32	59.87	61.92	59.73	59.73	59.64	64.42	60.94
Al_2O_3	22.99	23.17	23.87	26.86	26.54	27.09	27.88	21.00	20.53	24.86	23.14	21.27	24.98	26.70	27.36	24.04	21.84	23.87	23.17	24.11	24.11	24.13	20.93	23.68
FeO	0.00	0.00	0.00	0.00	0.58	0.00	0.25	0.17	0.66	0.59	0.52	0.24	0.55	0.40	0.20	0.49	0.57	0.53	0.39	0.54	0.00	0.00	0.25	0.43
CaO	3.32	3.95	5.41	7.95	8.07	8.53	9.63	1.89	1.42	5.76	3.99	1.82	5.79	7.90	9.06	4.97	3.20	5.41	3.95	5.34	5.34	5.60	1.35	4.72
Na_2O	8.36	7.98	8.07	6.46	6.63	6.37	5.70	7.77	8.09	7.57	7.90	8.25	7.61	6.89	6.32	7.93	7.84	8.07	7.98	7.78	7.78	7.93	8.38	7.89
K_2O	2.68	2.51	1.61	0.61	0.56	0.51	0.46	3.78	3.84	1.50	2.38	3.87	1.29	0.73	0.73	1.69	2.95	1.61	2.51	1.63	1.63	1.56	4.15	1.86
BaO	0.00	0.00	0.00	0.00	0.58	0.00	0.25	0.17	0.66	0.59	0.52	0.24	0.55	0.40	0.20	0.49	0.57	0.00	0.00	0.00	0.00	0.00	0.00	0.00
An	15.4	18.5	24.7	39.0	38.9	41.3	47.0	9.2	6.9	27.1	18.9	8.5	27.5	37.2	42.4	23.3	15.3	24.7	18.5	25.0	25.0	25.7	6.3	22.3
Ab	69.9	67.6	66.6	57.4	57.9	55.8	50.3	68.8	71.0	64.5	67.7	69.9	65.3	58.7	53.6	67.3	67.9	66.6	67.6	65.9	65.9	65.8	70.7	67.3
Or	14.7	14.0	8.8	3.6	3.2	2.9	2.7	22.0	22.2	8.4	13.4	21.6	7.3	4.1	4.0	9.4	16.8	8.8	14.0	9.1	9.1	8.5	23.0	10.4

All mineral analyses were recalculated to 100 %. Pheno = phenocrysts and microphenocrysts (> 50 µm). Micro = microlites (< 50 µm); R = rim, C = core, I = intermediate, An = Anorthite, Ab = Albite, Or = Orthoclase (mol %).

Representative SEM-EDS analyses of K-feldspar.

Sample	**0749**																		
Litology	**Benmoreite**																		
position																			
Type	mpheno, R	mpheno, C	mpheno, R	mpheno, C	mpheno, R	mpheno, C	mpheno, C	pheno, C	micro	micro	micro, C	micro, R	mpheno, R	micro, C	micro, R	micro, C	micro, R	micro, C	micro, R
SiO_2	57.11	49.08	60.31	56.65	60.57	57.55	52.02	52.02	60.19	58.98	53.28	63.06	56.57	54.88	61.75	52.76	60.74	53.42	58.88
Al_2O_3	26.54	31.78	23.99	26.65	24.10	26.07	29.51	29.51	24.18	24.61	28.90	21.84	26.76	27.98	22.98	29.44	23.93	28.87	25.06
FeO	0.00	0.78	0.20	0.39	0.50	0.64	0.81	0.28	0.00	0.00	0.37	0.44	0.21	0.00	0.78	0.20	0.39	0.50	0.64
CaO	8.12	14.51	5.45	8.53	4.90	7.76	11.84	11.00	5.44	6.05	11.23	3.07	8.89	10.26	4.16	11.94	5.52	11.12	6.76
Na_2O	6.82	3.39	7.71	6.48	7.87	7.03	4.75	4.75	7.55	7.97	4.69	8.03	6.02	5.38	8.01	4.56	7.32	4.88	7.02
K_2O	0.88	0.26	1.58	0.71	1.75	0.92	0.53	1.00	1.69	1.33	0.47	2.72	0.82	0.52	1.69	0.29	1.32	0.44	0.95
BaO	0.00	0.78	0.20	0.39	0.50	0.64	0.00	0.00	0.00	0.00	0.37	0.44	0.21	0.00	0.78	0.20	0.39	0.50	0.64
An	37.8	69.3	25.6	40.4	23.1	36.0	56.2	52.9	25.8	27.4	55.4	14.7	42.8	49.8	20.1	58.1	27.1	54.3	32.8
Ab	57.3	29.2	65.5	55.5	67.1	59.0	40.8	41.4	64.7	65.4	41.9	69.7	52.5	47.2	70.1	40.2	65.1	43.1	61.7
Or	4.9	1.5	8.8	4.0	9.8	5.1	3.0	5.7	9.6	7.2	2.8	15.5	4.7	3.0	9.7	1.7	7.7	2.6	5.5

All mineral analyses were recalculated to 100 %. Pheno = phenocrysts and mpheno = microphenocrysts (> 50 µm). Micro = microlites (< 50 µm); R = rim, C = core, I = intermediate; An = Anorthite, Ab = Albite, Or = Orthoclase (mol %).

Representative SEM-EDS analyses of clinopyroxenes.

Sample	**0720**	**0721**		**0722**						**0723**				**0731**									
Formation	**Green Tuff**																						
Member	**A**	**B**		**C**						**D**				**E**									
	pumice fall	**Pumice flow**		**Weld. Eutax.**						**Weld. Fines-rich**				**Welded fines-depleted**									
Position	**Botton**			**Intermediate**										**Top**									
Type	*pheno*	*micr*	*pheno*	*pheno*	*pheno*	*mphen*	*mpheo*	*micro*	*micro*	*Pheno, R*	*pheno, C*	*mphen*	*pheno*	*pheno*	*phen*	*pheno*	*mphen*	*mphen*	*pheno*	*micro*	*micro*	*micro*	*micro*
name	*Hd*	*Hd*	*Hd*	*Agt*	*Agt*	*Agt*	*Agt*	*Acm*	*Acm*	*Agt*	*Agt*	*Agt*	*Acm*	*Aug*	*Aug*	*Aug*	*Aug*	*Aug*	*Aug*	*Acm*	*Acm*	*Acm*	*Agt*
SiO_2	50.19	51.55	50.03	49.40	48.25	49.25	48.71	48.75	52.66	49.31	48.20	50.69	54.05	49.98	49.48	48.83	49.98	49.48	50.06	54.42	53.73	54.66	53.81
TiO_2	0.43	0.45	0.44	0.47	0.68	0.38	0.48	0.36	0.43	0.51	0.49	1.67	0.77	0.63	0.73	0.42	0.63	0.73	0.55	0.31	0.31	1.53	6.52
Al_2O_3	0.37	0.43	0.39	0.56	0.51	0.51	0.70	0.50	1.28	0.53	0.44	0.56	0.98	0.89	0.97	0.48	0.89	0.97	0.92	0.78	0.89	3.21	5.93
FeO	25.53	24.27	25.59	21.91	27.61	26.91	25.68	25.92	28.97	25.80	26.72	27.18	28.09	17.27	17.25	25.05	17.27	17.25	16.54	25.40	27.81	24.49	20.26
MnO	1.68	1.64	1.21	1.73	1.38	1.25	1.40	1.43	1.08	1.43	1.75	1.45	0.85	1.23	1.03	1.33	1.23	1.03	1.22	0.44	1.83	0.62	0.74
MgO	3.06	3.74	3.63	5.98	2.22	2.22	3.28	2.85	0.20	2.75	2.89	0.76	0.14	8.68	9.01	3.49	8.68	9.01	9.12	0.56	0.21	0.00	2.45
CaO	17.96	16.76	17.54	18.69	16.11	16.11	17.08	18.28	1.97	17.23	16.66	7.02	0.51	20.27	20.30	18.58	20.27	20.30	20.64	2.03	1.47	0.65	1.65
Na_2O	1.40	1.50	1.00	1.24	3.13	3.01	2.43	2.20	13.26	2.53	2.40	9.98	14.82	0.99	1.20	1.56	0.99	1.20	0.86	15.45	12.22	13.96	6.39
Wo	38.4	36.3	38.0	34.4	34.5	36.4	39.0	3.9	4.3	36.8	35.8	14.4	1.0	42.0	41.8	39.9	42.0	41.8	42.6	4.0	3.0	1.3	3.3
En	9.1	11.3	10.9	6.6	6.6	9.7	8.4	0.6	1.0	8.2	8.6	2.2	0.4	25.0	25.8	10.4	25.0	25.8	26.2	1.5	0.6	0.0	6.8
Fs	39.6	41.1	43.0	29.7	32.4	30.4	30.8	0.0	5.5	32.1	31.4	6.4	0.0	21.1	17.9	33.7	21.1	17.9	20.1	0.0	6.1	0.9	31.8
Extra-Quad	12.7	11.3	8.0	29.2	26.5	23.4	21.8	95.5	89.2	23.0	24.2	77.1	98.6	11.9	14.4	16.0	11.9	14.4	11.1	94.5	90.3	97.8	58.1
Q	1.7	1.7	1.8	1.4	1.5	1.5	1.6	0.1	0.2	1.7	1.7	1.5	1.5	1.8	1.7	1.7	1.8	1.7	1.8	0.1	0.2	0.0	0.9
J	0.2	0.2	0.2	0.5	0.5	0.4	0.3	1.9	1.8	0.3	0.2	0.5	0.4	0.1	0.2	0.2	0.1	0.2	0.1	2.2	1.8	2.0	1.0

Pheno = phenocrysts and mpheno = microphenocrysts (> 50 µm). Micro = microlites (< 50 µm); R = rim, C = core; Wo, En, Fs = wollastonite, enstatite, ferrosilite (mole %). Extra-quad = jadeite + aegirine + tschermakite (mole %). Acm = aegirine (wo+en+fs < 20 %), Agt = Aegirine-Augite (wo+en+fs = 20-80 %), Hd = (Na-) hedembergite (wo+en+fs > 80 %). Q = Ca+Mg+Fe^{2+}, J = 2Na (atoms per formula unit).

Representative SEM-EDS analyses of clinopyroxenes.

Sample	**0718**																			
	Trachyte "Case Ricco"																			
Position																				
Type	*pheno,*	*pheno,*	*pheno,*	*pheno,*	*pheno,*	*pheno,*	*mpheno,*	*mpheno,*	*mpheno,*	*mpheno,*	*mpheno,*	*mpheno,*	*mpheno,*	*mpheno,*	*mpheno,*	*micro*	*micro*	*micro*	*micro*	*micro*	*micro*
name	*R*	*C*	*R*	*C*	*R*	*C*	*R*	*C*	*C*	*R*	*C*	*R*	*C*	*R*	*R*	*Fe-Aug*	*Fe-Aug*	*Fe-Aug*	*Fe-Aug*	*Fe-Aug*	*Fe-Aug*
	Aug	*Aug*	*Aug*	*Aug*	*Aug*	*Aug*	*Aug*	*Aug*	*Fe-Aug*	*Fe-Aug*	*Aug*	*Aug*	*Aug*	*Fe-Aug*							
SiO_2	51.75	51.63	51.38	51.85	50.43	50.31	50.98	51.28	49.45	50.18	50.02	50.34	50.47	50.23	50.97	50.15	50.95	50.12	51.00	50.23
TiO_2	0.41	0.51	0.42	0.68	0.69	0.47	0.51	0.50	0.71	0.59	0.58	0.63	0.61	0.24	0.52	0.45	0.55	0.67	0.54	0.24
Al_2O_3	0.93	0.44	0.66	0.83	1.04	1.01	0.91	0.61	0.85	1.01	1.06	1.09	1.11	0.64	0.48	0.48	0.14	0.38	0.47	0.64
FeO	16.50	16.24	16.63	15.23	16.04	15.68	16.35	15.00	19.17	16.28	16.10	15.82	14.64	18.25	17.77	21.42	22.48	21.47	17.96	18.25
MnO	1.18	1.08	1.13	0.95	0.91	1.05	1.01	0.96	1.25	1.08	0.92	1.03	0.90	1.00	1.31	1.40	1.61	1.49	1.17	1.22
MgO	9.36	10.27	9.93	10.56	9.89	10.36	10.07	10.89	8.75	10.11	9.90	10.15	10.54	8.25	9.55	6.87	3.55	7.24	9.55	8.25
CaO	19.31	19.30	19.52	19.81	20.42	20.26	19.78	20.46	18.95	19.96	20.39	20.22	20.71	19.58	18.86	18.29	17.60	17.84	18.59	19.58
Na_2O	0.56	0.53	0.28	0.08	0.99	0.84	0.39	0.31	1.01	0.97	0.95	0.86	0.76	0.91	0.43	0.94	0.00	0.67	0.71	0.91
Wo	39.8	39.8	40.4	40.0	41.7	41.5	40.8	42.0	39.3	40.9	41.9	41.4	42.4	40.6	39.1	38.5	36.5	37.6	38.5	40.9
En	26.9	29.4	28.6	29.7	28.1	29.5	28.9	31.1	25.2	28.8	28.3	28.9	30.0	23.8	27.6	20.1	10.3	21.3	27.5	24.0
Fs	26.5	25.1	26.8	24.0	18.5	17.9	24.6	22.0	22.5	18.2	18.0	18.8	17.8	24.7	27.4	31.1	36.4	33.2	26.1	24.5
Extra-Quad	6.8	5.7	4.2	6.3	11.6	11.1	5.7	5.0	12.9	12.2	11.9	10.9	9.8	10.9	5.9	10.3	16.8	7.9	7.9	10.6
Q	1.9	1.9	1.9	1.9	1.8	1.8	1.9	1.9	1.7	1.8	1.8	1.8	1.8	1.8	1.9	1.8	1.8	1.8	1.8	1.8
J	0.1	0.1	0.0	0.0	0.2	0.1	0.1	0.1	0.1	0.1	0.1	0.1	0.1	0.1	0.1	0.1	0.0	0.1	0.1	0.1

Pheno = phenocrysts and mpheno = microphenocrysts (> 50 μm). Micro = microlites (< 50 μm); R = rim, C = core; Wo, En, Fs = wollastonite, enstatite, ferrosilite (mole %). Extra-quad = jadeite + aegirine + tschermakite (mole %). Acm = aegirine (wo+en+fs < 20 %), Agt = Aegirine-Augite (wo+en+fs = 20-80 %), Hd = (Na-) hedembergite (wo+en+fs > 80 %). Q = Ca+Mg+Fe^{2+}, J = 2Na (atoms per formula unit).

Representative SEM-EDS analyses of clinopyroxenes.

Sample	**0748**																	
Member																		
	Trachyte "M.gna Grande Sud"																	
Position																		
Type	*pheno, R*	*pheno, C*	*pheno, R*	*pheno, C*	*pheno, R*	*pheno, C*	*mpheno, R*	*mpheno, C*	*mpheno, R*	*mpheno, R*	*mpheno, C*	*micro*	*micro*	*micro*	*micro*	*micro*	*micro*	*micro*
name	*Aug*	*Aug*	*Aug*	*Aug*	*Aug*	*Aug*	*Aug*	*Aug*	*Fe-Aug*	*Fe-Aug*	*Fe-Aug*	*Fe-Aug*	*Fe-Aug*	*Fe-Aug*	*Fe-Aug*	*Fe-Aug*	*Acm*	*Agt*	*Agt*
SiO_2	50.25	50.89	51.04	50.56	49.90	49.59	50.62	50.36	49.72	49.70	50.24	49.39	48.88	49.07	49.64	48.25	52.33	50.62	51.00
TiO_2	0.61	0.72	0.52	0.84	0.70	0.94	0.54	0.36	0.52	0.47	0.35	0.71	1.92	0.91	0.47	0.83	0.54	0.78	2.68
Al_2O_3	1.01	1.11	0.70	0.88	0.87	1.63	0.91	1.06	1.24	1.25	1.21	0.60	0.91	1.85	1.25	0.58	2.10	2.19	0.69
FeO	16.01	14.55	16.70	15.56	16.87	15.04	14.66	14.43	17.71	18.82	20.06	21.45	25.18	18.53	18.82	26.01	25.90	24.43	29.49
MnO	0.86	0.98	0.97	0.86	1.05	0.98	1.08	0.75	0.97	0.96	1.75	1.59	1.31	1.55	0.96	1.61	0.69	0.62	0.94
MgO	9.76	10.90	8.77	10.07	9.36	11.11	10.39	11.53	9.08	8.66	7.49	7.12	4.80	8.45	8.66	5.15	0.90	3.03	0.42
CaO	20.55	20.56	19.93	20.63	20.44	20.07	20.65	19.96	20.29	18.96	17.23	17.43	11.94	18.12	16.76	15.99	5.17	9.68	4.15
Na_2O	0.73	0.79	0.37	1.01	0.95	0.86	0.70	1.06	0.91	0.78	1.44	1.07	4.31	1.21	1.15	1.15	11.44	8.63	9.49
Wo	42.3	41.7	41.5	42.1	4.1	40.8	42.5	40.7	41.7	39.5	36.0	42.3	41.7	42.1	41.4	42.0	10,4	19.5	19.5
En	28.0	30.8	25.4	28.6	26.8	31.4	29.7	32.7	26.0	25.1	21.8	28.0	30.8	28.5	28.2	27.7	2.5	8.5	8.5
Fs	20.3	17.5	27.6	17.9	19.2	15.3	18.8	13.9	20.1	25.2	26.9	20.3	17.5	20.3	21.3	21.8	1.7	4.4	4.4
Extra-Quad	9.4	9.9	4.5	11.4	12.0	12.4	9.1	12.8	12.2	10.1	15.3	9.4	9.9	9.1	9.0	8.4	85.4	67.6	67.6
Q	1.8	1.8	1.9	1.8	1.8	1.8	1.8	1.7	1.8	1.8	1.7	1.8	1.8	1.8	1.8	1.8	0.3	0.6	0.6
J	0.1	0.1	0.1	0.1	0.1	0.1	0.1	0.2	0.1	0.1	0.2	0.1	0.1	0.1	0.1	0.1	1.7	1.3	1.3

Pheno=phenocrysts and mpheno = microphenocrysts (> 50 µm). Micro = microlites (< 50 µm); R = rim, C = core; Wo, En, Fs = wollastonite, enstatite, ferrosilite (mole %).
Extra-quad = jadeite + aegirine + tschermakite (mole %). Acm = aegirine (wo+en+fs < 20 %), Agt = Aegirine-Augite (wo+en+fs = 20-80 %), Hd = (Na-) hedembergite (wo+en+fs > 80 %).
Q = Ca+Mg+Fe^{2+}, J = 2Na (atoms per formula unit).

Representative SEM-EDS analyses of clinopyroxenes.

Sample	**0750**																		
Member	**Trachyte "Montagna Grande Nord"**																		
Position																			
Type	*pheno, R*	*pheno, C*	*pheno, R*	*pheno, C*	*pheno, R*	*pheno, C*	*pheno, R*	*pheno, C*	*pheno, R*	*pheno, C*	*mpheno, R*	*mpheno, R*	*mpheno, R*	*mpheno, R*	*micro*	*micro*	*micro*	*micro*	*micro*
name	*Aug*	*Aug*	*Aug*	*Aug*	*Aug*	*Aug*	*Aug*	*Aug*	*Aug*	*Aug*	*Aug*	*Aug*	*Aug*	*Aug*	*Aug*	*Aug*	*Aug*	*Aug*	*Aug*
SiO_2	49.63	49.99	50.49	50.07	50.74	49.67	51.02	51.16	49.67	50.19	51.01	50.63	49.88	48.90	50.90	51.19	50.91	51.09	51.17
TiO_2	1.05	1.41	0.58	0.43	0.62	1.43	0.57	0.66	1.43	1.15	0.91	0.53	0.56	1.99	0.42	0.60	0.60	0.86	0.82
Al_2O_3	2.64	3.10	0.79	0.90	1.35	2.95	0.95	1.15	2.95	2.73	1.38	1.34	0.99	3.70	0.75	1.29	1.16	1.52	1.54
FeO	11.10	9.37	14.36	16.47	11.90	9.39	14.43	15.39	9.39	10.67	11.53	14.29	16.61	11.05	15.77	12.81	12.66	11.71	11.55
MnO	0.34	0.30	0.90	1.36	0.82	0.48	0.74	0.77	0.48	0.37	0.80	0.91	1.01	0.40	1.20	0.92	1.05	0.56	0.60
MgO	12.92	13.53	10.92	10.56	12.89	12.80	11.50	9.69	12.80	13.31	12.91	11.24	10.18	12.69	10.76	12.63	12.40	13.25	13.28
CaO	20.75	21.44	20.81	18.79	20.61	22.25	19.80	20.06	22.25	20.46	20.43	19.87	19.74	19.91	19.15	19.26	19.90	20.14	19.81
Na_2O	1.16	0.80	0.97	1.20	1.03	0.85	0.96	0.92	0.85	0.85	0.86	0.92	0.93	1.03	1.06	0.95	0.88	0.87	0.92
Wo	41.6	42.7	42.4	38.5	41.3	44.5	40.2	41.2	44.5	41.0	41.1	40.5	40.5	40.0	39.1	39.0	40.3	40.5	39.8
En	36.0	37.5	31.0	30.1	36.0	35.6	32.5	27.7	35.6	37.1	36.2	31.9	29.1	35.5	30.6	35.5	34.9	37.0	37.2
Fs	7.7	8.5	14.8	16.7	9.7	7.7	16.5	22.1	7.7	10.6	12.3	16.5	18.2	10.9	18.1	14.6	13.7	12.3	12.5
Extra-Quad	14.6	11.3	11.8	14.8	12.9	12.1	10.7	9.0	12.1	11.2	10.4	11.2	12.1	13.5	12.2	10.9	11.1	10.2	10.5
Q	1.7	1.8	1.8	1.7	1.7	1.8	1.8	1.8	1.8	1.8	1.8	1.8	1.8	1.7	1.8	1.8	1.8	1.8	1.8
J	0.2	0.1	0.1	0.2	0.1	0.1	0.1	0.1	0.1	0.1	0.1	0.1	0.1	0.1	0.2	0.1	0.1	0.1	0.1

Pheno = phenocrysts and mpheno = microphenocrysts (> 50 µm). Micro = microlites (< 50 µm); R = rim, C = core; Wo, En, Fs = wollastonite, enstatite, ferrosilite (mole %).
Extra-quad = jadeite + aegirine + tschermakite (mole %). Acm = aegirine (wo+en+fs < 20 %), Agt = Aegirine-Augite (wo+en+fs = 20-80 %), Hd = (Na-) hedembergite (wo+en+fs > 80 %).
Q = Ca+Mg+Fe^{2+}, J = 2Na (atoms per formula unit).

Representative SEM-EDS analyses of clinopyroxenes.

Sample	**0732**															
Member																
	Trachyte "Mueggen"															
Position																
Type	*pheno, R*	*pheno, C*	*pheno, C*	*pheno, R*	*pheno, C*	*pheno, R*	*mpheno*	*mpheno, C*	*mpheno, R*	*mpheno, C*	*mpheno, R*	*mpheno*	*micro*	*micro*	*micro*	*micro*
name	*Fe-Aug*	*Fe-Aug*	*Fe-Aug*	*Fe-Aug*	*Fe-Aug*	*Fe-Aug*	*Fe-Aug*	*Fe-Aug*	*Fe-Aug*	*Fe-Aug*	*Fe-Aug*	*Fe-Aug*	*Fe-Aug*	*Fe-Aug*	*Fe-Aug*	*Fe-Aug*
SiO_2	48.26	48.80	48.82	48.51	49.61	48.86	48.40	49.22	48.80	48.64	49.53	48.94	48.92	47.36	48.26	48.93
TiO_2	0.66	0.38	0.43	0.50	0.32	0.31	0.41	0.36	0.55	0.52	0.41	0.36	0.69	1.06	0.63	0.63
Al_2O_3	0.60	0.49	0.62	0.46	0.54	0.63	0.63	0.45	0.49	0.44	0.47	0.60	0.69	0.51	0.42	0.48
FeO	24.80	23.25	23.67	23.42	20.67	22.83	22.04	22.84	23.05	23.20	22.51	23.48	23.89	29.17	24.80	22.48
MnO	1.65	1.21	1.53	1.53	1.07	1.47	1.41	1.13	1.37	1.41	1.47	1.22	1.53	1.93	1.65	1.61
MgO	4.14	4.68	4.42	4.69	6.45	4.68	5.39	5.16	4.76	4.76	4.87	4.29	4.48	2.94	4.14	3.58
CaO	18.10	20.33	19.12	19.23	20.22	19.88	20.17	19.92	19.64	19.58	19.45	19.52	18.28	15.20	18.10	17.00
Na_2O	1.56	1.26	1.22	1.33	1.16	1.33	1.17	1.15	1.43	1.16	1.24	1.41	1.69	1.68	1.57	2.02
Wo	38.7	43.0	40.8	41.0	42.4	42.2	42.8	42.1	41.6	41.8	41.3	41.6	38.8	33.0	38.7	37.4
En	12.3	13.8	13.1	13.9	18.8	13.8	15.9	15.2	14.0	14.1	14.4	12.7	13.2	8.9	12.3	10.9
Fs	31.4	28.5	32.0	29.5	25.7	28.5	26.3	29.7	28.4	30.3	31.1	30.6	30.3	39.1	32.4	34.2
Extra-Quad	17.6	14.8	14.1	15.6	13.1	15.5	14.9	13.0	15.9	13.8	13.2	15.0	17.7	19.0	16.6	17.5
Q	1.6	1.7	1.7	1.7	1.7	1.7	1.7	1.7	1.7	1.7	1.7	1.7	1.6	1.6	1.6	1.6
J	0.2	0.2	0.2	0.2	0.2	0.2	0.2	0.2	0.2	0.2	0.2	0.2	0.3	0.3	0.2	0.3

Pheno = phenocrysts and mpheno = microphenocrysts (> 50 µm). Micro = microlites (< 50 µm); R = rim, C = core; Wo, En, Fs = wollastonite, enstatite, ferrosilite (mole %). Extra-quad = jadeite + aegirine + tschermakite (mole %). Acm = aegirine (wo+en+fs < 20 %), Agt = Aegirine-Augite (wo+en+fs = 20-80 %), Hd = (Na-) hedembergite (wo+en+fs > 80 %). Q = Ca+Mg+Fe^{2+}, J = 2Na (atoms per formula unit).

Representative SEM-EDS analyses of clinopyroxenes.

Sample	**Pant24**															
Member																
	Trachyte enclave															
Position	**In Pumice cone "C. Randazzo"**															
Type	*pheno, R*	*pheno, C*	*pheno, R*	*pheno, C*	*pheno*	*mpheno*	*mpheno*	*mpheno*	*mpheno*	*micro*	*micro*	*micro*	*micro*	*micro*	*micro*	*micro*
name	*Fe-Aug*	*Fe-Aug*	*Fe-Aug*	*Fe-Aug*	*Fe-Aug*	*Fe-Aug*	*Fe-Aug*	*Fe-Aug*	*Fe-Aug*	*Agt*	*Agt*	*Fe-Aug*	*Fe-Aug*	*Fe-Aug*	*Fe-Aug*	*Agt*
SiO_2	49.51	48.91	48,.55	48.87	48.07	49.05	49.03	47.93	49.34	48.93	46.89	46.81	46.64	46.56	47.85	48.37
TiO_2	0.72	0.50	0.69	0.56	0.56	0.55	0.49	0.47	0.46	0.50	1.04	1.03	1.42	1.20	0.85	0.62
Al_2O_3	0.84	0.88	0.97	0.72	0.69	0.78	0.72	0.58	0.83	0.53	0.92	1.58	1.38	1.03	0.68	0.44
FeO	21.54	21.22	20.88	21.05	23.59	21.17	22.04	24.63	20.15	26.71	28.22	27.30	26.94	26.36	28.87	28.03
MnO	1.14	1.28	1.35	1.07	1.32	1.27	1.21	1.46	1.21	1.34	1.65	1.52	1.50	1.63	1.74	1.50
MgO	5.81	5.60	6.08	5.83	3.87	5.65	5.31	3.17	6.95	1.82	1.68	1.60	2.15	1.88	2.01	1.75
CaO	20.75	20.65	20.33	20.62	20.76	21.01	20.60	20.35	20.97	17.25	17.30	18.55	18.64	18.61	16.92	16.86
Na_2O	0.89	0.91	0.88	0.86	0.89	0.85	0.79	0.97	0.86	2.62	1.73	1.38	1.43	1.44	1.44	2.27
Wo	43.3	43.6	42.9	43.7	44.5	44.2	43.6	43.9	43.7	37.1	37.7	40.4	40.3	40.8	36.7	36.4
En	16.9	16.5	17.9	17.2	11.6	16.6	15.6	9.5	20.1	5.4	5.1	4.8	6.5	5.7	6.1	5.3
Fs	28.7	28.0	26.9	28.2	31.9	27.8	30.3	33.7	24.3	33.8	36.6	38.0	35.7	36.3	41.1	36.5
Extra-Quad	11.1	11.9	12.3	11.9	12.0	11.4	10.5	12.8	11.9	23.7	20.5	16.8	17.5	17.1	16.2	21.8
Q	1.8	1.8	1.8	1.8	1.8	1.8	1.8	1.7	1.8	1.5	1.6	1.7	1.7	1.7	1.7	1.6
J	0.1	0.1	0.1	0.1	0.1	0.1	0.1	0.2	0.1	0.4	0.3	0,.2	0.2	0.2	0.2	0.4

Pheno = phenocrysts and mpheno = microphenocrysts (> 50 μm). Micro = microlites (< 50 μm); R = rim, C = core; Wo, En, Fs = wollastonite, enstatite, ferrosilite (mole %). Extra-quad = jadeite + aegirine + tschermakite (mole %). Acm = aegirine (wo+en+fs < 20 %), Agt = Aegirine-Augite (wo+en+fs = 20-80 %), Hd = (Na-) hedembergite (wo+en+fs > 80 %). Q = Ca+Mg+Fe^{2+}, J = 2Na (atoms per formula unit).

Representative SEM-EDS analyses of clinopyroxenes.

Sample	**Pant21**																
Member																	
	Trachyte enclave																
Position	**In Pumice cone "C. Randazzo"**																
Type	*pheno, R*	*pheno, C*	*pheno, R*	*pheno, C*	*pheno R*	*pheno, C*	*pheno, R*	*pheno, C*	*mpheno, C*	*mpheno, R*	*mpheno, C*	*mpheno, R*	*mpheno, C*	*micro*	*micro*	*micro*	*micro*
name	*Fe-Aug*	*Fe-Aug*	*Agt*	*Fe-Aug*	*Fe-Aug*	*Fe-Aug*	*Fe-Aug*	*Fe-Aug*	*Fe-Aug*	*Fe-Aug*	*Fe-Aug*	*Fe-Aug*	*Fe-Aug*	*Agt*	*Fe-Aug*	*Fe-Aug*	*Fe-Aug*
SiO_2	50.90	49.39	48.82	50.84	51.62	49.39	51.72	51.12	52.16	53.09	52.99	49.83	52.59	46.88	48.93	47.93	51.52
TiO_2	0.50	0.22	0.57	0.48	0.30	0.47	0.33	0.29	0.29	0.44	0.26	0.34	0.11	0.77	0.52	0.46	0.54
Al_2O_3	0.52	0.54	0.60	0.51	0.55	0.55	0.45	0.62	0.55	0.56	0.46	0.45	0.37	0.80	0.38	0.33	0.32
FeO	22.75	23.05	26.02	20.80	20.43	21.90	19.59	20.00	20.58	18.50	19.04	22.06	20.17	26.14	22.18	24.38	21.03
MnO	2.26	2.22	2.28	1.22	1.73	1.72	1.93	1.66	1.83	1.38	1.25	1.71	1.89	1.99	2.19	1.94	1.31
MgO	5.54	5.76	4.69	6.58	6.44	5.98	6.33	6.72	6.30	7.17	6.74	6.16	6.72	4.81	7.17	4.99	6.00
CaO	15.89	17.33	14.55	17.85	16.85	18.69	17.60	17.69	16.54	17.38	17.65	17.86	16.03	15.78	17.35	18.69	17.60
Na_2O	1.68	1.50	1.92	1.64	1.77	1.24	1.93	1.78	1.66	1.59	1.60	1.58	1.97	2.36	1.17	1.44	1.87
Wo	33.7	36.6	31.2	37.4	35.7	39.5	37.1	36.9	35.5	36.5	37.4	37.6	34.4	33.6	36.6	39.7	37.0
En	16.4	16.9	14.0	19.2	19.0	17.6	18.6	19.5	18.8	21.0	19.9	18.0	20.0	14.3	21.0	14.7	17.6
Fs	34.8	29.0	34.6	29.1	31.3	28.6	28.7	27.4	34.5	30.4	31.5	27.9	32.5	25.0	26.8	26.9	31.0
Extra-Quad	15.1	17.5	20.2	14.4	14.0	14.3	15.6	16.2	11.2	12.1	11.2	16.5	13.1	27.2	15.6	18.6	14.4
Q	1.7	1.7	1.6	1.7	1.7	1.7	1.7	1.7	1.7	1.7	1.7	1.7	1.7	1.5	1.7	1.6	1.7
J	0.3	0.2	0.3	0.2	0.3	0.2	0.3	0.3	0.3	0.2	0.2	0.2	0.3	0.4	0.2	0.2	0.3

Pheno = phenocrysts and mpheno= microphenocrysts (> 50 μm). Micro = microlites (< 50 μm); R = rim, C = core; Wo, En, Fs = wollastonite, enstatite, ferrosilite (mole %). Extra-quad = jadeite + aegirine + tschermakite (mole %). Acm = aegirine (wo+en+fs < 20 %), Agt = Aegirine-Augite (wo+en+fs = 20-80 %), Hd = (Na-) hedembergite (wo+en+fs > 80 %). Q = Ca+Mg+Fe^{2+}, J = 2Na (atoms per formula unit).

Representative SEM-EDS analyses of clinopyroxenes.

Sample	**Pan23**												
Member													
	Trachyte enclave												
Position	**In Pumice C. Randazzo**												
Type	*pheno, C*	*pheno R*	*pheno, R*	*pheno, R*	*micro*	*pheno, R*	*pheno, Int*	*pheno, Int*	*mpheno, R*	*mpheno, Int*	*mpheno C*	*micro*	*micro*
name	*Aug*	*Aug*	*Aug*	*Aug*	*Aug*	*Aug*	*Hd*	*Hd*	*Hd*	*Hd*	*Aug*	*Aug*	*Hd*
SiO_2	50.90	51.21	51.37	50.97	50.03	49.86	48.71	48.55	48.84	49.15	49.00	50.34	49.00
TiO_2	0.67	0.63	0.83	0.52	0.93	0.95	0.56	0.69	0.78	0.72	0.57	1.03	0.49
Al_2O_3	0.76	0.56	0.62	0.67	1.21	1.31	0.70	0.68	0.68	0.59	1.33	0.97	0.85
FeO	18.68	18.31	18.06	17.28	18.38	16.32	20.01	21.45	21.94	19.76	18.51	17.38	19.38
MnO	0.91	1.14	1.24	1.13	1.36	1.26	1.41	1.33	1.13	1.41	1.18	1.09	0.87
MgO	7.88	7.90	8.49	9.16	8.18	9.13	6.43	5.81	5.27	6.47	8.09	8.04	7.63
CaO	20.06	20.17	19.40	19.88	19.43	19.82	20.99	20.48	20.36	20.39	20.57	20.63	20.78
Na_2O	0.15	0.09	0.00	0.35	0.45	1.00	0.99	1.07	0.74	1.13	1.02	0.93	0.77
Wo	41.49	41.44	39.34	41.24	40.59	40.98	44.14	43.17	43.40	42.93	42.53	42.67	43.47
En	22.68	22.59	23.96	26.44	23.78	26.26	18.81	17.04	15.63	18.96	23.28	23.14	22.23
Fs	30.16	29.36	28.59	27.28	28.89	20.84	23.59	25.99	31.69	24.80	19.98	24.11	23.43
Extra-Quad	5.67	6.61	8.11	5.04	6.75	11.92	13.46	13.81	9.27	13.31	14.21	10.09	10.88
Q	1.9	1.9	1.9	1.9	1.9	1.7	1.7	1.7	1.8	1.7	1.7	1.8	1.8
J	0.1	0.1	0.1	0.1	0.1	0.2	0.2	0.2	0.2	0.2	0.2	0.2	0.2

Pheno = phenocrysts and mpheno = microphenocrysts (> 50 µm). Micro = microlites (< 50 µm); R = rim, C = core; Wo, En, Fs = wollastonite, enstatite, ferrosilite (mole %). Extra-quad = jadeite + aegirine + tschermakite (mole %). Acm = aegirine (wo+en+fs < 20 %), Agt = Aegirine-Augite (wo+en+fs = 20-80 %), Hd = (Na-) hedembergite (wo+en+fs > 80 %). Q = Ca+Mg+Fe^{2+}, J = 2Na (atoms per formula unit).

Representative SEM-EDS analyses of clinopyroxenes.

Sample	**Pan0749**																		
Member																			
Position	**Benmoreite In trachyte Montagna Grande**																		
Type name	*pheno, C Aug*	*pheno Int Aug*	*pheno, R Aug*	*pheno, C Aug*	*pheno, R Aug*	*pheno, C Aug*	*pheno, Int Aug*	*pheno, R Aug*	*pheno, C Aug*	*pheno, Int Aug*	*pheno, R Aug*	*pheno, C Aug*	*pheno, R Aug*	*pheno, R Aug*	*pheno, C Aug*	*pheno, Int Aug*	*pheno R Aug*	*pheno C Aug*	*pheno R Aug*
SiO_2	50.62	50.34	50.27	49.72	50.67	49.97	50.63	50.76	49.97	50.63	50.76	51.49	51.37	50.34	51.34	51.49	50.15	51.04	49.33
TiO_2	0.76	0.80	1.47	0.54	0.45	0.32	0.66	0.47	0.32	0.66	0.47	0.54	1.04	1.03	0.45	0.46	1.94	1.33	2.13
Al_2O_3	0.96	0.71	2.32	0.76	0.93	0.76	1.22	1.09	0.76	1.22	1.09	0.61	1.34	0.97	0.47	0.75	2.98	2.66	3.63
FeO	14.65	16.09	9.83	16.82	15.54	16.54	16.05	15.56	16.54	16.05	15.56	15.02	10.8	17.38	16.07	15.16	10.16	7.87	9.76
MnO	1.10	1.07	0.24	1.18	0.87	1.43	1.10	0.88	1.43	1.10	0.88	1.02	0.65	1.09	1.15	1.04	0.3	0.24	0.2
MgO	11.32	10.88	14.51	10.26	10.70	9.13	10.77	11.13	9.13	10.77	11.13	11.33	14.14	8.04	10.23	11.49	13.54	15.42	13.7
CaO	19.96	18.60	20.38	19.38	20.01	19.34	19.36	19.73	19.34	19.36	19.73	19	19.89	20.63	19.31	18.69	20.18	20.58	20.62
Na_2O	0.95	0.98	0.66	1.05	0.74	0.99	0.95	1.00	0.99	0.95	1.00	0.81	0.74	0.93	0.97	0.92	0.74	0.55	0.63
Wo	40.54	38.25	40.69	41.24	40.97	40.47	39.26	39.96	40.47	39.26	39.96	38.76	39.77	42.67	39.61	38.06	40.37	40.72	41.18
En	32.68	31.12	40.32	29.34	30.49	26.58	30.39	31.36	26.58	30.39	31.36	32.17	39.34	23.14	29.20	32.56	37.69	42.45	38.08
Fs	15.98	19.28	9.46	17.28	19.07	20.00	19.00	18.00	20.00	19.00	18.00	20.26	11.82	24.11	21.05	19.44	12.45	8.60	10.80
Extra-Quad	11.46	11.33	9.46	13.54	9.46	12.95	11.35	10.68	12.95	11.35	10.68	8.78	9.06	10.09	10.13	9.92	9.47	8.21	9.92
Q	1.8	1.8	1.8	1.7	1.8	1.7	1.7	1.7	1.8	1.7	1.7	1.8	1.8	1.8	1.8	1.8	1.8	1.8	1.8
J	0.1	0.1	0.1	0.2	0.1	0.2	0.2	0.2	0.2	0.2	0.2	0.2	0.2	0.2	0.1	0.1	0.1	0.1	0.1

Pheno = phenocrysts and mpheno = microphenocrysts (> 50 μm). Micro = microlites (< 50 μm); R = rim, C = core; Wo, En, Fs = wollastonite, enstatite, ferrosilite (mole %). Extra-quad = jadeite + aegirine + tschermakite (mole %). Acm = aegirine (wo+en+fs < 20 %), Agt = Aegirine-Augite (wo+en+fs = 20-80 %), Hd = (Na-) hedembergite (wo+en+fs > 80 %). Q = Ca+Mg+Fe^{2+}, J = 2Na (atoms per formula unit).

Representative SEM-EDS analyses of clinopyroxenes.

Sample	**Pan0749**																		
Member																			
Position	**Benmoreite In trachyte Montagna Grande**																		
Type	*pheno, C*	*pheno R*	*pheno, R*	*pheno, C*	*pheno, R*	*pheno, C*	*pheno, R*	*pheno, Int*	*pheno, Int*	*pheno, Int*	*pheno, R*	*pheno, Int*	*pheno, C*	*pheno R*	*pheno Int*	*pheno C*	*pheno R*	*pheno Int*	*pheno C*
name	*Aug*	*Aug*	*Aug*	*Aug*	*Aug*	*Aug*	*Aug*	*Aug*	*Aug*	*Aug*	*Aug*	*Aug*	*Aug*	*Aug*	*Aug*	*Aug*	*Aug*	*Aug*	*Aug*
SiO_2	51.42	51.04	50.76	50.59	50.01	50.65	50.54	50.55	50.22	50.07	51.15	50.58	50.92	50.01	50.64	50.13	51.28	49.99	49.37
TiO_2	0.66	0.93	1.47	1.34	1.35	0.65	0.93	0.66	0.60	1.95	0.73	0.52	1.23	0.73	0.64	1.23	0.68	0.65	1.95
Al_2O_3	1.39	0.89	2.15	2.55	2.70	0.77	1.62	1.08	0.80	4.05	1.45	1.07	1.91	1.14	0.93	6.92	1.14	0.93	3.77
FeO	15.99	15.01	9.59	9.97	9.48	15.72	10.50	14.77	16.21	7.05	11.70	15.38	10.22	14.57	15.54	9.64	11.77	15.90	8.83
MnO	0.20	0.20	0.36	0.38	0.16	0.85	0.58	0.79	1.28	0.51	0.67	0.98	0.36	1.03	0.93	0.42	0.42	1.13	0.45
MgO	10.94	11.15	13.90	13.41	15.10	10.57	13.96	11.07	10.30	15.93	13.21	10.81	13.61	11.54	10.88	14.71	13.78	10.89	13.43
CaO	18.56	19.81	20.87	20.74	20.02	19.00	20.94	20.07	19.65	20.05	20.66	20.15	20.96	19.60	19.79	20.29	19.84	19.27	21.83
Na_2O	0.74	0.83	0.74	0.90	0.80	0.93	0.91	0.94	1.02	0.41	0.86	0.93	0.73	1.01	1.00	0.83	0.97	0.97	0.50
Wo	37.97	40.44	41.71	41.44	39.80	39.21	40.36	40.78	40.70	42.44	41.27	40.94	41.93	39.95	40.25	37.09	40.15	39.49	43.54
En	31.14	31.67	38.65	37.30	41.77	30.37	39.07	31.30	29.69	39.06	36.73	30.59	37.89	32.73	30.79	39.35	37.90	31.04	37.27
Fs	24.20	19.99	10.42	10.33	7.07	20.56	8.99	15.39	22.39	10.52	11.10	16.73	11.12	14.37	17.15	9.40	12.30	16.95	9.49
Extra-Quad	6.69	7.90	9.23	10.93	11.37	9.87	11.58	12.52	7.23	7.99	10.90	11.75	9.07	12.95	11.81	14.16	9.65	12.53	9.69
Q	1.9	1.8	1.8	1.8	1.8	1.8	1.8	1.7	1.9	1.8	1.8	1,8	1,8	1.7	1.8	1.7	1.8	1.7	1.8
J	0.1	0.1	0.1	0.1	0.1	0.1	0.1	0.2	0.1	0.1	0.1	0,1	0,1	0.1	0.1	0.1	0.1	0.1	0.1

Pheno = phenocrysts and mpheno = microphenocrysts (> 50 µm). Micro = microlites (< 50 µm); R = rim, C = core; Wo, En, Fs = wollastonite, enstatite, ferrosilite (mole %). Extra-quad = jadeite + aegirine + tschermakite (mole %). Acm = aegirine (wo+en+fs < 20 %), Agt = Aegirine-Augite (wo+en+fs = 20-80 %), Hd = (Na-) hedembergite (wo+en+fs > 80 %). Q = Ca+Mg+Fe^{2+}, J = 2Na (atoms per formula unit).

Representative SEM-EDS analyses of clinopyroxenes.

Sample	**Pan0749**																		
Member																			
Position	**Benmoreite In trachyte Montagna Grande**																		
Type	*mpheno, C*	*mpheno R*	*mpheno, C*	*mpheno, R*	*mpheno, C*	*mpheno, Int*	*mpheno, R*	*mpheno, C*	*mpheno, R*	*mpheno, R*	*mpheno C*	*mpheno, R*	*mphen C*	*micro*	*micro*	*micro*	*micro*	*micro*	*micro*	*micro*
name	*Aug*	*Aug*	*Aug*	*Aug*	*Aug*	*Aug*	*Aug*	*Di*	*Di*	*Aug*	*Aug*	*Aug*	*Aug*	*Aug*	*Di*	*Di*	*Aug*	*Di*	*Di*	*Aug*
SiO_2	51.55	51.56	47.93	49.56	50.62	50.34	50.28	47.70	47.62	50.76	50.59	47.70	47.62	51.01	46.00	48.23	50.67	46.00	48.23	51.01
TiO_2	0.64	0.97	2.30	1.91	0.76	0.81	1.47	2.37	2.46	1.47	1.34	2.37	2.46	1.00	3.15	1.90	1.26	3.15	1.90	1.00
Al_2O_3	0.48	1.54	4.55	2.95	0.97	0.71	2.32	6.61	4.87	2.15	2.55	6.61	4.87	1.56	6.53	4.81	1.78	6.53	4.81	1.56
FeO	14.62	10.69	8.20	9.77	14.56	16.10	9.84	6.59	7.88	9.59	9.97	6.59	7.88	10.02	8.90	9.60	9.82	8.90	9.60	10.02
MnO	0.97	0.29	0.24	0.42	1.10	1.07	0.25	0.17	0.32	0.36	0.38	0.17	0.32	0.38	0.00	0.47	0.27	0.00	0.47	0.38
MgO	11.9	13.81	14.04	13.73	11.32	10.88	14.52	13.41	13.60	13.97	13.41	13.41	13.60	14.02	12.36	13.04	13.86	12.36	13.04	14.02
CaO	19.18	20.36	21.69	20.24	19.96	18.61	20.38	22.41	22.12	20.87	20.74	20.87	20.74	21.02	22.30	21.14	21.08	22.30	21.14	21.02
Na_2O	0.61	0.78	0.72	1.03	0.92	0.99	0.67	0.65	0.83	0.74	0.90	0.65	0.83	0.94	0.65	0.79	0.93	0.65	0.79	0.94
Wo	39.08	40.70	43.15	40.46	40.57	38.22	40.70	44.37	44.02	41.65	41.42	41.97	41.83	41.87	44.63	42.17	42.14	44.63	42.18	41.87
En	33.74	38.41	38.88	38.20	32.03	31.10	40.33	36.95	37.67	38.79	37.29	37.52	38.18	38.86	34.41	36.19	38.55	34.41	36.20	38.86
Fs	20.06	12.33	4.62	8.36	16.00	19.27	9.51	5.23	3.70	10.21	10.33	8.40	6.53	8.14	6.57	7.62	8.47	6.57	7.62	8.14
Extra-Quad	7.12	8.56	13.34	12.99	11.40	11.41	9.46	13.45	14.61	9.36	10.96	12.12	13.45	11.12	14.40	14.03	10.84	14.40	14.00	11.12
Q	1.9	1.8	1.7	1.7	1.8	1.8	1.8	1.7	1.7	1.8	1.8	1.8	1.7	1.8	1.7	1.7	1.8	1.7	1.7	1.8
J	0.1	0.1	0.1	0.1	0.1	0.1	0.1	0.1	0.1	0.1	0.1	0.1	0.1	0.1	0.1	0.1	0.1	0.1	0.1	0.1

Pheno = phenocrysts and mpheno = microphenocrysts (> 50 μm). Micro = microlites (< 50 μm); R = rim, C = core; Wo, En, Fs = wollastonite, enstatite, ferrosilite (mole %). Extra-quad = jadeite + aegirine + tschermakite (mole %). Acm = aegirine (wo+en+fs < 20 %), Agt = Aegirine-Augite (wo+en+fs = 20-80 %), Hd = (Na-) hedembergite (wo+en+fs > 80 %). Q = Ca+Mg+Fe^{2+}, J = 2Na (atoms per formula unit).

Representative SEM-EDS analyses of clinopyroxenes*

Sample	**Pan0749**										
Member											
	Benmoreite										
Position	**In trachyte Montagna Grande**										
Type	*pheno, *R*	*pheno I*	*pheno, C*	*pheno, R*	*pheno, Int*	*pheno, C*	*pheno, R*	*pheno, 1*	*pheno, 2*	*pheno, 3*	*pheno C*
name	*Di*	*Aug*	*Aug*	*Aug*	*Aug*	*Aug*	*Di*	*Aug*	*Aug*	*Aug*	*Aug*
SiO_2	47,28	49,79	50,03	51,05	51,20	51,01	50,77	50,76	50,35	51,15	50,90
TiO_2	1,67	1,37	1,47	0,52	0,48	0,40	1,95	1,01	1,42	0,73	0,84
Al_2O_3	5,24	4,27	3,43	0,60	0,65	0,80	2,05	2,71	2,85	1,45	1,12
FeO	6,70	7,49	8,26	15,86	15,92	16,00	7,05	8,55	8,73	11,70	11,90
MnO	0,10	0,32	0,18	1,01	1,04	1,00	0,51	0,08	0,24	0,67	0,80
MgO	15,78	15,75	14,90	11,32	11,11	11,00	15,93	15,42	14,89	13,21	12,66
CaO	21,61	20,62	20,84	18,99	19,07	19,10	20,75	21,28	20,55	20,66	21,01
Na_2O	0,43	0,38	0,48	0,55	0,61	0,70	0,81	0,56	0,74	0,86	0,80
Wo	42,90	40,63	41,45	38,91	39,04	39,08	40,98	41,91	40,80	41,27	42,29
En	43,61	43,20	41,23	32,26	31,63	31,32	43,77	42,27	41,15	36,73	35,48
Fs	0,24	6,41	8,44	21,44	21,62	20,78	4,93	6,36	7,64	11,10	11,93
Extra-Quad	13,25	9,75	8,87	7,39	7,71	8,83	10,32	9,45	10,41	10,90	10,29
Q	1,7	1,8	1,8	1,9	1,8	1,8	1,8	1,8	1,8	1,8	1,8
J	0,1	0,1	0,1	0,1	0,1	0,1	0,1	0,1	0,1	0,1	0,1

Pheno = phenocrysts and mpheno = microphenocrysts (> 50 µm). Micro = microlites (< 50 µm); R = rim, C = core; Wo, En, Fs = wollastonite, enstatite, ferrosilite (mole %). Extra-quad = jadeite + aegirine + tschermakite (mole %). Acm = aegirine (wo+en+fs < 20 %), Agt = Aegirine-Augite (wo+en+fs = 20-80 %), Hd = (Na-) hedembergite (wo+en+fs > 80 %). Q = Ca+Mg+Fe^{2+}, J = 2Na (atoms per formula unit).

Selected analyses of olivines.

Sample	**0720**				**0731**												
Formation	**Green Tuff**				**Green Tuff**												
Member	**A**				**E**												
	Pumice fall				**Welded fines-depleted**												
Position	**Botton**				**Top**												
Type	pheno	pheno	mpheno, R	mpheno, C	pheno, R	pheno, C	pheno, R	pheno, C	pheno, R	pheno,C	mpheno, R	mpheno, C	mpheno, R	mpheno, C	micro	micro	micro
SiO_2	31.54	31.54	31.54	31.37	30.98	30.67	31.12	31.01	30.98	31.15	30.74	31.13	30.45	30.47	29.67	35.76	31.88
TiO_2	0.00	0.00	0.00	0.00	0.00	0.00	0.00	0.00	0.00	0.00	0.00	0.00	0.00	0.00	0.00	0.00	0.00
Al_2O_3	0.00	0.00	0.00	0.00	0.00	0.00	0.00	0.00	0.00	0.00	0.00	0.00	0.00	0.00	0.00	0.00	0.00
FeO	63.00	63.50	64.00	62.01	54.36	54.54	53.62	54.65	55.37	54.32	54.76	54.35	58.43	59.65	61.32	54.68	55.75
MnO	5.00	4.00	3.00	4.06	3.10	3.13	3.35	3.16	3.16	2.85	2.94	2.93	3.77	3.85	4.24	4.20	4.07
MgO	2.08	2.08	2.08	2.14	9.82	10.05	10.13	9.91	9.84	9.76	10.11	10.87	5.51	4.55	3.00	2.78	1.29
CaO	0.41	0.70	0.36	0.41	0.55	0.45	0.47	0.59	0.49	0.49	0.53	0.46	0.49	0.48	0.42	0.20	0.79
Fo	5.6	5.5	5.5	5.8	24.37	24.73	25.19	24.4	24.1	24.2	24.8	26.3	14.4	12.0	8.0	8.3	4.0
Fa	87.8	89.1	90.5	88.7	72.47	72.12	71.43	72.3	72.7	72.0	72.3	70.9	81.1	83.2	86.4	85.6	89.7
Tefr	7.1	5.7	4.3	5.9	4.18	4.19	4.52	3-2	4.2	3.9	3.9	3.9	5.3	5.4	6.0	6.7	6.6

Sample	**0718**																						
Member																							
	Trachyte “Case Ricco”																						
Position																							
Type	pheno, R	pheno, I	pheno, C	pheno, R	pheno, C	pheno, R	pheno, C	pheno, C	pheno, R	pheno, C	pheno, R	pheno	pheno, C	pheno, R	pheno, C	pheno, C	mpheno, R	mpheno, C	mpheno, C	mpheno, R	micro	micro	micro	micro
SiO_2	31.77	31.52	32.47	32.22	32.35	32.09	32.83	31.21	30.69	31.51	31.17	31.10	31.29	31.24	31.15	31.07	30.89	31.07	31.01	30.67	3.31	30.20	30.61	30.63
TiO_2	0.00	0.00	0.00	0.00	0.00	0.00	0.00	0.00	0.00	0.00	0.00	0.00	0.00	0.00	0.00	0.00	0.00	0.00	0.00	0.00	0.00	0.00	0.00	0.00
Al_2O_3	0.00	0.00	0.00	0.00	0.00	0.00	0.00	0.00	0.00	0.00	0.00	0.00	0.00	0.00	0.00	0.00	0.00	0.00	0.00	0.00	0.00	0.00	0.00	0.00
FeO	56.08	55.31	53.48	55.17	52.66	55.98	52.34	54.24	56.00	53.73	55.88	54.77	53.55	54.95	55.19	54.25	55.81	56.70	54.54	54.79	62.22	62.69	63.24	63.74
MnO	3.30	3.15	3.11	3.19	2.94	3.07	2.93	2.78	2.97	2.77	2.92	2.64	2.63	3.16	2.88	2.72	2.87	2.95	3.11	2.88	3.72	3.83	4.35	3.96
MgO	8.23	9.45	10.36	9.02	11.48	8.52	11.36	10.80	8.40	10.66	8.96	9.93	10.92	8.91	9.00	9.98	8.55	8.23	9.14	9.45	2.61	2.49	1.35	1.14
CaO	0.48	0.44	0.40	0.30	0.40	0.35	0.42	0.47	0.55	0.41	0.47	0.46	0.34	0.36	0.40	0.42	0.39	0.47	0.43	0.46	0.33	0.37	0.28	0.29
Fo	19.8	22.4	24.6	21.6	26.9	20.4	26.8	25.2	20.2	25.2	21.3	23.5	25.7	21.5	21.6	23.8	20.6	19.7	22.0	22.6	6.6	6.3	3.4	2.9
Fa	75.7	73.4	71.2	74.1	69.2	75.4	69.3	71.1	75.7	71.1	74.7	72.9	70.8	74.2	74.5	72.5	75.5	76.2	73.7	73.5	88.1	88.3	90.3	91.4
Tefr	4.5	4.2	4.2	4.3	3.9	4.2	3.9	3.7	4.1	3.7	4.0	3.6	3.5	4.3	3.9	3.7	3.9	4.1	4.3	3.9	5.3	5.5	6.3	5.7

Pheno = phenocrysts and mpheno= microphenocrysts (> 50 µm). Micro = microlites (< 50 µm); R = rim, C = core. Fo = forsterite, Fa = fayalite and Tefr = tefroite (mole %).

Selected analyses of olivines.

Sample	**0748**																
Member																	
	Trachyte "M.gna Grande Sud"																
Position																	
Type	pheno, R	pheno, C	pheno, R	pheno, I	pheno, C	pheno, R	pheno, C	mpheno	mpheno, R	pheno, C	mpheno, R	mpheno, I	mpheno, R	mpheno, I	mpheno, C	micro	micro
SiO_2	32.77	31.74	30.80	31.74	31.04	31.33	32.26	31.92	31.33	32.26	31.96	31.29	31.32	31.41	31.75	30.37	29.75
TiO_2	0.00	0.00	0.00	0.00	0.00	0.00	0.00	0.00	0.00	0.00	0.00	0.00	0.00	0.00	0.00	0.00	0.00
Al_2O_3	0.00	0.00	0.00	0.00	0.00	0.00	0.00	0.00	0.00	0.00	0.00	0.00	0.00	0.00	0.00	0.00	0.00
FeO	51.54	53.06	53.66	53.51	52.55	53.01	52.54	52.73	53.01	52.54	53.00	53.32	53.58	53.03	54.49	59.71	61.38
MnO	2.60	2.79	3.46	2.66	2.86	3.01	2.75	2.74	3.01	2.75	2.93	2.84	2.65	3.03	3.18	5.75	3.45
MgO	11.25	11.29	10.11	11.09	11.20	11.06	11.39	10.87	11.06	11.39	10.95	11.22	10.80	11.27	8.57	3.17	3.77
CaO	0.51	0.40	0.45	0.44	0.45	0.41	0.47	0.61	0.41	0.47	0.31	0.41	0.27	0.26	0.54	0.06	0.24
Fo	27.1	26.5	24.0	26.1	26.5	26.0	26.9	25.9	26.0	26.9	25.9	26.2	25.5	26.4	20.9	7.9	9.4
Fa	69.4	69.8	71.4	70.4	69.7	70.0	69.5	70.4	70.0	69.5	70.2	70.0	70.9	69.6	74.7	83.9	85.7
Tefr	3.5	3.7	4.6	3.5	3.8	4.0	3.6	3.7	4.0	3.7	3.9	3.8	3.6	4.0	4.4	8.2	4.9

Sample	**0750**																
Member																	
	Trachyte "Montagna Grande Nord"																
Position																	
Type	pheno, R	pheno, C	pheno, C	pheno, R	pheno, C	pheno, R	pheno, C	mpheno	mpheno	mpheno	mpheno	micro	micro	micro	micro	micro	micro
SiO_2	32.90	32.19	32.51	32.64	33.05	33.11	32.95	33.13	32.39	33.36	32.60	32.76	32.49	32.47	32.63	32.81	33.07
TiO_2	0.00	0.00	0.00	0.00	0.00	0.00	0.00	0.00	0.00	0.00	0.00	0.00	0.00	0.00	0.00	0.00	0.00
Al_2O_3	0.00	0.00	0.00	0.00	0.00	0.00	0.00	0.00	0.00	0.00	0.00	0.00	0.00	0.00	0.00	0.00	0.00
FeO	46.64	46.26	46.44	46.81	46.31	46.49	46.88	47.11	47.24	47.11	46.79	46.72	47.39	46.88	47.25	46.65	46.88
MnO	2.17	2.45	1.97	2.06	2.08	2.18	2.41	2.41	2.20	2.20	2.19	2.46	2.39	2.28	2.17	2.22	2.32
MgO	16.27	16.62	17.37	16.50	16.86	16.72	16.56	16.01	16.28	15.89	16.16	16.10	15.69	15.77	15.98	16.53	16.03
CaO	0.41	0.70	0.36	0.41	0.35	0.24	0.38	0.27	0.27	0.31	0.35	0.34	0.37	0.49	0.62	0.47	0.34
Fo	37.3	39.0	40.0	38.6	39.3	39.1	38.6	37.7	38.1	37.6	38.1	37.0	37.1	37.5	36.6	38.7	37.9
Fa	59.9	59.0	58.5	59.8	59.0	59.1	59.5	60.3	60.1	60.6	60.0	60.0	60.8	60.5	60.6	59.4	60.1
Tefr	2.8	2.0	2.5	2.7	2.7	2.8	3.1	3.1	2.8	2.9	2.9	3.0	3.1	3.0	2.8	2.9	3.0

Pheno = phenocrysts and mpheno = microphenocrysts (> 50 µm). Micro = microlites (< 50 µm); R = rim, C = core. Fo = forsterite, Fa = fayalite and Tefr = tefroite (mole %).

Selected analyses of olivines.

Sample	**0732**										
Member											
	Trachyte "Mueggen"										
Position											
Type	pheno, R	pheno, C	pheno, R	pheno, C	mpheno, R	mpheno, I	mpheno, C	mpheno, R	mpheno, C	micro	micro
SiO_2	29.42	29.51	31.34	29.93	31.02	29.89	29.83	31.23	29.63	30.12	29.94
TiO_2	0.00	0.00	0.00	0.00	0.00	0.00	0.00	0.00	0.00	0.00	0.00
Al_2O_3	0.00	0.00	0.00	0.00	0.00	0.00	0.00	0.00	0.00	0.00	0.00
FeO	61.14	61.20	59.67	61.08	59.39	60.60	61.35	60.45	61.19	60.85	60.59
MnO	4.10	3.67	3.83	3.92	3.50	4.09	4.01	3.88	3.87	3.72	3.97
MgO	3.57	3.56	3.36	3.36	4.00	3.51	3.42	3.90	3.53	3.60	3.79
CaO	0.35	0.61	0.57	0.38	0.24	0.39	0.19	0.46	0.60	0.30	0.35
Fo	8.9	8.9	8.6	8.4	10.2	8.9	8.5	9.7	8.8	9.1	8.5
Fa	85.3	85.9	85.8	86.0	84.7	85.3	85.8	84.8	85.7	84.4	85.9
Tefr	5.8	5.2	5.6	5.6	5.1	5.8	5.7	5.5	5.5	5.5	5.6

Sample	**Pant24**														
Member	**Trachyte enclave**														
Position	**Pumice cone "C. Randazzo"**														
Type	pheno, R	pheno, C	pheno, C	pheno, R	pheno, C	pheno, R	mpheno	mpheno	mpheno	mpheno	micro	micro	micro	micro	micro
SiO_2	29.31	29.29	29.14	28.91	30.14	30.51	29.15	30.18	28.72	28.83	29.19	29.31	29.47	29.01	29.36
TiO_2	0.00	0.00	0.00	0.00	0.00	0.00	0.00	0.00	0.00	0.00	0.00	0.00	0.00	0.00	0.00
Al_2O_3	0.00	0.00	0.00	0.00	0.00	0.00	0.00	0.00	0.00	0.00	0.00	0.00	0.00	0.00	0.00
FeO	61.47	61.60	62.58	61.98	57.81	58.29	64.08	58.20	64.65	64.41	63.61	64.62	63.28	64.32	64.81
MnO	4.26	4.08	3.85	4.09	3.60	3.47	3.99	3.49	3.87	4.29	3.88	4.16	4.16	4.17	3.96
MgO	3.67	3.85	3.59	3.14	6.38	6.28	1.20	6.37	1.20	0.99	1.35	1.13	1.30	1.18	1.27
CaO	0.81	0.73	0.83	0.62	0.52	0.55	0.28	0.69	0.24	0.32	0.31	0.32	0.40	0.33	0.27
Fo	9.0	9.4	8.8	7.8	15.6	15.4	3.0	15.5	3.1	2.5	3.4	2.8	3.3	3.0	3.2
Fa	85.0	84.9	85.9	86.4	79.4	79.8	91.2	79.6	91.4	91.3	90.9	91.2	90.7	91.0	91.2
Tefr	6.0	5.7	5.4	5.8	5.0	4.8	5.8	4.8	5.5	6.2	5.7	6.0	6.0	6.0	5.6

Pheno = phenocrysts and mpheno = microphenocrysts (> 50 µm). Micro = microlites (< 50 µm); R = rim, C = core. Fo = forsterite, Fa = fayalite and Tefr = tefroite (mole %).

Selected analyses of olivines.

Sample	**Pant21**																	
Member	**Trachyte enclave**																	
Position	**Pumice cone "C. Randazzo"**																	
Type	pheno, R	pheno, C	pheno, R	pheno, C	pheno, R	pheno, C	pheno, R	pheno, C	mpheno	mpheno	mpheno	mpheno	mpheno	mpheno	micro	micro	micro	micro
SiO_2	29.86	29.71	29.92	29.48	30.28	29.39	30.09	29.69	28.92	29.47	30.05	28.92	29.69	29.87	29.55	29.68	29.57	28.95
TiO_2	0.00	0.00	0.00	0.00	0.00	0.00	0.00	0.00	0.00	0.00	0.00	0.00	0.00	0.00	0.00	0.00	0.00	0.00
Al_2O_3	0.00	0.00	0.00	0.00	0.00	0.00	0.00	0.00	0.00	0.00	0.00	0.00	0.00	0.00	0.00	0.00	0.00	0.00
FeO	61.30	61.13	61.16	61.81	60.20	60.94	61.01	61.45	64.65	63.63	63.75	64.16	61.28	61.36	64.91	64.65	64.09	64.37
MnO	4.04	4.08	4.10	4.34	3.87	4.09	3.90	3.81	3.87	4.04	3.95	4.27	4.10	3.86	3.94	3.70	3.99	4.20
MgO	3.89	3.98	3.78	3.06	4.51	3.57	4.11	4.02	1.90	1.96	1.98	1.80	3.82	3.84	0.94	1.25	1.37	1.83
CaO	0.66	0.71	0.70	0.58	0.73	0.62	0.68	0.62	0.24	0.41	0.30	0.35	0.68	0.73	0.34	0.35	0.52	0.33
Fo	9.6	9.8	9.3	7.6	16.2	8.9	15.1	9.9	4.7	4.9	4.9	4.5	9.4	13.5	2.3	3.2	3.5	4.6
Fa	84.8	84.5	84.9	86.3	78.4	85.3	79.4	84.8	89.8	89.4	89.5	89.5	84.8	80.1	92.0	91.5	90.8	89.5
Tefr	5.6	5.7	5.8	6.1	5.4	5.8	5.5	5.3	5.5	5.7	5.6	6.0	5.8	5.4	5.7	5.3	5.7	5.9

Sample	**Pan23**										
Member	**Trachyte enclave**										
Position	**In pumice C. Randazzo**										
Type	mpheno	mpheno	pheno	pheno	pheno	pheno	pheno, C	pheno, R	pheno, C	micro	micro
SiO_2	***32,66***	***32,76***	***29,00***	***31,97***	***32,03***	***31,87***	***32,32***	***31,10***	***31,08***	***30,95***	***30,50***
TiO_2	0.00	0.00	0.00	0.00	0.00	0.00	0.00	0.00	0.00	0.00	0.00
Al_2O_3	0.00	0.00	0.00	0.00	0.00	0.00	0.00	0.00	0.00	0.00	0.00
FeO	***50,92***	***51,71***	***64,44***	***53,86***	***53,68***	***53,81***	***53,28***	***56,38***	***55,11***	***55,26***	***58,55***
MnO	***2,86***	***2,86***	***4,32***	***3,23***	***3,27***	***3,19***	***3,29***	***3,25***	***3,49***	***3,46***	***3,34***
MgO	***13,08***	***12,11***	***1,58***	***10,12***	***10,34***	***10,40***	***10,63***	***8,38***	***8,67***	***8,50***	***5,72***
CaO	***0,48***	***0,57***	***0,30***	***0,61***	***0,57***	***0,56***	***0,48***	***0,55***	***0,48***	***0,66***	***0,61***
Fo	31,4	29,5	24,0	25,1	25,6	25,6	26,2	20,9	21,9	21,5	14,8
Fa	66,6	68,5	72,5	71,4	70,9	70,9	70,3	75,6	74,6	75,0	81,7
Tefr	2.00	2.09	3,8	4,1	4,4	4,8	3,5	4,3	3,5	3,7	3,6

Pheno = phenocrysts and mpheno = microphenocrysts (> 50 µm). Micro = microlites (< 50 µm); R = rim, C = core. Fo = forsterite, Fa = fayalite and Tefr = tefroite (mole %).

Selected analyses of olivines.

Sample	**0749**																				
Member	**BENMOREIITE**																				
Position	**IN TRACHYTE**																				
Type	**pheno, C**	**pheno, R**	**pheno, C**	**pheno, R**	**pheno, C**	**pheno, R**	**pheno, C**	**pheno, R**	**pheno**	**pheno, R**	**pheno, C**	**pheno, C**	**pheno, I**	**pheno, R**	**pheno, C**	**pheno, I**	**pheno, R**	**pheno, R**	**pheno, C**	**pheno, R**	**pheno, C**
SiO_2	38.96	34.60	39.48	34.73	33.88	35.56	38.83	37.74	34.85	35.29	38.92	39.70	39.17	36.14	39.20	37.93	35.00	36.16	39.37	36.97	38.85
TiO_2	0.00	0.00	0.00	0.00	0.00	0.00	0.00	0.00	0.00	0.00	0.00	0.00	0.00	0.00	0.00	0.00	0.00	0.00	0.00	0.00	0.00
Al_2O_3	0.00	0.00	0.00	0.00	0.00	0.00	0.00	0.00	0.00	0.00	0.00	0.00	0.00	0.00	0.00	0.00	0.00	0.00	0.00	0.00	0.00
FeO	15.80	34.17	14.39	32.59	37.40	35.55	15.19	19.48	34.57	35.62	16.04	14.92	18.39	33.01	16.69	20.79	35.00	30.57	14.81	23.36	15.34
MnO	0.26	0.92	0.18	0.90	1.34	0.92	0.22	0.29	1.01	1.27	0.09	0.26	0.18	1.11	0.23	0.45	1.06	0.73	0.25	0.55	0.13
MgO	43.70	28.44	44.60	28.53	25.51	26.06	44.71	40.88	27.50	26.16	43.75	44.86	42.04	29.43	43.12	39.48	27.53	30.98	43.92	37.43	44.19
CaO	0.16	0.24	0.38	0.31	0.35	0.51	0.41	0.51	0.27	0.31	0.06	0.26	0.23	0.30	0.16	0.31	0.40	0.27	0.36	0.29	0.35
Fo	83.1	59.1	84.7	60.9	54.9	56.7	83.8	78.8	58.9	56.9	82.9	84.0	80.3	60.4	81.0	76.5	58.9	63.0	82.8	78.3	58.8
Fa	16.6	39.8	15.2	38.6	44.4	42.9	16.0	21.0	40.9	42.6	17.0	15.7	19.7	38.3	18.0	23.0	40.9	36.0	17.0	21.4	40,7
Tefr	0.3	1.1	0.1	1.1	1.6	1.1	0.2	0.3	1.2	1.5	0.1	0.3	0.2	1.3	1.0	0.5	1.3	1.0	0.2	0.3	0.5

Sample	**0749**											
Member	**BENMOREIITE**											
Position	**IN TRACHYTE**											
Type	**mpheno, R**	**mpheno, C**	**mpheno, R**	**mpheno, C**	**pheno, R**	**mpheno, C**	**mpheno, R**	**micro**	**micro**	**micro**	**micro**	**micro**
SiO_2	34.53	35.05	35.75	38.79	35.51	35.00	35.81	34.90	34.56	34.89	34.46	34.99
TiO_2	0.00	0.00	0.00	0.00	0.00	0.00	0.00	0.00	0.00	0.00	0.00	0.00
Al_2O_3	0.00	0.00	0.00	0.00	0.00	0.00	0.00	0.00	0.00	0.00	0.00	0.00
FeO	37.43	36.98	34.20	16.79	31.64	35.00	36.35	36.46	36.73	37.48	38.04	36.54
MnO	1.13	0.89	1.07	0.11	0.79	1.06	1.17	0.98	0.91	0.89	0.95	0.84
MgO	25.38	25.96	28.45	43.10	30.67	27.53	26.20	25.40	25.05	24.58	24.59	25.80
CaO	0.40	0.41	0.28	0.32	0.36	0.40	0.46	0.43	0.40	0.41	0.44	0.45
Fo	54.7	55.6	59.7	82.1	63.3	58.4	56.2	55.4	54.9	53.9	53.5	55.7
Fa	43.9	43.0	38.8	16.9	35.5	40.3	42.5	43.1	43.7	44.6	45.0	42.8
Tefr	1.4	1.4	1.5	1.0	1.2	1.3	1.3	1.5	1.4	1.5	1.5	1.5

Pheno = phenocrysts and mpheno = microphenocrysts (> 50 µm). Micro = microlites (< 50 µm); R = rim, C = core. Fo = forsterite; Fa = fayalite; Tefr = tefroite (mole %)

Selected analyses of Fe-Ti oxides.

Sample	**0720**	**0722**		**0723**			**0731**			
Member	**A**	**C**		**D**			**E**			
	Pumice fall	**Weld. Eutax.**		**Weld. Fines-rich**			**Welded fines-depleted**			
Position	**Botton**	**intermediate**					**Top**			
Type	*micro*	*micro*	*micro*	*mpheno*	*micro*	*micro*	*micro*	*micro*	*micro*	*micro*
SiO_2	0.51	0.21	0.34	0.18	0.32	0.20	0.30	0.34	0.32	0.30
TiO_2	48.45	50.58	52.83	51.02	52.00	52.55	52.85	52.26	51.92	52.85
Al_2O_3	0.28	0.10	0.14	0.05	0.03	0.26	0.17	0.07	0.22	0.17
FeO	41.92	44.22	44.80	41.51	44.88	45.96	46.34	45.09	45.35	46.34
MnO	4.52	2.14	2.12	6.53	2.41	1.68	1.78	1.96	1.98	1.78
MgO	0.28	0.12	0.12	0.21	0.39	0.18	0.53	0.48	0.97	0.53
Usp										
Ilm	97.2	99.1	99.5	97.3	98.9	99.4	98.7	99.4	97.5	97.8

Sample	**0722**	**0723**		**0731**					
Member	**B**	**D**		**E**					
	Weld. Eutax.	**Weld. Fines-rich**		**Welded fines-depleted**					
Position	**intermediate**			**Top**					
Type	*micro*	*mpheno*	*micro*	*mpheno*	*mpheno*	*mpheno*	*mpheno*	*mpheno*	*mpheno*
SiO_2	2.18	0.19	2.37	0.14	0.27	0.33	0.35	0.29	0.22
TiO_2	19.11	24.22	20.83	28.84	29.24	28.06	27.03	26.63	25.11
Al_2O_3	0.38	0.56	0.51	0.27	0.26	0.39	0.35	0.29	0.24
FeO	62.56	72.05	60.03	67.12	65.80	67.80	66.89	68.23	67.15
MnO	2.21	3.57	2.91	1.73	1.75	1.54	1.59	1.81	1.43
MgO	0.17	0.18	0.34	0.19	0.27	0.24	0.31	0.52	0.42
Usp	66.8	66.7	73.0	82.2	84.3	80.6	79.0	75.9	74.0
Ilm									

Pheno = phenocrysts and mpheno = microphenocrysts (> 50 µm). Micro = microlites (< 50 µm); R = rim, C = core Usp = ulvospinel mole %; Ilm = ilmenite mole %.

Selected analyses of Fe-Ti oxides.

Sample	**0718**					
Member	**Trachyte "Casa Ricco"**					
Position	**intermediate**					
Type	*micro*	*micro*	*micro*	*mpheno*	*pheno*	*pheno*
SiO_2	0.21	0.29	0.40	0.25	0.29	0.35
TiO_2	23.02	21.36	20.95	25.14	24.82	22.39
Al_2O_3	0.60	0.27	0.25	0.43	0.95	1.21
FeO	69.31	70.20	70.14	66.63	68.87	69.49
MnO	1.44	1.37	1.54	1.45	1.17	1.35
MgO	0.33	0.37	0.07	0.32	0.71	0.80
Usp	68.2	62.9	62.6	75.1	73.2	67.2
Ilm						

Sample	**0750**						
Member	**Trachyte "Montagna Grande Nord"**						
Position	**Less evolved**						
Type	*micro*	*micro*	*micro*	*mpheno*	*mpheno*	*pheno*	*pheno*
SiO_2	0.34	0.36	0.26	0.48	0.23	0.14	0.40
TiO_2	23.58	22.57	22.07	23.82	24.23	51.24	50.89
Al_2O_3	1.01	0.77	1.26	1.74	1.25	0.22	0.09
FeO	71.20	67.89	67.83	70.50	67.59	44.16	46.02
MnO	1.28	1.29	1.22	1.04	1.28	1.46	1.25
MgO	1.79	1.27	1.50	1.69	1.69	2.43	2.13
Usp	66.1	67.0	66.0	63.1	63.1		
Ilm						95.8	97.4

Pheno = phenocrysts and mpheno = microphenocrysts (> 50 µm). Micro = microlites (< 50 µm); R = rim, C = core Usp = ulvospinel mole %; Ilm = ilmenite mole %.

Selected analyses of Fe-Ti oxides.

Sample	**0732**					
Member	**Trachyte "Mueggen"**					
Position	**More evolved**					
Type	*micro*	*micro*	*micro*	*mpheno*	*pheno*	*pheno*
SiO_2	0.27	0.21	0.39	0.16	0.30	0.39
TiO_2	23.67	24.08	24.80	51.22	50.51	51.62
Al_2O_3	0.40	0.27	0.34	0.04	0.09	0.05
FeO	70.77	71.05	69.73	46.83	46.78	45.79
MnO	1.50	1.66	1.57	1.92	1.94	1.95
MgO	0.38	0.27	0.48	0.44	0.43	0.38
Usp	68.1	68.6	71.2			
Ilm				96.5	95.8	98.2

Sample	**Pant24**													
Member	**Trachyte enclave**													
Position	**Pumice "C.Randazzo"**													
Type	*Micro*	*Micro*	*mpheno*	*mpheno*	*mpheno*	*mpheno*	*mpheno*	*mpheno*	*Micro*	*Micro*	*Micro*	*Micro*	*Micro*	*Micro*
SiO_2	5.47	3.57	2.30	0.31	0.31	0.45	0.30	0.70	0.85	1.68	0.27	0.21	0.42	0.32
TiO_2	21.10	23.60	23.67	27.01	27.55	27.43	27.11	27.03	50.63	49.69	51.74	52.56	51.62	52.00
Al_2O_3	0.21	0.47	0.60	0.51	0.77	0.75	0,.38	0.75	0.10	0.42	0.19	0.19	0.33	0.13
FeO	69.67	67.81	68.86	69.35	67.89	67.81	67.67	67.88	46.72	45.63	46.02	45.75	45.90	46.50
MnO	2.38	1.63	1.56	1.54	1.56	1.74	182	1.76	2.11	1.89	1.93	1.94	1.64	1.94
MgO	0.32	0.36	0.11	0.18	-0.01	0.54	0.14	0.33	0.12	0.20	0.16	0.21	0.21	0.39
Usp	72.0	74.5	77.5	80.7	79.4	78.5	79.5	77.2						
Ilm									97.1	98.7	98.5	99.4	98.9	97.8

Pheno = phenocrysts and mpheno = microphenocrysts (> 50 µm). Micro = microlites (< 50 µm); R = rim, C = core Usp = ulvospinel mole %; Ilm = ilmenite mole %.

Selected analyses of Fe-Ti oxides

Sample	**Pant21**											
Member												
Position	**In Pumice cone "C.Randazzo"**											
Type	*mpheno*	*mpheno*	*mpheno*	*mpheno*	*mpheno*	*mpheno*	*micro*	*micro*	*micro*	*micro*	*micro*	*mpheno*
SiO_2	2.30	0.31	0.45	0.30	0.70	0.23	0.31	0.33	0.41	0.76	0.58	0.32
TiO_2	23.67	27.55	27.43	27.11	27.03	25.68	27.14	51.72	51.43	52.07	49.83	52.00
Al_2O_3	0.60	0.77	0.75	0.38	0.75	0.72	0.78	0.19	0.19	0.18	0.44	0.13
FeO	68.86	67.89	67.81	67.67	67.88	69.03	69.99	45.52	45.00	45.88	43.96	46.00
MnO	1.56	1.56	1.74	1.82	1.76	1.48	1.61	2.14	2.30	2.28	1.97	1.94
MgO	0.11	-0.01	0.54	0.14	0.33	0.31	0.41	0.08	0.20	0.21	0.21	0.39
Usp	74.5	80.7	79.4	78.5	79.5	75.0	77.2					
Ilm								99.0	98.9	99.1	99.1	98.3

Sample	**Pant23**					
Member						
Position	**In Pumice cone "C.Randazzo"**					
Type	*pheno, R*	*pheno, C*	*pheno, R*	*micro*	*micro*	*micro*
SiO_2	0.46	0.51	0.40	0.33	1.68	0.27
TiO_2	26.01	27.67	24.73	52.23	49.69	51.74
Al_2O_3	0.35	0.72	0.30	0.26	0.42	0.19
FeO	69.67	68.97	71.12	43.79	45.63	46.02
MnO	1.93	1.45	1.02	2.58	1.89	1.93
MgO	0.15	0.50	0.63	0.34	0.20	0.16
Usp	74.2	79.5	70.2			
Ilm				99.9	98.7	98.5

Pheno = phenocrysts and mpheno = microphenocrysts (> 50 µm). Micro = microlites (< 50 µm); R = rim, C = core Usp = ulvospinel mole %; Ilm = ilmenite mole %.

Selected analyses of Fe-Ti oxides.

Sample	**0749**														
Member	**BENMOREIITE**														
Position	**IN TRACHYTE**														
Type	*micro*	*micro*	*mpheno*	*mpheno*	*mpheno*	*mpheno*	*mpheno*	*mpheno*	*micro*	*micro*	*micro*	*micro*	*micro*	*micro*	*micro*
SiO_2	0.05	0.34	0.45	0.40	0.40	0.22	0.40	0.23	0.30	0.30	0.40	0.40	4.04	2.11	0.26
TiO_2	23.52	22.83	22.21	23.12	24.15	24.02	23.12	24.79	50.55	50.55	50.55	50.05	45.55	47.29	50.94
Al_2O_3	0.61	2.13	0.66	2.36	2.07	2.14	2.36	2.02	0.41	0.41	0.41	0.41	1.37	0.46	0.29
FeO	67.15	68.17	73.31	66.63	66.16	67.07	66.63	68.17	44.01	44.03	44.03	45.03	43.37	45.52	43.21
MnO	2.10	0.80	2.10	0.97	0.88	0.92	0.97	1.01	0.85	0.95	0.95	0.95	0.88	0.66	0.83
MgO	2.55	3.21	0.69	2.57	3.10	3.01	2.57	3.12	2.61	2.71	2.71	2.71	1.82	1.50	2.93
Usp	65.0	65.8	62.2	69.9	71.3	70.2	69.9	70.5							
Ilm									95.7	95.4	95.5	93.9	94.6	94.9	95.9

Sample	**0749**																			
Member	**BENMOREIITE**																			
Position	**IN TRACHYTE**																			
Type	*Micro*	*Micro*	*Micro*	*Micro*	*Micro*	*Micro*	*Micro*	*Micro*	*Micro*	*Micro*	*Micro*	*Micro*	*Micro*	*Micro*	*mpheno*	*mpheno*	*mpheno*	*mpheno*	*mpheno*	*mpheno*
SiO_2	0.55	0.26	0.29	0.33	0.35	0.20	0.26	0.31	0.47	0.27	0.22	3.00	0.50	0.39	0.03	0.19	0.45	0.50	0.48	0.18
TiO_2	7.69	4.22	4.90	17.09	15.19	7.67	4.58	15.45	7.46	4.87	3.66	3.69	16.62	11.40	19.45	17.07	20.39	16.62	20.82	17.14
Al_2O_3	11.17	19.77	22.67	3.50	3.82	11.14	20.24	4.84	20.25	18.58	20.96	18.00	4.45	5.91	2.77	3.91	2.86	4.45	2.74	7.41
FeO	52.60	40.93	30.80	57.72	59.73	53.28	36.02	59.14	36.94	42.76	31.43	42.24	56.45	53.71	63.42	60.29	63.57	56.45	63.13	51.91
MnO	0.29	0.42	0.32	0.72	0.69	0.74	0.23	0.64	0.29	0.58	0.17	0.51	0.69	0.62	0.62	0.56	0.38	0.69	0.62	0.67
MgO	4.58	7.49	12.59	4.32	3.30	4.78	10.49	4.30	11.44	8.27	11.28	5.80	4.19	4.09	3.11	3.28	2.86	4.19	3.00	7.04
CR_2O_3	17.96	23.25	27.52	13.00	14.66	18.14	25.79	12.41	22.53	22.62	30.21	21.60	13.19	21.49	7.17	12.36	6.92	13.19	5.31	10.24
MgCr2O4 (Mg-cromite)	6.62	11.45	19.95	7.61	5.51	6.74	16.69	6.05	15.80	11.99	20.45	9.24	7.27	7.91	4.33	5.39	4.56	7.27	4.50	9.15
FeCr2O4 (crom)	18.44	18.61	13.42	10.33	14.80	17.82	15.78	11.05	11.95	16.69	17.26	20.27	11.07	21.72	5.59	11.76	5.11	11.07	2.75	4.78

Pheno = phenocrysts and mpheno = microphenocrysts (> 50 µm). Micro = microlites (< 50 µm); R = rim, C = core Usp = ulvospinel mole %; Ilm = ilmenite mole %.

Representative SEM-EDS analyses of glasses.

Sample	**0720**						**0721**						**0722**							
member	**A**						**B**						**C**							
position	**Pumice fall botton**						**Pumice flow**						**Weld. eutax. intermediate**							
SiO_2	72.17	73.84	73.53	72.32	72.27	72.59	70.70	71.69	71.75	72.30	72.77	73.60	65.81	69.32	71.49	67.42	75.62	72.36	65.77	74.89
Al_2O_3	8.16	8.56	8.63	10.01	10.84	8.98	11.05	8.57	9.84	9.51	9.90	8.64	12.79	11.51	9.26	11.76	8.47	9.51	13.08	8.95
FeO	7.93	7.88	7.98	8.05	8.09	7.45	7.99	7.58	7.81	8.05	8.09	7.98	5.16	4.95	6.23	5.71	4.88	6.12	5.85	5.44
MnO	0.41	0.41	0.17	0.41	0.42	0.17	0.21	0.41	0.21	0.41	0.10	0.17	0.06	0.19	0.17	0.41	0.36	0.17	0.18	0.18
MgO	0.15	0.08	0.18	0.16	0.09	0.13	0.20	0.16	0.17	0.16	0.09	0.13	0.18	0.15	0.10	0.15	0.13	0.10	0.10	0.10
CaO	0.34	0.24	0.47	0.38	0.23	0.41	0.63	0.33	0.34	0.38	0.23	0.41	0.32	0.14	0.44	0.00	0.39	0.00	0.00	0.00
Na_2O	5.21	3.73	4.12	4.08	3.83	4.12	3.78	6.64	5.12	4.08	3.87	4.21	6.29	6.43	6.52	8.35	5.81	5.80	6.49	5.17
K_2O	5.13	4.82	4.46	4.56	4.95	4.47	4.96	4.23	4.36	4.56	4.61	4.62	9.37	7.41	5.76	6.27	4.40	5.93	8.52	5.27
A.I.	1.7	1.3	1.3	1.2	1.1	1.3	1.0	1.8	1.3	1.2	1.1	1.4	1.6	1.6	1.8	1.7	1.7	1.7	1.5	1.6

Sample	**0723**				**0731**			
member	**D**				**E**			
position	**Weld. fines-rich**				**Welded fines-depleted Top**			
SiO_2	66.59	67.85	65.97	65.66	65.04	67.36	66.68	66.87
Al_2O_3	14.45	10.89	13.67	13.16	17.70	17.33	17.20	17.88
FeO	4.34	7.26	5.77	6.19	4.07	2.85	3.06	2.69
MnO	0.06	0.47	0.40	0.18	0.16	0.04	0.00	0.22
MgO	0.17	0.11	0.14	0.10	0.16	0.22	0.24	0.35
CaO	0.31	0.39	0.37	0.44	0.19	0.46	0.33	0.42
Na_2O	6.51	6.54	6.06	7.09	7.20	7.14	5.97	6.77
K_2O	7.54	5.43	7.49	7.16	4.59	4.90	5.60	5.18
A.I.	1.3	1.5	1.3	1.5	0.9	1.0	0.9	0.9

AI = Agpaitic index molar ($Na_2O + K_2O)/Al_2O_3$)

Representative SEM-EDS analyses of glasses.

Sample	**0748**				
litologia	**Trachyte "Montagna Grande Sud"**				
position	**intermediate**				
Type	m.i.	m.i.	m.i.	gdm	gdm
SiO_2	66.55	67.95	69.32	74.79	67.78
Al_2O_3	15.43	15.25	15.90	18.01	18.10
FeO	2.46	2.56	2.76	2.10	3.37
MnO	0.96	0.70	0.40	0.01	0.33
MgO	0.50	0.19	0.14	0.19	0.14
CaO	0.08	0.17	0.09	0.17	0.41
Na_2O	4.50	4.57	4.29	4.66	6.67
K_2O	4.98	4.84	4.26	4.32	5.54
A.I.	0.9	0.9	0.8	1.1	1.0

Sample	**0750**																								
litologia	**Trachyte "Montagna Grande nord"**																								
position	**intermediate**																								
Type	gdm	gdm	gdm	gdm	gdm	gdm	*m.i.*	*m.i.*	*m.i.*	*m.i.*	*m.i.*	*m.i.*	*m.i.*	*m.i.*	*m.i.*	*m.i.*	*m.i.*	*m.i.*	*m.i.*	*m.i.*	*m.i.*	*m.i.*	*m.i.*	*m.i.*	*m.i.*
SiO_2	65.90	65.09	65.92	67.16	67.96	67.12	66.17	66.03	67.85	68.78	68.25	65.94	67.65	65.90	69.26	65.90	67.65	65.90	69.26	65.90	67.53	64.85	67.68	65.65	63.30	65.12
Al_2O_3	15.02	14.94	14.45	14.54	14.48	14.49	16.62	16.12	16.06	15.28	15.89	14.78	14.92	15.02	13.71	15.02	14.92	15.02	13.71	15.02	16.25	16.64	14.62	16.30	20.36	18.91
FeO	5.77	5.68	5.81	5.55	5.56	5.37	5.36	5.79	4.45	4.34	4.46	5.49	3.75	5.77	4.55	5.77	3.75	5.77	4.55	5.77	5.62	4.78	5.00	5.02	4.79	5.10
MnO	0.04	0.03	0.42	0.00	0.05	0.15	0.10	1.13	0.49	0.24	0.18	-0.14	0.35	0.04	0.28	0.04	0.35	0.04	0.28	0.04	0.12	0.45	0.19	0.43	0.16	0.09
MgO	0.32	0.68	0.30	0.40	0.37	0.46	0.27	0.30	0.17	0.17	0.20	0.44	1.13	0.32	0.30	0.32	1.13	0.32	0.30	0.32	0.21	0.35	0.24	0.60	0.39	0.23
CaO	0.60	0.41	0.38	0.47	0.32	0.19	0.71	0.94	0.94	0.69	0.52	0.63	0.59	0.60	0.35	0.60	0.59	0.60	0.35	0.60	0.31	1.83	0.40	0.34	0.76	0.77
Na_2O	5.80	6.15	5.54	4.92	4.79	4.75	6.24	6.29	6.66	6.21	5.98	6.26	6.21	5.80	5.88	5.80	6.21	5.80	5.88	5.80	5.86	6.54	6.46	7.22	6.66	5.94
K_2O	5.77	5.68	5.81	5.55	5.56	5.37	5.36	5.79	4.45	4.34	4.46	5.49	3.75	5.77	4.55	5.77	3.75	5.77	4.55	5.77	5.62	4.78	5.00	5.02	4.79	5.10
A.I.	1.05	1.09	1.07	0.97	0.96	0.94	0.97	1.03	0.98	0.98	0.92	1.10	0.96	1.05	1.07	1.05	0.96	1.05	1.07	1.05	0.97	0.96	1.10	1.06	0.79	0.81

AI = Agpaitic index molar ($Na_2O + K_2O$)/Al_2O_3) and M.I.= melt inclution Gdm =groundmass

Representative SEM-EDS analyses of glasses.

Sample	**Pant21**																							
litologia	**Trachyte enclaves**																							
position	**In Pumice cone "C.Randazzo"**																							
Type	gdm	gdm	gdm	gdm	gdm	gdm	gdm	gdm	gdm	gdm	gdm	gdm	gdm	gdm	gdm	gdm	gdm	gdm	*m.i.*	*m.i.*	*m.i.*	*m.i.*	*m.i.*	*m.i.*
SiO_2	71.19	70.30	71.36	69.33	70.21	71.69	71.95	72.04	71.22	71.05	72.87	71.00	71.01	70.63	69.77	70.23	70.72	71.68	70.07	69.47	69.48	68.69	68.69	68.57
Al_2O_3	6.48	8.02	7.52	9.81	6.81	7.36	6.56	7.11	7.41	7.23	8.74	8.39	8.48	8.50	8.53	8.59	8.63	7.82	12.29	15.92	14.98	15.52	15.25	11.69
FeO	11.69	10.19	10.85	8.45	11.70	10.57	10.60	10.60	10.19	10.64	9.93	9.60	9.50	9.99	10.03	9.48	9.52	10.15	7.55	3.78	4.68	4.15	5.03	6.93
MnO	0.48	0.29	0.32	0.20	0.48	0.41	0.36	0.18	0.39	0.45	0.21	0.49	0.35	-0.14	0.56	0.40	0.22	0.43	0.41	0.09	0.26	0.44	0.44	0.32
MgO	0.02	0.19	0.26	0.17	0.12	0.15	0.15	0.10	0.09	0.23	0.21	0.13	0.16	0.45	0.52	0.37	0.18	0.18	0.20	0.18	0.04	0.61	0.61	0.11
CaO	0.48	0.40	0.50	0.32	0.40	0.39	0.39	0.46	0.39	0.40	0.42	0.48	0.59	0.63	0.92	0.90	0.38	0.50	0.46	0.11	0.33	0.34	0.34	0.28
Na_2O	4.69	5.23	4.29	6.12	5.08	4.35	4.91	4.43	5.01	4.82	5.14	4.75	4.81	4.62	4.57	4.85	5.20	4.84	4.30	5.21	4.97	5.15	5.13	4.43
K_2O	3.89	4.59	4.11	4.81	4.12	4.13	4.29	4.12	4.30	4.29	4.29	4.30	4.40	4.31	4.42	4.44	4.40	4.11	4.10	5.04	5.00	4.91	4.89	4.47
A.I.	1.84	1.69	1.53	1.56	1.88	1.58	1.94	1.65	1.74	1.74	1.50	1.49	1.49	1.44	1.44	1.49	1.54	1.59	0.94	0.88	0.91	0.89	0.90	1.04

Sample	**0749**															
litologia	**BENMOREIITE**															
position	**IN TRACHYTE**															
Type	gdm	gdm	gdm	gdm	gdm	gdm	*m.i*	*m.i.*	*m.i.*	*m.i.*	*m.i.*	*m.i.*	*m.i.*	*m.i.*	*m.i.*	*m.i.*
SiO_2	62.81	60.65	66.16	63.15	63.26	62.31	60.87	52.75	59.93	67.67	66.22	71.40	60.01	66.54	66.42	66.42
TIO2	1.57	2.03	2.13	1.19	1.12	1.02	1.77	2.87	1.56	0.87	0.87	1.83	1.42	0.86	1.28	1.28
Al_2O_3	17.12	15.34	13.68	17.26	17.96	18.28	16.96	22.70	16.19	14.79	14.91	15.18	15.76	14.55	14.96	14.96
FeO	3.86	5.62	5.57	3.93	3.02	3.55	4.08	3.13	5.84	6.53	6.45	0.01	5.94	6.42	5.38	6.42
MnO	0.08	0.11	0.02	0.13	0.13	0.09	0.03	-0.04	0.00	0.21	0.35	0.17	0.15	0.21	0.21	0.21
MgO	0.44	0.61	0.47	0.68	0.43	0.60	0.69	1.00	0.72	0.24	0.39	0.47	1.86	0.24	0.39	0.39
CaO	0.82	3.40	1.13	1.07	1.25	1.44	3.23	4.83	3.68	1.03	1.28	1.29	5.22	1.02	1.28	1.28
Na_2O	6.43	6.46	5.19	5.95	6.13	6.96	6.76	9.24	6.36	4.55	4.72	4.82	5.72	4.47	4.73	4.60
K_2O	6.84	5.75	5.62	7.01	6.68	5.73	5.56	3.48	5.69	4.07	4.78	4.79	3.59	4.01	4.80	4.57
A.I.	1.05	1.10	1.07	1.01	0.96	0.97	1.01	0.84	1.03	0.80	0.87	0.86	0.84	0.80	0.87	0.84

AI = Agpaitic index molar ($Na_2O + K_2O$)/Al_2O_3) and M.I.= melt inclution Gdm = groundmass